

5-1-2014

Binary Technetium Halides

Erik Vaughan Johnstone

University of Nevada, Las Vegas, Erikvjohnstone@gmail.com

Follow this and additional works at: <https://digitalscholarship.unlv.edu/thesesdissertations>



Part of the [Radiochemistry Commons](#)

Repository Citation

Johnstone, Erik Vaughan, "Binary Technetium Halides" (2014). *UNLV Theses, Dissertations, Professional Papers, and Capstones*. 2099.

<https://digitalscholarship.unlv.edu/thesesdissertations/2099>

This Dissertation is protected by copyright and/or related rights. It has been brought to you by Digital Scholarship@UNLV with permission from the rights-holder(s). You are free to use this Dissertation in any way that is permitted by the copyright and related rights legislation that applies to your use. For other uses you need to obtain permission from the rights-holder(s) directly, unless additional rights are indicated by a Creative Commons license in the record and/or on the work itself.

This Dissertation has been accepted for inclusion in UNLV Theses, Dissertations, Professional Papers, and Capstones by an authorized administrator of Digital Scholarship@UNLV. For more information, please contact digitalscholarship@unlv.edu.

BINARY TECHNETIUM HALIDES

By

Erik Vaughan Johnstone

Bachelor of Science in Biochemistry
College of Charleston
2008

Bachelor of Science in Chemistry
College of Charleston
2009

A dissertation submitted in partial fulfillment

of the requirements for the

Doctor of Philosophy - Radiochemistry

Department of Chemistry

College of Sciences

The Graduate College

University of Nevada, Las Vegas

May 2014



THE GRADUATE COLLEGE

We recommend the dissertation prepared under our supervision by

Erik Vaughan Johnstone

entitled

Binary Technetium Halides

is approved in partial fulfillment of the requirements for the degree of

Doctor of Philosophy - Radiochemistry

Department of Chemistry

Kenneth Czerwinski, Ph.D., Committee Chair

Frederic Poineau, Ph.D., Committee Member

Alfred Sattelberger, Ph.D., Committee Member

Ralf Sudowe, Ph.D., Committee Member

Thomas Hartmann, Ph.D., Graduate College Representative

Kathryn Hausbeck Korgan, Ph.D., Interim Dean of the Graduate College

May 2014

ABSTRACT

Binary Technetium Halides

By

Erik Vaughan Johnstone

Dr. Kenneth Czerwinski, Advisory Committee Chair
Professor of Chemistry
Chair of the Department of Radiochemistry
University of Nevada, Las Vegas

In this work, the synthetic and coordination chemistry as well as the physico-chemical properties of binary technetium (Tc) chlorides, bromides, and iodides were investigated. Resulting from these studies was the discovery of five new binary Tc halide phases: α/β -TcCl₃, α/β -TcCl₂, and TcI₃, and the reinvestigation of the chemistries of TcBr₃ and TcX₄ (X = Cl, Br). Prior to 2009, the chemistry of binary Tc halides was poorly studied and defined by only three compounds, i.e., TcF₆, TcF₅, and TcCl₄. Today, ten phases are known (i.e., TcF₆, TcF₅, TcCl₄, TcBr₄, TcBr₃, TcI₃, α/β -TcCl₃ and α/β -TcCl₂) making the binary halide system of Tc comparable to those of its neighboring elements.

Technetium binary halides were synthesized using three methods: reactions of the elements in sealed tubes, reactions of flowing HX(g) (X = Cl, Br, and I) with Tc₂(O₂CCH₃)₄Cl₂, and thermal decompositions of TcX₄ (X = Cl, Br) and α -TcCl₃ in sealed tubes under vacuum. Binary Tc halides can be found in various dimensionalities such as molecular solids (TcF₆), extended chains (TcF₅, TcCl₄, α/β -TcCl₂, TcBr₃, TcI₃), infinite layers (β -TcCl₃), and bidimensional networks of clusters (α -TcCl₃); eight structure-types with varying degrees of metal-metal interactions are now known. The

coordination chemistry of Tc binary halides can resemble that of the adjacent elements: molybdenum and ruthenium (β -TcCl₃, TcBr₃, TcI₃), rhenium (TcF₅, α -TcCl₃), platinum (TcCl₄, TcBr₄), or can be unique (α -TcCl₂ and β -TcCl₂) in respect to other known transition metal binary halides. Technetium binary halides display a range of interesting physical properties that are manifested from their electronic and structural configurations. The thermochemistry of binary Tc halides is extensive. These compounds can selectively volatilize, decompose, disproportionate, or convert to other phases. Ultimately, binary Tc halides may find application in the nuclear fuel cycle and as precursors in inorganic and organometallic chemistry.

Acknowledgements

The work that has been presented in this document would not have been possible without the help, support, motivation, and teachings of many people in my life.

Academically, my past and current professors and mentors have molded me and have guided me through my vocational studies and research. Specifically, I would like to thank my dissertation committee. Each member of the committee has taught me valuable lessons and information pertaining to the field of radio- and Tc chemistry. The guidance, advice, and friendships of professors Frederic Poineau, Alfred Sattelberger, Thomas Hartmann, and Ralf Sudowe have been invaluable in my scientific, moral, and professional development. My gratitude goes out to my graduate advisor Prof. Kenneth Czerwinski for giving me the opportunity to grow and learn in such a unique field of science, and for showing me priceless leadership skills and a relentless work ethic that shall benefit me for the rest of my life.

I would also like to thank my friends and my family for all the support, love, and care that has nurtured, driven, and allowed me to reach my goals. My mother, Carol Clayton, and father, Helmuth Johnstone, and my siblings, Dylan and Lisa, have taught me how to live as an honest, hard-working man. I will always cherish their sacrifices that have helped me become who I am. I am forever indebted to my girlfriend, Brittany Duncan, and her family for all their motivation and love that has helped me through the toughest of times and celebrated with me in the light of my successes. Last, but not least, I would like to thank all of my friends who have stuck with me to see me through everything. Thank you all.

Background

The binary transition metal halides are compounds with the stoichiometry MX_n , where M is a transition metal, X a halogen (F, Cl, Br, I), and n can vary from 1 to 7 [1, 2]. Because of its radioactivity and short-half life (longest lived isotope: ^{210}At , $t_{1/2} = 8.1$ hr), astatine can be negated when considering this class of compounds [3]. There are over 200 binary halides that are known for the transition metals. These compounds exhibit interesting structural and physicochemical properties, and they play a major role in synthetic and industrial applications as well. For example, transition metal halides have been demonstrated as useful catalysts for laboratory to industrial scale productions; PdCl_2 has been employed in reactions for oxidizing olefins to aldehydes or ketones and esterifications. An assortment of 2nd and 3rd row transition metal chlorides, i.e., WCl_6 , MCl_5 (M = Nb, Ta, Mo, Re, W), MCl_4 (M = Zr, Hf), MCl_3 (M = Mo, Re, Ru, Os, Rh), and MCl_2 (M = Pd, Pt), have been classified on activity and selectivity for the addition of a silyl enol ether to aldehyde and/or aldimine functional groups. High valent Group V and VI metals, i.e., WCl_6 and MCl_5 (M = Mo, Nb, Ta) were shown to catalytically cleave C-O bonds in ethers [1, 4, 5, 6, 7]. Binary halides have also been integrated for use in photographic films and emulsions. The physical properties of transition metal halides can be used for chemical vapor deposition, separations, and purification. Transition metal halides are ideal precursors in inorganic and organometallic synthetic chemistry. They can be converted to other binary compounds [1, 8] and organometallic compounds, such as the complexes $\text{Cl}_3\text{Mo}(\mu\text{-CH}_2)_2\text{MoCl}_3$ and $\text{Cl}_2(\text{RO})_2\text{W}(\mu\text{-O})_2\text{W}(\text{OR})_2\text{Cl}_2$ (R = Et, *n*-Pr) used in Kauffmann olefinations. These complexes are capable of converting aldehydes and ketones to olefins [9] or other d^0 organoimido complexes [10].

Binary transition metal halides can be prepared by different synthetic routes: reaction of the elements, reaction of a molecular dimer and flowing HX(g), halide exchange, metallothermic reduction of higher halides, thermal disproportionation or decomposition of higher halides [2]. Binary transition metal halides form a diverse array of crystal structures from infinite chains and layers to molecular clusters shown in Table 1. Molecular structures are typically found for metal atoms in hexavalent and pentavalent states, which include: monomeric octahedron [11, 12], bioctahedral dimers, [13, 14], trimeric units [12], and tetrameric units [1, 12, 15, 16]. Infinite chain structures include repetitious units of MX_6 octahedra. These units can be classified by the bridging interactions of the halide atoms, metal-metal interactions between each unit, and the resulting degree of deformation of the MX_6 octahedra. Included in these structures are infinite repeating units of either corner-sharing [17, 18], edge-sharing [19, 20], or face-sharing [21] MX_6 octahedral subunits [1, 2, 22]. Similar to extended-chain structures, infinite-layered structures are also formed from repetitious subunits linked together as infinite sheets [23, 24, 25]. Within both infinite chain and sheet structures, metal-metal interactions often occur [22]. Additionally, there is an abundance of metal halide cluster structures that have been identified [26, 27, 28]. Trinuclear clusters exist as linked subunits that form bidimensional layers. Binary halides containing hexanuclear clusters are commonly found and form tridimensional networks [29, 30, 31].

Table 1. Types of crystal structure arrangements observed for binary transition metal halides and examples of each.

Molecular				Infinite Chain			Layered	Cluster	
Monomeric	Dimeric	Trimeric	Tetrameric	Corner-sharing	Edge-sharing	Face-sharing		Trinuclear	Hexanuclear
MF ₆ , M = Mo, W, Tc, Re, Ru, Os, Ir, Pt	M ₂ Cl ₁₀ , M = Nb, Ta, Mo, W, Re	((RuF ₅) ₃)	((MF ₅) ₄), M = Nb, Ta, Mo, Ru, Os	MF ₅ , M = Tc, Re	MCl ₄ , M = Zr, Hf, Nb, Ta, Mo, W, Tc, Os, Pt; MBr ₄ , M = Tc, Os, Pt	MBr ₃ , M = Mo, Ru; MI ₃ , M = Zr, Hf, Nb, Mo, Ru, Os	α-MCl ₃ M = Mo, Ru; β-MoCl ₄	Re ₃ X ₉ , M ₃ X ₈ , M = Nb, Ta	M ₆ X ₁₂ , M = Mo, W; M ₆ X ₁₄ , M = Nb, Ta; M ₆ X ₁₅ , M = Nb, Ta

One element whose binary halide chemistry has been significantly undeveloped is technetium (Tc, Z = 43), the lightest radioelement. Due to the late discovery of Tc and its radioactive nature, Tc halide chemistry is still drastically behind those of its neighboring 2nd and 3rd row elements. For Tc, there are only five known binary halide compounds, dramatically less than heavier congener, Re (Table 2). The first binary Tc halides synthesized were TcF₆, TcF₅, and TcCl₄, followed by the additions of the first Tc bromides, TcBr₃ and TcBr₄. Notably, only one chloride phase has been identified, and no binary Tc halides in oxidation states lower than +IV or binary Tc iodides have been reported. Considering this, it is of interest to investigate the binary Tc halides and determine what new phases may exist and how their chemistry will compare with the surrounding elements [32].

Table 2. Binary Tc (bold) reported in 2009 and Re halides [1, 2]

Oxidation State	Fluorides		Chlorides		Bromides		Iodides	
	Tc	Re	Tc	Re	Tc	Re	Tc	Re
I	-	-	-	-	-	-	-	ReI
II	-	-	-	-	-	-	-	ReI ₂
III	-	-	-	ReCl ₃	TcBr₃	ReBr ₃	-	ReI ₃
IV	-	ReF ₄	TcCl₄	ReCl ₄	TcBr₄	ReBr ₄	-	ReI ₄
V	TcF₅	ReF ₅	-	ReCl ₅	-	ReBr ₅	-	-
VI	TcF₆	ReF ₆	-	ReCl ₆	-	-	-	-
VII		ReF ₇	-	-	-	-	-	-

The objective of this thesis is to study binary Tc halides related to fundamental chemistry and nuclear fuel cycle applications. For fundamental chemistry, understanding the chemical behavior of Tc compared to its surrounding elements will better elucidate the periodicity within the transition metals. For nuclear fuel cycle applications, Tc binary halides could potentially prove useful for separations, i.e., halide volatility, and the development of a robust waste form material.

The goal of the dissertation research is the synthesis and characterization of binary Tc chlorides, bromides, and iodides. This manuscript is composed of five chapters. The binary Tc phases investigated in this study are presented in three chapters (Chapter 3, 4 and 5), each of these chapter focuses on a single oxidation state. In Chapter 1, the fundamental and applied chemistry of Tc is reviewed. The binary halide chemistry of Tc is presented in details. Chapter 2 provides detailed information on the experimental methods, materials, and instrumentation used for the preparation and characterization of binary Tc halides.

Chapter 3 focuses on tetravalent binary halides and includes the reinvestigation of the chemistries of TcCl_4 and TcBr_4 . For TcCl_4 , its synthesis has been revisited, its crystallographic structure redetermined and its magnetic properties measured. The synthetic and coordination chemistry of TcCl_4 are discussed and compared to other transition metal tetrachlorides. The thermal properties of TcBr_4 were studied and the new $\text{Na}\{[\text{Tc}_6\text{Br}_{12}]_2\text{Br}\}$ salt obtained from the decomposition of TcBr_4 .

Chapter 4 focuses on the trivalent halides and three new binary Tc halides phases are reported: $\alpha\text{-TcCl}_3$, $\beta\text{-TcCl}_3$, and TcI_3 . The solid-state structure and thermal properties of these trihalides were investigated. For the trichlorides, their electronic structure and

transport properties were investigated by theoretical methods. For TcBr_3 , its thermal properties have been investigated and a new method for its preparation reported. The chemistries of the trivalent Tc halides are compared with those of surrounding elements.

Chapter 5 focuses on divalent binary Tc halides and two new phases (i.e., $\alpha\text{-TcCl}_2$ and $\beta\text{-TcCl}_2$) are reported. The crystallographic structure of these phases has been determined and both dichlorides exhibit new structure-types. Physical and thermal properties of $\beta\text{-TcCl}_2$ were investigated. Theoretical calculations were used to understand the electronic structure as well as the physical properties of these compounds. The chemistries of the dichlorides are compared with those of surrounding elements.

The conclusion summarizes the most important findings on the synthetic and coordination chemistry, as well as on the thermo-chemistry of binary Tc halides. Finally, the potential applications of Tc binary halides are discussed.

TABLE OF CONTENTS

ABSTRACT.....	iii
Acknowledgements.....	v
Background.....	vi
Table of Contents.....	xii
List of Tables.....	xvi
List of Figures.....	xviii
Chapter 1: Introduction to Technetium Chemistry.....	1
1.1 Technetium Background.....	1
1.2 Technetium Coordination Chemistry.....	4
1.3 Technetium Multiple Metal-Metal Bond Chemistry.....	13
1.4 Binary Technetium Halide Chemistry.....	19
1.4.1 Binary Technetium Fluorides.....	19
1.4.2 Binary Technetium Chlorides.....	21
1.4.3 Binary Technetium Bromides.....	23
1.5 Conclusion.....	25
Chapter 2: Experimental Methods and Materials.....	27
2.1 Reagents and Materials.....	27
2.2 Preparation of Starting Materials.....	28
2.2.1 Purification of Ammonium Pertechnetate.....	29
2.2.2 Technetium Metal.....	30
2.2.3 Preparation of Bis(μ -tetraacetate)dichloride Ditechnetate.....	32
2.3 Experimental Procedures.....	36
2.3.1 Sealed Tube Reactions between the Elements.....	36
2.3.2 Reactions between $Tc_2(O_2CCH_3)_4Cl_2$ under Flowing $HX(g)$	40
2.3.3 Sealed Tube Vacuum Decomposition.....	42
2.4 Instrumentation.....	44
Chapter 3: Technetium Tetrachloride and Tetrabromide.....	51
3.1 Technetium Tetrachloride.....	51
3.1.1 Introduction.....	51

3.1.2 Experimental Details.....	52
3.1.3 Results and Discussion	54
3.1.3.1 Synthesis of TcCl_4	54
3.1.3.2 Characterization of TcCl_4	55
3.1.3.3 Physical Properties of TcCl_4	62
3.1.3.4 Thermal Behavior of TcCl_4	63
3.1.3.5 Comparison of TcCl_4 with Other MCl_4 Systems	65
3.1.4 Summary	68
3.2 Technetium Tetrabromide.....	69
3.2.1 Introduction.....	69
3.2.2 Experimental Details.....	70
3.2.3 Results and Discussion	71
3.2.3.1 Thermal Behavior of TcBr_4	71
3.2.3.2 Characterization of $\text{Na}\{[\text{Tc}_6\text{Br}_{12}]_2\text{Br}\}$	74
3.2.4 Summary	80
3.3 Conclusion	81
Chapter 4: Technetium Trichlorides, Tribromide, and Triiodide	83
4.1 Technetium Trichlorides: α - TcCl_3 and β - TcCl_3	83
4.1.1 Introduction.....	83
4.1.2 Alpha-Technetium Trichloride	85
4.1.2.1 Experimental Details.....	85
4.1.2.2. Results and Discussion	86
4.1.2.2.a Synthesis of α - TcCl_3	86
4.1.2.2.b Characterization of α - TcCl_3	87
4.1.2.2.c Thermal Properties of α - TcCl_3	93
4.1.2.2.d Computational Studies on α - TcCl_3	94
4.1.3 Beta-Technetium Trichloride.....	96
4.1.3.1 Experimental Details.....	96
4.1.3.2 Results and Discussion	97
4.1.3.2.a Synthesis of β - TcCl_3	97
4.1.3.2.b Characterization of β - TcCl_3	98

4.1.3.2.c Thermal Behavior of β -TcCl ₃	102
4.1.3.2.d Computational Studies on β -TcCl ₃	103
4.1.4 Summary	105
4.2 Technetium Tribromide	106
4.2.1 Introduction.....	106
4.2.2 Experimental Details.....	108
4.2.3 Results and Discussion	110
4.2.3.1 Synthesis of TcBr ₃	110
4.2.3.2 Characterization of TcBr ₃	111
4.2.3.3 Thermal Behavior of TcBr ₃	114
4.2.4 Summary	118
4.3 Technetium Triiodide.....	119
4.3.1 Introduction.....	119
4.3.2 Experimental Details.....	120
4.3.3 Results and Discussion	122
4.3.3.1 Synthesis of TcI ₃	122
4.3.3.2 Characterization of TcI ₃	122
4.3.3.3 Thermal Behavior of TcI ₃	132
4.3.3.4 Comparison of TcI ₃ with Other MI ₃ Systems	133
4.3.4 Summary	137
4.4 Conclusion	137
Chapter 5: Technetium Dichlorides	140
5.1 Technetium Dichlorides α -TcCl ₂ and β -TcCl ₂	140
5.1.1 Introduction.....	140
5.1.2 Experimental Details.....	141
5.1.3 Results and Discussion	142
5.1.3.1 Preparation of β -TcCl ₂	142
5.1.3.2 Characterization of β -TcCl ₂	143
5.1.3.3 Characterization of α -TcCl ₂	151
5.1.3.4 Physical Properties of β -TcCl ₂	152
5.1.3.5 Thermal Behavior of β -TcCl ₂	155

5.1.3.6 Computational Studies on α -TcCl ₂ and β -TcCl ₂	156
5.1.3.7 Comparison of α/β -TcCl ₂ with Other Transition Metal Dichlorides	157
5.1.4 Conclusion	164
Conclusion	166
Appendix I	174
Appendix II	185
Bibliography	189
Curriculum Vitae	204

LIST OF TABLES

Table 1. Types of crystal structure arrangements observed for binary transition metal halides and examples of each.....	viii
Table 2. Binary Mo, Tc (bold) reported in 2009, Re, and Ru halides [1, 2].....	ix
Table 3. Common isotopes of Tc and their atomic and nuclear properties [32].....	2
Table 1.1. Tc(V)-cores and characteristic complexes formed for each [32].	7
Table 1.2. Multiple Tc-Tc Bonds in Tc_2^{n+} dimers and Characteristic Electron Configurations.....	14
Table 1.3. Hexanuclear Trigonal Prismatic Tc Clusters and Tc-Tc Distances.....	18
Table 2.1 Gases used for experiments.	28
Table 3.1. Structural parameters obtained by adjustment of the k^3 -EXAFS spectra of $TcCl_4$. Adjustment between $k = [2-14] \text{ \AA}^{-1}$. ΔE_0 (eV) = 1.79 eV. The values found by SCXRD in $TcCl_4$ are in italics [125]. MS stands for multi-scattering.....	61
Table 3.2. Structure-types and Metal–Metal Separations in Transition-Metal Tetrachlorides. ^a Not reported. ^b Characterized by powder XRD and interatomic distances not reported.	67
Table 3.3. Summary of Transition-Metal Tetrachloride Decompositions.....	68
Table 3.4. Selected Bond Distances (\AA) in the Tc_6Br_{12} Cluster in $Na\{[Tc_6Br_{12}]_2Br\}^a$ and $(Et_4N)_2\{[Tc_6Br_{12}]Br_2\}^b$ (Experimental Values in Bold and Calculated Values in Italics). ^a Represents an average value. ^b Reference 154.	78
Table 4.1. Structural parameters obtained by adjustment of k^3 -EXAFS spectra of α - $TcCl_3$ obtained from the reaction of $Tc_2(O_2CCH_3)_4Cl_2$ with $HCl(g)$ at 300 °C. Adjustment between $k = 2.5$ and 14 \AA^{-1} considering the structure of α - $TcCl_3$. ΔE_0 (eV) = 2.29 eV. Reduced $\chi^2 = 70$. Values found by SCXRD in α - $TcCl_3$ are in italic.....	93
Table 4.2. M-M and M··M distances in α - MCl_3 (M = Mo, Ru) and β - $TcCl_3$	102
Table 4.3. Products obtained from the reaction of metal-metal bonded acetates with flowing $HX(g)$ (X = Cl, Br, I) at various temperatures. [a] Reaction occurs at 250 °C, [b] Reaction occurs at 340 °C, [c] NR: not reported	111
Table 4.4. Structural parameters obtained by adjustment of the k^3 -EXAFS spectra of the compound obtained from the reaction of $Tc_2(O_2CCH_3)_4Cl_2$ with $HI(g)$ at 150 °C. Adjustment between $k = [2 -14.5] \text{ \AA}^{-1}$ considering the structure of $TcBr_3$. ΔE_0 (eV) = -4.09 eV. Reduced- $\chi^2 = 80$	128
Table 4.5. 2θ (°) and corresponding d-spacing (\AA) derived from the powder XRD of TcI_3	130
Table 4.6. Reactions of 2 nd and 3 rd row transition metals of Group 6, 7, 8 with I_2 . [a] This work. [b] Not reported.	134
Table 5.1. Chemical shifts (eV) of the technetium K-edge relative to NH_4TcO_4 measured for: (<i>n</i> -Bu ₄ N) $TcNCl_4$, (<i>n</i> -Bu ₄ N) $TcOCl_4$, $(Me_4N)_2TcCl_6$, (<i>n</i> -Bu ₄ N) $_2Tc_2Cl_8$, $Tc_2Cl_4(PMe_2Ph)_4$ ¹⁰⁴ and β - $TcCl_2$	149
Table 5.2. Structural parameters obtained by adjustment of the k^3 -EXAFS spectra of β - $TcCl_2$. The adjustment was performed between $k = 2.5 - 14 \text{ \AA}^{-1}$. $\Delta E_0 = 1.82$ eV. $S_0^2 = 0.9$	151
Table 5.3. Average bond distances (Figure 5.6) found by SCXRD, EXAFS [205], and DFT in β - $TcCl_2$ and found by SCXRD for α - $TcCl_2$ (Figure 5.10) [143] ^a . ^a	

Estimated standard deviations are in parentheses.^b SCXRD measurements were performed at 100 K for β -TcCl₂ and 140 K for α -TcCl₂.^c No perpendicular units are present in α -TcCl₂. 156

Table 5.4. Second and third row transition metal MCl₂ phases (M = Hf, Zr, Mo, W, Tc, Pd, and Pt) and their method of synthesis. ^a X-ray structure not reported 160

Table 5.5. Shortest metal-metal separation (M-M in Å) in second and third row transition metal dichlorides 164

LIST OF FIGURES

Figure 1.1. Decay scheme of the A = 99 isobar from ^{99}Mo to ^{99}Ru .	2
Figure 1.2. Characteristic UV-Vis spectrum of TcO_4^- in H_2O .	5
Figure 1.3. Ball-and-stick representation of the TcO_4^- anion. Tc atoms in black and O atoms in blue.	6
Figure 1.4. Ball-and-stick representation of the TcOCl_4^- anion in $(\text{Bu}_4\text{N})\text{TcOCl}_4$. Tc atom in black, O atom in blue, and Cl atoms in red.	8
Figure 1.5. Characteristic UV-Vis spectrum of TcOCl_4^- in 0 °C HCl.	8
Figure 1.6. Characteristic UV-Vis spectrum of TcCl_6^{2-} in HCl.	9
Figure 1.7. Ball-and-stick representation of the <i>hcp</i> structure of Tc metal displaying the packing of atoms down the <i>c</i> axis. Tc atoms in black.	13
Figure 1.8. Molecular orbitals involved in the quadruple bond.	14
Figure 1.9. Ball-and-stick representation of quadruply bonded Tc dimers: $\text{Tc}_2\text{Cl}_8^{2-}$ anion (left) and $\text{Tc}_2(\text{O}_2\text{CCH}_3)_4\text{Cl}_2$ (right). Tc atoms in black, Cl atoms in red, O atoms in blue, C atoms in grey, and H atoms in pink.	16
Figure 1.10. Ball-and-stick representations of the hexa- (left) and octanuclear (right) cluster cores containing multiple metal-metal bonding. Tc atoms in black, Cl atoms in red, and Br atoms in orange.	17
Figure 1.11. Ball-and-stick representation of two Tc_2Cl_8 units within a chain of $\text{K}_2\text{Tc}_2\text{Cl}_6$. Tc atoms in black and Cl atoms in red.	18
Figure 1.12. Ball-and-stick representation of the structures of binary technetium fluorides: TcF_6 (left) and TcF_5 (right). Tc atoms in black and F atoms in green.	21
Figure 1.13. Ball-and-stick representation of the binary technetium chloride, TcCl_4 . Tc atoms in black and Cl atoms in red.	23
Figure 1.14. Ball-and-stick representations of the structures of binary technetium bromides: TcBr_4 (left) and TcBr_3 (right). Tc atoms in black and Br atoms in orange.	25
Figure 2.1. Purification of NH_4TcO_4 starting with the impure material from ORNL (left) to purified NH_4TcO_4 (right).	30
Figure 2.2. Technetium metal obtained after the decomposition of NH_4TcO_4 under $\text{H}_2(\text{g})$ at 750 °C.	32
Figure 2.3. A: $(n\text{-Bu}_4\text{N})\text{TcO}_4$ after drying at 90 °C. B and C, respectively: $(n\text{-Bu}_4\text{N})\text{TcOCl}_4$ and $(n\text{-Bu}_4\text{N})_2\text{Tc}_2\text{Cl}_8$ after recrystallization with acetone:diethyl ether. D: $\text{Tc}_2(\text{O}_2\text{CCH}_3)_4\text{Cl}_2$ after diethyl ether washes.	36
Figure 2.4. Experimental setup used to prepare sealed tubes: a) Schlenk line; b) connection from inlet gas (i.e., Ar or Cl_2); c) connection to vacuum pump; d) stopcock-controlled port; e) Teflon tubing; f) Pyrex or quartz reaction tube; g) liquid nitrogen dewar; h) solid sample.	39
Figure 2.5. Flame-sealed Pyrex tubes of technetium metal with elemental chlorine (top), bromine (middle) and iodine (bottom) prior to reacting.	39
Figure 2.6. Experimental apparatus for flowing gas reactions using HCl gas: a) connection from inlet gas; b) Teflon-jointed glass connector; c) clamshell furnace; d) quartz tube; e) connection to bubbler filled with H_2SO_4 .	41
Figure 2.7. Experimental apparatus for flowing gas reactions using HX gas (X = Br, I): a) connection from Ar(g); b) connection from HX(g) (X = Br or I); c) T-shaped	

stopcock; d) Teflon-jointed glass connector; e) quartz tube; f) clamshell furnace; g) connection to bubbler filled with H ₂ SO ₄	42
Figure 2.8. Sealing a Pyrex tube under vacuum on a high vacuum Schlenk line.....	43
Figure 2.9. Vacuum sealed tube containing a binary technetium before (left) and after (right) thermal decomposition.....	43
Figure 2.10. Flowchart of experimental characterizations and the instrumentations used in the studies of binary technetium halides.....	44
Figure 3.1. EDX spectrum of a TcCl ₄ crystal displaying Tc-K _α , Tc-L _α , and the Cl-K _α lines. The Cu and Fe peaks are due to the sample holder. O ₁ (red) indicates the selected area measured on the crystal.....	55
Figure 3.2. SEM images of the TcCl ₄ powder: (A) x200; (B) x1000.....	56
Figure 3.3. Experimental PXRD pattern (blue) of TcCl ₄ with a Le Bail fit (red) confirming the <i>Pbca</i> space group. The difference between the experimental and fitted pattern is shown in grey (R-Bragg = 0.218).....	57
Figure 3.4. Ball-and-stick representation of TcCl ₄ . Two edge-sharing octahedra and a portion of a third octahedron are represented. Distances are in Å and angles in degrees.....	58
Figure 3.5. Ball-and-stick representation of the TcCl ₄ cluster used for the EXAFS calculations.....	59
Figure 3.6. Adjustment of experimental k ³ -EXAFS spectra (bottom) and Fourier transform of k ³ -EXAFS spectra (top) of TcCl ₄ . Adjustment performed between k = [2-14] Å ⁻¹	60
Figure 3.7. Normalized Tc K-edge XANES spectrum of TcCl ₄	61
Figure 3.8. Magnetic susceptibility as a function of temperature of TcCl ₄ . Measurement performed between 10 K and 300 K on TcCl ₄ (34.1 mg) in a 0.1 T magnetic field. The black line represents the experiment data. The red line represents the fit $\chi =$ $f(T)$ of χ vs. (T) above 50 K.....	63
Figure 3.9. SEM images of the powder (A, x200) and crystals (B, x100) obtained after decomposition of TcCl ₄ at 450 °C under vacuum for 14 h.....	64
Figure 3.10. SEM images of the surface of a TcCl ₄ crystal (A, x500; B, x4000) obtained after decomposition of TcCl ₄ at 450 °C under vacuum for 2 h.....	65
Figure 3.11. Ball-and-stick representations of second- and third-row transition-metal tetrachloride structure-types: (A) Zr, Hf, Tc, and Pt; (B) Os; (C) β-Mo; (D) Nb, Ta, α-Mo, and W; (E) β-Re. The metal atoms are in black, and the Cl atoms are in red.....	66
Figure 3.12. Left: Optical microscopy image of a single rail spike crystal of Na{[Tc ₆ Br ₁₂] ₂ Br}. Right: Scanning electron microscopy (SEM) image of a single rail spike crystal of Na{[Tc ₆ Br ₁₂] ₂ Br} at x500 magnification.....	72
Figure 3.13. XRD powder pattern of product (blue) obtained after decomposition of TcBr ₄ in Pyrex. The refinement (red) shows the presence of Tc metal (P63/mmc; $a = 2.742(1)$ Å and $b = 4.398(1)$ Å) and TcBr ₃ (Pmmn; $a = 11.206(1)$ Å, $b =$ $6.018(1)$ Å, and $c = 6.4777(1)$ Å). The difference between the experimental and fitted pattern is shown in green.....	73
Figure 3.14. XRD powder pattern of product (blue) obtained after decomposition of TcBr ₄ in quartz. The fit (red) shows the presence of Tc metal (P63/mmc; $a =$	

	2.743(1) Å and $c = 4.400(1)$ Å). The difference between the experimental and fitted pattern is shown in green.	74
Figure 3.15.	EDX measurement of Na{[Tc ₆ Br ₁₂] ₂ Br} crystal displaying Na-K _α , Tc-K _α , Tc-L _α , and the Br-K _α lines. The Cu peaks are due to the sample holder. O ₁ (red) indicates the selected area measured on the crystal.	75
Figure 3.16.	Ball-and-stick representation of the Tc ₆ Br ₁₂ cluster in Na{[Tc ₆ Br ₁₂] ₂ Br}. Tc atoms are in black and Br atoms in orange. Selected distances (Å): Tc _{A1} -Tc _{A2} 2.687(9), Tc _{A2} -Tc _{A3} 2.667(6), Tc _{A3} -Tc _{A1} 2.673(5), Tc _{A1} -Tc _{B1} 2.165(1), Tc _{A2} -Tc _{B2} 2.177(9), Tc _{A3} -Tc _{B3} 2.177(5).	77
Figure 3.17.	Ball-and-stick representation of two Tc ₆ Br ₁₂ clusters joined by a capping bromine in Na{[Tc ₆ Br ₁₂] ₂ Br}. Tc atoms in black, bromine atoms in orange.	78
Figure 3.18.	The Natural Bond Order (NBO) occupancy of the Tc-Tc bonds in Tc ₆ Br ₁₂	80
Figure 4.1.	Ball-and-stick representations of the structures exhibited by a) ReCl ₃ and b) α-MCl ₃ (M = Mo, Ru). Metal atoms are in black, chlorine atoms are in red.	84
Figure 4.2.	Top: Mechanism of formation of α-TcCl ₃ from Tc ₂ (O ₂ CCH ₃) ₄ Cl ₂ . Bottom: Ball and stick representation of A) Tc ₂ (O ₂ CCH ₃) ₄ Cl ₂ and B) Tc ₂ (O ₂ CCH ₃) ₂ Cl ₄ . Color of atoms: Tc in black, Cl in red, O in red, and C in grey. Selected distances(Å) in Tc ₂ (O ₂ CCH ₃) ₂ Cl ₄ : Tc-Tc 2.150(1), Tc-O 2.021(2), Tc-Cl _a 2.290(1), Tc-Cl _b 2.334(1).	87
Figure 4.3.	IR spectrum of α-TcCl ₃ (black) and Tc ₂ (O ₂ CCH ₃) ₄ Cl ₂ (red).	88
Figure 4.4.	Left: Ball-and-stick representation of the Tc ₃ Cl ₉ cluster in α-TcCl ₃ . Portions of the three neighboring clusters are also presented. Angles (°) and distances (Å) are shown. Right: SEM Image (x1000) of a single crystal of α-TcCl ₃	90
Figure 4.5.	Structural view of α-TcCl ₃ from the <i>c</i> -axis.	90
Figure 4.6.	Ball-and-stick representations of the α-TcCl ₃ (left) and β-TcCl ₃ (right) clusters used for EXAFS calculations. Tc and Cl atoms are in black and red, respectively. Tc0 represents the absorbing atom.	91
Figure 4.7.	Fits of the <i>k</i> ³ -EXAFS spectra (top) and Fourier transform of <i>k</i> ³ -EXAFS spectra (bottom) for α-TcCl ₃ obtained from the reaction of Tc ₂ (O ₂ CCH ₃) ₄ Cl ₂ with HCl(g) at 300 °C. Adjustment was performed between <i>k</i> = 2.5 and 14 Å ⁻¹ considering the structure of α-TcCl ₃ . Experimental data are in blue, and the fit is in black.	92
Figure 4.8.	PXRD pattern of the product obtained from the thermal decomposition of α-TcCl ₃ under vacuum at 450 °C (black). PXRD of TcCl ₂ single crystals (red).	94
Figure 4.9.	Ball-and-stick representation of the calculated structure of Tc trichloride with the ReCl ₃ structure (<i>R</i> $\bar{3}m$). Tc atoms are in black, Cl atoms are in red.	96
Figure 4.10.	PXRD pattern (black) of the dark hygroscopic product obtained at the cold end of the sealed tube after the reaction of Tc metal and chlorine gas at 450 °C. Simulated positions presented of the most intense peaks for: TcCl ₄ (red), TcCl ₂ (black), α-TcCl ₃ (green), and β-TcCl ₃ (blue).	98
Figure 4.11.	EDX spectrum of β-TcCl ₃ displaying the Tc-K _α , Tc-L _α , and the Cl-K _α lines. The Cu line is due to the sample holder. SEM image of a layered hexagonal β-TcCl ₃ crystal (x1000).	99

Figure 4.12. Ball-and-stick representation of a β -TcCl ₃ layer. View perpendicular to the <i>ab</i> plane (top) and in the <i>a</i> direction (bottom). Tc and Cl atoms are in black and red, respectively.	101
Figure 4.13. Ball-and-stick representation of the edge-sharing octahedra in β -TcCl ₃ . The Cl and Tc atoms are red and black, respectively. Selected distances (Å) and angles (°): Distances: Tc _a -Tc _b 2.861(3), Tc _a -Tc' 3.601(2), Tc _a -Cl1 _(a,b) 2.316(3), Tc _a -Cl2 _(a,b) 2.434(3), Tc _a -Cl2 _(c,d) 2.403(2), Cl1 _a -Cl1 _b 3.642(4). Angles: Tc _b -Tc _a -Cl2 _(c,d) 95.13(6), Cl1 _a -Tc _a -Cl1 _b 103.71(12), Cl2 _a -Tc _a -Cl2 _b 85.50(8), Cl2 _c -Tc _a -Cl1 _a 94.07(10), Cl2 _c -Tc _a -Cl1 _b 92.25(10), Cl2 _c -Tc _a -Cl2 _a 88.69(8), Cl2 _c -Tc _a -Cl2 _b 83.78(9).....	102
Figure 4.14. Total and partial DOSs per formula unit of (a) β -TcCl ₃ and (b) α -TcCl ₃ . Orbital-projected DOSs are represented for Tc 4d and Cl 2p orbitals. Positive and negative values of the DOS correspond to spin-up and spin-down contributions.	105
Figure 4.15. Ball-and-stick representation of the structure of MBr ₃ (M = Mo, Tc, Ru). Metals atoms are in black and Br atoms are in orange.	108
Figure 4.16. IR spectra of Tc ₂ (O ₂ CCH ₃) ₄ Cl ₂ (burgundy) and the products obtained from reactions of Tc ₂ (O ₂ CCH ₃) ₄ Cl ₂ and HBr(g) at 150 °C (blue) and 300 °C (black).	112
Figure 4.17. EDX spectrum of TcBr ₃ displaying Tc-L α , and Br-L α lines; area of TcBr ₃ analyzed (top right).	113
Figure 4.18. PXRD pattern of the products obtained from the reaction of Tc ₂ (O ₂ CCH ₃) ₄ Cl ₂ with HBr(g) at 150 °C (green) and 300 °C (blue) and the calculated (red) pattern of TcBr ₃ . The amorphous “hump” from 2 θ = 20 to 30° is due to a radiological containment dome.	114
Figure 4.19. Resulting tubes from the thermal decomposition of TcBr ₃ in a) Pyrex yielding rail spike crystals adjacent to the powder (black circle) and needle crystals at the end of the tube and in b) quartz with only sublimed needle-shaped crystals.	116
Figure 4.20. SEM image (x35) of TcBr ₃ single crystals as individual and clusters of needles ranging in size from 100 μ m to 2 mm.	117
Figure 4.21. PXRD pattern of the products obtained from the decomposition of TcBr ₃ in Pyrex at 450 °C (olive green) and calculated (red) pattern fit for TcBr ₃	117
Figure 4.22. PXRD pattern of the products obtained from the thermal decomposition of TcBr ₃ in quartz at 450 °C (blue) and calculated pattern (red) fit with TcBr ₃ and Tc metal.	118
Figure 4.23. IR spectra of Tc ₂ (O ₂ CCH ₃) ₄ Cl ₂ (burgundy) and the product obtained from reaction of Tc ₂ (O ₂ CCH ₃) ₄ Cl ₂ and HI(g) at 150 °C (purple).	123
Figure 4.24. Normalized Tc K-edge XANES spectra of Cs ₂ TcI ₆ (A in black) and TcI ₃ (B in blue).	124
Figure 4.25. Ball-and-stick representations of the clusters used for EXAFS calculations: (a) cluster with the ReI ₃ structure-type; (b) cluster with the TcBr ₃ structure-type. Tc and I atoms are in black and blue, respectively. Tc0 represents the absorbing atom.	125
Figure 4.26. Fits of the experimental k^3 -weighted EXAFS spectra (bottom) and Fourier transform of k^3 -weighted EXAFS spectra (top) for the compound obtained from	

the reaction of $\text{Tc}_2(\text{O}_2\text{CCH}_3)_4\text{Cl}_2$ with $\text{HI}(\text{g})$ at $150\text{ }^\circ\text{C}$. Adjustment was performed between $k = 2$ and 14.5 \AA^{-1} considering the structure of TcBr_3 . Experimental data are in blue, and the fits are in black.	126
Figure 4.27. Fits of the experimental k^3 - EXAFS spectra (bottom) and Fourier transform of k^3 -EXAFS spectra (top) for the compound obtained from the reaction of $\text{Tc}_2(\text{O}_2\text{CCH}_3)_4\text{Cl}_2$ with $\text{HI}(\text{g})$ at $150\text{ }^\circ\text{C}$. Adjustment performed between $k = [2 - 14.5]\text{ \AA}^{-1}$ considering the structure of ReI_3 . Reduced- $\chi^2 = 9195$. Experimental data are in blue and the fits are in black.....	127
Figure 4.28. PXRD pattern of products obtained from the reaction of $\text{Tc}_2(\text{O}_2\text{CCH}_3)_4\text{Cl}_2$ with $\text{HI}(\text{g})$ at $150\text{ }^\circ\text{C}$ (purple) and $300\text{ }^\circ\text{C}$ (orange) after sintering for 5 days at the respective temperatures.....	129
Figure 4.29. EDX spectrum of TcI_3 displaying Tc-L α and I-L α lines; secondary electron image (x500) of TcI_3 sampled shown at top right.....	130
Figure 4.30. SEM images of TcI_3 : (a) powder at x200 magnification; (b) individual pieces of powder at x500 magnification; (c) crystalline inclusion of TcI_3 at x5000 magnification.	131
Figure 4.31. PXRD pattern of the products obtained from the reaction of Tc metal and I_2 at $400\text{ }^\circ\text{C}$ for 2 weeks (black) and fit with Tc metal (red). Inset: comparison of the product (black) to TcI_3 from the reaction of $\text{Tc}_2(\text{O}_2\text{CCH}_3)_4\text{Cl}_2$ with $\text{HI}(\text{g})$ (purple).	132
Figure 4.32. PXRD pattern (purple) of the product obtained from the decomposition of TcI_3 under vacuum at $450\text{ }^\circ\text{C}$ in a gold envelope and the fit (red) with Tc metal.	133
Figure 4.33. Ball-and-stick representations of second- and third-row transition-metal triiodide structure-types for: (a) Zr, Hf, β -Nb, Mo, Tc, Ru, and Os; (b) Nb; (c) Re; (d) Rh and Ir; (e) Pt. Metal atoms are in black, and I atoms are in purple.	136
Figure 5.1. SEM image of the TcCl_2 /Tc metal powder obtained after the stoichiometric reaction of Tc metal with $\text{Cl}_2(\text{g})$ in sealed tubes at $450\text{ }^\circ\text{C}$	143
Figure 5.2. PXRD pattern (black open circles) of the powder obtained after reaction of Tc metal and Cl_2 at $450\text{ }^\circ\text{C}$ in a sealed tube. The fit against the experimental pattern is represented in a red solid line. Position of peaks of Tc metal and TcCl_2 is marked in green and blue lines, respectively.	144
Figure 5.3. SEM images of β - TcCl_2 needles (bottom left, x35; bottom right, x200) obtained after the stoichiometric reaction of Tc metal with $\text{Cl}_2(\text{g})$ in sealed tubes.	145
Figure 5.4. The EDX spectrum of β - TcCl_2 . Carbon and Cu peaks are due to the sample holder.	145
Figure 5.5. Ball-and-stick representation of the structure of β - TcCl_2 . (A) Single β - TcCl_2 chain. The orientation of the $\text{Tc}\equiv\text{Tc}$ bond changes every two Tc_2Cl_8 units within a single chain. (B) View along the c -axis of the $2 \times 2 \times 4$ supercell of β - TcCl_2 showing the packing of the chains. (C) View down the c -axis of a single β - TcCl_2 chain. Tc atoms are in black and chlorine atoms in red.....	147
Figure 5.6. Ball-and-stick representation of a portion of a β - TcCl_2 chain. Selected distances (\AA): Tc-Tc _a 2.136(3), Tc-Tc _b , 3.425(2), Tc-Tc _c 4.037(3), Tc-Tc _(d,e) 3.744(2). Tc atoms are in black and chlorine atoms are in red.	147
Figure 5.7. The XANES spectrum of β - TcCl_2	148

Figure 5.8. Chemical shift ΔE (eV) of the Tc-K edge relative to NH_4TcO_4 versus formal oxidation state for (a) $(n\text{-Bu}_4\text{N})\text{TcNCl}_4$, (b) $(n\text{-Bu}_4\text{N})\text{TcOCl}_4$, (c) $(\text{Me}_4\text{N})_2\text{TcCl}_6$, (d) $(n\text{-Bu}_4\text{N})_2\text{Tc}_2\text{Cl}_8$, (e) $\text{Tc}_2\text{Cl}_4(\text{PMe}_2\text{Ph})_4$, and (f) $\beta\text{-TcCl}_2$ (red dot).	149
Figure 5.9. Fitted experimental k^3 -EXAFS spectra (top) and Fourier transform of k^3 -EXAFS spectra (bottom) of $\beta\text{-TcCl}_2$. Adjustment between $k = 2.5\text{--}14 \text{ \AA}^{-1}$. Experimental data (blue) and fit (black).	150
Figure 5.10. Ball-and-stick representation of a portion of a $\beta\text{-TcCl}_2$ chain. Color of atoms: Tc in black and Cl in red. Selected distances (\AA): Tc-Tc _a 2.136(3), Tc-Tc _b 3.417(2), Tc-Tc _c 4.025(2).	152
Figure 5.11. (A) Molar magnetic susceptibility of the TcCl_2 powder as a function of temperature. (B) Diffuse reflectance spectrum of the TcCl_2 powder as a function of temperature. Fit of the absorption edge is in red. (C) Resistivity as a function of temperature of a $\beta\text{-TcCl}_2$ single crystal. Red solid line represents the Arrhenius fit with an activation energy of 0.17(2) eV. (D) Seebeck coefficient as a function of temperature of $\beta\text{-TcCl}_2$	154
Figure 5.12. PXRD pattern (blue) of the solid obtained after thermal treatment of $\beta\text{-TcCl}_2$ at 800 °C under vacuum in a sealed tube fit with a homogenous phase of Tc metal (red) and the difference (green).	155
Figure 5.13. Relaxed structures of $\alpha\text{-TcCl}_2$ and $\beta\text{-TcCl}_2$ chains calculated using spin-polarized density functional theory. The relative total energy difference per formula unit (f.u.), ΔE , is also reported. Tc atoms are in black and Cl atoms are in red.	157
Figure 5.14. Ball and stick representation of the structural motif in 2 nd and 3 rd transition metal dichlorides: (A) $\alpha\text{-TcCl}_2$; (B) $\beta\text{-TcCl}_2$; (C) $\beta\text{-MoCl}_2$; (D) $\alpha\text{-MoCl}_2$, WCl_2 ; (E) $\alpha\text{-PtCl}_2$, $\alpha\text{-PdCl}_2$, $\delta\text{-PdCl}_2$; (F) $\gamma\text{-PdCl}_2$; (G) $\beta\text{-PdCl}_2$, $\beta\text{-PtCl}_2$; (H) ZrCl_2 . Metal atoms are in black and Cl atoms are in red.	163
Figure 6.1. Ball-and-stick representations of the ten binary Tc halide phases.	167
Figure 6.2. Flowchart of the synthetic and thermo-chemistries of binary technetium chlorides.	169
Figure 6.3. Flowchart of the synthetic and thermo-chemistries of binary technetium bromides.	171
Figure 6.4. Flowchart summarizing the synthetic and thermo-chemistries of TcI_3	172

Chapter 1

Introduction to Technetium Chemistry

1.1 Technetium Background

Technetium is a Group VII second row transition metal located centrally on the periodic table. Technetium was first predicted by D. Mendeleev in 1869 and discovered by C. Perrier and E. Segrè in 1936 from an irradiated Mo foil at the Berkeley cyclotron run by E. O. Lawrence. Its name was given by C. Perrier and E. Segrè after the Greek word for “artificial,” “τεχνητόζ” [33]. Technetium is the lightest inherently radioactive element on the periodic table; its isotopes range from masses of $A = 86$ to 117. An empirical explanation of the radioactive nature of Tc is presented in Appendix I.

The most common occurring and longest-lived isotopes are ^{97}Tc , ^{98}Tc , and ^{99}Tc (Table 3). Whereas ^{97}Tc and ^{98}Tc are produced by bombardment reactions in a cyclotron, ^{99}Tc is found as a major fission product ($A = 99$ isobar, fission yield = 6.1 %) from the spent fuel in nuclear reactors, making it much more abundant than the other two long-lived isotopes. The isotope ^{99}Tc is a pure beta emitter ($E_{\text{max}} = 294$ keV) and decays into stable ^{99}Ru (Figure 1.1). The weak beta emission and low specific activity (629 kBq/mg) of ^{99}Tc allow for laboratory handling and storage using standard glass labware [32].

Table 3. Common isotopes of Tc and their atomic and nuclear properties [32].

Isotope	Atomic Mass (amu)	Spin and Parity [h/2π]	Half-life (t _{1/2})	Mode and Energy of Decay (keV)
⁹⁷ Tc	96.906364	9/2+	4.2 x 10 ⁶ y	ε
⁹⁸ Tc	97.907215	(6)+	4.2 x 10 ⁶ y	β ⁻ 397; γ 745, 652
⁹⁹ Tc	99.907657	9/2+	2.1 x 10 ⁵ y	β ⁻ 292, 203
^{99m} Tc	-	1/2-	6.006 h	IT 140, 143; β ⁻ ; e ⁻ ; γ 322, 233

The isotope ^{99m}Tc is primarily a low-energy gamma emitter (Table 3) that has found wide application in the radiopharmaceutical industry and is used in over 30 million nuclear diagnostic imaging procedures a year. The isotope ^{99m}Tc can be produced from the fission of nuclear fuel or irradiation of natural Mo or enriched ⁹⁸Mo with thermal neutrons in a nuclear reactor (Figure 1.1). After irradiation, ^{99m}Tc is eluted-off as pertechnetate (^{99m}TcO₄⁻) in isotope generators that separate the Tc from its parent nuclide (⁹⁹Mo, t_{1/2} = 67 h). These ^{99m}TcO₄⁻ solutions undergo “one-pot” reactions with a specific ligand, and reducing agent to quickly form low-valent complexes ready for injection. Many Tc core compounds have been synthesized in various oxidation states (Tc(V), Tc(III) and Tc(I)). Ligands have been developed as site specific agents [32, 34].

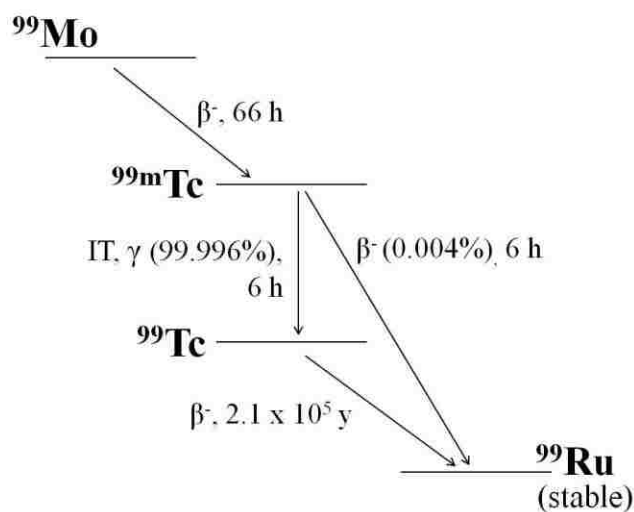


Figure 1.1. Decay scheme of the A = 99 isobar from ⁹⁹Mo to ⁹⁹Ru.

In the nuclear fuel cycle, ^{99}Tc is a major fission product formed from actinides. It is also generated from the fission of ^{232}Th , ^{233}U , ^{238}U , and ^{239}Pu . Other Tc isotopes with masses of 100 or greater produced in nuclear reactors have half-lives less than 20 min and decay during storage of the fuel in spent fuel pools; the formation of ^{97}Tc and ^{98}Tc from the fission of actinide fuels by thermal neutron is considered negligible [35]. In the spent nuclear fuel, Tc is present in the elemental form as the metal or as alloys with Mo, Ru, Rh, and Pd (i.e., epsilon-phases) [36].

The PUREX (Plutonium Uranium Recovery by Extraction) process is employed to treat spent fuel [37]. In the PUREX process, the fuel rods without cladding are initially dissolved into hot nitric acid. Technetium metal in the fuel is then oxidized to pertechnetate while the epsilon-phases remain at the bottom of the dissolution tank [32]. Technetium is extracted as $\text{HTcO}_4 \cdot 3\text{TBP}$ into an organic phase (30 vol.% *n*-dodecane with 70 vol.% tributyl phosphate (TBP)). In the presence of uranyl nitrate (i.e., $\text{UO}_2(\text{NO}_3)_2$) and TBP, Tc extraction is increased due to formation of $\text{UO}_2(\text{NO}_3)(\text{TcO}_4) \cdot 2\text{TBP}$. After back-extraction into nitric acid, Tc is vitrified with the high-level waste. In the UREX process after extraction of Tc(VII) and U(VI) into the organic phase, Tc would be separated from U using an anion exchange resin [38]. Note: there is no plan to develop UREX as a process. After separation, Tc would be incorporated in a robust waste form for geological disposal [39]. Ongoing research has focused on the development of new waste form materials for Tc as ceramics, alloys, and glass.

1.2 Technetium Coordination Chemistry

The ground state electronic configuration of Tc is $[\text{Kr}]4d^55s^2$. The half-filled 4d shell allows for nine oxidation states: from -I to +VII. In comparison to its neighboring Group VII elements, Tc chemistry resembles that of its heavier congener Re than of the lighter Mn [32]. Technetium coordination chemistry is extensive, forming a range of binary compounds to large inorganic and organometallic coordination complexes. The oxidation states of Tc can be classified into 3 categories: high-valent (Tc(VII), Tc(VI) and Tc(V)), mid-valent (Tc(IV) and Tc(III)), and low valent (Tc(II), Tc(I), Tc(0) and Tc(-I)). In the following, an overview of the model complexes for each category will be presented.

High-Valent: Tc(VII), Tc(VI), Tc(V)

The highest oxidation state achievable for Tc is +VII. In this oxidation state, oxide (e.g., Tc_2O_7), oxyhalides (e.g., TcO_3X , X = F, Cl, Br, I), oxo-salts (e.g., MTcO_4 , M = Li, Na, K, Cs), and coordination complexes with the $(\text{TcO}_3)^+$ core [40] (e.g., $\text{TcO}_3(\text{HB}(\text{pz})_3)$, pz = pyrazolyl) are found. For Tc(VII), one of the most commonly occurring class of compound are the pertechnetate salts. In these salts, the TcO_4^- anion exhibits the tetrahedral geometry (Figure 1.3). Pertechnetate salts are found with many cationic units, such as Group I and II elements, the uranyl cation (UO_2^{2+}), lanthanides, and organic cations ($n\text{-(CH}_3(\text{CH}_2)_n)_4\text{N}^+$ and $(\text{Ph}_4\text{As})^+$). The characteristic UV-Visible spectrum of pertechnetate exhibits two absorptions at 244 nm ($\epsilon = 5690 \text{ M}^{-1}\cdot\text{cm}^{-1}$) and 287 nm ($\epsilon = 2170 \text{ M}^{-1}\cdot\text{cm}^{-1}$) and resembles the spectra of its Re homologue [41].

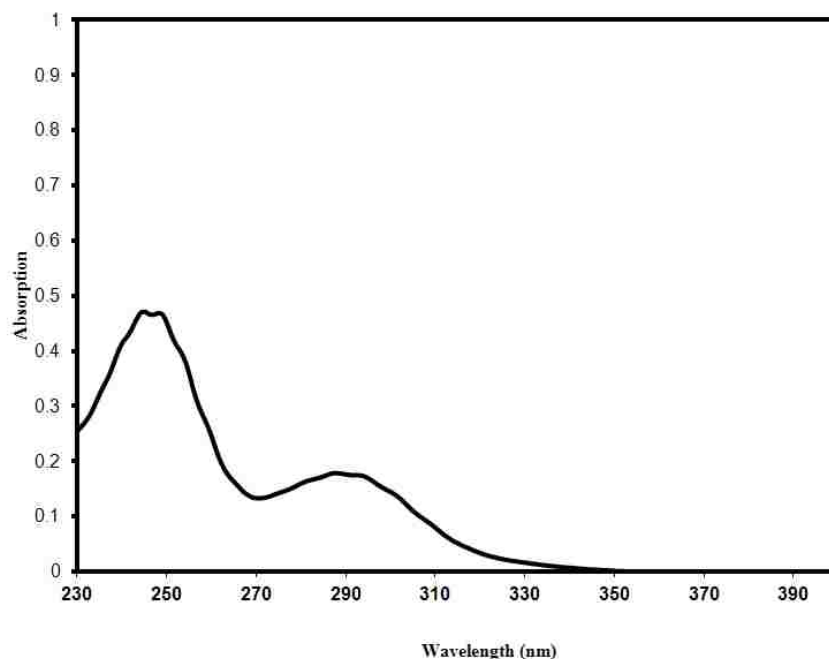


Figure 1.2. Characteristic UV-Visible spectrum of TcO_4^- in H_2O .

A common Tc(VII) pertechnetate salt is NH_4TcO_4 , which is often used as a starting material for inorganic Tc chemistry. In concentrated sulfuric and perchloric acids, the pertechnetate anion is protonated and pertechnetic acid, HTcO_4 , is the dominant species [42]. Alternative synthetic methods for preparing HTcO_4 include the dissolution of Tc_2O_7 in water and passing solutions of KTcO_4 through a strong-acid cation exchange column [43]. The highly volatile heptavalent, Tc_2O_7 , is formed as a yellow crystalline solid when Tc metal or TcO_2 are treated at elevated temperatures in the presence of O_2 [44]. Technetium heptaoxide is a molecular solid, it crystallizes as centrosymmetric Tc_2O_7 molecules and is structurally more similar to Mn_2O_7 than Re_2O_7 [45]. Technetium trioxide halides of the formula TcO_3X ($\text{X} = \text{F}, \text{Cl}, \text{Br}$) can be synthesized from the reaction of TcO_2 with $\text{X}_2(\text{g})$ at elevated temperatures; these compounds are often found

as impurities during the synthesis of binary Tc halides in the presence of unwanted O₂ [32, 46].

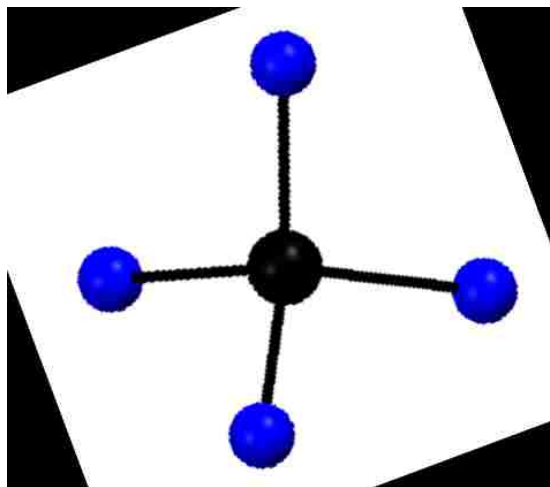


Figure 1.3. Ball-and-stick representation of the TcO₄⁻ anion. Tc atoms in black and O atoms in blue.

The chemistry for Tc(VI) is dominated by complexes containing the (Tc≡N)³⁺ core. One of the model compounds is the (*n*-Bu₄N)TcNCl₄ salt, which is synthesized from the reaction of (*n*-Bu₄N)TcO₄ with concentrated HCl and NaN₃. The TcNCl₄⁻ anion exhibits the square-pyramidal geometry with a short Tc≡N bond distance (i.e., 1.581(5) Å) [47].

Due to the large role of Tc(V) complexes in the development of radiopharmaceutical synthesis and design, a myriad of pentavalent Tc complexes have been synthesized. The majority of these complexes contain the isoelectronic (Tc=O)³⁺ or (Tc≡N)²⁺ cores and form a wide range of coordination complexes (Table 1.1) [32]. Many of the (Tc=O)³⁺-core complexes are derived from (*n*-Bu₄N)TcOCl₄. This salt can be

prepared from the reduction of (*n*-Bu₄N)TcO₄ with 0 °C concentrated HCl or in aqueous solutions of HCl with the addition of H₃PO₂ [48]. The detailed preparation of (*n*-Bu₄N)TcOCl₄ is presented in Chapter 2. The TcOCl₄⁻ anion (Figure 1.4) and many of its derivatives exhibit the square-pyramidal geometry with the capping Tc=O (~ 1.59-1.68 Å). The M₂TcOCl₅ salts, which contain the octahedral TcOCl₅²⁻ anion, can be obtained in low yield after the reduction of NH₄TcO₄ in cold HCl and precipitation with Group I cations [49]. The UV-Visible spectrum of TcOCl₄⁻ in cold HCl exhibits two intense absorption bands at 234 nm and 293 nm (Figure 1.5).

Table 1.1. Tc(V)-cores and characteristic complexes formed for each [32].

Tc(V) core	Characteristic complex
(TcO) ³⁺	(<i>n</i> -Bu ₄)TcOCl ₄
(TcS) ³⁺	(AsPh ₄)[TcS(edt) ₂] (edt = ethane-1,2-dithiol)
<i>trans</i> -(TcO ₂) ⁺	[TcO ₂ (en) ₂]Cl (en = ethylenediamine)
(TcN) ²⁺	(AsPh ₄) ₂ [TcN(NCS) ₄]

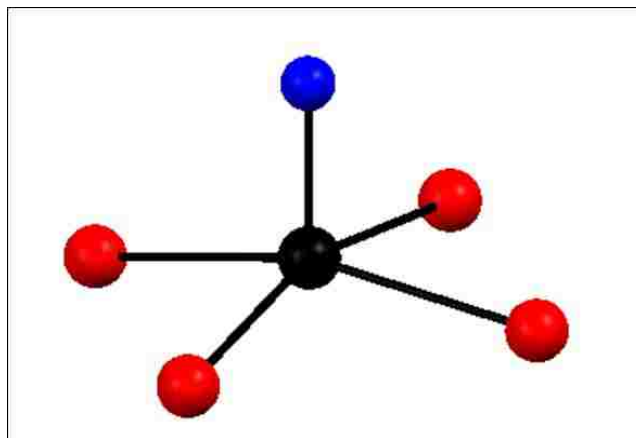


Figure 1.4. Ball-and-stick representation of the TcOCl_4^- anion in $(\text{Bu}_4\text{N})\text{TcOCl}_4$. Tc atom in black, O atom in blue, and Cl atoms in red.

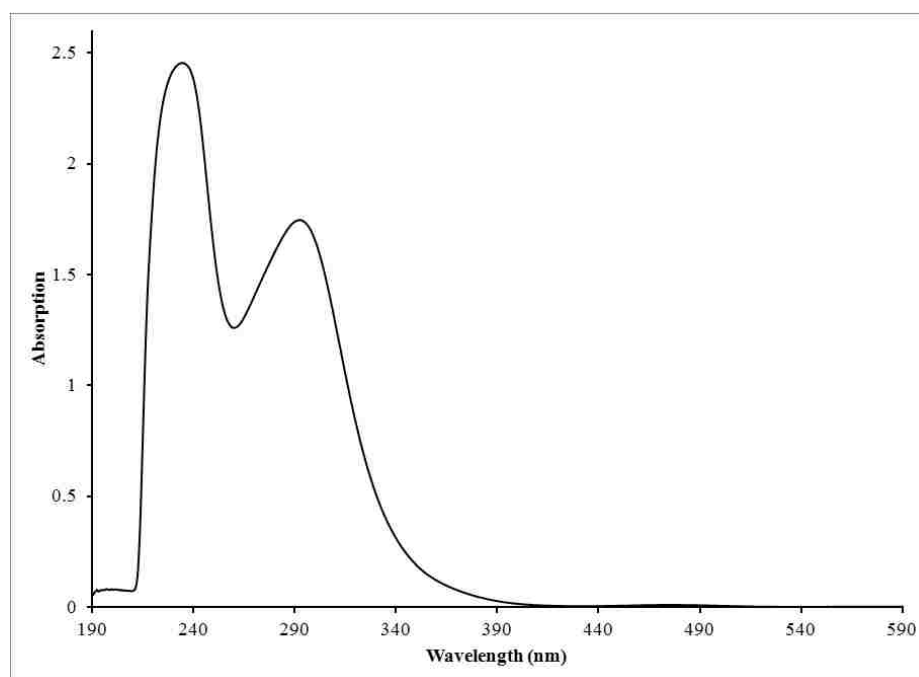


Figure 1.5. Characteristic UV-Visible spectrum of TcOCl_4^- in 0°C HCl .

Mid-Valent: Tc(IV) and Tc(III)

Technetium(IV) is another thermodynamically stable oxidation state for Tc forming d^3 complexes. For Tc(IV), two characteristic compounds are TcO_2 and salts

containing the TcX_6^{2-} ($\text{X} = \text{F}, \text{Cl}, \text{Br}, \text{I}$) species. Technetium dioxide can be synthesized in the solid-state from the decomposition of NH_4TcO_4 under an inert atmosphere at elevated temperatures. Technetium dioxide crystallizes in the monoclinic space-group $\text{P2}_1/\text{c}$ and is similar to MO_2 ($\text{M} = \text{Mo}, \text{Re}$); occupancies of TcO_2 are slightly different from those of ReO_2 [50]. Hydrated TcO_2 ($\text{TcO}_2 \cdot n\text{H}_2\text{O}$, $n = 1.6$) is often formed as a brown precipitate from the hydrolysis of Tc(IV) complexes in aqueous solutions. Other methods to prepare hydrated TcO_2 include the electrochemical or chemical reduction (hydrazine) of TcO_4^- in neutral to basic media [51]. The TcX_6^{2-} anion is formed from the reduction of NH_4TcO_4 in concentrated hydrohalic HX ($\text{X} = \text{F}, \text{Cl}, \text{Br}, \text{I}$) solutions. Salts of TcX_6^{2-} can be easily precipitated with Group I cations, NH_4^+ , and Me_4N^+ . In the salts, the TcX_6^{2-} anion exhibits the O_h geometry. The UV-Visible spectrum of TcCl_6^{2-} exhibits two major bands at 236 nm and 340 nm (Figure 1.6) [52].

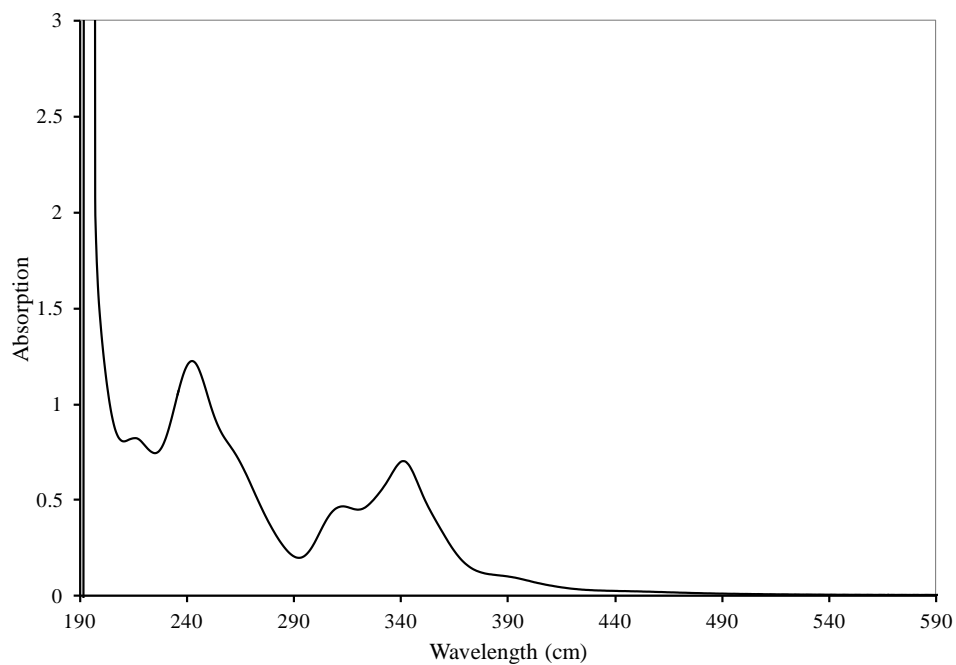


Figure 1.6. Characteristic UV-Visible spectrum of TcCl_6^{2-} in HCl .

Technetium(III) represents the second most numerous class of compounds after those of Tc(V). The archetypal compounds of Tc(III) are the halogeno-phosphine complexes TcX_2L_2^+ and TcX_3L_3 where X = Cl or Br and L = mono- or bidentate phosphine-based ligand, i.e. PR_3 (R = Me, Et, and Ph), dppe (1,2-bis(diphenylphosphino)ethane), dmpe (1,2-bis(dimethylphosphino)ethane). These compounds can be synthesized using a variety of different starting materials; for example, $\text{TcCl}_3(\text{Me}_2\text{PhP}_3)$ is obtained by refluxing NH_4TcO_4 , Me_2PhP , and HCl in EtOH [53]. These halogeno-phosphine complexes often exhibit the tetragonal geometry where the halogen and phosphine-based ligands are situated either *trans* or *mer* in respect to each other [32, 54]. Finally, many of Tc(III) complexes are dinuclear and contain multiple Tc-Tc bonds (*vide infra*).

Low-Valent: Tc(II), Tc(I), Tc(0), Tc(-I)

For Tc(II), complexes containing nitrosyl groups, nitrogen heterocycles, halogeno-phosphine ligands, and polynuclear complexes are the most encountered species. Technetium(II) halogeno-phosphine complexes are typically prepared from a mid-valent precursor and reduced with a strong reducing agent, such as NaBH_4 , or in the presence of a reducing ligand. In these compounds, the Tc atom is coordinated to halogen and phosphine ligands in the tetragonal geometry. Two examples of this class of compounds are $\text{TcX}_2(\text{dppe})_2$ (X = Cl, Br) [32, 55]. Nitrosyl compounds of Tc(II), such as $(n\text{-Bu}_4\text{N})\text{Tc}(\text{NO})\text{Br}_4$, have been prepared from the reaction of hydrated TcO_2 and $\text{NO}(\text{g})$ at 75 °C in aqueous HBr and followed by the precipitation with $(n\text{-Bu}_4\text{N})\text{Br}$. Exchange of the Br ligand with Cl and I resulted in analogous compounds $(n\text{-Bu}_4\text{N})\text{Tc}(\text{NO})\text{Cl}_4$ and $(n\text{-Bu}_4\text{N})\text{Tc}(\text{NO})\text{I}_4$, respectively [56]. Diffraction studies on $(n\text{-Bu}_4\text{N})\text{Tc}(\text{NO})(\text{MeOH})\text{Cl}_4$

obtained from the reduction of TcCl_6^{2-} or TcOCl_4^- with NH_2OH in MeOH , yielded a distorted octahedral geometry with the nitrosyl and MeOH groups situated in *trans* arrangement to each other [57].

The Tc(I) , Tc(0) , and Tc(-I) oxidation states are dominated by carbonyl chemistry. Typical complexes each of these oxidation states are $\text{Tc(CO)}_5\text{X}$ ($\text{X} = \text{Cl, Br, I}$), $\text{Tc}_2(\text{CO})_{10}$, and HTc(CO)_5 , respectively [58]. The $\text{Tc(CO)}_5\text{X}$ complexes can be prepared from the reaction of $\text{Tc}_2(\text{CO})_{10}$ with the respective elemental halogens in CCl_4 . The compounds $\text{Tc(CO)}_5\text{X}$ ($\text{X} = \text{Cl, Br, I}$) were characterized by X-ray Diffraction (XRD) and Infrared (IR) spectroscopy and all exhibit the C_{4v} symmetry [59]. Ditechnetium decacarbonyl, $\text{Tc}_2(\text{CO})_{10}$, and its synthetic derivatives constitute the few complexes of Tc(0) known. The compound $\text{Tc}_2(\text{CO})_{10}$ can be synthesized in up to gram quantities from the high temperature and pressure reactions of a variety of Tc species (i.e., TcO_2 , Tc_2O_7 , NH_4TcO_4 , NaTcO_4) with CO(g) in stainless steel autoclaves. The addition of copper powder to the reaction has proven to be beneficial in these reactions [60]. The $\text{Tc}_2(\text{CO})_{10}$ dimer exhibits the staggered D_{4d} geometry comparable to other Group VII $\text{M}_2(\text{CO})_{10}$ ($\text{M} = \text{Mn, Re}$) compounds. As for other carbonyl compounds, $\text{Tc}_2(\text{CO})_{10}$ is volatile and can be purified via vacuum sublimation [61].

For Tc(-I) , HTc(CO)_5 and $(\text{Et}_4\text{N})(\text{TcFe}_2(\text{CO})_{12})$ are the only two compounds with Tc atom in the (-I) oxidation state reported. The compound HTc(CO)_5 can be prepared by reduction of $\text{Tc}_2(\text{CO})_{10}$ with a 1 % Na-Hg amalgam in THF . The compound has been characterized by IR spectroscopy and its spectrum is similar to the ones of homologous Mn and Re complexes [59].

Tchnetium metal can be synthesized using three primary techniques: the hydrogen reduction of NH_4TcO_4 at elevated temperatures, the decomposition of $(\text{NH}_4)_2\text{TcCl}_6$ under inert atmosphere, or the electrodeposition of TcO_4^- from dilute H_2SO_4 solutions [62]. A detailed experimental preparation of Tc metal is presented in Chapter 2. Tchnetium metal appears bright silvery grey, and though it is brittle it can be manipulated into a variety of physical forms: rods, foils, plates, or wires [63]. The melting point of the metal was determined to be on average 2167°C , and its boiling point estimated to 5173°C . The density of Tc metal was measured to be 11.47 g/cm^3 [64]. Tchnetium metal crystallizes in the hexagonal close-packed space group P63/mmc (Figure 1.7) with cell parameters $a = 2.7364\text{ \AA}$ and $c = 4.3908\text{ \AA}$ at 4.2 K [65]. Physical measurements have shown Tc to be a high temperature superconductor with transition temperatures at 11.2 K and 9.3 K for powder metal and an arc-melted sample, respectively; it has the 2nd highest transition temperature for any element following that of niobium [66]. The magnetic susceptibility was measured at 298 K to be $2.7 \times 10^{-6}\text{ cm}^3 \cdot \text{g}^{-1}$ [64]. The catalytic behavior of Tc metal has been predicted and compared to that of other platinum-group metals. Experimentally it has shown to be quite effective in a number of catalytic reactions (e.g., hydrogenation of benzene to cyclohexane) [32, 67].

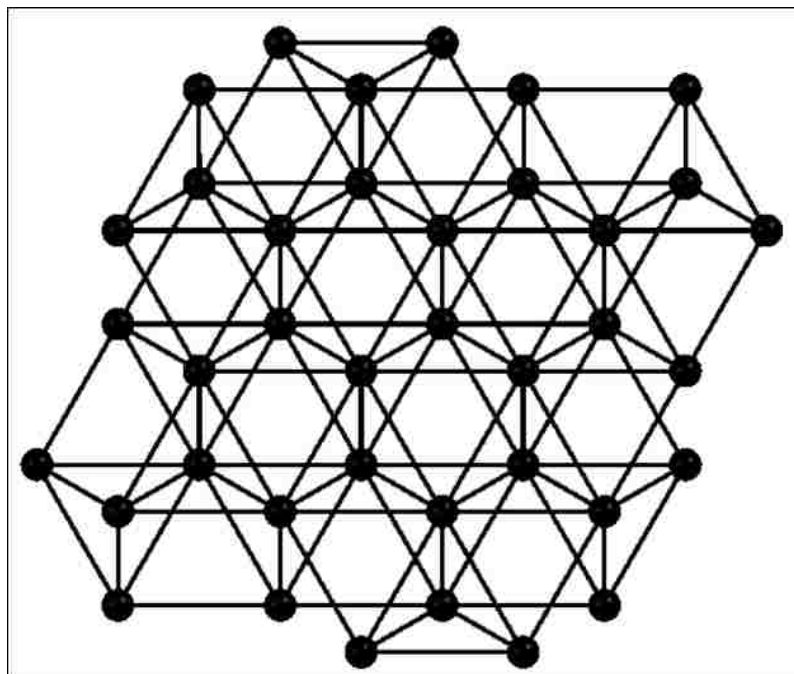


Figure 1.7. Ball-and-stick representation of the *hcp* structure of Tc metal displaying the packing of atoms down the *c* axis.

1.3 Technetium Multiple Metal-Metal Bond Chemistry

Transition metals are capable of forming single to quintuple bonds with other metal atoms. The formation of bonds with bond orders greater than 3, which result in quadruple and quintuple bonds, are only accessible between two transition metal atoms with significant d orbital overlap. This interaction forms σ , π , and δ orbitals. For Tc multiple Tc-Tc bonds are observed in dinuclear compounds, heteroatomic clusters, and extended-structure compounds. In these compounds, Tc can be found in the oxidation state Tc(III), Tc(II), and Tc(I) [68].

Multiple Metal-Metal Bonded Dimers

Dinuclear compounds can exhibit the core structure Tc_2^{n+} ($n = 6, 5, 4$); quadruple bonds are observed for $n = 6$, a weak quadruple bonds for $n = 5$ and triple bonds for $n =$

4. Quadruple bonds are derived from d orbital overlaps and consist of one σ , two π and one δ orbitals (Figure 1.8). The electronic configurations and corresponding bond orders of the Tc_2^{n+} ($n = 6, 5, 4$) are presented in Table 1.2.

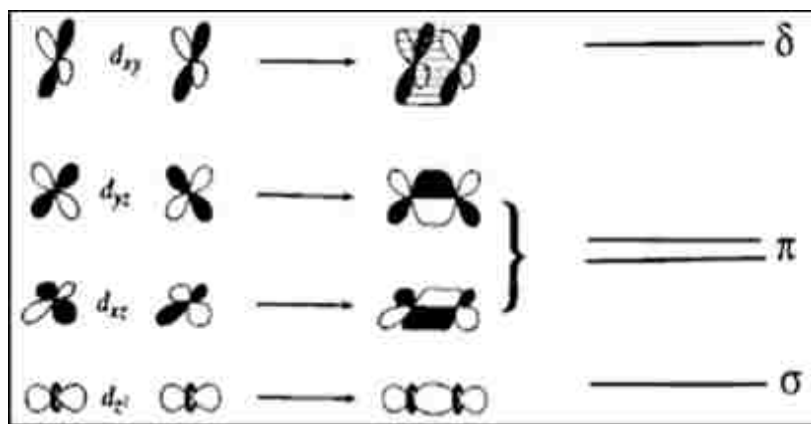


Figure 1.8. Molecular orbitals involved in the quadruple bond.

Table 1.2. Multiple Tc-Tc Bonds in Tc_2^{n+} dimers and Characteristic Electron Configurations

Tc_2^{n+}	Number of Electrons	Electron Configuration	Bond Order (BO)
$n = 6$	8	$\sigma^2 \pi^4 \delta^2$	4
$n = 5$	9	$\sigma^2 \pi^4 \delta^2 \delta^{*1}$	3.5
$n = 4$	10	$\sigma^2 \pi^4 \delta^2 \delta^{*2}$	3

Prior to 2010, only five quadruple bonded dimers had been structurally characterized. The archetypal examples of these compounds are $(n\text{-Bu}_4\text{N})_2Tc_2Cl_8$ and $Tc_2(O_2CCH_3)_4Cl_2$. The $(n\text{-Bu}_4\text{N})_2Tc_2Cl_8$ salt can be prepared by different methods: reduction of $(NH_4)_2TcCl_6$ by mossy Zn in aqueous HCl followed by cation exchange with Bu_4NCl [69] or reduction of $(n\text{-Bu}_4\text{N})TcOCl_4$ by $(Bu_4N)BH_4$ in THF followed by

acidification with HCl(g) in CH₂Cl₂. A detailed preparation of (*n*-Bu₄N)₂Tc₂Cl₈ is presented in Chapter 2. The (*n*-Bu₄N)₂Tc₂Cl₈ can easily be converted to the Br analogue in dichloromethane with HBr(g) [70]. In (*n*-Bu₄N)₂Tc₂Cl₈, the Tc₂Cl₈²⁻ anion (Figure 1.9) consists of two eclipsed TcCl₄ units linked by a Tc-Tc quadruple bond (i.e., Tc-Tc = 2.147(4) Å) [71]. The (*n*-Bu₄N)₂Tc₂Cl₈ salt is highly soluble in polar solvents, i.e., acetone and CH₂Cl₂, and exhibits the characteristic δ→δ* transition (670 nm) in its UV-Visible spectra [72].

The Tc₂(O₂CCH₃)₄Cl₂ complex was first synthesized from the hydrogen reduction of KTcO₄ in HCl/acetic acid mixture in an autoclave; it was later derived from the reaction of (*n*-Bu₄N)₂Tc₂Cl₈ in refluxing mixture of acetic anhydride/acetic acid [73]. A detailed experimental procedure for the preparation of Tc₂(O₂CCH₃)₄Cl₂ is presented in Chapter 2. The crystal structure of Tc₂(O₂CCH₃)₄Cl₂ was recently determined (Figure 1.9); it exhibits the paddle-wheel motif with four bridging acetate ligands and two axial chlorides. The Tc-Tc separation, 2.1758(3) Å, is indicative of a quadruple Tc-Tc bond and is comparable to other Tc(III) carboxylate dimers [74].

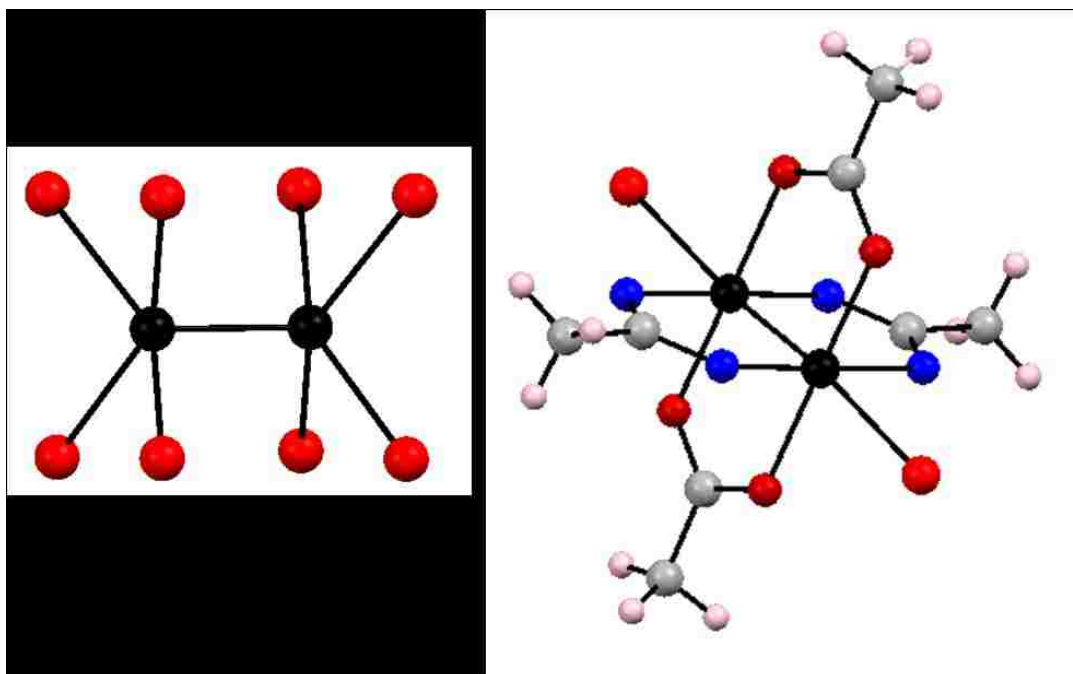


Figure 1.9. Ball-and-stick representation of quadruply bonded Tc dimers: $\text{Tc}_2\text{Cl}_8^{2-}$ anion (left) and $\text{Tc}_2(\text{O}_2\text{CCH}_3)_4\text{Cl}_2$ (right). Tc atoms in black, Cl atoms in red, O atoms in blue, C atoms in grey, and H atoms in pink.

Clusters Containing Multiple Metal-Metal Bonds

Multiple metal-metal bonds are found in hexa- and octanuclear clusters with trigonal or tetragonal prismatic geometries, respectively. Technetium trigonal prismatic clusters have been synthesized using high-pressure autoclave techniques (Table 1.3). The $(\text{Me}_4\text{N})_3\{[\text{Tc}_6(\mu\text{-Cl})_6\text{Cl}_6]\text{Cl}_2\}$ and $(\text{Me}_4\text{N})_2[\text{Tc}_6(\mu\text{-Cl})_6\text{Cl}_6]$ salts were prepared from the hydrogen reduction of $(\text{Me}_4\text{N})_2\text{TcCl}_6$ or $(\text{Me}_4\text{N})\text{TcO}_4$ in HCl at 30-50 atm and 140-180 °C [75, 76]. The corresponding Br analogue was synthesized under similar conditions with HBr. Starting with $(\text{Et}_4\text{N})_2\text{TcCl}_6$, the major product is $(\text{Et}_4\text{N})_2\{[\text{Tc}_6(\mu\text{-Br})_6\text{Br}_6]\text{Br}_2\}$. The triangular prismatic structures (Figure 1.10) contain short Tc-Tc distances that extend perpendicular to the triangular faces indicative of triple bonds. The Tc-Tc

distances along the triangular edge are much longer in comparison and are indicative of single bonds (Table 1.3).

Tetragonal prismatic octanuclear bromide and iodide clusters have also been identified: $[\text{Tc}_8(\mu\text{-Br})_8\text{Br}_4]\text{Br}\cdot 2\text{H}_2\text{O}$, $(\text{H}_5\text{O}_2)[\text{Tc}_8(\mu\text{-Br})_8\text{Br}_4]\text{Br}$, $(\text{H}_5\text{O}_2)_2[\text{Tc}_8(\mu\text{-Br})_8\text{Br}_4]\text{Br}_2$, and $(\text{Bu}_4\text{N})_2[\text{Tc}_8(\mu\text{-Br})_4(\mu\text{-I})_4\text{Br}_2\text{I}_2]\text{I}_2$ [77]. Similarly to the hexanuclear chloride and bromide clusters, these were prepared using autoclave methods with concentrated HBr and HI solutions. Within the $[\text{Tc}_8(\mu\text{-Br})_8\text{Br}_4]^+$ cluster, the shorter Tc-Tc bonds ($\sim 2.145(2) \text{ \AA} - 2.147(2) \text{ \AA}$) perpendicular to the rhomboidal top and bottom faces are characteristic of triple bonds, while the Tc-Tc bonds surrounding the edges of the faces ($2.521(2) \text{ \AA}$ to $2.689(2) \text{ \AA}$) are characteristic of single bonds (Figure 1.10) [68].

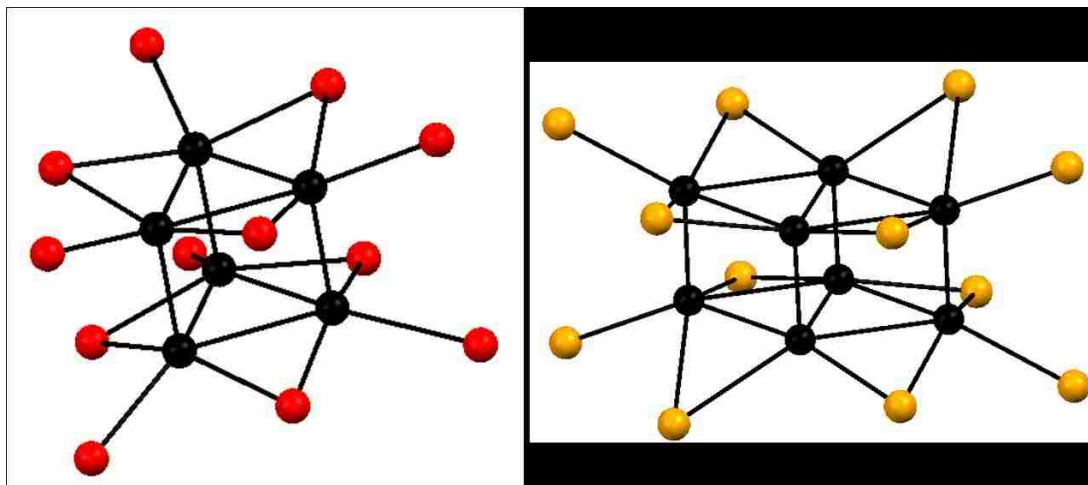


Figure 1.10. Ball-and-stick representations of the hexa- (left) and octanuclear (right) cluster cores containing multiple metal-metal bonding. Tc atoms in black, Cl atoms in red, and Br atoms in orange.

Table 1.3. Hexanuclear Trigonal Prismatic Tc Clusters and Tc-Tc Distances

Compound	Core	Tc-Tc Bond Length (Å)	Tc≡Tc Bond Length (Å)
(Me ₄ N) ₂ [Tc ₆ (μ-Cl) ₆ Cl ₆]	Tc ₆ ¹⁰⁺	2.69(1)	2.16(1)
(Me ₄ N) ₃ {[Tc ₆ (μ-Cl) ₆ Cl ₆]Cl ₂ }	Tc ₆ ¹¹⁺	2.57(1)	2.22(1)
(Et ₄ N) ₃ {[Tc ₆ (μ-Br) ₆ Br ₆]Br ₂ }	Tc ₆ ¹¹⁺	2.702(2)	2.154(5)
(Et ₄ N) ₂ {[Tc ₆ (μ-Br) ₆ Br ₆]Br ₂ }	Tc ₆ ¹²⁺	2.66(2)	2.188(5)

Extended Structures Containing Multiple Metal-Metal Bonds

The K₂Tc₂Cl₆ compound is the only example of a compound with an extended structure containing multiple metal-metal bonds reported. This compound was synthesized in an autoclave at ~30 atm from the reaction KTcO₄ with HCl and H₂(g) at 140 °C. The structure of K₂Tc₂Cl₆ consists of infinite zigzag chains of edge-sharing Tc₂Cl₈ units (Figure 1.11). Within the Tc₂Cl₈ unit, the Tc-Tc distance (i.e., 2.044(1) Å) is consistent with the presence of a triple bond; the electronic configuration of the Tc≡Tc triple bond being $\sigma^2\pi^4\delta^2\delta^*2$ [78].

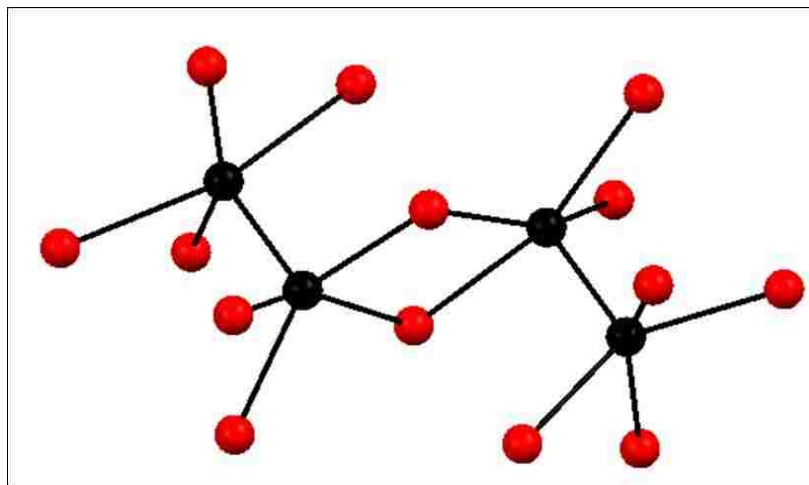


Figure 1.11. Ball-and-stick representation of two Tc₂Cl₈ units within a chain of K₂Tc₂Cl₆.

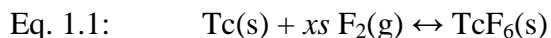
Tc atoms in black and Cl atoms in red.

1.4 Binary Technetium Halide Chemistry

The chemistry of binary Tc halides was dominated by TcF_6 , TcF_5 , and TcCl_4 . During this time period, work done toward these compounds was focused on the chlorine system, and a second binary chloride TcCl_6 was proposed at high temperatures under a chlorine atmosphere, but no further characterization has been reported. Similarly, gas phase experiments reported the existence of a trichloride in the form of Tc_3Cl_9 homologous to the Re analogue, but the compound was never isolated in the solid-state [79]. In 2009, the first binary Tc bromides TcBr_3 and TcBr_4 were reported. In comparison to the binary Re halides, for which there are 15 known and characterized, the fundamental chemistry of binary Tc halides was notably undeveloped prior to this work.

1.4.1 Binary Technetium Fluorides

Technetium(VI) hexafluoride was reported in 1961. It can be isolated in purities greater than 90% after fractional sublimation when prepared from the direct fluorination of the metal in a nickel can at 400 °C (Eq. 1.1) or in lower yields when Tc metal is treated in a stream of $\text{F}_2/\text{N}_2(\text{g})$ at 350 °C [80]. It is a volatile golden-yellow solid that melts at 37.4 °C and boils at 55.3 °C. The compound is stable and can be stored in nickel or dried Pyrex vessels for extend periods.

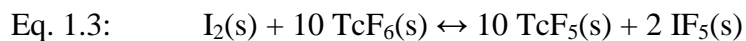
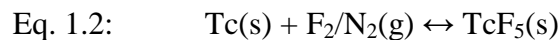


At room temperature, TcF_6 crystallizes in the body center cubic Bravais lattice with lattice parameter $a = 6.16 \text{ \AA}$ ($Z = 2$). The compound undergoes a solid phase transition under -6 °C from bcc to orthorhombic where it crystallizes in the space group $Pnma$ with unit cell dimensions $a = 9.360(3) \text{ \AA}$, $b = 8.517(3) \text{ \AA}$, $c = 4.934(2) \text{ \AA}$, ($Z = 4$) (Figure 1.12A). This transition from the bcc phase has been identified by XRD for other

isotypic MF₆ compounds (M = Mo, Ru, Rh, W, Re, Os, Ir, and Pt) [80]. Technetium hexafluoride is isomorphous with its rhenium congener and is composed of molecular TcF₆ octahedra. The magnetic susceptibility of TcF₆ was measured from 295 K to 14 K and is inversely proportional to temperature (1/T), and the magnetic moment was determined to be 0.45 B.M. [81]. In aqueous NaOH solutions, TcF₆ disproportionates into amorphous TcO₂ and TcO₄⁻ [80a]. As a starting material, the compound has been shown to react with iodine yielding TcF₅ [82]. It also reacts with NO, NOF, and NO₂F to form NOTcF₆, (NO)₂TcF₈, and NO₂TcF₇, respectively [83]. In HF, the compound reacts with N₂H₆F₂; N₂H₆(TcF₆)₂ is obtained from the reaction of excess TcF₆ with N₂H₆F₂ while the addition of excess hydrazinium fluoride yields the Tc(IV) species N₂H₆TcF₆ [84]. In the nuclear fuel cycle, TcF₆ is formed during the gaseous diffusion enrichment of ²³⁵U as a contaminant with UF₆ [85].

Technetium(V) pentafluoride was first reported in 1963, it can be obtained along with TcF₆ as a by-product when a mixture of F₂/N₂(g) is reacted with Tc metal at elevated temperature (Eq. 1.2) [86]. Alternatively, TcF₅ is also formed by the reaction of elemental iodine with an excess of TcF₆ yielding oxidized IF₅ and reduction of the hexafluoride to the pentafluoride (Eq. 1.3) [82]. The compound forms a low-melting point (50 °C) yellow solid that can be purified by vacuum sublimation, though when subjected to higher temperatures (60 °C) will decompose. Technetium pentafluoride crystallizes in the orthorhombic space group *Pmcn* with cell parameters $a = 5.76 \text{ \AA}$, $b = 17.01 \text{ \AA}$, $c = 7.75 \text{ \AA}$, ($Z = 8$) [87]. The compound consists of infinite chains of corner-sharing TcF₆ octahedra that run along the *a*-axis and is isomorphous to CrF₅, VF₅, and ReF₅ (Figure 1.12B) [86]. Magnetic properties of TcF₅ have been determined; its

magnetic moment is 3.00 B.M., approximately the spin-only value for two unpaired electrons, and a Weiss constant of 156° [82].



Unlike rhenium that forms ReF_7 and ReF_4 , there is no experimental evidence that TcF_7 and TcF_4 have been prepared, though first-principle calculations have predicted the compounds to be stable [32, 88, 89].

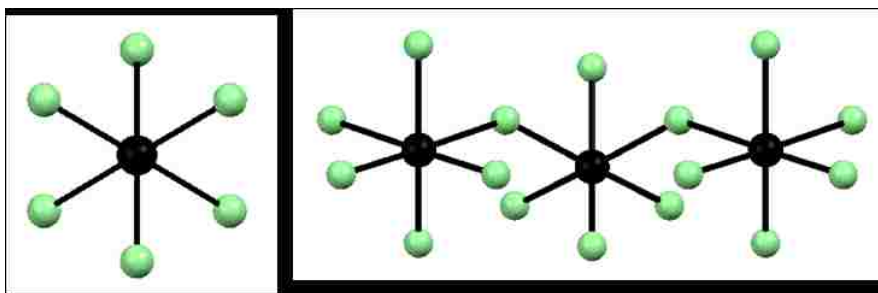
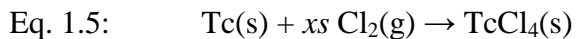
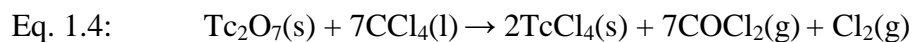


Figure 1.12. Ball-and-stick representation of the structures of binary technetium fluorides: TcF_6 (left) and TcF_5 (right). Tc atoms in black and F atoms in green.

1.4.2 Binary Technetium Chlorides

Technetium tetrachloride was first reported in 1957 from the reaction of CCl_4 with Tc_2O_7 in a sealed tube contained inside a metal bomb at 400 °C in 80 % yield (Eq. 1.4). A second synthetic approach for producing TcCl_4 was reported from the solid-state reaction of flowing dry Cl_2 over the metal between 200-400 °C (Eq. 1.5). The reaction forms a blood-red solid that can be sublimed in a stream of Cl_2 gas at 300 °C [90].



Suitable single crystals of TcCl_4 were obtained and its structure was solved by Single-Crystal X-ray Diffraction (SCXRD); TcCl_4 crystallizes in the orthorhombic space group $Pbca$ with cell parameters of $a = 11.65 \text{ \AA}$, $b = 14.06 \text{ \AA}$, $c = 6.03 \text{ \AA}$, ($Z = 8$). The structure of TcCl_4 is composed of infinite zigzag chains of distorted edge-sharing TcCl_6 octahedra (Figure 1.13). Within the chains, three types of Tc-Cl linkages occur: terminal Tc-Cl linkages (2.24 \AA); bridging Tc-Cl linkages parallel to the chain (2.38 \AA); bridging Tc-Cl linkages perpendicular to the chain length (2.49 \AA) [91]. Magnetic measurements have shown TcCl_4 to be paramagnetic. The magnetic moment was determined to be $\mu = 3.14 \mu\text{B}$, a lower value than expected for a d^3 octahedral complex, and the Weiss constant $\theta = -57 \text{ K}$ [92].

The chemistry of TcCl_4 is more developed than that of the other known binary Tc halides. This is primarily due to its ease of preparation and manipulation in comparison with the reactivity and special precautions required for the fluorides. When dissolved in 12 M HCl, TcCl_4 is converted into the TcCl_6^{2-} , whereas in aqueous and basic solutions it hydrolyses to amorphous TcO_2 [2]. Tetravalent Tc complexes in the form TcCl_4L_2 can be synthesized from the reaction of TcCl_4 with monodentate L donor ligands ($\text{L} = \text{PPh}_3$, PMe_2Ph , OPPh_3 , AsPh_3 , THF, CH_3CN , DMSO, TO, and H_2O) [93]. A Tc nitrido chloride (TcNCl_3) was prepared from the reaction of TcCl_4 and IN_3 in CCl_4 ; this nitrido chloride can be converted to the TcNCl_4^- anion by addition to a solution of $(\text{Ph}_4\text{As})\text{Cl}$ in CH_2Cl_2 [94]. Other reactions of TcCl_4 with aromatic π -complexes (i.e., $[\text{Tc}(\text{C}_6\text{H}_6)_2]\text{PF}_6$ and $\{\text{Tc}[\text{C}_6(\text{CH}_3)_6]_2\}\text{PF}_6$) and crown ethers (i.e., $\{[\text{TcCl}_5(\text{H}_2\text{O})][(\text{15-Crown-5})(\text{H}_3\text{O})](\text{15-Crown-5})\}$) have also been reported [95].

Technetium(VI) hexachloride has been reported as a green volatile co-product from the chlorination of Tc metal. Limited information and chemical analysis have been performed on the compound, and its existence is still questionable [90, 46]. Other Tc chlorides, i.e., Tc_3Cl_9 and $\text{Tc}_3\text{Cl}_{12}$, have been observed in the gas phase, but have not been synthesized in the solid-state and no structural or chemical information is available [79]. These experiments and the existence of their Re homologues ReCl_6 , Re_3Cl_9 , and $\text{Re}_3\text{Cl}_{12}^{3-}$, which have been isolated in weighable quantities, gives great hope of isolating these binary Tc chlorides in the solid-state [96].

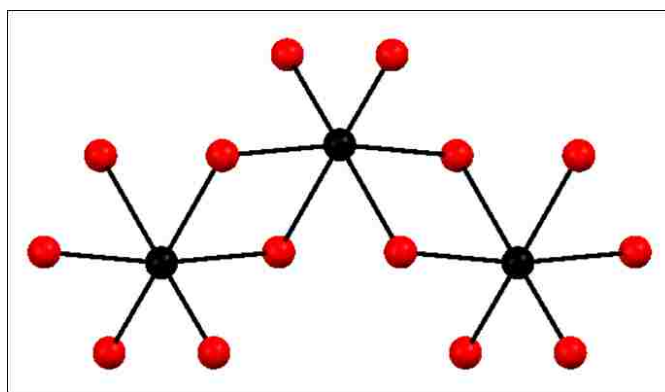
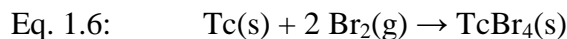


Figure 1.13. Ball-and-stick representation of the binary technetium chloride, $\text{TcCl}_4.\text{Tc}$ atoms in black and Cl atoms in red.

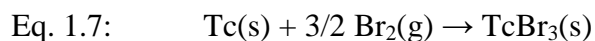
1.4.3 Binary Technetium Bromides

The first binary Tc bromides TcBr_3 and TcBr_4 were not reported until 2009. Technetium tetrabromide was prepared congruently with TcBr_3 from the reaction of the elements ($\text{Tc}:\text{Br} \sim 1:4$) in a sealed Pyrex tube at $400\text{ }^\circ\text{C}$ (Eq. 1.6) [97]. The compound was sublimed as black needle single-crystals and analyzed by SCXRD. Technetium tetrabromide crystallizes in the orthorhombic space group $Pbca$ with cell dimensions of $a = 6.3237(5)\text{ \AA}$, $b = 12.1777(9)\text{ \AA}$, and $c = 14.7397(11)\text{ \AA}$ and is isomorphous with TcCl_4 ,

PtBr₄, and OsBr₄ (Figure 1.14) [91b, 98]. The structure of TcBr₄ consists of infinite zigzag chains of edge-sharing TcBr₆ octahedral; inside the chain, the Tc-Tc distances (3.7914(4) Å) preclude metal-metal interactions. Similarly to TcCl₄, there are three distinct Tc-Br distances observed with two bridging ($d_{av} = 2.6234[4]$ Å and 2.5256[4]) and one terminal (2.3953(4) Å).



Technetium tribromide was synthesized from the stoichiometric reaction of Tc metal with elemental bromine with (Tc:Br ~1:3) in sealed Pyrex tubes at 350-400 °C for 8 h (Eq. 1.7) [97]. The compound was isolated as sublimed black single-crystals suitable for SCXRD measurements. TcBr₃ crystallizes in the orthorhombic space group *Pmmn* with cell parameters $a = 11.0656(2)$ Å, $b = 5.9717(1)$ Å, and $c = 6.3870(1)$ Å (Figure 1.14). It exhibits the TiI₃ structure-type and is isomorphous to MBr₃ (M = Ru, Mo) [98]. It consists of infinite chains of face-sharing distorted TcBr₆ octahedra that extend parallel to the *c*-axis. Within the chain, the Tc-Tc distances repetitively alternate between long (3.1434(4) Å) and short separations (2.8283(4) Å); the shorter separations are indicative of metal-metal bonding [22]. The disparity between the two different distances of the Tc-Tc separations follow the order $\Delta\text{RuRu} > \Delta\text{MoMo} > \Delta\text{TcTc}$ [99]. Technetium tribromide has been used as a precursor in synthetic chemistry; two new divalent complexes, TcBr₂(PMe₃)₄ and Tc₂Br₄(PMe₃)₄ have been obtained from the reaction of TcBr₃ with trimethylphosphine and NaBEt₃H in THF [100].



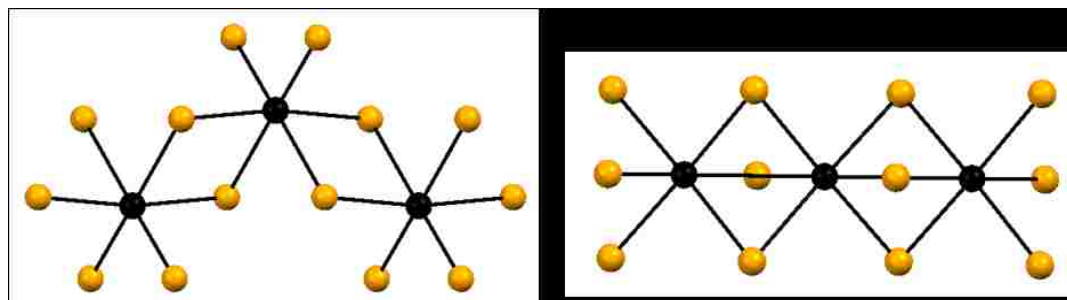


Figure 1.14. Ball-and-stick representations of the structures of binary technetium bromides: TcBr_4 (left) and TcBr_3 (right). Tc atoms in black and Br atoms in orange.

1.5 Conclusion

Discovered in 1936, Tc is the lightest radioelement. There are 31 isotopes of Tc reported, the two most common being ^{99}Tc , a major fission product of the nuclear industry and $^{99\text{m}}\text{Tc}$ the workhorse of diagnostic nuclear medicine. Due to its radioactivity and late discovery, there is little known about Tc chemistry in comparison to its heavier homologue, Re. An example of this gap in knowledge between the two elements is their respective halide chemistries; for Re 15 compounds are reported whereas for Tc there is only five.

For half a century, the halide chemistry of Tc has been defined by three compounds, TcF_6 , TcF_5 , and TcCl_4 , the first binary Tc bromides TcBr_3 and TcBr_4 were not reported until 2009. The absence of Tc divalent and trivalent chlorides as well as binary iodides is surprising considering the existence of such compounds for all of the elements surrounding Tc. The common synthetic routes used to obtain binary halides of the neighboring elements, e.g., sealed tube reactions between elements and flowing gas reactions between a molecular complex and HX gas ($X = \text{Cl}, \text{Br}, \text{I}$) had not been reported for Tc. Using these routes, the halide chemistry of Tc is revisited. In this dissertation, the

preparation, structure, and properties of new binary Tc halides is described and their chemistry compared to neighboring element analogs. This allows for a better understanding of the fundamental chemistry of Tc and the physicochemical trends within the periodic table.

Chapter 2

Experimental Methods and Materials

This chapter will provide detailed information on the experimental methods, materials, and instrumentation used for the preparation and characterization of binary Tc halides. In section 2.1, reagents and materials will be presented. Section 2.2 will be devoted to the experimental procedures used for synthesizing the necessary Tc precursors, this includes the purification of ammonium pertechnetate, the preparation of metallic Tc and $\text{Tc}_2(\text{O}_2\text{CCH}_3)_4\text{Cl}_2$. The synthetic techniques used for preparing binary Tc halides will be detailed in section 2.3. The instrumentation used for characterizing the synthesized materials will be presented in section 2.4.

2.1 Reagents and Materials

Caution! ^{99}Tc is a weak β -emitter ($E_{\text{max}} = 292 \text{ keV}$). All manipulations were performed in a laboratory designed for handling radioactive materials using efficient HEPA-filtered fume hoods, Schlenk and glovebox techniques and following locally approved radiochemistry handling and monitoring procedures. Laboratory coats, disposable gloves, and protective eyewear were worn at all times.

Technetium was purchased as ammonium pertechnetate (NH_4TcO_4) from Oak Ridge National Laboratory (ORNL). Other necessary chemicals listed in the experimental sections were either purchased from Sigma-Aldrich, Strem Chemicals Inc., Fischer, or Alfa Aesar and were used as received. The gases used in the experiments are presented in Table 2.1.

Table 2.1 Gases used for experiments.

Gas	Purity (%)	Manufacturer
Ar	99.998 %	Praxis
95% Ar, 5% H ₂	1 ppm – 99.999%	Praxis
HX (X = Cl, Br)	≥ 99.0%	Sigma-Aldrich
HI	99.9%	Matheson-Trigas
Cl ₂	≥ 99.5%	Sigma-Aldrich

The Pyrex tubes (L = 1 m, 10 mm outer diameter, 7 mm inner diameter) and fused silica (quartz) tubes (L = 1 m, 10 outer diameter, 8 inner diameter) used for the sealed tube reactions (refer to sections 2.3.1 and 2.3.3) were obtained from Chemglass, Inc. The composition of the Pyrex is: SiO₂ 83.34%, B₂O₃ 11.19%, Na₂O 4.08%, Al₂O₃ 1.33%, K₂O 0.04%.

The furnace used in the preparation of Tc metal, in the sealed tube and flowing gas reactions was a Thermo Fisher Scientific Lindberg/Blue M Mini-Mite clamshell furnace. This furnace allows to performed experiments in temperature up to 1100 °C.

2.2 Preparation of Starting Materials

The Tc precursors used in the preparation of Tc binary halides are Tc metal and Tc₂(O₂CCH₃)₄Cl₂. Technetium metal was used in sealed tube reactions between the elements (Cl₂, Br₂ and I₂) at elevated temperature. The compound Tc₂(O₂CCH₃)₄Cl₂ was used in flowing gas reaction with HX(g) (X = Cl, Br, I). Both compounds, Tc metal and Tc₂(O₂CCH₃)₄Cl₂, originate from NH₄TcO₄, the only commercially available Tc precursor. Ammonium pertechnetate, purchased from ORNL, is an impure black solid.

The impurity is likely TcO_2 , which is likely produced from the radiolytic autoreduction of NH_4TcO_4 . Prior to use in synthetic chemistry, the impure NH_4TcO_4 was purified.

2.2.1 Purification of Ammonium Pertechnetate

The procedure of purification is applicable from milligram to gram amounts; it can be completed using either a rotary evaporator (rotavap) or directly on a hotplate in an Erlenmeyer flask.

With the rotavap, the impure black solid (785.0 mg) was transferred to 100 mL round bottom flask (RBF) and deionized H_2O (5 mL), NH_4OH (0.5 mL), and H_2O_2 (0.4 mL) were added. A thin layer of grease was applied to the rim of the RBF connected to the rotavap, and the RBF was lowered into a mineral oil bath. The RBF was heated to ebullition and the solution boiled for 15 minutes. After the reaction, the contents were put under vacuum, the solution was slowly evaporated and a white solid (NH_4TcO_4) precipitated. The solid was then washed with an aliquot of *i*-PrOH (2 mL x 2) and diethyl ether (2 mL x 2). The solid was dried under a light flux of Ar(g) and using a handheld heat gun. The white solid (782.0 mg, 4.320 mmol) was transferred to a glass vial and stored for future use.

Using a hotplate and an Erlenmeyer flask, a weighted amount of the black solid (204.0 mg) was transferred to a 50 mL Erlenmeyer flask containing a small Teflon magnetic stir bar. The solid was suspended into deionized H_2O (2.5 mL) and NH_4OH (130 μL) and H_2O_2 (200 μL) were added. Using a hotplate, the suspension was heated to its boiling point. As the solid dissolved, the color of the solution changed from brown to a pale yellow. When the black solid was solubilized, the reaction was continued for 10 minutes at temperature. The volume of solution was evaporated down to 0.5 mL under a

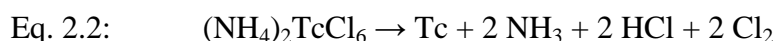
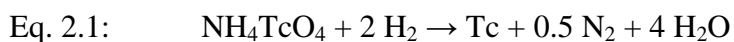
flux of Ar(g) and a white solid was precipitated; the remaining solution was removed via pipette from the precipitate. The solid (Figure 2.1) was then washed with a small amount of *i*-PrOH (2 mL x 2) and diethyl ether (2 mL x 2). The solid was taken to dryness under a light flux of Ar(g) and a handheld heat gun. The compound (138.0 mg, 0.762 mmol) was transferred to a glass vial for storage. Ammonium pertechnetate was characterized by UV-visible spectroscopy in water; the TcO_4^- exhibits characteristic bands at 244 nm and 288 nm (see section 1.2).



Figure 2.1. Purification of NH_4TcO_4 starting with the impure material from ORNL (left) to purified NH_4TcO_4 (right).

2.2.2 Technetium Metal

Technetium metal can be prepared by thermal decomposition of NH_4TcO_4 (Eq.2.1) or $(\text{NH}_4)_2\text{TcCl}_6$ (Eq. 2.2) under flowing $\text{H}_2(\text{g})$ at elevated temperatures. In this work, Tc metal used for the preparation of binary halides has been primarily obtained from the decomposition of NH_4TcO_4 under $\text{H}_2(\text{g})$.



For the decomposition of NH_4TcO_4 under $\text{H}_2(\text{g})$, a sample of NH_4TcO_4 (782.0 mg, 4.320 mmol) was transferred to an 8-cm-long quartz boat using a disposable funnel. The quartz boat was then inserted into a quartz tube situated into the middle of a 50-cm-long quartz tube fitted with Solv-Seal end joints in the clamshell furnace. The flowing gas apparatus was purged with $\text{H}_2(\text{g})$ for 15 minutes at room temperature, and then the temperature was increased to 750 °C (10 °C /min) and held there for two hours. Following the reaction, the contents were cooled to room temperature under a constant flow of $\text{H}_2(\text{g})$. The sample was collected as a fine grey powder (Figure 2.2) into a glass vial using a disposable funnel (355.0 mg, 3.586 mmol). Yield: 83.0%. The compound was characterized by Powder X-ray Diffraction (PXRD), which shows the presence of hexagonal close-packed (hcp) metallic Tc as a single phase.

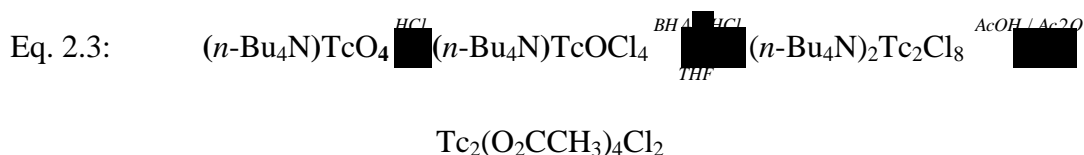
For the decomposition of $(\text{NH}_4)_2\text{TcCl}_6$ under $\text{H}_2(\text{g})$, a quantity of $(\text{NH}_4)_2\text{TcCl}_6$ (529.7 mg, 1.522 mmol) was transferred to a quartz boat and inserted into a quartz tube flowing as setup. The system was purged with $\text{H}_2(\text{g})$ for 15 minutes, and the temperature was increased (10 °C/min) to 750 °C. Around 395°C, a color change from yellow to black (i.e. TcN_x) was observed and a volatile white solid (i.e. NH_4Cl) was sublimed on the quartz tube outside of the furnace. At approximately 500 °C, a second color change was observed and the black solid turned to a pale grey, i.e., Tc metal (Figure 2.2). The reaction was continued for 2 hours at 750 °C after which the sample was cooled to room temperature under a constant flow of $\text{H}_2(\text{g})$. The grey metal (150.6 mg, 1.521 mmol) was transferred to a glass vial using a disposable funnel. Yield: 99.9%.



Figure 2.2. Technetium metal obtained after the decomposition of NH_4TcO_4 under $\text{H}_2(\text{g})$ at $750\text{ }^\circ\text{C}$.

2.2.3 Preparation of Bis(μ -tetraacetate)dichloride Ditechnetate

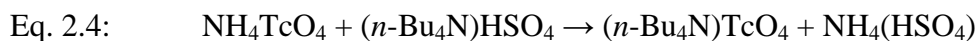
The preparation of $\text{Tc}_2(\text{O}_2\text{CCH}_3)_4\text{Cl}_2$ is a multistep procedure (Eq. 2.3) which involves the successive reduction of $(n\text{-Bu}_4\text{N})\text{TcO}_4$ to $(n\text{-Bu}_4\text{N})\text{TcOCl}_4$ and to $(n\text{-Bu}_4\text{N})_2\text{Tc}_2\text{Cl}_8$ followed by treatment of $(n\text{-Bu}_4\text{N})_2\text{Tc}_2\text{Cl}_8$ in refluxing acetic acid/acetic anhydride.



The preparations of the precursors involved in the multistep reaction are presented below.

a. Tetrabutylammonium Pertechetate

Tetrabutylammonium pertechnetate (i.e., $(n\text{-Bu}_4\text{N})\text{TcO}_4$) is best prepared from the precipitation of an aqueous NH_4TcO_4 solution with $(n\text{-Bu}_4\text{N})\text{HSO}_4$ (Eq. 2.4).

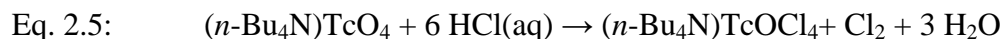


A quantity of impure NH_4TcO_4 (1.044 g, ~ 5.768 mmol) was transferred into a 25 mL Erlenmeyer flask with a disposable funnel. Deionized H_2O (20 mL), NH_4OH (1 mL), and H_2O_2 (0.5 mL) were added to the flask and the suspension was gently heated until

complete dissolution. The resulting liquid was evenly pipetted into six 15 mL glass centrifuge tubes (3 mL/tube). To each tube, 3 mL of an aqueous solution of tetrabutylammonium bisulfate (3.15 mg in 12 mL) was added and a fluffy white solid ((*n*-Bu₄N)TcO₄) was instantaneously precipitated. Each tube was centrifuged and the supernatant was removed via pipette. The remaining solid was washed with cold H₂O (3 mL x 2) and the tubes were dried at 90 °C overnight. The resulting vivid white solid (2.201 g, 5.429 mmol) (Figure 2.3) was scraped from the tubes and transferred directly to a glass vial for storage. Yield: 94.1%.

b. Tetrabutylammonium Oxotetrachlorotechnetate

Tetrabutylammonium oxotetrachlorotechnetate (i.e., (*n*-Bu₄N)TcOCl₄) is best prepared from the reduction of (*n*-Bu₄N)TcO₄ with cold 12 M HCl(aq) (Eq. 2.5).

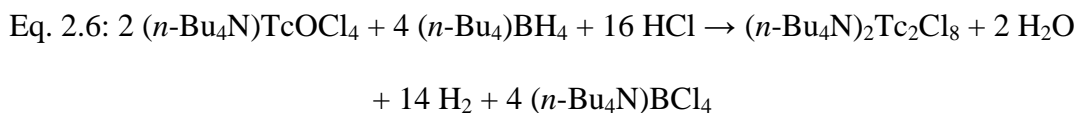


A weighted quantity of (*n*-Bu₄N)TcO₄ (2.201 g, 5.429 mmol) was evenly transferred into six 15 mL glass centrifuge tubes (~ 367 mg/tube). To each of the glass centrifuge tubes, 3 mL of cold (0 °C) 12 M HCl(aq) was added. The tubes were shaken for 20 minutes, evolution of chlorine gas and color changes from white to orange/red and finally to a yellow/green accompanied by the precipitation of a green solid were observed. After 20 minutes, the tubes were centrifuged and the supernatant removed using a disposable glass pipette. The green solid was then washed with *i*-PrOH (2 mL x 2) and recrystallized twice from a 1:4 mixture of acetone (2 mL) and diethyl ether (8 mL). The resulting solid was washed a final time with diethyl ether (10 mL). The remaining solvent was removed under a slight flux of Ar(g) and the solid was taken to dryness with a handheld heat gun. The solid was collected as a silvery-grey powder (*n*-Bu₄N)TcOCl₄ (1.894 g, 3.788 mmol)

and transferred to a glass vial via a disposable funnel for storage (Figure 2.3). Yield: 70.0%. The compound was characterized by UV-visible, infrared and EXAFS spectroscopy. The UV-visible spectra of (*n*-Bu₄N)TcOCl₄ in HCl exhibits the bands at 234 nm and 293 nm.

c. Bis(tetrabutylammonium) Octachloroditechnetate

The compound (*n*-Bu₄N)₂Tc₂Cl₈ was prepared by a modification of the procedure reported by Preetz et al. [69, 101] and was obtained after the reduction of (*n*-Bu₄N)TcOCl₄ by (*n*-Bu₄N)BH₄ in THF followed by acidification of the products with HCl(g) in CH₂Cl₂ (Eq. 2.6).

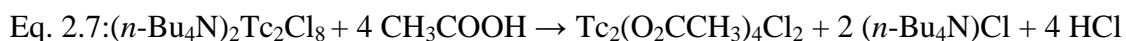


The preparation was performed in a 250 mL round-bottomed flask equipped with a three-hole rubber stopper. The compound (*n*-Bu₄N)TcOCl₄ (933.0 mg, 1.866 mmol) was dissolved in THF (20 mL) under an Ar(g) atmosphere. A solution of (*n*-Bu₄N)BH₄ (967.0 mg, 3.764 mmol) in THF (20 mL) was slowly added dropwise and reacted for 5 minutes. The resulting brown solution was decanted from the precipitate, and the remaining brown solid was washed with THF (10 mL x 2) and ether (20 mL x 2); the resulting solid was dried under an Ar(g) flux yielding a yellow-green solid. Dichloromethane (20 mL) was added to the flask, the yellow-green solid immediately dissolved and the solution was treated with a slight flux of HCl(g) for 7 minutes. An immediate change of color from yellow-green to emerald-green was observed. After the reaction, hexane (60 mL) was added to the flask and green (*n*-Bu₄N)₂Tc₂Cl₈ was precipitated. The supernatant was removed and the solid was washed with hexane (20 mL) and ether (20 mL) and dried

under a stream of Ar(g). The solid was dissolved in 8 mL of acetone and transferred to four 15 mL glass centrifuge tubes (2 mL/tube) and precipitated with the addition of an equal volume of diethyl ether (2 mL/tube). The tubes were centrifuged and the solids were isolated followed by a second recrystallization in a 1:1 mixtures of acetone and ether, yielding pure $(n\text{-Bu}_4\text{N})_2\text{Tc}_2\text{Cl}_8$ (333.0 mg, 0.345 mmol) (Figure 2.3). Yield: 37.0%. The compound was characterized by UV-visible spectroscopy in CH_2Cl_2 and exhibits the bands characteristic at 330 nm and 670 nm.

d. Bis(μ -tetraacetate)dichloride Ditechnetate

The compound $\text{Tc}_2(\text{O}_2\text{CCH}_3)_4\text{Cl}_2$ was prepared by a modification of the procedure reported by Preetz et al. [102] and was obtained after treatment of $(n\text{-Bu}_4\text{N})_2\text{Tc}_2\text{Cl}_8$ in refluxing acetic acid/ acetic anhydride (Eq. 2.7).



A quantity (728.0 mg, 0.755 mmol) of $(n\text{-Bu}_4\text{N})_2\text{Tc}_2\text{Cl}_8$ was added to a 25 mL Schlenk flask using a disposable funnel. To the flask, an aliquot (6 mL) of a 1:4 mixture of glacial acetic acid and acetic anhydride was added and lightly refluxed. The green solid slowly dissolved resulting in a greenish yellow solution. After several minutes, a dark precipitate was formed in the solution and the flask was quickly cooled to room temperature. The solid and supernatant were pipetted as a suspension into two 10 mL glass centrifuge tubes. The tubes were centrifuged and the liquid was removed from the solid. The crimson solid ($\text{Tc}_2(\text{O}_2\text{CCH}_3)_4\text{Cl}_2$) was washed with acetone (3 mL x 2) and diethyl ether (3 mL x 2). The remaining solvent was removed under a light flux of Ar(g) and taken to dryness with a handheld heat gun. The red powder (242.1 mg, 0.480 mmol) (Figure 2.3) was transferred directly from the centrifuge tubes into a glass vial for storage. Yield:

63.5%. Overall yield based on $\text{NH}_4\text{TcO}_4 = 15.5\%$. The compound was characterized by infrared spectroscopy (see section 4.1.2.2).



Figure 2.3. A: $(n\text{-Bu}_4\text{N})\text{TcO}_4$ after drying at $90\text{ }^\circ\text{C}$. B and C, respectively: $(n\text{-Bu}_4\text{N})\text{TcOCl}_4$ and $(n\text{-Bu}_4\text{N})_2\text{Tc}_2\text{Cl}_8$ after recrystallization with acetone:diethyl ether. D: $\text{Tc}_2(\text{O}_2\text{CCH}_3)_4\text{Cl}_2$ after diethyl ether washes.

2.3 Experimental Procedures

Three solid-state techniques were used for synthesizing binary Tc halides: 1) sealed tube reactions between Tc metal and the elements (Cl_2 , Br_2 and I_2) at elevated temperatures, 2) reaction of $\text{Tc}_2(\text{O}_2\text{CCH}_3)_4\text{Cl}_2$ with a flowing $\text{HX}(\text{g})$ ($\text{X} = \text{Cl}, \text{Br}, \text{I}$), and 3) thermal decomposition of a binary halide under vacuum. Each of these techniques will be detailed in the following sections.

2.3.1 Sealed Tube Reactions between the Elements

Binary Tc halides can be prepared from the reaction of fresh Tc metal with the Cl_2 , Br_2 , or I_2 in a sealed tube. This technique allows for various conditions to be utilized,

such as amount of reactants, temperatures, and pressures. The reactants can be varied from sub-stoichiometric to excess. Reactions performed from room temperature up to 500 °C are done in Pyrex tubes. Temperatures higher than 500 °C to 1100 °C are performed in quartz tubes. The pressure from atmospheric pressure up to ~ 5 atmospheres within the reaction tube can be controlled depending on the amount of reactants.

Preparing sealed tubes for reactions of the elements can be completed using a Schlenk line (Figure 2.4); this equipment allows for manipulation of the chemicals free of oxygen under specific gas, e.g., Cl₂, or under vacuum. In a typical preparation, technetium metal was transferred to a Pyrex (L = 30 - 45 cm) or quartz (L = 30 - 45 cm) tube using a disposable paper funnel. The tube and its contents were connected to the Schlenk line using a piece of thick-walled Tygon tube and the contents placed under vacuum. The tube was flamed under vacuum to remove any residual oxygen and moisture and cooled to room temperature. To the resulting tube, the desired halogen was introduced as the element.

The Cl₂ was introduced as a gas. A lecture bottle was connected to the Schlenk line equipped with a bubbler of CCl₄ and the gas was backfilled into the tube. To remove any remaining oxygen, an alternation of the vacuum and backfilling with the gas was performed three times. Finally, the gas and metal can be isolated from the Schlenk line, the end of the tube was cooled in liquid nitrogen and the gas condensed on the metal. The resulting tube and its contents were flame-sealed under partial vacuum.

For solid I₂ or liquid Br₂, the flamed tube containing the metal was backfilled with Ar(g) and removed from the Schlenk line; the liquid was added with a volumetric micropipette and the solid added with a disposable funnel directly into the tube. The tube

and its contents were connected to the Schlenk line, the tube was backfilled with Ar(g), the end of the tube cooled in liquid nitrogen (LN₂) and the contents condensed under an Ar(g) atmosphere. After the contents were condensed, a vacuum was introduced, the LN₂ Dewar was removed, and the contents were slowly allowed to warm to room temperature under dynamic vacuum (to remove any remaining O₂). Before the halide was volatilized under dynamic vacuum, the vacuum was switched off and the contents were put under inert atmosphere and condensed again. These steps were repeated a minimum of three times to remove any remaining oxygen. Finally, the contents were condensed, put under vacuum, and the tube flame-sealed (L ~ 18 cm). The resulting tubes with technetium metal and halide (Figure 2.5) were then placed inside of a 50-cm-long quartz tube fitted in a clamshell furnace and reacted under the desired conditions.

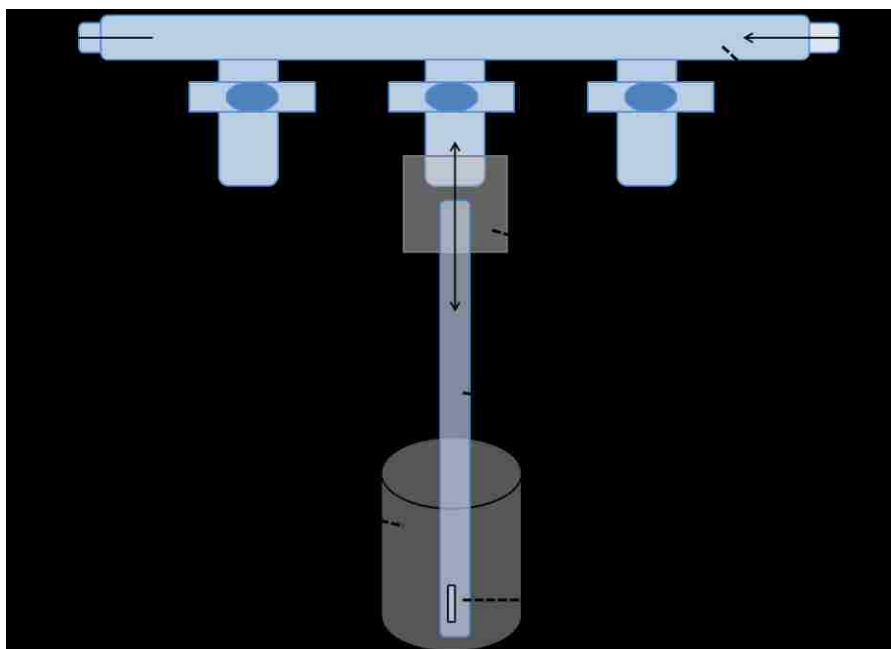


Figure 2.4. Experimental setup used to prepare sealed tubes: a) Schlenk line; b) connection from inlet gas (i.e., Ar or Cl₂); c) connection to vacuum pump; d) stopcock-controlled port; e) Teflon tubing; f) Pyrex or quartz reaction tube; g) liquid nitrogen dewar; h) solid sample.

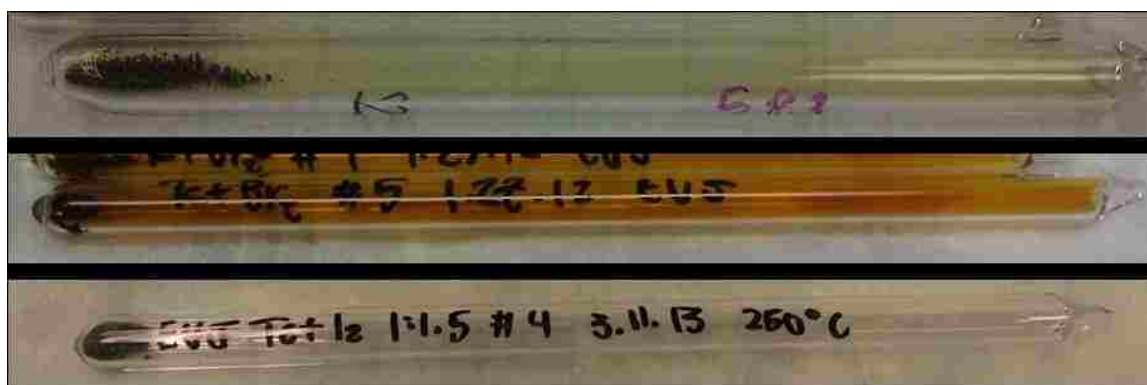
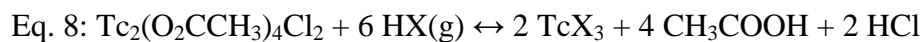


Figure 2.5. Flame-sealed Pyrex tubes of technetium metal with elemental Cl (top), Br (middle) and I (bottom) prior to reacting.

2.3.2 Reactions between $\text{Tc}_2(\text{O}_2\text{CCH}_3)_4\text{Cl}_2$ under Flowing $\text{HX}(\text{g})$

An alternative synthetic route for preparing binary transition metal halides is the reaction of a dinuclear acetate complex with flowing $\text{HX}(\text{g})$ ($\text{X} = \text{Cl}, \text{Br}, \text{I}$) (Equation 8). This reaction involves the exchange of the acetate ligands with halogen atoms. The starting complex for this reaction is $\text{Tc}_2(\text{O}_2\text{CCH}_3)_4\text{Cl}_2$. These reactions are performed at elevated temperatures to remove liberated acetic acid. Using this method, the compound can be prepared in weighable quantities with excellent yields.



Two experimental set-ups have been used to prepare Tc binary halides from the reaction of $\text{Tc}_2(\text{O}_2\text{CCH}_3)_4\text{Cl}_2$ and $\text{HX}(\text{g})$ ($\text{X} = \text{Cl}, \text{Br}, \text{I}$). The experimental set-up in Figure 2.6 has been used for the experiment under HCl gas. In this method, the starting Tc compound ($\text{Tc}_2(\text{O}_2\text{CCH}_3)_4\text{Cl}_2$) was evenly dispersed in an 8-cm-long quartz boat that inserted into a 50-cm-long quartz tube fitted with two Solv-Seal end joints and two gas inlets/outlets. The HCl reaction gas was connected to one end joint and a sulfuric acid bubbler to the opposite end joint. The quartz tube was placed in clamshell furnace. The tube was initially purged with the gas and followed by the reaction under the desired conditions. After completion, the reacted solid can be collected into a storage vial using a disposable funnel. This method has been applied for the preparation of $\alpha\text{-TcCl}_3$ (see section 4.1.2.1).

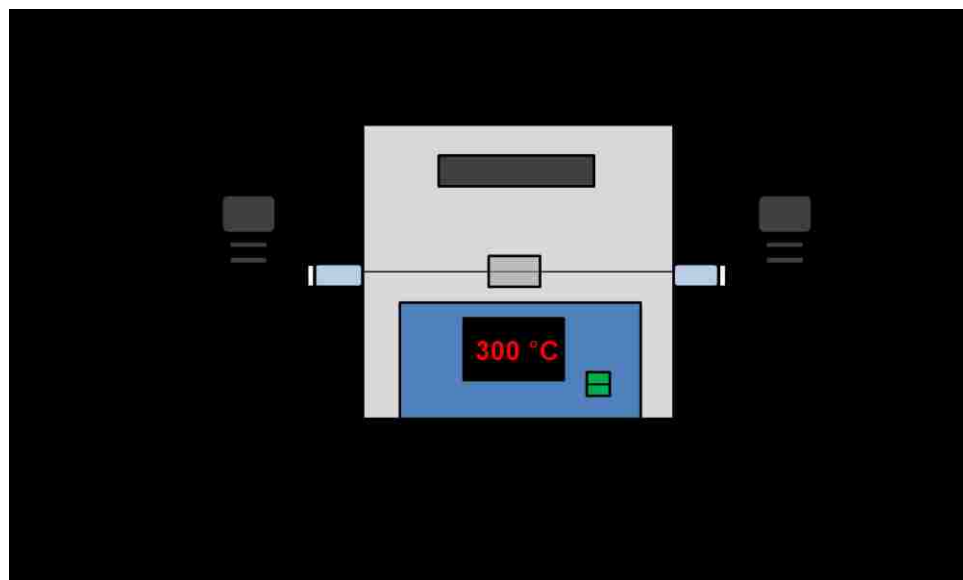


Figure 2.6. Experimental apparatus for flowing gas reactions using HCl gas: a) connection from inlet gas; b) Teflon-jointed glass connector; c) clamshell furnace; d) quartz tube; e) connection to bubbler filled with H₂SO₄.

A modification of the experimental set-up using for flowing gas reaction has been developed for the reaction with HX(g) (X = Br, I). In the new setup (Figure 2.7), the 50 cm long quartz tube fitted with Solv-Seal end joints and two gas inlets/outlets was used. The inlet was connected with Teflon tubing to a T-shaped stopcock controlling the flow of HX(g) or Ar(g), and the outlet was connected to a bubbler trap filled with concentrated H₂SO₄. The tube was placed in the clamshell furnace with a 8-cm-long quartz boat containing Tc₂(O₂CCH₃)₄Cl₂ located directly above the thermocouple of the furnace. For each reaction, the tube was initially purged with flowing Ar(g) and the temperature was increased to 150 °C and held there for a minimum of 10 min, after which the atmosphere was switched to HX(g) and the temperature was then increased (10 °C/min) to the desired temperature. This was done to prevent the premature reaction of HX(g) with the

compound, resulting in the release of acetic acid below its boiling point (117 °C). This method has been applied for the preparation of TcI_3 and $TcBr_3$ (see Chapter 4).

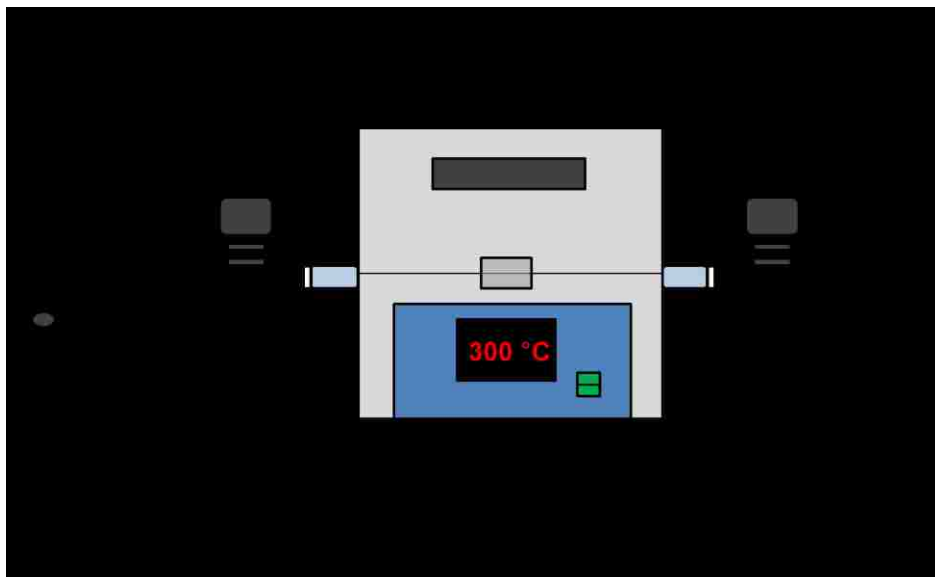


Figure 2.7. Experimental apparatus for flowing gas reactions using HX gas (X = Br, I): a) connection from $Ar(g)$; b) connection from HX(g) (X = Br or I); c) T-shaped stopcock; d) Teflon-jointed glass connector; e) quartz tube; f) clamshell furnace; g) connection to bubbler filled with H_2SO_4 .

2.3.3 Sealed Tube Vacuum Decompositions

In order to investigate the thermal behavior of Tc binary halides, sealed tube reactions were performed under vacuum at elevated temperatures. The starting Tc binary halide was inserted into a Pyrex or quartz tube with a disposal funnel, and the resulting tube and contents were connected to a Schlenk line (Figure 2.8 and Figure 2.9). The contents were put under vacuum, and the tube lightly flamed to remove any excess oxygen or moisture. The tube and its contents were flame-sealed under vacuum with or

without the use of liquid nitrogen. The resulting tube was placed in a quartz tube and reacted in a furnace under the desired conditions.



Figure 2.8. Sealing a Pyrex tube under vacuum on a high vacuum Schlenk line.

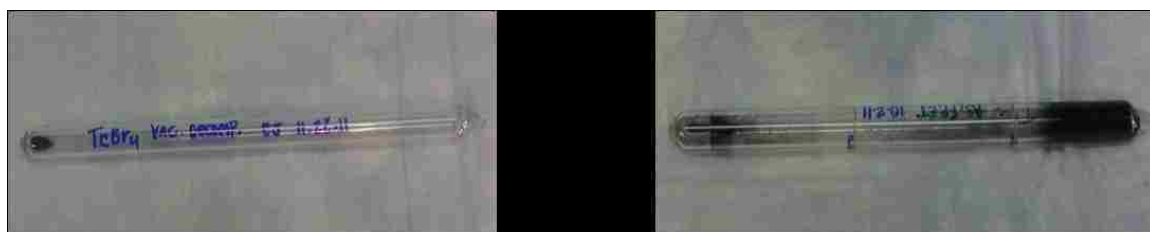


Figure 2.9. Vacuum sealed tube containing a binary technetium before (left) and after (right) thermal decomposition.

2.4 Instrumentation

Binary Tc halides were characterized by diffraction, microscopic and spectroscopic techniques and their physical properties measured (Figure 2.10).

Furthermore, the solid state and electronic structure as well as the physical properties of binary Tc halides were investigated by theoretical methods.

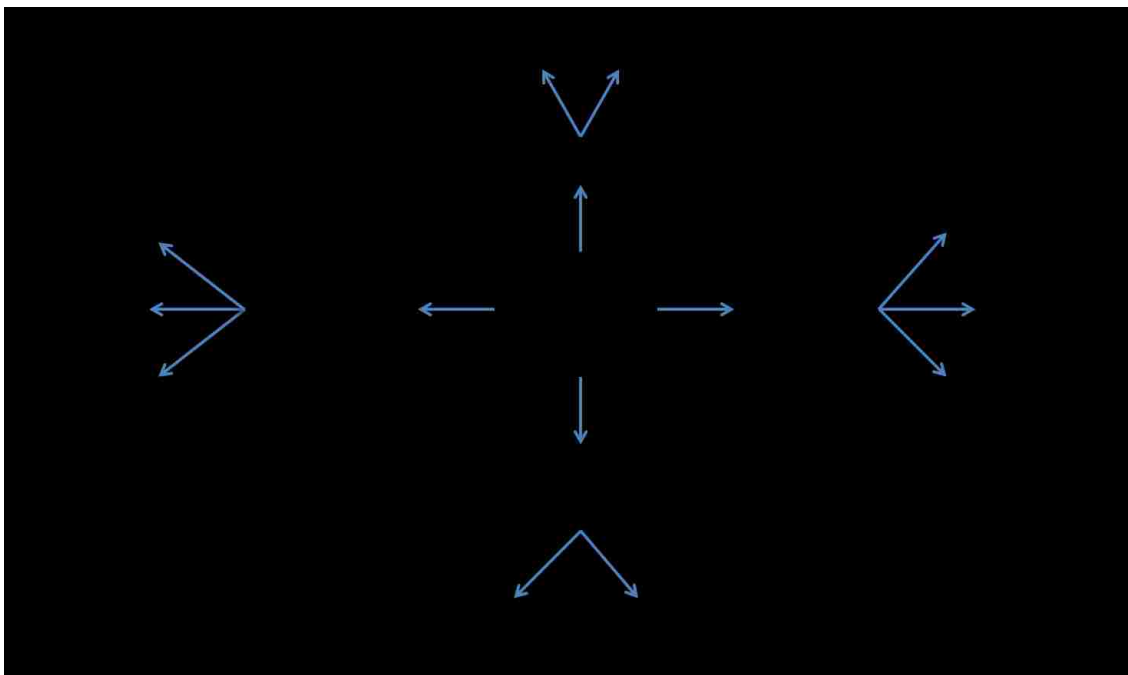


Figure 2.10. Flowchart of experimental characterizations and the instrumentations used in the studies of binary technetium halides.

Diffraction techniques

Single-Crystal X-ray Diffraction measurement were performed in collaboration with Dr. Paul M. Forster in the Department of Chemistry at UNLV, Dr. Brian Scott at Los Alamos National Laboratory, and Dr. Christos Malliakas in the Department of Chemistry at Northwestern University. This technique was used to determine the solid

state structures of the new synthesized materials. At UNLV, single-crystal XRD data were collected on a Bruker Smart Apex II system equipped with an Oxford nitrogen cryostream operating at 150 K. Crystals were mounted under Paratone on a glass fiber. Data processing was performed using the *Apex II* suite and an absorption correction performed with *SADABS*. Structure solution (direct methods) and refinement were carried out using *SHELX97* [103].

Powder X-ray Diffraction (PXRD) measurements were performed in collaboration with Dr. Thomas Hartmann in the Department of Engineering at UNLV. This technique was used for identification of the crystalline phases present in the sample. PXRD patterns were obtained using a Bruker D8 advanced diffractometer employing Cu $K\alpha_1$ X-rays from 10 to 120° (2 θ) with a step size of 0.008° (2 θ) and 0.65 s/step. The PXRD patterns were quantified by Rietveld analysis using *Topas 4.0* software. The samples (~10–20 mg) were ground in an agate mortar and dispersed on a low-background silicon disk sample holder, covered with a radiological containment dome, and placed in the instrument for measurement.

Spectroscopy techniques

X-ray Absorption Fine-Structure (XAFS) spectroscopy measurements were performed in collaboration with Dr. Frederic Poineau at UNLV and Dr. Sungsik Lee at Argonne National Laboratory. X-ray Absorption Near-Edge Structure (XANES) spectra can give information about the oxidation state of the absorbing atoms [104], while the Extended X-ray Absorption Fine Structure (EXAFS) spectrum contains information on the chemical environment around the absorbing atoms [101, 105]. The XAFS measurements were done at the Advanced Photon Source (APS) at the BESSRC-CAT 12

BM station at Argonne National Laboratory. Synthesized compounds were diluted in boron nitride, ground in a mortar, and placed in an aluminum sample holder equipped with Kapton windows. The XAFS spectra were recorded at the Tc-K edge (21,044 eV) in transmission and/or fluorescence mode at room temperature using a 13 element germanium detector. A double crystal of Si (111) was used as a monochromator. The energy was calibrated using a molybdenum foil (Mo-K edge = 20,000 eV). The EXAFS spectra were extracted using *Athena* software, and data analysis was performed using *Winxas* [106]. For the fitting procedure, the amplitude and phase shift functions were calculated by *FEFF* 8.2 [107]. Input files were generated by *Atoms* [108]. Adjustments of the k^3 -weighted EXAFS spectra were under the constraints $S_0^2 = 0.9$. For the XANES spectra, the energy of the absorption edge was determined using the first derivative method.

Attenuated Total Reflectance FT-IR (ATR- FT-IR) spectra were obtained on a Varian Excalibur spectrometer using a KBr beam splitter and an integrated Durasampler diamond ATR. This technique was primarily used to probe the presence of acetate and organic ligands in the reaction products.

UV-visible spectra were recorded in a quartz cell (1 cm) on a Cary 6000i double beam photospectrometer. This was used for determining purity of starting materials and Tc elemental concentrations using the Beer-Lambert law.

Microscopy techniques

Scanning Electron Microscopy (SEM) and Energy Dispersive X-Ray Spectroscopy (EDX) were performed in collaboration with Dr. Minghua Ren in the microscopy laboratory at UNLV. Microscopic techniques can give information on the

morphology of the sample and on their composition. Scanning electron microscopy imaging and EDX measurements were performed on a JEOL model JSM-5610 scanning electron microscope equipped with secondary-electron and backscattered-electron detectors.

Transmission Electron Microscopy (TEM) was performed in collaboration with Dr. Longzhou Ma at the Harry Reid Center at UNLV. TEM and EDX were performed on a TECNAI-G2-F30 Supertwin transmission electron microscope with a 300 keV field emission gun. The elemental composition of the sample was analyzed by energy-dispersive X-ray spectroscopy under the scanning transmission electron microscopy (STEM) mode. For the STEM/EDS mode, a 0.2 nm electron probe was used to examine a dedicated area of the sample. The TEM samples were prepared by a solution-drop method. A total of 2 - 5 mg of the sample material was ground with hexane in an agate mortar. After slight shaking, one drop of the suspension was placed onto a 3-mm-diameter carbon-coated copper grid using a small-tipped transfer pipette. The liquid was evaporated at room temperature, leaving the fine particulate sample deposited on the carbon film.

Physical properties

Physical properties including magnetic and conductivity measurements were performed in collaboration with Dr. Andrew Cornelius and Mr. Daniel Antonio in the Department of Physics and Astronomy at UNLV and with Dr. Christos D. Malliakas in the Department of Chemistry at Northwestern University. At UNLV, magnetic measurements were performed using a Quantum Design PPMS. The sample was prepared by placing a weighted quantity of powder (~ 30 mg) in the bottom of a gelatin capsule

packed with cotton. The capsule was wrapped and sealed with Kapton tape and firmly inserted into the bottom of a plastic straw, which was fitted onto the sample holder. At Northwestern University, magnetic measurements were performed using a Quantum Design Magnetic Properties Measurement System (MPMS) superconducting quantum interference device (SQUID) magnetometer. Temperature-dependent magnetic susceptibilities were measured in a gelatin capsule containing powdered sample (~ 20 mg).

Band gap measurements were performed at Northwestern University using a Nicolet 6700 IR spectrometer equipped with a diffuse-reflectance kit was used for the 4000-400 cm^{-1} spectral region. The spectrum was referenced against a metallic mirror used as a non-absorbing reflectance standard. The generated reflectance-versus-wavelength data were used to estimate the band gap of the material by converting reflectance to absorbance data according to the Kubelka-Munk equation: $\alpha/S = (1-R)^2/(2R)$, where R is the reflectance and α and S are the absorption and scattering coefficients, respectively [109].

Charge transport measurements were performed at Northwestern using a four-probe high-temperature electrical resistivity measurements device under vacuum from room-temperature to 530 K on single crystal. A custom-made resistivity apparatus equipped with a nanovoltmeter (Keithley 2182A), precision direct current (DC) source (Keithley 6220), and a high- temperature vacuum chamber controlled by a temperature controller (K-20 MMR Technologies) was used. Data acquisition was computer controlled by custom-written software [110]. Seebeck coefficient measurements were performed using a commercial MMR SB-100 Seebeck Measurement System under

vacuum between 308 and 530 K. The sample was mounted with silver paste in parallel with a constantan reference to monitor the temperature difference across the samples.

Technetium elemental analyses

The compositions of the materials were ascertained by technetium elemental analysis. In this method a known mass of sample (~ 10 mg) was suspended in a known volume of concentrated acid (HCl or HClO₄) or in NH₄OH/H₂O₂ solution and the solution warmed (100 °C) until complete dissolution of the sample. After cooling to room temperature, the Tc concentration can be determined by UV–visible spectroscopy in HCl using the absorbance at 340 nm of the TcCl₆²⁻ anion [111] or by liquid scintillation counting (LSC) using a Packard 2500 scintillation analyzer. The scintillation cocktail was ULTIMA GOLD ABTM (Packard).

Theoretical calculations

Theoretical calculations were used to analyze the solid state and electronic structures, as well as the physical properties (magnetic susceptibility and conductivity) of technetium binary halides. Density Functional Theory (DFT) computational calculations were performed by Dr. Phil Weck at Sandia National Laboratories, Dr. Eunja Kim in the Department of Physics and Astronomy at UNLV, and Dr. Justin Grant and Dr. Laura Gagliardi at the University of Minnesota. First-principles total energy calculations were performed using the DFT as implemented in the Vienna *ab initio* simulation package (VASP) [112]. The exchange-correlation energy was calculated using the generalized gradient approximation (GGA) with the parameterization of Perdew and Wang (PW91) [113]. The PW91 functional was found to accurately reproduce structural parameters observed experimentally for Tc halide systems [89, 100]. Natural Bond Order occupancy

(NBO) analysis was performed using the DFT implementation of the Gaussian 09 software package [114]. Structural relaxation was performed without symmetry constraints and the exchange-correlation energy was calculated using the GGA and the Becke 3-parameter, Lee, Yang and Parr [115] (B3LYP) hybrid functional. The Dunning-Huzinaga valence double-zeta basis set [116] (D95V) was used for Cl atoms in combination with the Stuttgart/Dresden effective core potentials [117] (SDD ECPs) for the Tc metal atoms. The effective bond order concept was employed in the discussion of the Tc-Tc chemical bonding [118].

Chapter 3

Technetium Tetrachloride and Tetrabromide

This chapter includes the reinvestigation of the chemistries of TcCl_4 (section 3.1) and TcBr_4 (section 3.2). For TcCl_4 , its synthesis has been revisited, its crystal structure redetermined and its magnetic properties measured. The synthetic and coordination chemistry of TcCl_4 are discussed and compared to other transition metal tetrachlorides. The thermal properties of TcCl_4 and TcBr_4 were studied under vacuum at elevated temperatures, their decomposition products were characterized by diffraction and microscopic techniques.

3.1 Technetium Tetrachloride

3.1.1 Introduction

Transition-metal tetrahalides exhibit a wide range of structural and physical properties [1, 2]. For Tc, two tetrahalides have been reported: TcCl_4 and TcBr_4 [32, 97]. In comparison, its heavier congener, Re, forms tetrahalides with fluorine, chlorine, bromine, and iodine [119, 120, 121, 122]. Of the second-row transition metals, Tc is the last element in the series to form an isolable, structurally characterized tetrachloride. Though the structure of TcCl_4 has been determined (see section 1.4.2), there is a discrepancy between the two sets of unit cell parameters published for this compound [91]. Theoretical calculations on the structure of TcX_4 ($X = \text{F}, \text{Cl}, \text{Br}, \text{I}$) have been performed and for TcCl_4 the calculated Tc-Cl distances are within $\sim 1\%$ of the published experimental values [89].

Previous magnetic studies of TcCl_4 gave an effective magnetic moment of 3.14 μB [92]. This value is significantly lower than the theoretical one, *viz.*, 3.87 μB , expected for a spin-only d^3 paramagnet. The low value reported for the magnetic moment and the lack of characterization raise questions about the purity of the TcCl_4 sample analyzed [92]. To the best of our knowledge, neither a powder X-ray diffraction pattern nor any microscopy characterization has been reported for TcCl_4 . The chemistry of TcCl_4 is also sparse, for example there are no reports on its thermal behavior at elevated temperatures. For other transition-metal tetrahalides, thermal decomposition and/or disproportionation often occurs and lead to divalent and trivalent binary halides [123, 124]. Similarly, TcCl_4 seemed a likely precursor to the Tc(II) or -(III) binary chlorides.

In this work, a new method for the preparation of TcCl_4 and its characterization by spectroscopic (EXAFS, EDX), microscopy techniques (SEM), and PXRD are reported. Its solid-state structure has also been redetermined by single crystal XRD. Its magnetic properties have also been measured. Finally, the thermal behavior of TcCl_4 was investigated, and its decomposition products were characterized [125].

3.1.2 Experimental Details

Preparation of TcCl_4 . Technetium metal (20.1 mg, 0.203 mmol) was placed in a Pyrex tube ($L = 43$ cm), connected to a Schlenk line, and flamed under vacuum. After backfilling with Cl_2 ($\text{Tc}:\text{Cl}$, $\approx 1:6$) at ambient temperature and pressure, the tube was isolated from the Schlenk line and the lower end of the tube was cooled in liquid nitrogen to condense the gas. The tube was flame-sealed ($L = 18$ cm) and placed in an open-ended quartz tube packed with glass wool at each end. The tubes were inserted into a clamshell furnace with the metal end of the sealed tube located in the center. The temperature was

increased to 450 °C (7.5 °C/min) and held at that temperature for 14 hours. After cooling to room temperature, a reddish-black crystalline powder was observed at the cool end of the tube together with a red amorphous film. The crystalline powder was removed, placed in a second Pyrex tube of identical dimensions as the first, sealed under a Cl₂ atmosphere (Tc:Cl, ■1:6), and reacted as before. The reddish-black powder (33.8 mg, yield: 69%) and several small red needles (■1 mg) in the middle of the tube were recovered. The purity of the compound was confirmed by PXRD (*vide infra*).

Thermal Decomposition of TcCl₄ to TcCl₂. A sample of TcCl₄ (39.5 mg, 0.164 mmol) was placed in a 30-cm-long Pyrex tube, and the tube was then evacuated and sealed at 18 cm. The tube was placed in a tube furnace for 14 hours at 450 °C with the solid at the center. After cooling to room temperature, the reaction yielded a black crystalline powder (6.2 mg) at one end of the tube, lustrous black needles in the middle, and a black amorphous film at the coolest end. The resulting products were analyzed by SCXRD, PXRD and SEM.

Thermal Decomposition of TcCl₄ to α-TcCl₃. A sample of TcCl₄ powder (23.2 mg, 0.096 mmol) was placed in a 30-cm-long Pyrex tube, and the tube was then evacuated, sealed at 18 cm, and reacted for 2 hours at 450 °C. After the reaction, red needles and small purple hexagonal plates were located near the center of the tube, an amorphous black film was observed at the coolest end of the tube, and no remaining product was seen at the hottest portion of the tube. The hexagonal plates were characterized by SCXRD and SEM (*vide infra*).

3.1.3 Results and Discussion

3.1.3.1 Synthesis of TcCl_4

Technetium tetrachloride was synthesized in a sealed glass tube from the elements at elevated temperature. A subsequent treatment of the resulting powder with excess chlorine at 450 °C for 14 hours was required to yield pure, single crystalline TcCl_4 phase. In comparison to the flowing gas system, sealed tube reactions give somewhat lower yields but avoid the generation of volatile Tc oxychlorides (i.e., TcO_3Cl and TcOCl_4), which are observed even in the presence of low-oxygen-content Cl_2 streams [46]. It also represents a safe, convenient way to handle and manipulate small quantities of a volatile radioactive sample.

The behavior of Tc metal in a Cl_2 atmosphere can be compared to that of other second- and third-row transition metals. Tetrachlorides are obtained directly from the reactions of Cl_2 with Zr [126], Hf [126], Os [127, 128], and Pt metal [129]. Reacting Mo metal and excess Cl_2 yields MoCl_5 . The β - MoCl_4 compound is obtained from the reaction of the pentachloride with MoCl_3 in a sealed tube at 250 °C [130], while the α - MoCl_4 is synthesized by refluxing MoCl_5 with tetrachloroethylene and carbon tetrachloride [131]. Chlorination of W metal yields WCl_6 , which can then be reduced with Al to form the tetrachloride [132]. For Re, the direct chlorination of the metal results in a mixture of ReCl_5 and ReCl_6 [133, 134]. Two phases of Re tetrachloride have been identified: β - ReCl_4 [135] and γ - ReCl_4 [136]. The β -phase, which is the only structurally characterized phase, was obtained via the reaction of ReCl_5 with either ReCl_3 or SbCl_3 [133]. Ruthenium and Rh trichlorides are both formed from the reaction of the elements, and neither element forms a stable tetrachloride in the solid state [137, 138].

3.1.3.2 Characterization of TcCl_4

SEM and TEM Analysis

The EDX spectrum of TcCl_4 (Figure 3.1) shows the presence of the Tc K_α , Tc L_α , and Cl K_α lines, confirming the formation of a binary Tc chloride. The integrated areas of the Cl K_α and Tc K_α lines were used to calculate an atomic ratio of chlorine to Tc of 3.99(5). SEM images (Figure 3.2) reveal the morphology of the tetrachloride as being a combination of small rods and larger rectangular plates ranging in size from 10 to 100 μm . These crystalline rods and plates are typically found in clusters throughout the powder. After thermal decomposition of TcCl_4 , the rods contained in the initial powder are transformed into crystals with other morphologies.

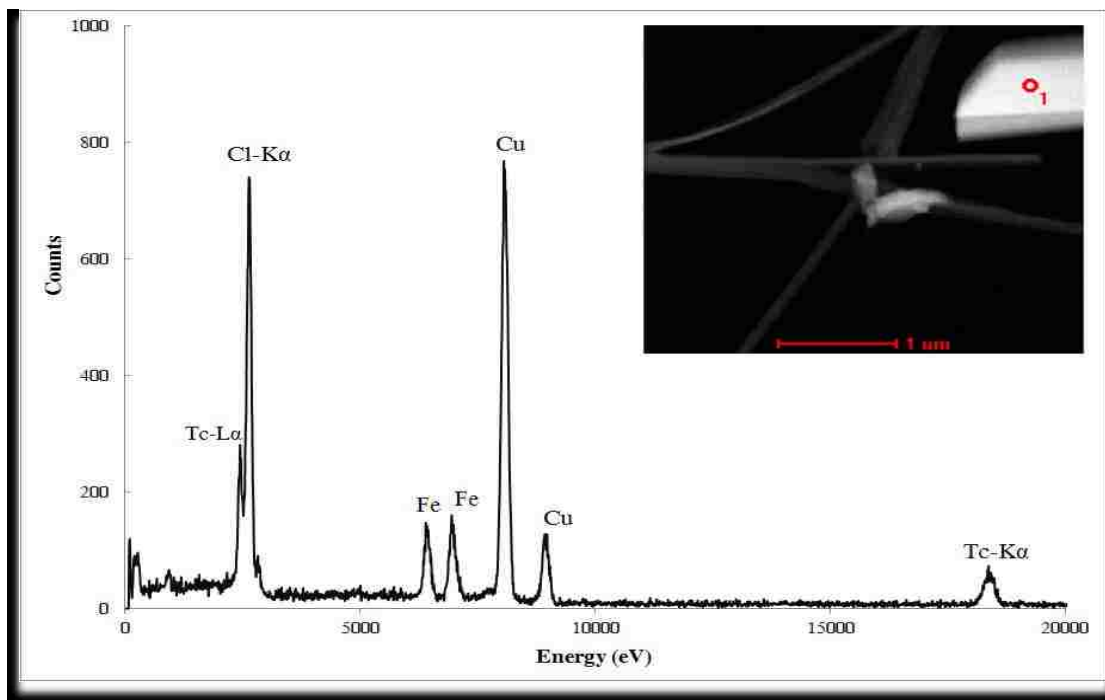


Figure 3.1. EDX spectrum of a TcCl_4 crystal displaying Tc- K_α , Tc- L_α , and the Cl- K_α lines. The Cu and Fe peaks are due to the sample holder. O_1 (red) indicates the selected area measured on the crystal.

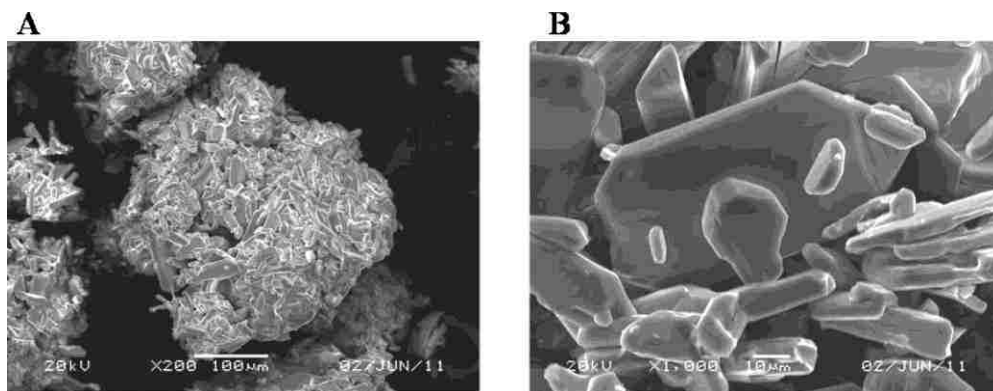


Figure 3.2. SEM images of the TcCl_4 powder: (A) x200; (B) x1000.

Powder X-ray Diffraction

The PXRD pattern (Figure 3.3) shows a crystalline single phase of TcCl_4 and the absence of Tc metal. A LeBail fit of the PXRD pattern confirms that the compound crystallizes at room temperature in the $Pbca$ space group with lattice parameters $a = 6.0258(5) \text{ \AA}$, $b = 11.6460(4) \text{ \AA}$, and $c = 14.0289(1) \text{ \AA}$. Rietveld analysis of the pattern gave a less satisfactory fit because of the strong texture within the sample.

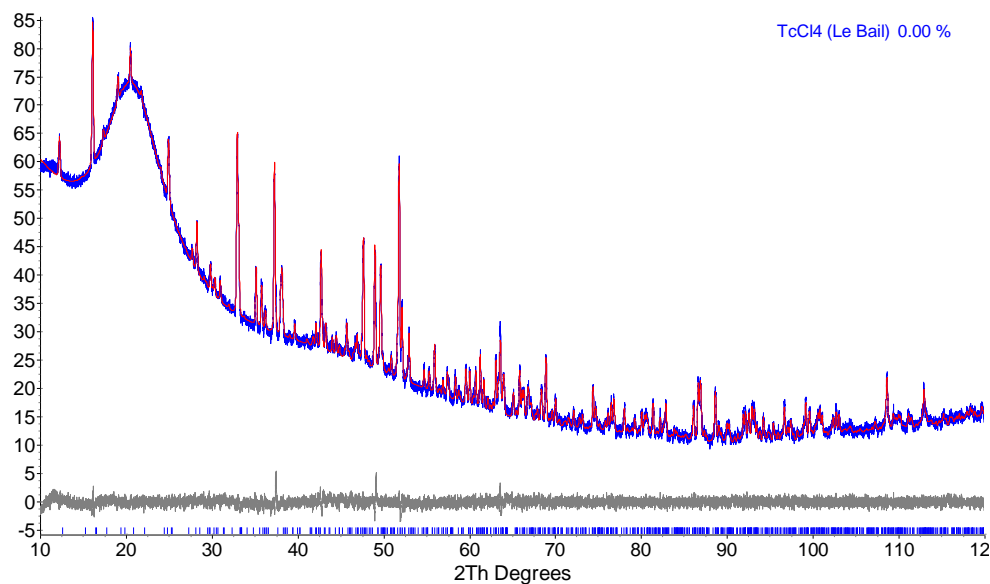


Figure 3.3. Experimental PXRD pattern (blue) of TcCl_4 with a LeBail fit (red) confirming the $Pbca$ space group. The difference between the experimental and fitted pattern is shown in grey ($R\text{-Bragg} = 0.218$).

Single Crystal X-ray Diffraction

The structure of TcCl_4 was redetermined by SCXRD. Single crystals were grown in the presence of a Cl_2 atmosphere as a phase transport agent within a sealed Pyrex tube. In agreement with previous results, TcCl_4 crystallizes in the orthorhombic space group $Pbca$ and consists of infinite ordered zigzag chains of edge-sharing TcCl_6 octahedra (Figure 3.4) [91]. Technetium tetrachloride is isostructural with PtCl_4 [20] and TcBr_4 [97]. The cell parameters at 100 K are $a = 6.0111(4) \text{ \AA}$, $b = 11.5308(9) \text{ \AA}$, and $c = 13.9334(10) \text{ \AA}$. The $\text{Tc}\cdots\text{Tc}$ separation of $3.6048(3) \text{ \AA}$ within the chain precludes any direct metal–metal bonding. Within a given octahedron, three different $\text{Tc}\text{--Cl}$ distances are observed. The shortest distance is attributed to the two cis terminal chlorines, Cl3 and Cl4 (average $\text{Tc}\text{--Cl} = 2.2368[6] \text{ \AA}$). The other two distances are associated with two

different sets of bridging chlorine atoms. Of these, the bonded chlorine atoms Cl1' and Cl2' perpendicular to the chain are the longest (average Tc–Cl = 2.4808[6] Å), whereas the chlorine atoms Cl1 and Cl2 parallel to the chain are slightly shorter (average Tc–Cl = 2.3797[6] Å). Additional crystallographic data are provided in the Appendix II.

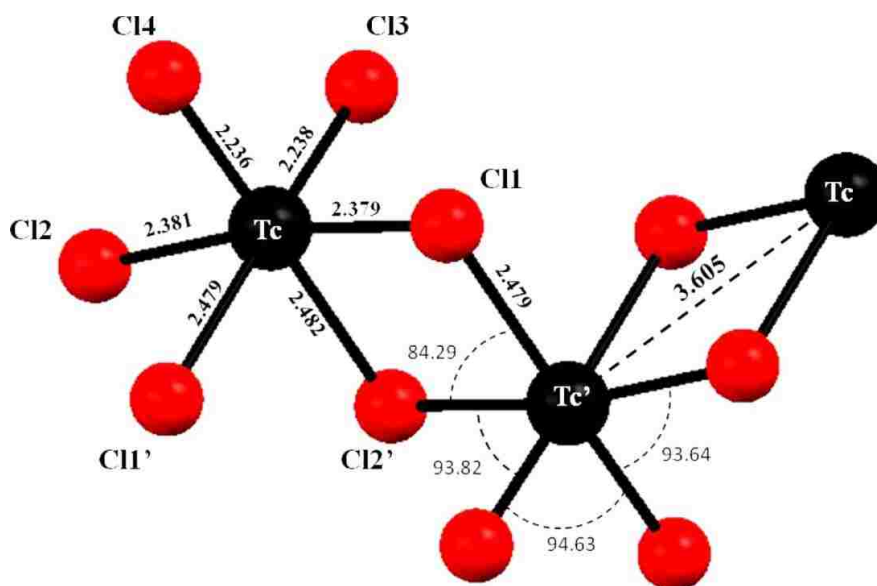


Figure 3.4. Ball-and-stick representation of TcCl_4 . Two edge-sharing octahedra and a portion of a third octahedron are represented. Distances are in Å and angles in degrees. Tc atoms in black and Cl atoms in red.

X-ray Absorption Fine Structure Spectroscopy

Technetium tetrachloride was also analyzed using XAFS spectroscopy [139]. The EXAFS spectra of the compound were k^3 -weighted and the Fourier Transformation (FT) performed in the k -range [2-14] Å⁻¹. The EXAFS spectra were fitted using the scattering functions calculated in the structure of TcCl_4 (Figure 3.5). The spatial resolution (i.e., $\pi/2\Delta K = 0.131$ Å) using this technique could not differentiate between the Tc-ClA1 (i.e.,

2.237[2] Å) from the Tc-ClA2 (i.e., 2.380[2]) contribution, or the Tc-ClA2 from the Tc-ClA3 (i.e., 2.480[2] Å) contribution. Though, under these conditions the Tc-Tc contributions of the various Tc chlorides could be differentiated: TcCl₄ (i.e., 3.605(1) Å), α-TcCl₃ (i.e., 2.444(1) Å), β-TcCl₃ (i.e., 2.861(3) Å), and TcCl₂ (i.e., 2.127(2) Å).

For fitting the EXAFS spectra, the numbers were fixed at those of the crystal structure. The ΔE_0 was constrained to be the same value for each wave, and all the other parameters were allowed to vary. The results of the adjustments (Figure 3.6, Table 3.1) indicate that the chemical environment of the absorbing Tc atom consists of six Cl atoms at 2.34(2) Å, four Cl atoms at 4.24(4) Å and two Tc atoms at 3.66(4) Å. These results are consistent with the ones determined by SCXRD. EXAFS spectroscopy on the sample indicates that the reaction of Tc metal and chlorine gas in a sealed tube at elevated temperature produces a homogenous phase of TcCl₄ absent of any α/β-TcCl₃, TcCl₂, or unreacted Tc metal. Also, this demonstrates that TcCl₄ is stable for at least five days in the sample holder.

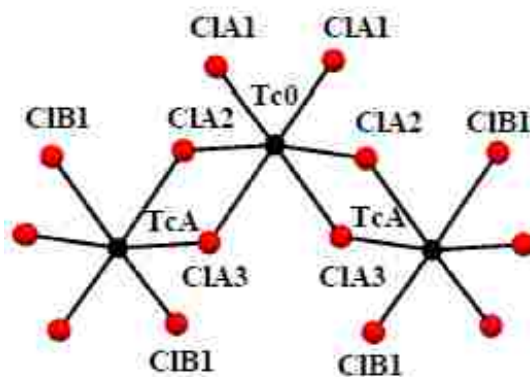


Figure 3.5. Ball-and-stick representation of the TcCl₄ cluster used for the EXAFS calculations.

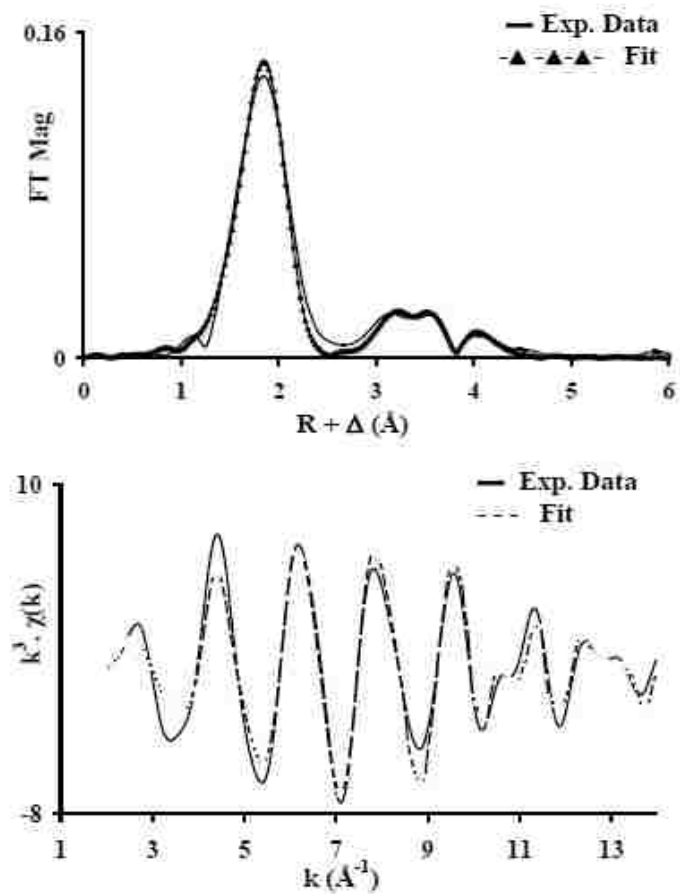


Figure 3.6. Adjustment of experimental k^3 -EXAFS spectra (bottom) and Fourier transform of k^3 -EXAFS spectra (top) of TcCl_4 . Adjustment performed between $k = [2-14] \text{\AA}^{-1}$.

Table 3.1. Structural parameters obtained by adjustment of the k^3 -EXAFS spectra of TcCl_4 . Adjustment between $k = [2-14] \text{ \AA}^{-1}$. ΔE_0 (eV) = 1.79 eV. The values found by SCXRD in TcCl_4 are in italics [125]. MS stands for multi-scattering.

Scattering	Structural Parameter		
	C.N.	R (\AA)	σ^2 (\AA^2)
$\text{Tc0} \rightleftharpoons \text{ClA}$	6	2.34(2), 2.366[4]	0.0072
$\text{Tc0} \rightleftharpoons \text{TcA}$	2	3.66(4), 3.605(1)	0.0058
$\text{Tc0} \rightleftharpoons \text{ClB}$	4	4.24(4), 4.292[4]	0.0091
MS $\text{Tc0} \rightleftharpoons \text{ClA}$	6	4.70(5)	0.0110

The XANES spectrum of TcCl_4 (Figure 3.7) was background subtracted, normalized, and the Tc K-edge position determined using the first derivative method. The absence of a pre-edge feature suggests there is no presence of TcO_4^- or TcOCl_4^- in the material [140]. The measured Tc-K edge position was determined to be 21053.0 eV. Compared to Tc-K edge position of NH_4TcO_4 , the chemical shift (ΔE vs. TcO_4^-) to lower energy is -10 eV and corresponds to an oxidation state of +4.

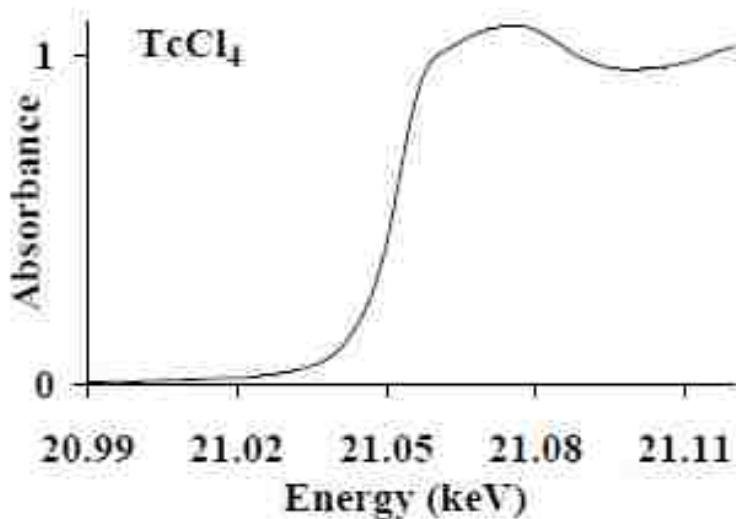


Figure 3.7. Normalized Tc K-edge XANES spectrum of TcCl_4 .

3.1.3.3 Physical Properties of TcCl₄

Previous magnetic susceptibility measurements were recorded on a sample of TcCl₄ prepared from the reaction of Tc₂O₇ with CCl₄ [32]. No magnetic measurements have been performed on a sample of TcCl₄ synthesized from the reaction of the metal with chlorine gas, and no data have been collected below 78 K. A plot of the magnetic susceptibility versus temperature (Figure 3.8) shows features typical of an antiferromagnet with a cusp indicating the Néel temperature (T_N) at about 24 K and of a paramagnet above T_N . A fit of the data above 50 K to the Curie–Weiss law (Eq. 3.1) gives a Curie temperature of $\theta = 51(1)$ K and a diamagnetic contribution of $\chi_0 = -3.1(8) \times 10^{-4}$ emu/mol.

$$\text{Eq. 3.1} \quad \chi = C/(T + \theta) + \chi_0$$

The effective moment at each Tc site is then $\mu_{\text{eff}} = (3Ck_B/N)^{1/2} = 3.76(3) \mu_B$. In comparison to the previously measured value of $3.14 \mu_B$ [92], this measurement is much closer to the theoretical, spin-only value (i.e., the orbital angular momentum is effectively zero) of $3.87 \mu_B$. This moment is similar to the one found in other $4d^3$ species, i.e., K₂TcCl₆ ($4.05 \mu_B$) [141] and K₃MoCl₆ ($3.79 \mu_B$) [142]. The magnetic behavior for TcCl₄ is similar to the one expected for an isolated Tc^(IV)Cl₆ octahedron and is consistent with the absence of a significant metal–metal interaction in TcCl₄ [92].

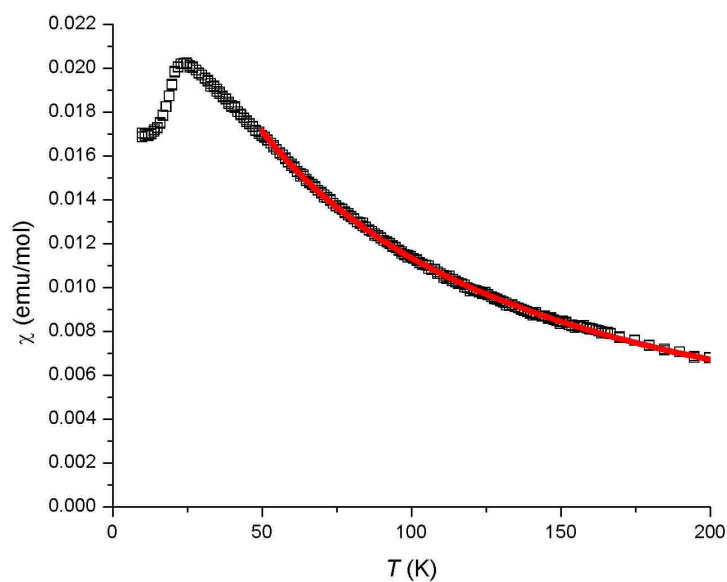


Figure 3.8. Magnetic susceptibility as a function of temperature of TcCl_4 . Measurement performed between 10 K and 300 K on TcCl_4 (34.1 mg) in a 0.1 T magnetic field. The black line represents the experiment data. The red line represents the fit $\chi = f(T)$ of χ vs. (T) above 50 K.

3.1.3.4 Thermal Behavior of TcCl_4

The thermal behavior of TcCl_4 was studied under flowing argon and in a sealed tube under vacuum at 450 °C. The latter temperature is one that we previously employed for the synthesis of TcCl_4 . Experiments under flowing argon at 250 – 500 °C for 14 h only resulted in volatilization of the starting material.

In a first experiment, TcCl_4 was reacted at 450 °C for 14 h. After the reaction, a dark black powder, needlelike crystals (center of the tube), and a black amorphous film (cold end of the tube) were observed. The powder XRD of the black powder indicates the presence of both TcCl_4 and TcCl_2 . The structure and properties of Tc dichloride are

presented in Chapter 5. The needle-like single crystals were indexed by SCXRD, yielding cell parameters and a space group identical with that of TcCl_2 [143]. The SEM analysis of the powder (Figure 3.9A) and single crystals (Figure 3.9B) show the “sea urchin” cluster arrangement of the needle-shaped crystals characteristic of TcCl_2 morphology.

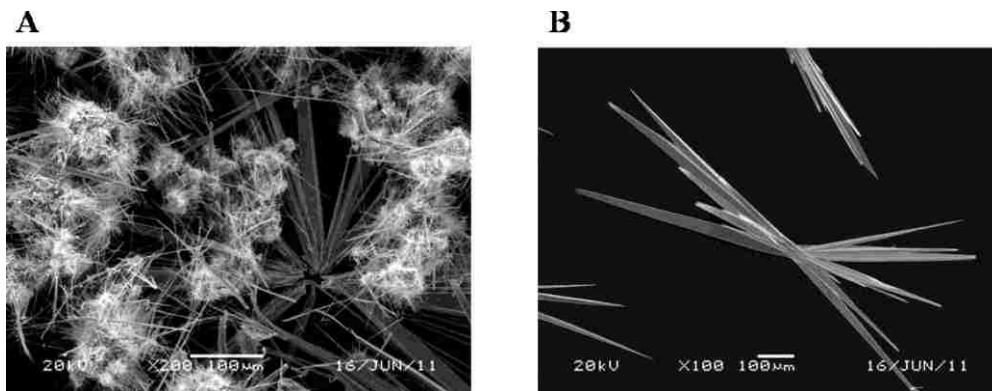


Figure 3.9. SEM images of the powder (A, $\times 200$) and crystals (B, $\times 100$) obtained after decomposition of TcCl_4 at $450\text{ }^\circ\text{C}$ under vacuum for 14 h.

In a second experiment, TcCl_4 was reacted at $450\text{ }^\circ\text{C}$ in a sealed tube under vacuum for 2 hours. After the reaction, red needles, small purple hexagonal plates, and an amorphous film were observed at the coolest end of the tube. The red needles were indexed using SCXRD as TcCl_4 , while the purple hexagonal plates were indexed as $\alpha\text{-TcCl}_3$. The structure, morphology and properties of $\alpha\text{-TcCl}_3$ are presented in Chapter 4.

Analysis of the decomposition products by SEM (Figure 3.10A) shows the edge of a TcCl_4 single crystal. Closer inspection of the TcCl_4 crystal (Figure 3.10B) revealed the presence of small hexagonal shaped crystals ($2 - 5\text{ }\mu\text{m}$) characteristic of $\alpha\text{-trichloride}$ morphology.

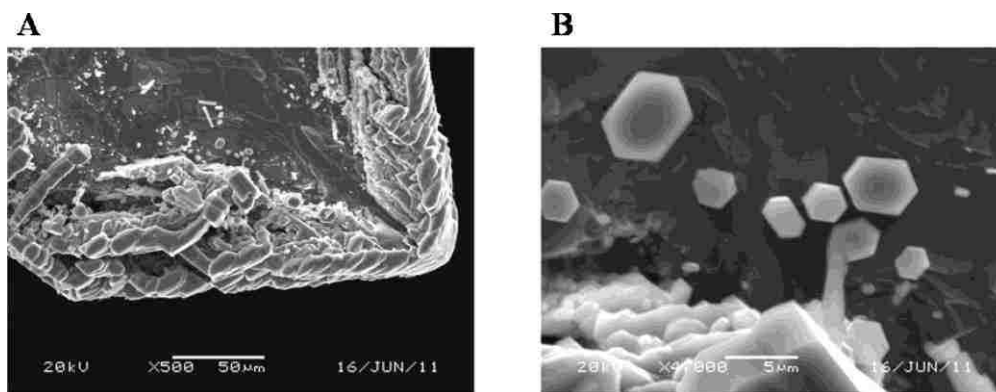


Figure 3.10. SEM images of the surface of a TcCl_4 crystal (A, $\times 500$; B, $\times 4000$) obtained after decomposition of TcCl_4 at $450\text{ }^\circ\text{C}$ under vacuum for 2 h.

It appears that the presence of a vacuum and elevated temperature are required for decomposition of TcCl_4 . Decomposition provides two products in the early stages of the reaction, and the isolation of $\alpha\text{-TcCl}_3$ after 2 h and TcCl_2 after 14 hours of reaction at $450\text{ }^\circ\text{C}$ suggests that the trichloride is likely the initial decomposition product.

3.1.3.5 Comparison of TcCl_4 with Other MCl_4 Systems

Five different structure-types have been identified for the second- and third-row transition-metal tetrachlorides spanning groups 4–10 ($d^0\text{--}d^6$) for Zr, Hf, Nb, Ta, Mo, W, Tc, Re, Os, and Pt. These tetrachlorides are comprised of MCl_6 edge- or face-sharing octahedra, forming either infinite chains or layers (Figure 3.11). These compounds can be differentiated based on the presence or absence of metal–metal bonding.

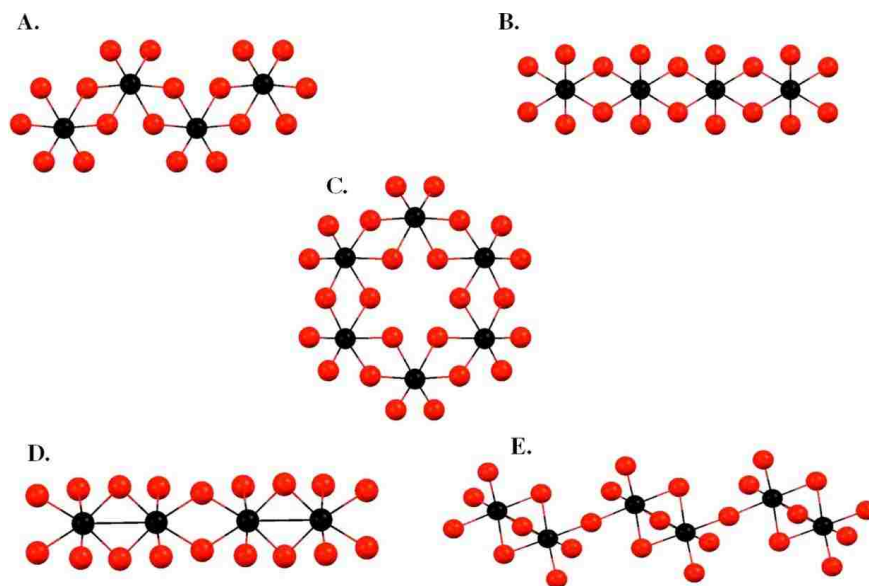


Figure 3.11. Ball-and-stick representations of second- and third-row transition-metal tetrachloride structure-types: (A) Zr, Hf, Tc, and Pt; (B) Os; (C) β -Mo; (D) Nb, Ta, α -Mo, and W; (E) β -Re. The metal atoms are in black, and the Cl atoms are in red.

The structure-types in Figure 3.11A–C are representative of transition-metal tetrachlorides that exhibit no metal–metal bonding. Similar to Tc, the tetrachlorides of Zr [144], Hf [145], and Pt [20] (Figure 3.11A) adopt the TcCl_4 structure-type. The M–M separations within the chains suggest little or no interaction between neighboring metal ions. The OsCl_4 [146] structure-type (Figure 3.11B) consists of infinite linear chains of edge-sharing OsCl_6 octahedra with a single $\text{Os}\cdots\text{Os}$ separation of 3.56(1) Å, suggesting the absence of metal–metal bonding. The β - MoCl_4 [25] structure-type consists of infinite layered sheets instead of chains of MCl_6 octahedra (Figure 3.11C); the $\text{Mo}\cdots\text{Mo}$ separation in this structure, 3.670(1) Å, also precludes any metal–metal bonding.

The structure-types for the transition-metal tetrachlorides that can be classified as metal–metal bonded are shown in Figure 3.11D and E. The NbCl_4 [147] structure-type

(Figure 3.11D) is also found for TaCl₄ [148], α -MoCl₄ [131], and WCl₄ [132]. These compounds consist of edge-sharing chains of distorted MCl₆ octahedra with alternating short and long metal–metal distances. The shorter distances suggest the presence of some metal–metal interaction. β -Re tetrachloride (Figure 3.11E) consists of infinite chains of distorted Re₂Cl₉ confacial bioctahedra linked by a terminal chlorine atom. In the Re₂Cl₉ unit, the Re–Re separation (i.e., 2.728(2) Å) is indicative of a strong metal–metal interaction.

Table 3.2. Structure-types and Metal–Metal Separations in Transition-Metal Tetrachlorides. ^a Not reported. ^b Characterized by powder XRD and interatomic distances not reported.

Electronic configuration	Metal	Structure-type	M–M and M...M (in italics) distances (Å)
d ⁰	Zr	TcCl ₄ (Figure 3.11A)	3.962(1)
	Hf	TcCl ₄	3.920(1)
d ¹	Nb	NbCl ₄ (Figure 3.11D)	3.029(2), 3.794(2)
	Ta	NbCl ₄	2.985(3), 3.791(3)
d ²	Mo	α : NbCl ₄	^b
		β : MoCl ₄ (Figure 3.11C)	3.670(1)
	W	NbCl ₄	2.688(1), 3.787(1)
d ³	Tc	TcCl ₄	3.604(8)
	Re	β : ReCl ₄ (Figure 3.11E)	2.728(2), 4.368(2)
d ⁴	Ru	^a	^a
	Os	OsCl ₄ (Figure 3.11B)	3.560(1)
d ⁵	Rh	^a	^a
	Ir	^a	^a
d ⁶	Pd	^a	^a
	Pt	TcCl ₄	^b

The transition-metal tetrachlorides are thermally unstable; they can decompose or disproportionate (Table 3.3). The thermal behavior of TcCl₄ is similar to that of PtCl₄, which also yields the dichloride as the final decomposition product [124]. Osmium

tetrachloride decomposes to OsCl_3 at 470 °C [128]. In contrast, ReCl_4 and $\beta\text{-MoCl}_4$ undergo disproportionation to the respective tri- and pentachloride [134, 135, 149, 150]. Tungsten(IV) chloride also disproportionates, forming WCl_2 and WCl_5 [132, 151]. In comparison to the surrounding elements, Tc displays unique thermal properties upon undergoing successive decomposition to the tri- and dichlorides.

Table 3.3. Summary of Transition-Metal Tetrachloride Decompositions.

Compound	Conditions	Products
$\beta\text{-MoCl}_4$	288 °C, under argon	MoCl_3 and MoCl_5
WCl_4	450–500 °C, vacuum	WCl_2 and WCl_5
TcCl_4	450 °C, 2 h, vacuum	$\alpha\text{-TcCl}_3$
	450 °C, 24 h, vacuum	TcCl_2
ReCl_4	300 °C, under nitrogen	ReCl_3 and ReCl_5
OsCl_4	470 °C, slight pressure of chlorine	OsCl_3
PtCl_4	350 °C, open system with flowing $\text{N}_2(\text{g})$	$\text{Pt}_6\text{Cl}_{12}$

3.1.4 Summary

Technetium tetrachloride was synthesized from the reaction of Tc metal with excess Cl_2 in sealed Pyrex tubes at elevated temperatures. This synthetic procedure is preferred for small samples and avoids the formation of unwanted oxychlorides. The phase purity of the compound obtained by this method was analyzed by PXRD and XAFS spectroscopy, which confirmed the presence of TcCl_4 as a single phase. The structure of TcCl_4 was revisited by SCXRD; more accurate structural parameters were obtained from this measurement. Magnetic measurements confirmed TcCl_4 to be paramagnetic above 50 K and to exhibit antiferromagnetic behavior below 24 K. The morphology of TcCl_4 was observed by SEM as rod-shaped clusters and used to track compositional changes at various temperatures under vacuum. The thermal behavior of TcCl_4 was investigated in sealed tubes under vacuum after 2 and 14 hours at 450 °C.

Diffraction and microscopic techniques show TcCl_4 to decompose to $\alpha\text{-TcCl}_3$ and TcCl_2 after 2 hours and to TcCl_2 without a trace of the trichloride after 14 hours. The $\alpha\text{-TcCl}_3$ appears to be the initial decomposition product, while TcCl_2 is the ultimate product of decomposition under the prevailing experimental conditions.

3.2 Technetium Tetrabromide

3.2.1 Introduction

Technetium tetrabromide has previously been synthesized from the reaction of the elements in sealed tubes and characterized by SCXRD (see section 1.4.3) [97]. Beyond its preparation and the determination of its crystal structure no other experiments on TcBr_4 have been reported. Our previous studies (*vide supra*) have shown that TcCl_4 is thermally unstable and decomposes under vacuum at 450 °C to lower-valent binary chlorides (i.e., $\alpha\text{-TcCl}_3$ and TcCl_2) [125]. Because TcCl_4 and TcBr_4 are isomorphous and thermal decomposition of the tetrachloride produces TcCl_2 , it was of interest to study the solid-state decomposition of TcBr_4 as possible precursor to the unknown TcBr_2 .

In this study, the thermal decomposition of TcBr_4 in sealed Pyrex tubes under vacuum at elevated temperatures was investigated and the formation of the new hexanuclear Tc bromide cluster, $\text{Na}\{[\text{Tc}_6\text{Br}_{12}]_2\text{Br}\}$ was reported. The stoichiometry of the compound was confirmed by EDX spectroscopy, and its structure was determined using SCXRD. First-principle calculations were employed to better understand the electronic structure and bonding of the trigonal prismatic hexanuclear $\text{Tc}_6\text{Br}_{12}$ cluster [152].

3.2.2 Experimental Details

Preparation of Technetium Tetrabromide. Technetium metal (31.5 mg, 0.32 mmol) was transferred into a Pyrex tube (L = 43 cm), connected to a Schlenk line and flamed under vacuum. The tube was backfilled with Ar(g), isolated from the Schlenk line and Br₂ (40 μL, 0.78 mmol) was added using a micropipette. The tube was reconnected to the Schlenk line and the end of the tube was cooled using liquid nitrogen. Once the Br₂ was condensed, the coolant was removed, and the tube was evacuated under vacuum while slowly warming the tube allowing the Br₂ to convert back to the liquid phase. After the Br₂ had become liquid, the tube was isolated and the contents condensed again in liquid nitrogen. This process was repeated three times. After the third time, the tube was placed in liquid nitrogen, evacuated under vacuum, and flame-sealed (L = 18 cm). The tube was inserted into a clamshell furnace with the metal end of the sealed tube located in the center of the furnace. The temperature was increased to 400 °C at 10 °C/min, and held at temperature for 24 hours. After cooling to room temperature, a purplish black crystalline powder was observed where the metal once was and a black amorphous film at the opposite end of the tube. The crystalline powder was removed and placed in a second Pyrex tube of identical dimensions as the first, sealed with bromine, and reacted as before. The purplish black powder (77.6 mg, yield: 58%) in the tube was recovered.

Thermal Decomposition of TcBr₄ to Na{[Tc₆Br₁₂]₂Br} in Pyrex. A sample of TcBr₄ (64.1 mg, 0.15 mmol) was placed in a 30-cm-long Pyrex tube, evacuated, and sealed at 18 cm. The tube was placed in a tube furnace for 24 hours at 450 °C with the solid at the center of the furnace. After cooling to room temperature, the reaction yielded a crystalline black powder (41.7 mg) and several purplish black rail spike crystals adjacent

to the powder. The tube and its contents were annealed at 200 °C for a period of 3 days to ensure crystallinity. The powder was analyzed by PXRD and the single-crystals by SCXRD, EDX, and SEM.

Thermal Decomposition of TcBr₄ in Quartz. A sample of TcBr₄ (54.0 mg, 0.13 mmol) was placed in a 30-cm-long quartz tube, evacuated, and sealed at 18 cm. The tube was placed in a tube furnace for 24 hours at 450 °C with the solid at the center of the furnace. After cooling to room temperature, the reaction yielded a grayish black powder (23.4 mg) and amorphous black film at the coolest end of the tube. The powder was analyzed using PXRD.

3.2.3 Results and Discussion

3.2.3.1 Thermal Behavior of TcBr₄

Technetium tetrabromide was prepared according to the method reported in the literature [97]. A small quantity (■64 mg) was placed in a Pyrex tube, and the tube was flame-sealed under vacuum, placed in a furnace, and reacted at 450 °C for 14 hours. After the reaction, a dark-purple/black crystalline powder (■42 mg) was obtained in the hottest part of tube, and purple crystals (■2 mg) were observed on the surface of the tube adjacent to the powder. The product was annealed at 200 °C for an additional 3 days. Analysis of the crystals by optical and scanning electron microscopy revealed a “rail spike” shape (Figure 3.12).



Figure 3.12. Left: Optical microscopy image of a single rail spike crystal of $\text{Na}\{[\text{Tc}_6\text{Br}_{12}]_2\text{Br}\}$. Right: Scanning electron microscopy (SEM) image of a single rail spike crystal of $\text{Na}\{[\text{Tc}_6\text{Br}_{12}]_2\text{Br}\}$ at x500 magnification.

The PXRD pattern of the bulk material obtained in Pyrex revealed a mixture of TcBr_3 and Tc metal with the absence of TcBr_4 (Figure 3.13). Identical reactions performed in quartz tubes (absence of sodium) did not yield any crystals. The PXRD pattern of the decomposition in quartz yielded a homogeneous phase of Tc metal (Figure 3.14). This suggests that the source of Na in the compound originates from the Pyrex tube (see Chapter 2 for Pyrex composition).

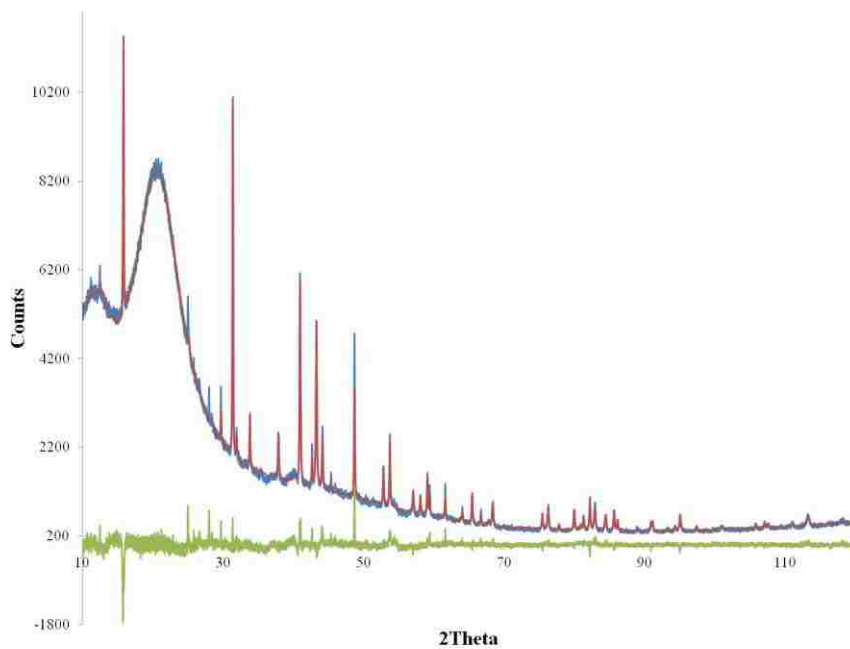


Figure 3.13. XRD powder pattern of product (blue) obtained after decomposition of TcBr_4 in Pyrex. The refinement (red) shows the presence of Tc metal (P63/mmc; $a = 2.742(1) \text{ \AA}$ and $b = 4.398(1) \text{ \AA}$) and TcBr_3 (Pmmn; $a = 11.206(1) \text{ \AA}$, $b = 6.018(1) \text{ \AA}$, and $c = 6.4777(1) \text{ \AA}$). The difference between the experimental and fitted pattern is shown in green.

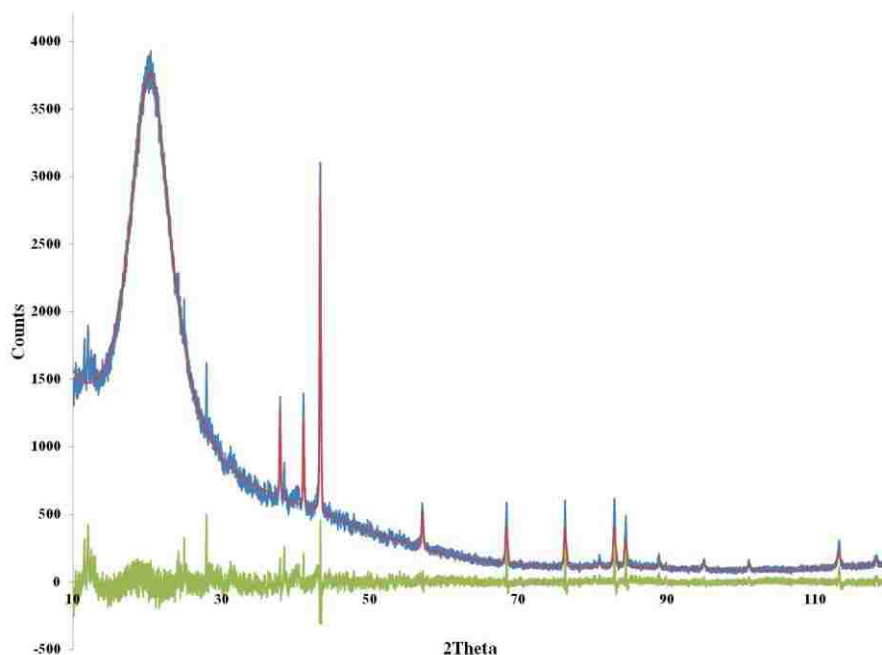


Figure 3.14. XRD powder pattern of product (blue) obtained after decomposition of TcBr_4 in quartz. The fit (red) shows the presence of Tc metal ($P63/mmc$; $a = 2.743(1) \text{ \AA}$ and $c = 4.400(1) \text{ \AA}$). The difference between the experimental and fitted pattern is shown in green.

3.2.3.2 Characterization of $\text{Na}[[\text{Tc}_6\text{Br}_{12}]_2\text{Br}]$

EDX Analysis

The EDX spectrum (Figure 3.15) of the crystals show characteristic Na- $K\alpha$, Tc- $K\alpha$ and Tc- $L\alpha$, and Br- $K\alpha$ and Br- $L\alpha$ lines, consistent with the presence of Na, Tc, and Br in the compound. A Br:Tc ratio of 2.0(3) was determined from the integrated intensities of the Tc- $K\alpha$ and Tc- $L\alpha$, and Br- $K\alpha$ and Br- $L\alpha$ peaks (Lighter Z elements are difficult to accurately quantify by EDX; absorption correction (ZAF) was applied).

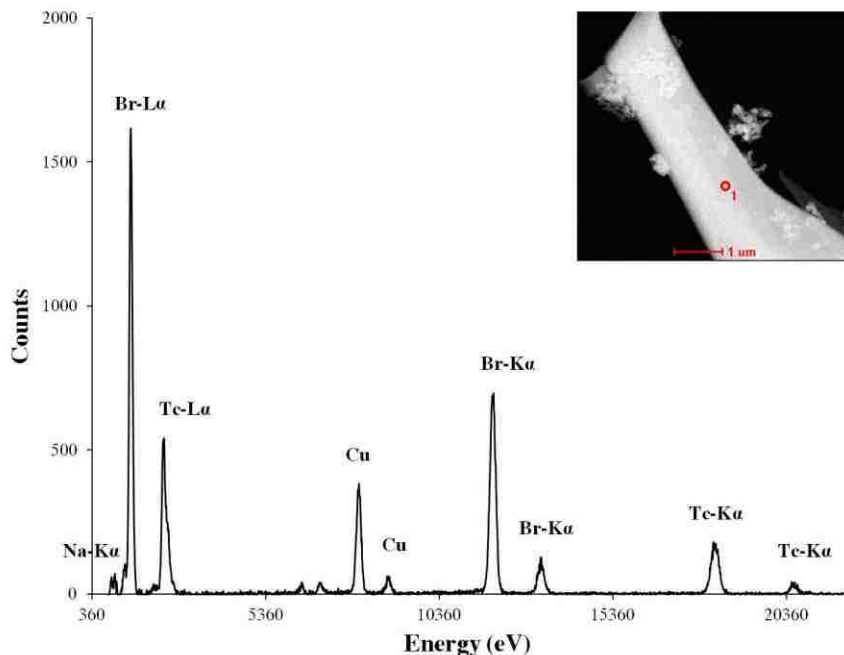


Figure 3.15. EDX measurement of $\text{Na}\{[\text{Tc}_6\text{Br}_{12}]_2\text{Br}\}$ crystal displaying $\text{Na-K}\alpha$, $\text{Tc-K}\alpha$, $\text{Tc-L}\alpha$, and the $\text{Br-K}\alpha$ lines. The Cu peaks are due to the sample holder. O_1 (red) indicates the selected area measured on the crystal.

Single Crystal X-ray Diffraction

A suitable crystal was selected for structural determination by SCXRD. The compound exhibits the stoichiometry $\text{Na}\{[\text{Tc}_6\text{Br}_{12}]_2\text{Br}\}$ and crystallizes in the triclinic space group $P-1$ ($a = 9.517(5) \text{ \AA}$, $b = 10.523(6) \text{ \AA}$, and $c = 11.141(6) \text{ \AA}$; $\alpha = 83.67(1)^\circ$, $\beta = 73.72(10)^\circ$, $\gamma = 84.84(1)^\circ$). Additional crystallographic data are provided in the Appendix II. The compound contains the trigonal-prismatic hexanuclear $\text{Tc}_6\text{Br}_{12}$ cluster (Figure 3.16 and Figure 3.17). The geometry of the $\text{Tc}_6\text{Br}_{12}$ cluster in $\text{Na}\{[\text{Tc}_6\text{Br}_{12}]_2\text{Br}\}$ is similar to that found for the $\text{Tc}_6\text{Br}_{12}$ cluster in $(\text{Et}_4\text{N})_2\{[\text{Tc}_6\text{Br}_{12}]\text{Br}_2\}$, the $\text{Tc}_6\text{Br}_{12}^-$ cluster in $(\text{Me}_4\text{N})_3\{[\text{Tc}_6\text{Br}_{12}]\text{Br}_2\}$ [153], and the $\text{Re}_6\text{Br}_{12}^{2+}$ cluster in $\{[\text{Re}_6\text{Br}_{12}]\text{Br}_2\}$ [154, 155]. All of these clusters were prepared in an autoclave via the hydrogen reduction of

MO_4^- ($\text{M} = \text{Tc}, \text{Re}$) or TcX_6^{2-} salts in concentrated HX_{aq} ($\text{X} = \text{Cl}, \text{Br}$) at elevated temperature [154, 156, 75]; it is the first time that a prismatic hexanuclear cluster of Group VII metal has been prepared from a solid-state reaction.

In $\text{Na}\{[\text{Tc}_6\text{Br}_{12}]_2\text{Br}\}$, the $\text{Tc}_6\text{Br}_{12}$ cluster is composed of two identical parallel Tc_3Br_6 units linked by multiple Tc–Tc bonds. In the Tc_3^{6+} unit, the $\text{Tc}_A\text{--Tc}_A$ distance (av. $\text{Tc--Tc} = 2.685(5) \text{ \AA}$) is characteristic of a Tc–Tc single bond [157]. This distance is longer than that found in the triangular Tc_3^{9+} core in $\alpha\text{-TcCl}_3$ (i.e., $2.444(1) \text{ \AA}$; Tc=Tc double bond) and similar to that found (Table 3.4) in the Tc_3^{6+} core of $(\text{Et}_4\text{N})_2\{[\text{Tc}_6\text{Br}_{12}]\text{Br}_2\}$ (i.e., $2.66(2) \text{ \AA}$) [153]. The $\text{Tc}_A\text{--Tc}_B$ distance between the Tc_3Br_6 units (av. $\text{Tc--Tc} = 2.174(5) \text{ \AA}$) is similar to that found in the $(\text{Et}_4\text{N})_2\{[\text{Tc}_6\text{Br}_{12}]\text{Br}_2\}$ salt (i.e., $2.188(5) \text{ \AA}$) and is characteristic of a Tc \equiv Tc triple bond [72]. Further evidence of a triple bond is provided by theoretical calculation (*vide infra*).

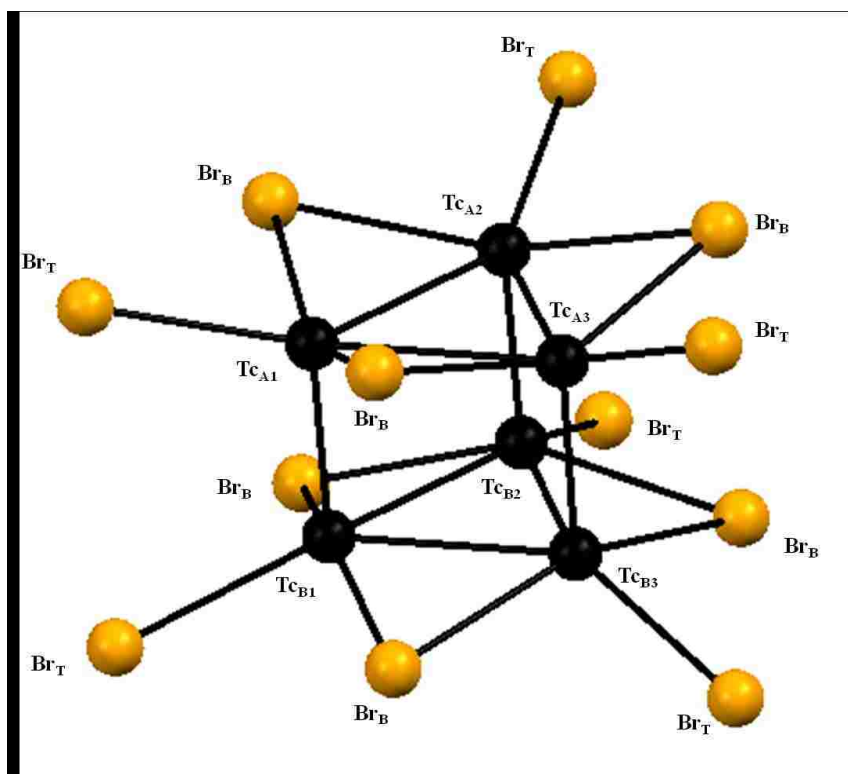


Figure 3.16. Ball-and-stick representation of the $\text{Tc}_6\text{Br}_{12}$ cluster in $\text{Na}\{[\text{Tc}_6\text{Br}_{12}]_2\text{Br}\}$. Tc atoms are in black and Br atoms in orange. Selected distances (\AA): $\text{Tc}_{\text{A}1}\text{--}\text{Tc}_{\text{A}2}$ 2.687(9), $\text{Tc}_{\text{A}2}\text{--}\text{Tc}_{\text{A}3}$ 2.667(6), $\text{Tc}_{\text{A}3}\text{--}\text{Tc}_{\text{A}1}$ 2.673(5), $\text{Tc}_{\text{A}1}\text{--}\text{Tc}_{\text{B}1}$ 2.165(1), $\text{Tc}_{\text{A}2}\text{--}\text{Tc}_{\text{B}2}$ 2.177(9), $\text{Tc}_{\text{A}3}\text{--}\text{Tc}_{\text{B}3}$ 2.177(5).

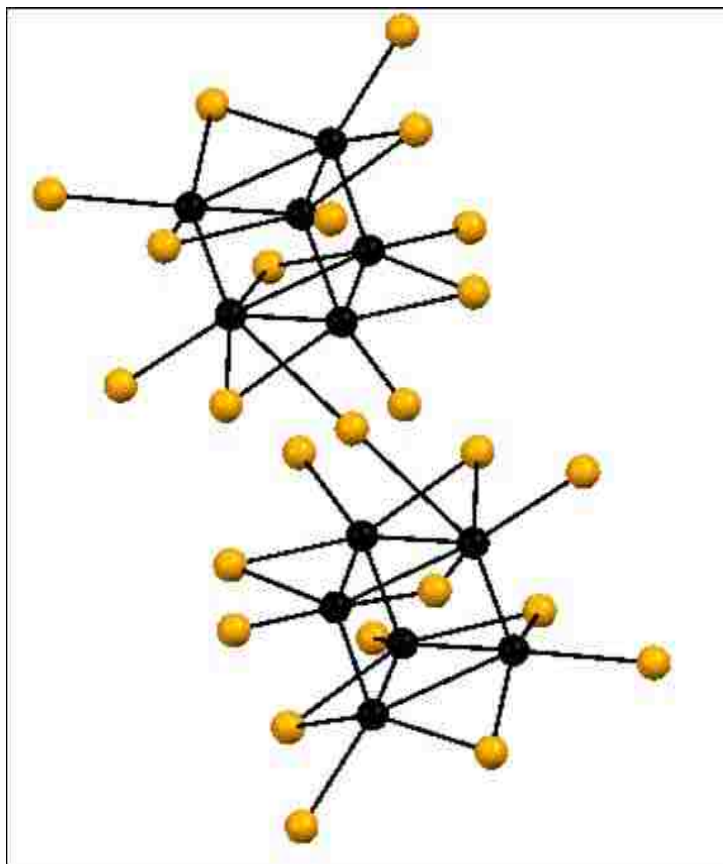


Figure 3.17. Ball-and-stick representation of two $\text{Tc}_6\text{Br}_{12}$ clusters joined by a capping bromine in $\text{Na}\{[\text{Tc}_6\text{Br}_{12}]_2\text{Br}\}$. Tc atoms in black, bromine atoms in orange.

Table 3.4. Selected Bond Distances (\AA) in the $\text{Tc}_6\text{Br}_{12}$ Cluster in $\text{Na}\{[\text{Tc}_6\text{Br}_{12}]_2\text{Br}\}$ ^a and $(\text{Et}_4\text{N})_2\{[\text{Tc}_6\text{Br}_{12}]\text{Br}_2\}$ ^b (Experimental Values in Bold and Calculated Values in Italics).^a Represents an average value.^b Reference 154.

Compound	$\text{Tc}_A\text{-Tc}_A$	$\text{Tc}_A\text{-Tc}_B$	Tc-Br_T	Tc-Br_B
$\text{Na}\{[\text{Tc}_6\text{Br}_{12}]_2\text{Br}\}$	2.6845(5)	2.1735(5)	2.4966(8)	2.4738(7)
$(\text{Et}_4\text{N})_2\{[\text{Tc}_6\text{Br}_{12}]\text{Br}_2\}$ ^b	2.66(2)	2.188(5)	2.50(1)	2.49(1)
$\text{Tc}_6\text{Br}_{12}$	<i>2.720</i>	<i>2.173</i>	<i>2.479</i>	<i>2.494</i>

Each of the Tc_3Br_6 units contains three terminal Br_T atoms (av. $\text{Tc-Br}_T = 2.4966(8) \text{ \AA}$) and three bridging Br_B atoms (av. $\text{Tc-Br}_B = 2.4738(7) \text{ \AA}$). In the $\text{Tc}_6\text{Br}_{12}$ cluster, one of the two Tc_3Br_6 units is capped by a Br atom (Br_C). The capping Br atom

lies above the center of the triangular face. The distances between the Br_C and Tc atoms of the Tc₃Br₆ unit (i.e., 3.1952(5) Å, 3.0994(4) Å, and 2.9636(5) Å) are significantly longer than those in other technetium(II) complexes (i.e., Tc–Br = 2.50 – 2.60 Å) and indicate that the Tc and Br atoms are coupled by a weak electrostatic interaction [32, 72, 100, 158]. The distances between the Br_C atom and the three bridging Br_B atoms (i.e., 3.472 Å, 3.482 Å, and 3.625 Å) of the Tc₃Br₆ unit indicate that those Br atoms are in van der Waals contact (sum of the van der Waals radii = 3.70 Å) [158]. The distances between Br_C and Br_T (i.e., 4.067 Å, 4.300 Å, and 4.447 Å) are larger than the sum of the van der Waals radii.

The environment of the Tc₆Br₁₂ cluster in Na{[Tc₆Br₁₂]₂Br} differs from that of Tc₆Br₁₂ in (Et₄N)₂{[Tc₆Br₁₂]₂Br₂}. In the latter compound, both Tc₃Br₆ units are capped by Br atoms. The shortest interatomic distance between the Tc₆Br₁₂ clusters (Br...Br = 3.935 Å) exceeds the sum of the Br van der Waals radii (3.70 Å), indicating that there are no direct interactions between the Tc₆Br₁₂ clusters. The Na atoms are located in the cavities between the clusters and hexagonally coordinated to three of the terminal Br atoms between two of the clusters (Na–Br = 2.96 – 3.26 Å).

Computational Study

In order to better understand the structure and bonding in the Tc₆Br₁₂ cluster, DFT calculations were performed. The interatomic distances found by DFT in Tc₆Br₁₂ are in excellent agreement with the crystallographic data. The largest discrepancy (± 0.036 Å) was found for the Tc_A–Tc_A distance in the Tc₃Br₆ unit. The calculated Tc_A–Tc_B distance (i.e., 2.173 Å) is identical with that found by SCXRD (2.1735 Å). The calculated Tc–Br_T and Tc–Br_B distances are respectively 0.018 Å shorter and 0.020 Å longer than the

experimental ones. The calculated $\text{Tc}_A\text{-Tc}_A\text{-Tc}_A$, $\text{Br}_{\text{Bri}}\text{-Tc}_A\text{-Br}_{\text{Bri}}$, and $\text{Tc}_A\text{-Br}_{\text{Bri}}\text{-Tc}_{\text{face}}$ angles are within 0.5° of the crystal data.

The electronic structure of the $\text{Tc}_6\text{Br}_{12}$ cluster has been investigated. Employing skeletal electron pair counting rules [159], it was found that $\text{Tc}_6\text{Br}_{12}$ has 30 bonding electrons within the metal framework, differing from the typical magic number of 18 electrons for trigonal prisms [160]. The molecular orbital analysis reveals bonding in $\text{Tc}_6\text{Br}_{12}$ to be electron-rich $\text{Tc}\equiv\text{Tc}$ bonds along the edge and $\text{Tc}\text{-Tc}$ single bonds in the triangles with an overall electronic configuration of $(\sigma^{12}\pi^{10}\delta^4\delta^*4)$. Natural bond orbital occupancy (NBO) calculations were performed to characterize the metal–metal bonding in the cluster (Figure 3.18). The NBO occupancy along the edge of $\text{Tc}_6\text{Br}_{12}$ is 5.4e, close to that of an ideal covalent triple bond (i.e., NBO = 6.0) and further confirms the presence of a $\text{Tc}\equiv\text{Tc}$ triple bond in the cluster. The NBO occupancy along the face is 1.5e, consistent with a $\text{Tc}\text{-Tc}$ single bond.

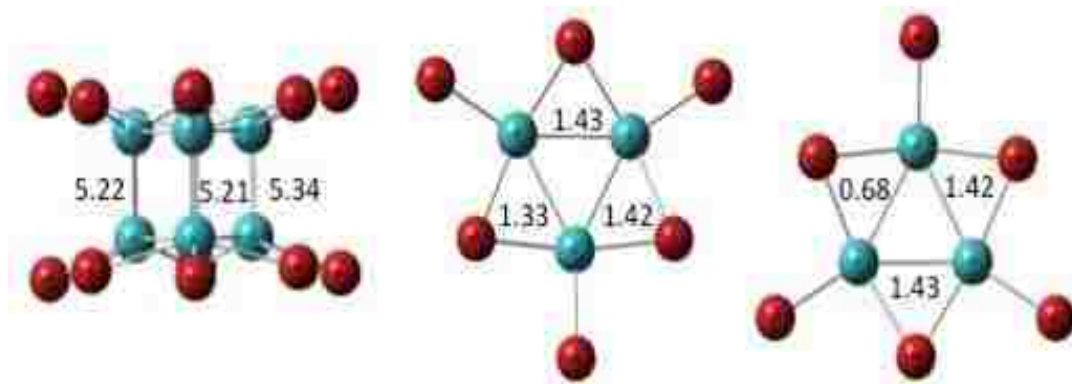


Figure 3.18. The Natural Bond Order (NBO) occupancy of the $\text{Tc}\text{-Tc}$ bonds in $\text{Tc}_6\text{Br}_{12}$.

3.2.4 Summary

The compounds $\text{Na}\{[\text{Tc}_6\text{Br}_{12}]_2\text{Br}\}$ and TcBr_3 were obtained from the decomposition of TcBr_4 under vacuum in a glass tube. The Br:Tc stoichiometry in

$\text{Na}\{[\text{Tc}_6\text{Br}_{12}]_2\text{Br}\}$ was confirmed using EDX spectroscopy and its structure determined using SCXRD. The compound contains the trigonal-prismatic hexanuclear $\text{Tc}_6\text{Br}_{12}$ cluster. It is the first Group VII trigonal-prismatic hexanuclear cluster to be synthesized from a solid-state reaction. Theoretical calculations have been used to investigate the geometrical and electronic structure of the $\text{Tc}_6\text{Br}_{12}$ cluster. The calculated structural parameters are in excellent agreement with the experimental data. NBO analyses indicate the presence of six Tc–Tc single and three $\text{Tc}\equiv\text{Tc}$ triple bonds within the Tc_6^{12+} core.

3.3 Conclusion

Technetium tetrachloride and tetrabromide have been synthesized in the solid-state and characterized by various techniques. Both compounds can be prepared from the reaction of the elements in sealed tubes at elevated temperatures. The crystal structures of TcCl_4 and TcBr_4 are isomorphic with their Pt analogues and are composed of extended zigzag chains of distorted TcX_6 ($X = \text{Cl}, \text{Br}$) octahedra. Technetium tetrachloride and tetrabromide are thermally unstable and decompose in sealed tubes under vacuum resulting in Tc(III) and Tc(II) species; TcCl_4 decomposes to $\alpha\text{-TcCl}_3$ and TcCl_2 while TcBr_4 to TcBr_3 and $\text{Na}\{[\text{Tc}_6\text{Br}_{12}]_2\text{Br}\}$. It is noted that $\text{Na}\{[\text{Tc}_6\text{Br}_{12}]_2\text{Br}\}$ is the first compound to contain a prismatic hexanuclear cluster to be synthesized from a solid phase reaction; this raises the question about the transport in gas phase of hexanuclear cluster. Akin to other transition metal tetrahalides, these materials have great potential for further use as precursors in an array of inorganic and organometallic chemistries, and notably their volatile behavior could be of the utmost interest for applications in separations or thin layer deposition. Other Tc tetrahalides are waiting to be discovered, those include

TcF₄ and TcI₄. It will be of interest to see if these materials would exhibit the structure predicted from DFT calculations [89].

Chapter 4

Technetium Trichlorides, Tribromide, and Triiodide

This chapter focuses on the trivalent binary Tc halides: Tc trichlorides (section 4.1), Tc tribromide (section 4.2) and triiodide (section 4.3). Herein, three new binary Tc halides phases are reported: α -TcCl₃, β -TcCl₃, and TcI₃. The solid-state structure and thermal properties of these trihalides were investigated by experimental methods. For the trichlorides, their electronic structure and transport properties were investigated by theoretical methods. For TcBr₃, its thermal properties have been investigated and a new method for its preparation reported. Finally, in each section the chemistries of the trivalent Tc halides are compared with those of surrounding elements.

4.1 Technetium Trichlorides: α -TcCl₃ and β -TcCl₃

4.1.1 Introduction

Binary transition metal trihalides display a diverse variety of chemical structures and properties; there are more than 20 known structure-types including chains, layers, three dimensional networks composed of metal halide clusters. These have been investigated in depth for Groups V, VI, and VIII [22]. Prior to 2010, Group VII trichlorides were only known for Re; ReCl₃ consists of Re₃Cl₉ clusters with the triangular Re₃⁹⁺ core (Figure 4.1A) [28]. Of the various methods for preparing ReCl₃, the reaction of Re₂(O₂CCH₃)₄Cl₂ with HCl(g) at elevated temperature is often the most direct and highest yielding route [27, 176]. As a precursor, ReCl₃ has served as a synthetic template for more than 50 known compounds that exhibit the Re₃⁹⁺ core, which has greatly expanded the multiply metal-metal bonded chemistry of this element [27]. For Group VI

and VIII, α - MoCl_3 and α - RuCl_3 exhibit the AlCl_3 structure-type and consist of infinite layers of edge-sharing MCl_6 octahedra (Figure 4.1B) [161, 23, 24, 29]. These trichlorides were prepared from the reaction between the elements in sealed tubes. Because the existence of TcCl_3 had been reported in the gas phase [79], it was of interest to pursue its solid-state synthesis. This can be achieved by transposing the methods used for the preparation of the Re, Ru, and Mo trihalides to Tc.

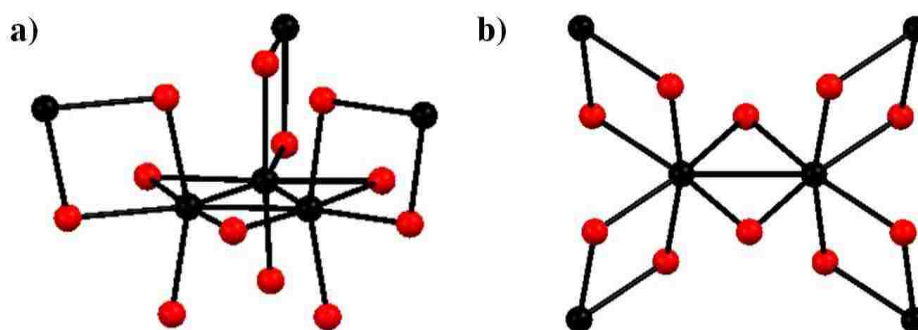


Figure 4.1. Ball-and-stick representations of the structures exhibited by a) ReCl_3 and b) α - MCl_3 ($\text{M} = \text{Mo}, \text{Ru}$). Metal atoms are in black, chlorine atoms are in red.

In this section, the reaction of $\text{Tc}_2(\text{O}_2\text{CCH}_3)_4\text{Cl}_2$ with flowing $\text{HCl}(\text{g})$ and the sealed tube reaction of Tc metal and chlorine gas at elevated temperatures are presented. These reactions lead to two polymorphs of technetium trichloride: α - TcCl_3 and β - TcCl_3 . The preparation, solid-state structure, and thermal properties of these trichlorides are reported. The electronic structure, magnetic, and transport properties of these phases were also analyzed by first principle calculations [162, 163].

4.1.2 Alpha-Technetium Trichloride

4.1.2.1 Experimental Details

Preparation of α -TcCl₃. Technetium trichloride was prepared by reacting Tc₂(O₂CCH₃)₄Cl₂ with HCl(g) at 300 °C using the experimental set-up presented in Chapter 2, Figure 6. A weighted quantity (43 mg, 0.099 mmol) of Tc₂(O₂CCH₃)₄Cl₂ was evenly dispersed in a quartz boat. The apparatus was purged with HCl(g) and the temperature was raised to 300 °C (10 °C/ min) and held there for 3 hours after which the system was cooled to room temperature. During the experiment, Tc₂(O₂CCH₃)₄Cl₂ was visually inspected and a change of color from pink to green occurred at ~100 °C and from green and black at ~ 250 °C. After the reaction, 32 mg of black powder were obtained. Yield = 77%. The black powder was analyzed by PXRD, IR and XAFS spectroscopy, and Tc elemental analysis.

After the reaction, a portion of the black powder (15 mg) was placed in a 30-cm-long Pyrex tube, evacuated (p = 1 mtorr) and the tube was flamed-sealed at 19 cm. The tube was placed in the furnace at 450 °C for 12 hours (10 °C/ min). Following the thermal treatment, a black film and small hexagonal crystals were observed at the cold part of the tube. A hexagonal crystal was selected for analysis by SCXRD.

Thermal decomposition of α -TcCl₃. A sample of α -TcCl₃ (14.6 mg, 0.071 mmol) was placed in a 30-cm-long Pyrex tube, and the tube was then evacuated and sealed at 18 cm. The tube was placed in a tube furnace for 14 hours at 450 °C with the solid at the center of the furnace. After cooling to room temperature, the reaction yielded a black crystalline powder (10.6 mg) at one end of the tube and a red-black amorphous film at the coolest end. The resulting products were analyzed by PXRD and EDX spectroscopy.

4.1.2.2 Results and Discussion

4.1.2.2.a Synthesis of α -TcCl₃

The reaction between Tc₂(O₂CCH₃)₄Cl₂ with HCl(g) is the method of choice for production of weighable amounts of α -TcCl₃. During the heating, a color change from pink to green (~100 °C) and to black (~250 °C) was noticed. Analysis had shown the green product to be Tc₂(O₂CCH₃)₂Cl₄ while the black amorphous compound to be α -TcCl₃.

The Tc₂(O₂CCH₃)₂Cl₄ complex is isostructural with Re₂(O₂CCH₃)₂Cl₄ and consists of two *trans*-acetate ligands bridging to the Tc₂⁶⁺ unit and four terminal chlorides (Figure 4.2). The Tc-Tc distance (2.150(1) Å) is similar to the one found in (*n*-Bu₄N)₂Tc₂Cl₈ (2.147(4) Å) and consistent with the presence of a metal-metal quadruple bond. The electronic spectrum of Tc₂(O₂CCH₃)₂Cl₄ in CH₂Cl₂ exhibits bands at 650 nm, 350 nm and 310 nm, similar to the spectrum of Tc₂Cl₈²⁻ [101]. By analogy with Tc₂Cl₈²⁻, the band at 650 nm is assigned to the $\delta \rightarrow \delta^*$ transition. The mechanism of formation of α -TcCl₃ mimics the one described for rhenium [164]; the dimer Tc₂(O₂CCH₃)₂Cl₄ is formed as an intermediate in the early stage of the reaction while technetium trichloride is later formed at 300 °C (Figure 4.2).

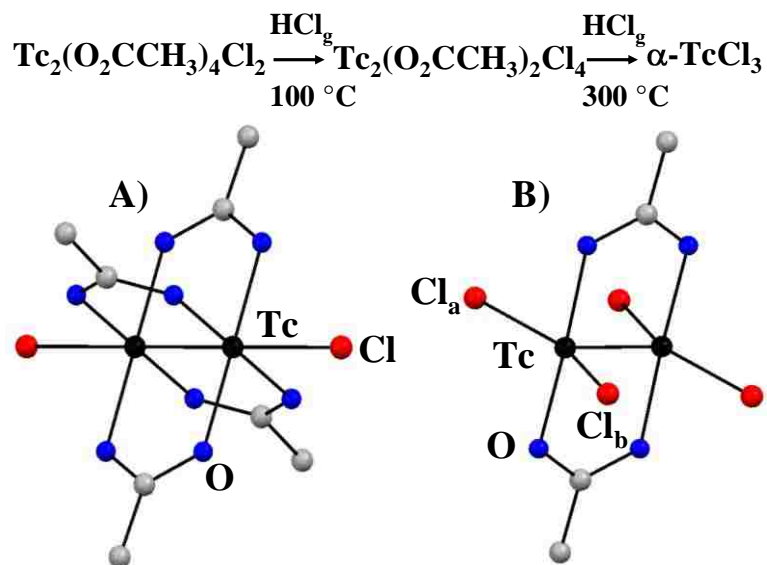


Figure 4.2. Top: Mechanism of formation of $\alpha\text{-TcCl}_3$ from $\text{Tc}_2(\text{O}_2\text{CCH}_3)_4\text{Cl}_2$. Bottom: Ball and stick representation of A) $\text{Tc}_2(\text{O}_2\text{CCH}_3)_4\text{Cl}_2$ and B) $\text{Tc}_2(\text{O}_2\text{CCH}_3)_2\text{Cl}_4$. Color of atoms: Tc in black, Cl in red, O in red, and C in grey. Selected distances(\AA) in $\text{Tc}_2(\text{O}_2\text{CCH}_3)_2\text{Cl}_4$: Tc-Tc 2.150(1), Tc-O 2.021(2), Tc-Cl_a 2.290(1), Tc-Cl_b 2.334(1).

4.1.2.2.b Characterization of $\alpha\text{-TcCl}_3$

Infrared Spectroscopy and Elemental Analysis

The IR spectrum displays no stretching in the region of $4000\text{-}500\text{ cm}^{-1}$ indicative that no $\text{Tc}_2(\text{O}_2\text{CCH}_3)_4\text{Cl}_2$ or $\text{Tc}_2(\text{O}_2\text{CCH}_3)_2\text{Cl}_4$ was present in the sample (Figure 4.3).

The compound is soluble in concentrated HCl(aq) and acetone. For Tc elemental analysis, the solid was suspended in 10 mL of concentrated HCl and warmed for 1 hour at $100\text{ }^\circ\text{C}$. After dissolution, the Tc concentration was determined by UV-visible spectroscopy using the absorbance at 340 nm of the TcCl_6^{2-} anion [111]. Results were consistent with the stoichiometry of TcCl_3 , Anal. Calcd for TcCl_3 : Tc, 48.2. Found: Tc, 47.3. The PXRD pattern of $\alpha\text{-TcCl}_3$ obtained after the reaction at $300\text{ }^\circ\text{C}$ shows the compound to be amorphous.

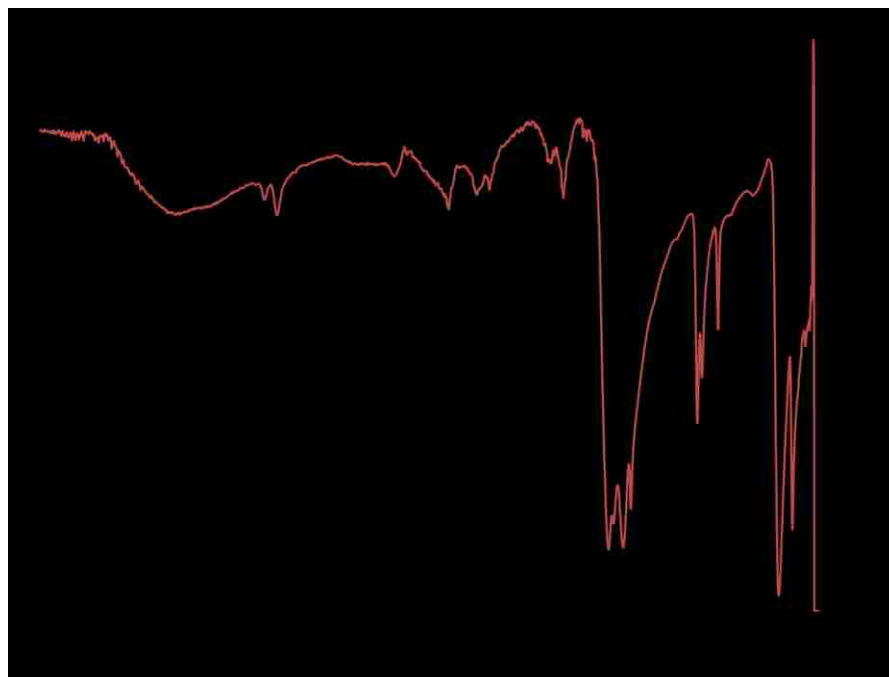


Figure 4.3. IR spectrum of α -TcCl₃ (black) and Tc₂(O₂CCH₃)₄Cl₂ (red).

Single Crystal X-ray Diffraction

The crystal structure of α -TcCl₃ was determined by SCXRD from one of the hexagonal-shaped crystals (Figure 4.4); Alpha-technetium trichloride crystallizes in the trigonal $R\bar{3}m$ space group with cell parameters: $a = b = 10.1035(19)$ Å, $c = 20.120(8)$ Å (full refinement details can be found in Appendix II). The compound is isostructural to ReCl₃ and is composed of triangular clusters of Tc₃Cl₉ units with C_{3v} symmetry [28]. In the Tc₃Cl₉ cluster, each of the Tc atoms is coordinated to two Tc neighbors and five chloride ligands (Figure 4.4). The Tc atoms form an equilateral triangle with Tc-Tc distances of 2.444(1) Å. This distance is 0.045 Å shorter than the Re-Re distance found in ReCl₃ and is indicative of a Tc=Tc double bond.

Each Tc_3Cl_9 unit possesses 3 terminal Cl atoms (Cl1), three bridging Cl atoms (Cl2), and six intermolecular bridging Cl atoms (Cl3) shared with three adjacent Tc_3Cl_9 units (Figure 4.4). The three terminal chlorine atoms are chemically equivalent and the Tc-Cl1 distance (2.237(2) Å) is significantly shorter than those found in several dinuclear Tc(III) complexes [68]. The three bridging Cl2 atoms are also equivalent and form an equilateral triangle (edge = 4.744(2) Å) that is shifted by 0.068(1) Å from the Tc_3^{9+} plane. The Tc-Cl2 distance (2.373(1) Å) is similar to the Tc-(μ -Cl) distance in the hexanuclear cluster $[\text{Me}_4\text{N}]_2[\text{Tc}_6\text{Cl}_6(\mu\text{-Cl})_6]$ [165]. The Cl3 bridging Cl atoms are not chemically equivalent as two distinct distances are noted (2.373(1) Å and 2.585(2) Å). The larger Tc-Cl distance is associated with the Cl atoms *trans* to Tc atoms; a similar distribution of metal-Cl bond distances has already been catalogued and discussed for the Re homologue [28]. The Tc_3Cl_9 units are joined by Cl atoms forming infinite layers four atoms thick (6.80 Å) and perpendicular to the *c*-axis. The shortest interlayer distance (Cl1...Cl2 = 3.451(2) Å) is lower than the sum of the van der Waals radii (3.60 Å) [166]. The intermolecular metallic distance $\text{Tc}\cdots\text{Tc}'$ (3.852(1) Å) precludes any metal-metal bonding between the units.

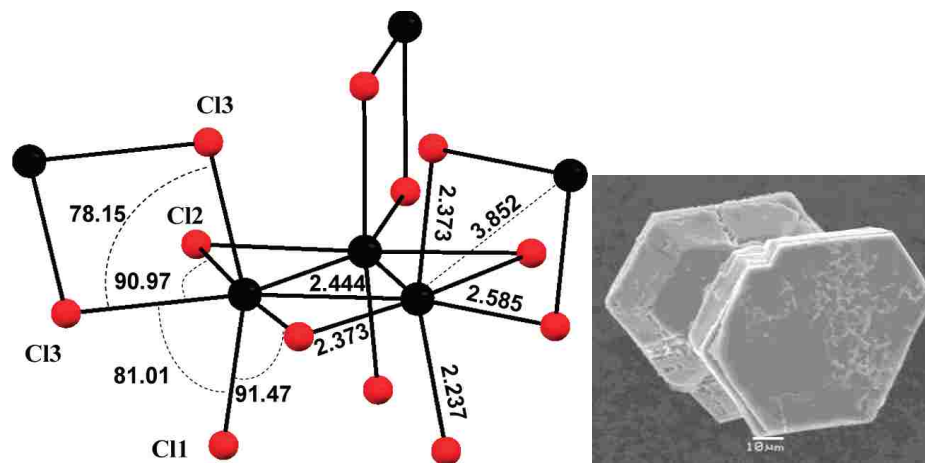


Figure 4.4. Left: Ball-and-stick representation of the Tc_3Cl_9 cluster in $\alpha-TcCl_3$. Portions of the three neighboring clusters are also presented. Angles ($^\circ$) and distances (\AA) are shown. Right: SEM Image (x1000) of a single crystal of $\alpha-TcCl_3$.

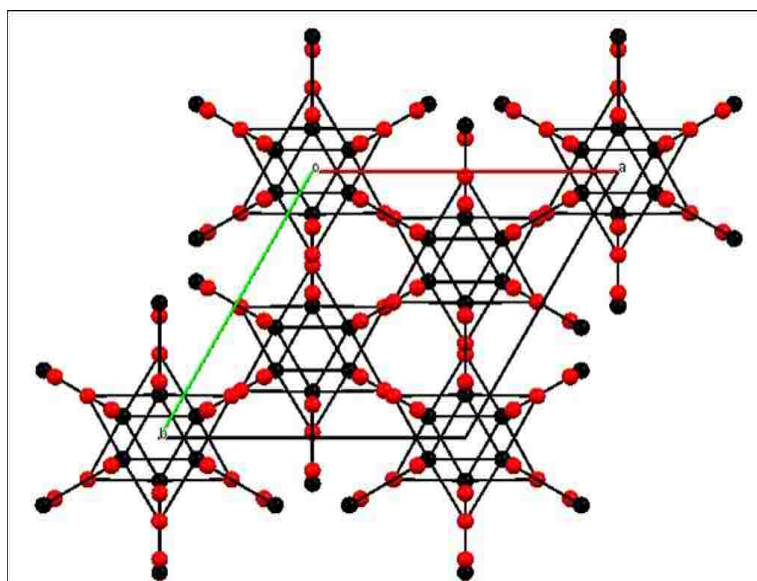


Figure 4.5. Structural view of $\alpha-TcCl_3$ from the c -axis.

X-ray Absorption Fine Structure Spectroscopy

The compound obtained from the reaction of $Tc_2(O_2CCH_3)_4Cl_2$ with $HCl(g)$ at $300\text{ }^\circ\text{C}$ was X-ray amorphous, did not contain any acetate ligands, and had a Tc content

consistent with TcCl_3 (*vide supra*). In order to determine whether it exhibits the $\alpha\text{-TcCl}_3$, $\beta\text{-TcCl}_3$ (*vide infra*), or some other structure, the compound was analyzed by EXAFS spectroscopy. The extracted EXAFS spectrum was k^3 -weighted and the FT done in the k range $2.5 - 14 \text{ \AA}^{-1}$. Two different adjustments were performed considering the structure of $\alpha\text{-TcCl}_3$ and $\beta\text{-TcCl}_3$ [162, 163]. The scattering functions used for the adjustment were calculated from the crystallographic structure of $\alpha\text{-TcCl}_3$ and $\beta\text{-TcCl}_3$ (Figure 4.6). For adjustment, the numbers of atoms were fixed at those of the crystal structures; ΔE_0 was constrained to be the same value for each wave; all other parameters were allowed to vary.

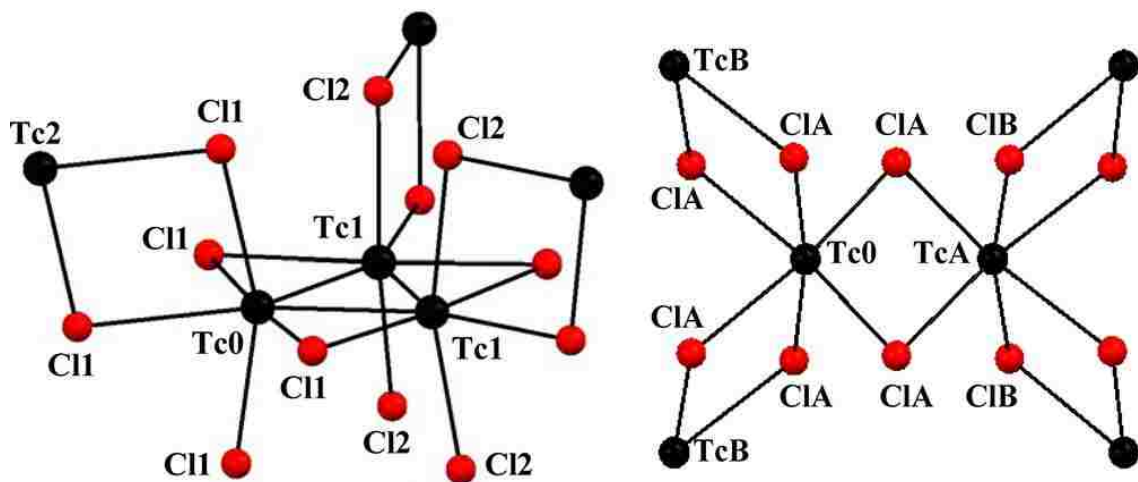


Figure 4.6. Ball-and-stick representations of the $\alpha\text{-TcCl}_3$ (left) and $\beta\text{-TcCl}_3$ (right) clusters used for EXAFS calculations. Tc and Cl atoms are in black and red, respectively. Tc0 represents the absorbing atom.

The best adjustment (Figure 4.7) was obtained considering the structure of $\alpha\text{-TcCl}_3$. Structural parameters (Table 4.1) show the presence of Tc atoms at $2.46(2) \text{ \AA}$ and

3.81(4) Å and of Cl atoms at 2.36(2) Å and 3.68(4) Å; those distances are in agreement with those found in the crystal structure of α -TcCl₃ [162].

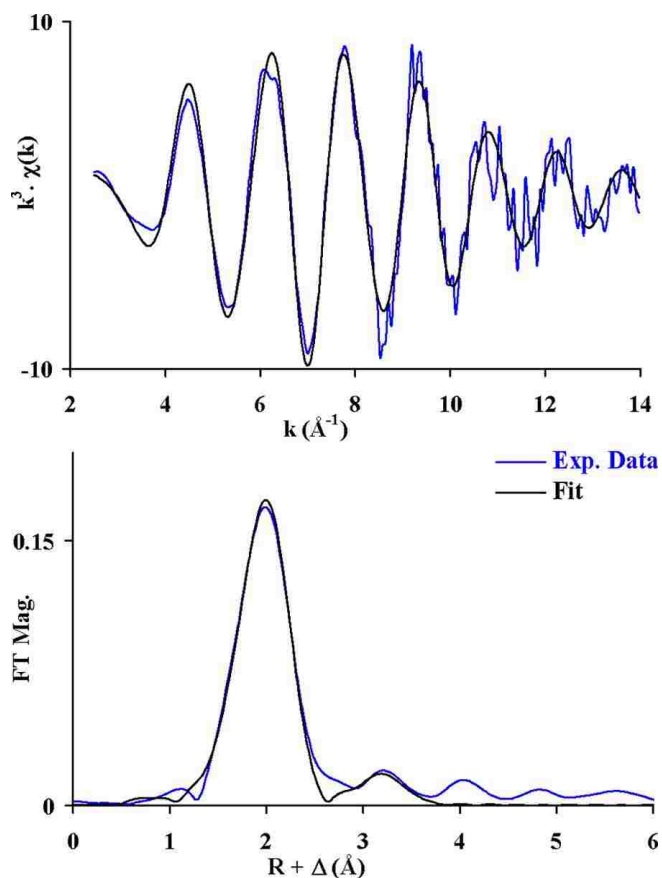


Figure 4.7. Fits of the k^3 -EXAFS spectra (top) and Fourier transform of k^3 -EXAFS spectra (bottom) for α -TcCl₃ obtained from the reaction of Tc₂(O₂CCH₃)₄Cl₂ with HCl(g) at 300 °C. Adjustment was performed between $k = 2.5$ and 14 \AA^{-1} considering the structure of α -TcCl₃. Experimental data are in blue, and the fit is in black.

Table 4.1. Structural parameters obtained by adjustment of k^3 -EXAFS spectra of α -TcCl₃ obtained from the reaction of Tc₂(O₂CCH₃)₄Cl₂ with HCl(g) at 300 °C. Adjustment between $k = 2.5$ and 14 \AA^{-1} considering the structure of α -TcCl₃. ΔE_0 (eV) = 2.29 eV. Reduced $\chi^2 = 70$. Values found by SCXRD in α -TcCl₃ are in italic.

Scattering	CN	R (Å)	σ^2 (Å ²)
Tc0 \leftrightarrow Cl1	5	2.36(2), 2.388(4)	0.0056
Tc0 \leftrightarrow Tc1	2	2.46(2), 2.4445(7)	0.0046
Tc0 \leftrightarrow Cl2	4	3.68(4), 3.614(4)	0.0083
Tc0 \leftrightarrow Tc2	1	3.81(4), 3.852(1)	0.0130

4.1.2.2.c Thermal Properties of α -TcCl₃

A sample of α -TcCl₃ was reacted in a sealed tube under vacuum at 450 °C for 14 h. After the reaction, a dark black powder and a dark red amorphous film (cold end of the tube) were observed. The PXRD of the black powder (Figure 4.8) indicates the presence of TcCl₂ (see Chapter 5) and Tc metal. A [Cl:Tc] ratio of 2.09(1) was determined by EDX spectroscopy from the integrated intensity of the Tc-K α and Cl-K α lines and is consistent with the TcCl₂ stoichiometry.

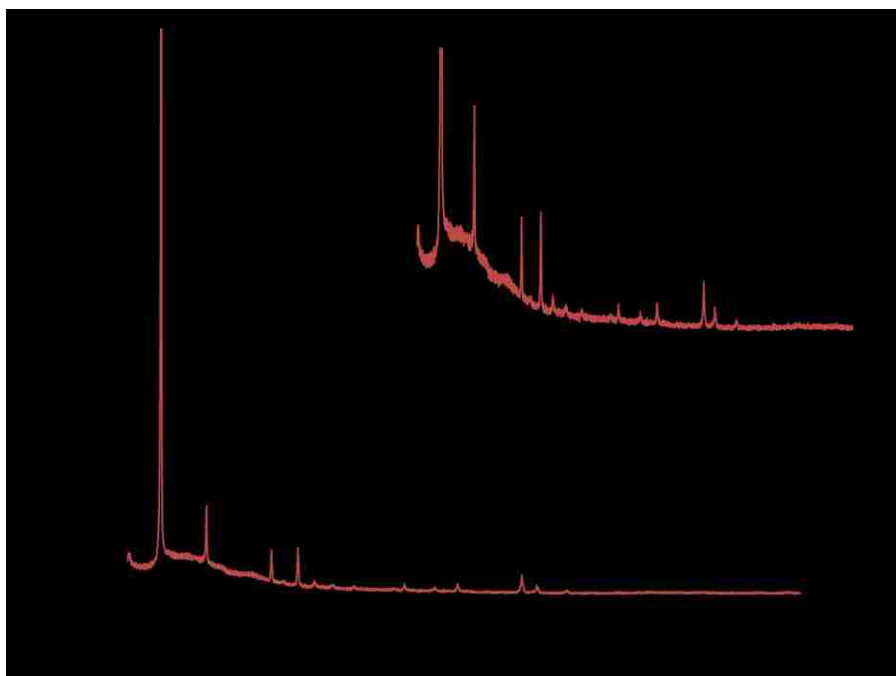


Figure 4.8. PXRD pattern of the product obtained from the thermal decomposition of α -TcCl₃ under vacuum at 450 °C (black). PXRD of TcCl₂ single crystals (red).

4.1.2.2.d Computational Studies on α -TcCl₃

Interestingly, α -TcCl₃ is isostructural with ReCl₃, while TcBr₃ is isostructural with MBr₃ (M = Mo, Ru) [97]. Prior to its isolation, it was assumed that TcCl₃ would crystallize either with the ReCl₃ structure ($R\bar{3}m$), the α -MoCl₃ structure ($C2/m$), or the TcBr₃ structure ($Pmmm$) [97]. In order to provide a theoretical framework, first-principles density functional theory calculations on Tc trichloride with the ReCl₃, TcBr₃, and α -MoCl₃ structures were carried out. This approach was previously found to accurately reproduce structural parameters observed experimentally for the Tc halide systems [89, 167].

The main candidate structures investigated for TcCl_3 were the ReCl_3 -type structure crystallizing in the $R\bar{3}m$ space group with the Tc_3Cl_9 motif, the TcBr_3 -type structure in the $Pm\bar{3}n$ space group, and the $\alpha\text{-MoCl}_3$ -type structure in the $C2/m$ space group symmetry. Structural relaxation and total energy calculations for the three types of structures were performed. Consistent with experimental results, the ReCl_3 -type structure with $R\bar{3}m$ symmetry (Figure 4.9) is found to be the most stable TcCl_3 structure ($E = -18.743$ eV/f.u.) with calculated lattice parameters $a = b = 10.31$ Å and $c = 22.41$ Å. The TcCl_3 structure crystallizing with the ReCl_3 motif is energetically more favorable than the ones with either the $\alpha\text{-MoCl}_3$ or TcBr_3 structures, by ca. 0.34 eV and 0.39 eV per formula unit, respectively. Chemical bonding in the Tc_3Cl_9 cluster has been analyzed by theoretical methods [168]. The results indicate the presence of a $\text{Tc}=\text{Tc}$ double bond between the Tc atoms within the Tc_3^{9+} core. Occupation number calculations of the $\text{Tc}=\text{Tc}$ bond show the presence of 1.99 electrons on both the σ and π orbitals, which lead to an effective bond order of 2. Density-of-state (DOS) calculations predict a band gap of 0.6 eV that indicates $\alpha\text{-TcCl}_3$ to be a semiconductor.

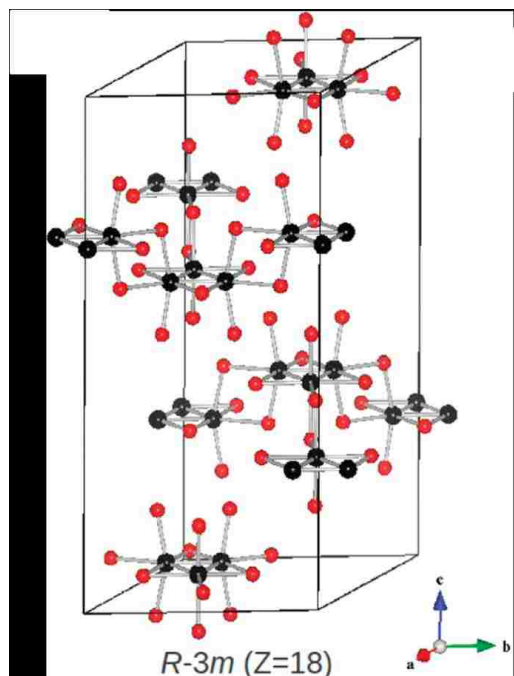


Figure 4.9. Ball-and-stick representation of the calculated structure of Tc trichloride with the ReCl_3 structure ($R\bar{3}m$). Tc atoms are in black, Cl atoms are in red.

4.1.3 Beta-Techneium Trichloride

4.1.3.1 Experimental Details

Synthesis of $\beta\text{-TcCl}_3$. Technetium metal (60.5 mg, 0.611 mmol), was placed in a Pyrex tube (L = 43 cm) and flamed under vacuum. After backfilling with Cl_2 , the end of the tube was cooled in liquid nitrogen and the gas (~17 mL, 0.68 mmol) was condensed. The tube was flame-sealed (L = 18 cm) and placed in a clamshell furnace; the temperature was increased (10 °C/min) and held for 24 hours at 450°C. After cooling to room temperature, a dark crystalline powder (82.4 mg) was observed at the end of the tube that contained the metal and some very thin dark needles were present on the surface of the central portion of the tube. At the end of the tube located in the coldest area of the

furnace, a dark hygroscopic product had formed. The dark hygroscopic product was analyzed by PXRD.

After the reaction, the product from the cool end of the tube was isolated and placed in a 30-cm-long Pyrex tube, evacuated to 1 mtorr, and sealed (L= 18 cm). The tube was placed in the furnace at 280 °C for 6 days. After this time, a dark crystalline product (2 mg) was produced in the hot part of the tube and a red film in the cold part. The crystalline product was analyzed by EDX spectroscopy and SCXRD.

Thermal Conversion of β -TcCl₃ to α -TcCl₃. Technetium metal (62.2 mg) was sealed with Cl₂ and reacted at 450°C. After the experiment, the compound at the cool end of the tube was removed and sealed in a 30-cm-long Pyrex tube and placed in the furnace at 280 °C for 16 days. After the reaction, the product was analyzed by SCXRD.

4.1.3.2 Results and Discussion

4.1.3.2.a Synthesis of β -TcCl₃

Technetium metal and chlorine gas were reacted (Tc:Cl; 1:2.5) in a sealed tube at 450 °C for 24 h [143]. After the reaction, a dark powder containing technetium metal and TcCl₂ (see Chapter 5) were obtained in the hot part of the tube, β -TcCl₂ needles in the center of the tube, and a dark hygroscopic product in the colder part of the tube. The dark hydroscopic product was analyzed by PXRD (Figure 4.10). The PXRD pattern of the dark product shows three characteristic diffraction peaks at $2\theta = 16.51^\circ$, 12.66° , and 15.11° (Figure 4.10). The first and third peak are consistent with the presence of TcCl₄ (hygroscopic) while the peak at 15.11° is attributed to β -TcCl₃ [162,91].

In order to separate TcCl₄ from the other crystalline products, the dark hygroscopic product was sealed in a tube under vacuum and treated for 6 days at 280 °C;

at this temperature TcCl_4 is volatile, allowing its separation from the remaining products [19]. After 6 days of treatment, a dark crystalline $\beta\text{-TcCl}_3$ was obtained. Unlike $\alpha\text{-TcCl}_3$ that can be easily produced in weighable quantities, $\beta\text{-TcCl}_3$ is formed in minute yields (~10 mg; yield: ~2%) from this reaction. Such low yields may indicate that the compound is thermally unstable under these conditions and ultimately decomposes to $\alpha\text{-TcCl}_3$ or TcCl_2 .

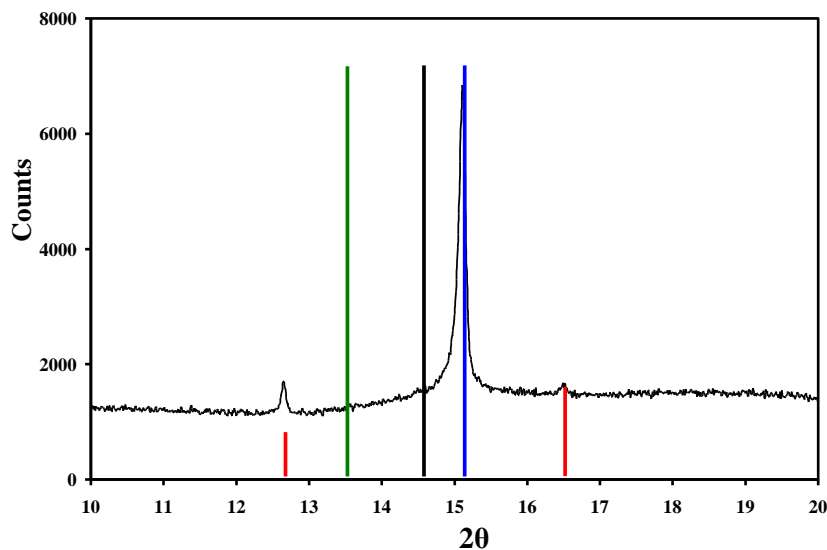


Figure 4.10. PXRD pattern (black) of the dark hygroscopic product obtained at the cold end of the sealed tube after the reaction of Tc metal and chlorine gas at 450 °C.

Simulated positions presented of the most intense peaks for: TcCl_4 (red), TcCl_2 (black), $\alpha\text{-TcCl}_3$ (green), and $\beta\text{-TcCl}_3$ (blue).

4.1.3.2.b Characterization of $\beta\text{-TcCl}_3$

SEM Analysis

Image analysis of $\beta\text{-TcCl}_3$ by SEM shows layered crystals approximately 100 μm in size with a hexagonal shape (Figure 4.11). The composition of these crystals was semi-

quantitatively determined by EDX spectroscopy (Figure 4.11). The spectrum yielded only lines from Tc-K α and Cl-K α indicating the product to be a binary Tc chloride. In addition, a [Cl:Tc] ratio of 2.99(9), determined from the integrated intensity of the Tc-K α and Cl-K α lines is consistent with the TcCl₃ stoichiometry.

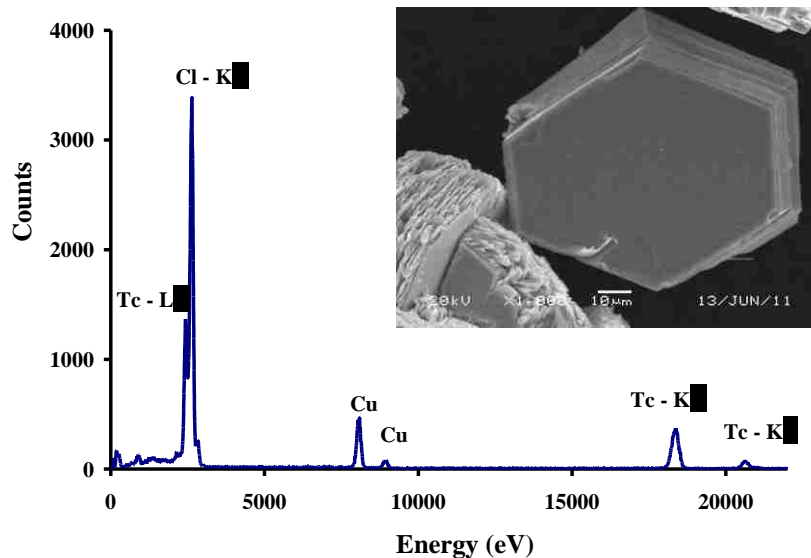


Figure 4.11. EDX spectrum of β -TcCl₃ displaying the Tc-K α , Tc-L α , and the Cl-K α lines. The Cu line is due to the sample holder. SEM image of a layered hexagonal β -TcCl₃ crystal (x1000).

Single crystal X-ray diffraction

A hexagonal crystal was used for the structure determination by SCXRD. The compound crystallizes with a distorted AlCl₃ structure-type in the monoclinic *C2/m* space group with cell parameters $a = 6.013(4)$ Å, $b = 9.713(4)$ Å, and $c = 6.207(3)$ Å, $\beta = 108.71^\circ$ (additional refinement parameters are presented in Appendix II). The compound is isostructural to α -MoCl₃ [23, 29]. The structure of β -TcCl₃ consists of

infinite ordered layers of edge-sharing TcCl_6 octahedron oriented parallel with the ab plane (Figure 4.12). Within a layer, the Tc atoms form an infinite sheet with a distorted honeycomb pattern sandwiched by two layers of Cl atoms. The stacking of the TcCl_3 layers is similar to the one in $\alpha\text{-MoCl}_3$ and a separation of 5.87 Å between the Tc sheets is observed. The shortest inter-atomic distance between TcCl_3 layers ($\text{Cl}\cdots\text{Cl} = 3.561$ Å) is lower than the sum of the van der Waals radii (3.60 Å) and indicate the layers to be in weak interaction. Within a layer, the coupling of Tc atoms into Tc_2^{6+} pair oriented along the b axis occurs and two set of Tc-Tc distances are observed (i.e., $\text{Tc-Tc} = 2.861(3)$ Å and $\text{Tc}\cdots\text{Tc}' = 3.601(2)$ Å). The Tc-Tc distance in the Tc_2^{6+} pair is characteristic of significant metal-metal-bonding interaction (*vide infra*), whereas the $\text{Tc}\cdots\text{Tc}'$ distance is similar to the one observed in TcCl_4 (i.e., 3.605(1) Å) which precludes any metal-metal bond formation [91]. Strong coupling between metal atoms occurs in other layered trichlorides, such as $\alpha\text{-MoCl}_3$ ($\text{Mo-Mo} = 2.757(3)$ Å). For $\alpha\text{-RuCl}_3$, coupling is still subject to discussion: Ru_2^{6+} pairs were not ascertained by XRD, but weak coupling has been proposed based on scanning tunneling microscopy measurements. The disparity (ΔMM) between paired and non-paired metal-metal distances in layered MCl_3 ($\text{M} = \text{Mo}, \text{Tc}, \text{Ru}$) (Table 4.2) follow the order $\Delta\text{MoMo} > \Delta\text{TcTc} > \Delta\text{RuRu}$. The reason for the disparity between the MM paired and nonpaired distances has already been discussed for trichlorides having the AlCl_3 structure-type [22], and a Peierls distortion is likely the origin of dimerization (i.e., formation of M_2^{6+} unit). Two significant structural consequences of the Tc-Tc coupling are the deformation of the TcCl_6 octahedron and of the Tc honeycomb ($b/a = 1.624$ Å) from the hexagonal geometry ($b:a = \sqrt{3} = 1.732$ Å). There are two types of

Cl atoms and three distinct Tc–Cl bond distances (Figure 4.13). The shortest bond involves the bridging Cl within the Tc_2^{6+} pair ($\text{Tc–Cl1} = 2.316(3) \text{ \AA}$), while the longest bonds are the $\text{Cl2}_{(a,b)}$ atoms in *trans* positions to the Cl1 atoms ($\text{Tc–Cl2}_{(a,b)} = 2.434(3) \text{ \AA}$). Finally, a Tc–Cl distance of $2.403(2) \text{ \AA}$ is observed for the $\text{Cl2}_{(c,d)}$ atoms located in *cis* positions to the Cl1 atom. As a result of metal–metal bond formation, the Cl1 atoms are pushed away from the center of the layer and are located in a plane 0.38 \AA above the plane formed by the Cl2 atoms.

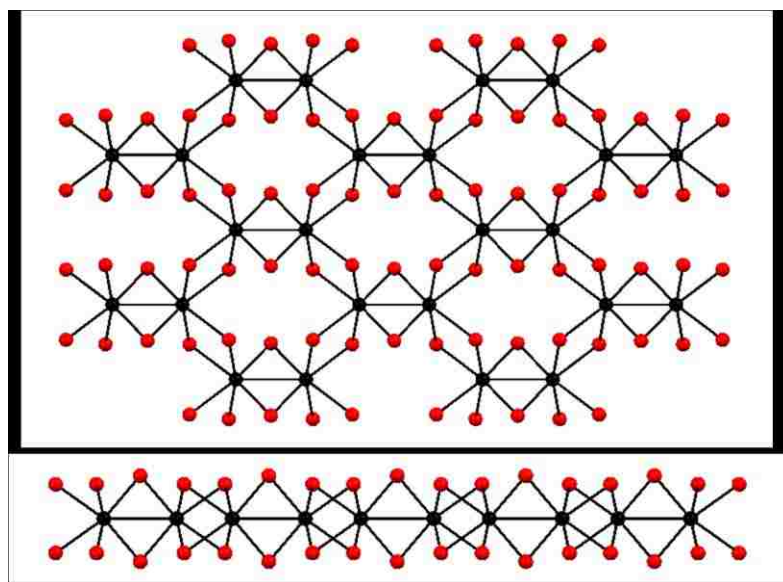


Figure 4.12. Ball-and-stick representation of a $\beta\text{-TcCl}_3$ layer. View perpendicular to the *ab* plane (top) and in the *a* direction (bottom). Tc and Cl atoms are in black and red, respectively.

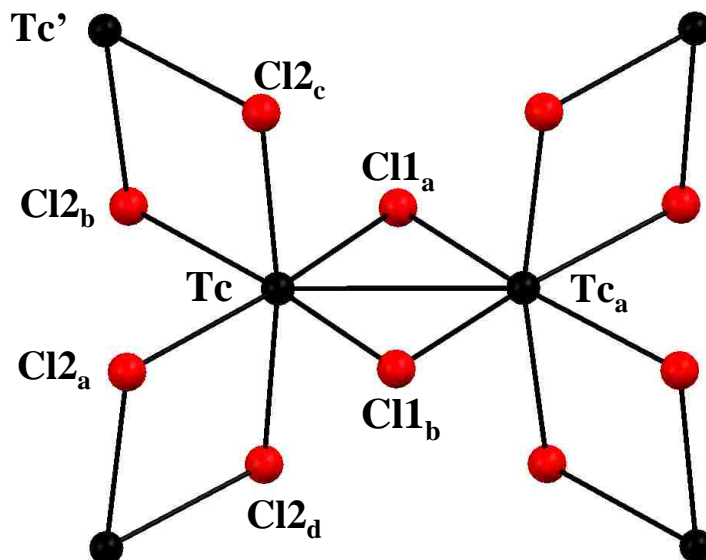


Figure 4.13. Ball-and-stick representation of the edge-sharing octahedra in β - TcCl_3 . The Cl and Tc atoms are red and black, respectively. Selected distances (\AA) and angles ($^\circ$): Distances: $\text{Tc}_a\text{-Tc}_b$ 2.861(3), $\text{Tc}_a\text{-Tc}'$ 3.601(2), $\text{Tc}_a\text{-Cl}_{1(a,b)}$ 2.316(3), $\text{Tc}_a\text{-Cl}_{2(a,b)}$ 2.434(3), $\text{Tc}_a\text{-Cl}_{2(c,d)}$ 2.403(2), $\text{Cl}_{1a}\text{-Cl}_{1b}$ 3.642(4). Angles: $\text{Tc}_b\text{-Tc}_a\text{-Cl}_{2(c,d)}$ 95.13(6), $\text{Cl}_{1a}\text{-Tc}_a\text{-Cl}_{1b}$ 103.71(12), $\text{Cl}_{2a}\text{-Tc}_a\text{-Cl}_{2b}$ 85.50(8), $\text{Cl}_{2c}\text{-Tc}_a\text{-Cl}_{1a}$ 94.07(10), $\text{Cl}_{2c}\text{-Tc}_a\text{-Cl}_{1b}$ 92.25(10), $\text{Cl}_{2c}\text{-Tc}_a\text{-Cl}_{2a}$ 88.69(8), $\text{Cl}_{2c}\text{-Tc}_a\text{-Cl}_{2b}$ 83.78(9).

Table 4.2. M-M and M...M distances in α - MCl_3 (M = Mo, Ru) and β - TcCl_3 .

Distance (\AA)	MoCl_3 ^[23]	TcCl_3	RuCl_3 ^[161]
M-M	2.757(3)	2.861 (3)	3.44(1)
M...M	3.714(3)	3.601(2)	3.45(1)
ΔMM	0.957(4)	0.740(3)	0.01(1)

4.1.3.2.c Thermal Behavior of β - TcCl_3

The compound β - TcCl_3 is thermally unstable, after 16 days at 280 $^\circ\text{C}$ it converted to hexagonal crystals. The crystals were analyzed by SCXRD and indexed as α - TcCl_3 ($R\bar{3}m$; $a = b = 10.16 \text{ \AA}$, $c = 20.26 \text{ \AA}$, $\alpha = \beta = 90^\circ$, $\gamma = 120^\circ$). These experimental results

are somewhat consistent with first principle calculations that have determined the α -phase to be the more energetically stable form of TcCl_3 [162, 163].

4.1.3.2.d Computational Studies on β - TcCl_3

The structure of β - TcCl_3 was further analyzed by DFT techniques. As shown previously (section 4.1.2.2.d), the relaxed β - TcCl_3 structure crystallizing in the space group $C2/m$ is energetically less favorable than the α - TcCl_3 structure with the $R\bar{3}m$ symmetry. The space group of the relaxed structure of β - TcCl_3 was determined with ± 0.01 Å accuracy. The computed lattice parameters of β - TcCl_3 are $a = 6.15$ Å, $b = 9.68$ Å, $c = 6.65$ Å, and $\beta = 107.7^\circ$. The calculations confirm the structural impact of the Tc–Tc bonding (i.e., deformation of the Tc honeycomb and of the TcCl_6 octahedra). The calculated bond distances (Tc–Tc = 2.74 Å, Tc \cdots Tc' = 3.72 Å, and Tc–Cl = 2.33 Å, 2.43 Å, and 2.46 Å) are in overall fair agreement with the experimental data.

An understanding of the metal–metal bonding in layered MCl_3 systems can be approached by the study of molecules containing the $\text{M}(\mu\text{-Cl})_2\text{M}$ fragment ($\text{M} = \text{Mo}, \text{Tc}$). Previous studies on the hypothetical $\text{Mo}_2\text{Cl}_6(\text{PH}_3)_4$ complex have shown that the metal–metal bond can be described as a double bond with σ and π character [169]. This result further supported the presence of a weak double bond in α - MoCl_3 that was reported [23, 29]. For technetium, the hypothetical $\text{Cl}_4\text{Tc}(\mu\text{-Cl})_2\text{TcCl}_4^{4-}$ fragment was studied. The occupancy of the metal-based orbitals in the metal–metal-bonded singlet state ($S = 0$) and the highest-multiplicity state ($S = 2$) for the d^4 – d^4 configuration can be idealized as $\sigma^2\pi^2\delta^2\delta^*\pi^*\sigma^*$ and $\sigma^1\pi^1\delta^2\delta^*\pi^*\sigma^*$, respectively [170]. The computed Tc–Tc bond distance was found to be 2.71 Å for $S = 0$ and 3.87 Å for $S = 2$. The Tc–Tc bond distance for $S = 0$ is close to the value of 2.74 Å found in the β - TcCl_3 crystal structure relaxed

with DFT. The effective bond order calculated for the $S = 0$ configuration (i.e., 1.38) indicates the presence of a weak double bond. Therefore, similar to the case of α - MoCl_3 , a weak $\text{Tc}=\text{Tc}$ double bond with σ and π character is suggested between the Tc atoms.

Calculations also predict β - TcCl_3 to be slightly paramagnetic, with a magnetization of $0.9 \mu_{\text{B}}/\text{Tc}$. This value is within the range of the experimentally observed magnetic moments for α - MoCl_3 ($0.49 \mu_{\text{B}}$) and α - RuCl_3 ($2.25 \mu_{\text{B}}$) [23, 24, 29, 171, 172]. Density-of-state calculations are consistent with metallic character; this contrasts with α - TcCl_3 , a semiconductor (Figure 4.14), and with α - RuCl_3 , which is a Mott insulator [173]. In β - TcCl_3 , the metallic character stems predominantly from Tc 4d orbitals, which are dominant in the vicinity of the Fermi level, with significant orbital hybridization with Cl 2p. The Cl 2p valence states become the major contribution to the DOS below ~ 2 eV.

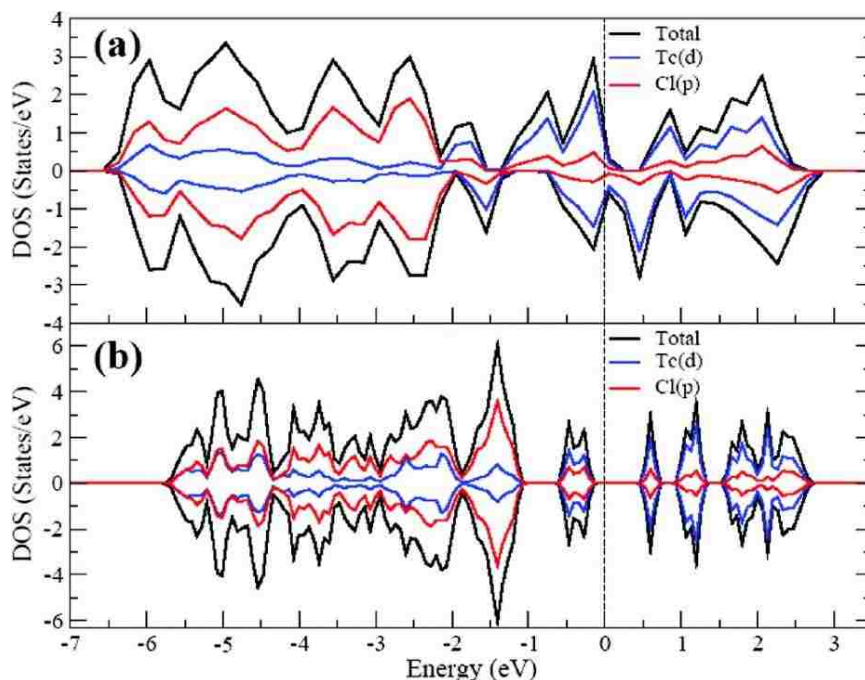


Figure 4.14. Total and partial DOSs per formula unit of (a) β -TcCl₃ and (b) α -TcCl₃.

Orbital-projected DOSs are represented for Tc 4d and Cl 2p orbitals. Positive and negative values of the DOS correspond to spin-up and spin-down contributions.

4.1.4 Summary

Two new polymorphs of TcCl₃ have been prepared and characterized: α -TcCl₃ and β -TcCl₃. Alpha-TcCl₃ has been synthesized in weighable quantities from the reaction between Tc₂(O₂CCH₃)₄Cl₂ and HCl(g) at 300 °C while β -TcCl₃ has been identified from the reaction between Tc metal and Cl₂(g). The mechanism of formation of α -TcCl₃ mimics the one described for Re and Tc₂(O₂CCH₃)₂Cl₄ is formed as intermediate in the early stage of the reaction. For β -TcCl₃, the compound is obtained congruently with TcCl₄ and TcCl₂. To the best of our knowledge, Tc is the only transition metal where three binary chloride phases in different oxidation states (i.e., TcCl₄, TcCl₃, and TcCl₂) are formed congruently from the reaction of elements. Concerning their solid-state

structure, α -TcCl₃ is isomorphous to ReCl₃ while β -TcCl₃ is to α -MCl₃ (M = Mo, Ru). Beta-TcCl₃ is the first example of a d⁴ metal with this structure-type. Concerning their thermal properties, both trichlorides are unstable: β -TcCl₃ is converted to α -TcCl₃ after 16 days at 280 °C and α -TcCl₃ decomposes to β -TcCl₂ and Tc metal after 12 h at 450 °C. The conversion of β -TcCl₃ to α -TcCl₃ is consistent with calculations that predict β -TcCl₃ to be energetically less stable than α -TcCl₃. Calculations also show that both α -TcCl₃ and β -TcCl₃ exhibit a Tc=Tc double bond with σ and π character; bond-order calculations show the Tc=Tc bond to be stronger for α -TcCl₃ than for β -TcCl₃. Similar calculations performed on the bromide system indicate that TcBr₃ with the Re₃Br₉ structure-type should be the most stable form of TcBr₃; the preparation of Tc₃Br₉ will be investigated in section 4.2 (*vide infra*).

4.2 Technetium Tribromide

4.2.1 Introduction

Because Tc is the lighter congener of Re, it often demonstrates chemically similar behaviour [32]. An example of this is the homologous reaction of Tc₂(O₂CCH₃)₄Cl₂ with flowing HCl(g) at 300 °C that yields α -TcCl₃ with the ReCl₃ structure-type [162, 28, 176]. Alpha-TcCl₃ has also been synthesized from the decomposition of TcCl₄ under vacuum at 450 °C and the thermal treatment of β -TcCl₃ at 280 °C under vacuum [163, 19]. Unlike α -TcCl₃, β -TcCl₃ exhibits structural similarities to the Ru and Mo analogues, crystallizing with the AlCl₃ structure-type [163]. This structural similarity with the Ru and Mo is also observed for TcBr₃.

Tchnetium tribromide has been obtained congruently with TcBr_4 from the stoichiometric reaction of the elements in a sealed tube at elevated temperature (see Chapter 1). This method yields a TcBr_3 phase with the TiI_3 structure-type, which consists of infinite chains of face-sharing TcBr_6 octahedra (Figure 4.15) [97]. A previous study mentioned that Tc_3Br_9 , which would be isostructural to $\alpha\text{-TcCl}_3$ and Re_3Br_9 , was obtained from the bromination of $[\text{Tc}(\text{CO})_3\text{Br}]_4$, but no crystallographic data were reported [174]. With regard to this information, the existence of Tc_3Cl_9 and the trending chemical behavior of the Re_3X_9 system ($\text{X} = \text{Cl}, \text{Br}, \text{I}$) [28], it was of interest to perform the reaction of $\text{Tc}_2(\text{O}_2\text{CCH}_3)_4\text{Cl}_2$ with flowing $\text{HBr}(\text{g})$ at elevated temperatures in an attempt to isolate Tc_3Br_9 .

The thermal decomposition of binary transition metal halides is a practical method for isolating low-valent phases [124, 175]. For Tc, previous studies performed at 450 °C under vacuum have shown that TcCl_4 decomposes sequentially to $\alpha\text{-TcCl}_3$ and TcCl_2 , while TcBr_4 decomposes to TcBr_3 and $\text{Na}\{[\text{Tc}_6\text{Br}_{12}]_2\text{Br}\}$ [19,152].

In this section, the reactions of $\text{Tc}_2(\text{O}_2\text{CCH}_3)_4\text{Cl}_2$ with flowing $\text{HBr}(\text{g})$ at 150 °C and 300 °C are reported. The reaction products were characterized using XRD, EDX spectroscopy, and IR spectroscopy. The thermal properties of TcBr_3 were studied under vacuum in sealed tubes at elevated temperature [21].

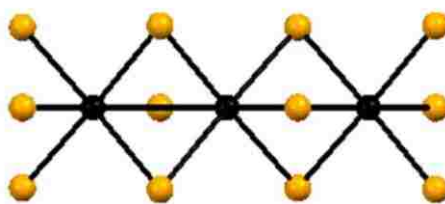


Figure 4.15. Ball-and-stick representation of the structure of MBr_3 ($M = Mo, Tc, Ru$).

Metals atoms are in black and Br atoms are in orange.

4.2.2 Experimental Details

Reaction of $Tc_2(O_2CCH_3)_4Cl_2$ with $HBr(g)$ at $150\text{ }^\circ C$. The experimental set-up used to prepare TcX_3 ($X = Cl, Br$) is presented in Chapter 2, Figure 2.7. The $Tc_2(O_2CCH_3)_4Cl_2$ (65.6 mg, 0.15 mmol) was evenly dispersed in a quartz boat. The boat was placed into the middle of a quartz tube situated in the clamshell furnace. The tube was initially purged with $Ar(g)$ for 15 minutes at room temperature; the temperature was then increased to $150\text{ }^\circ C$ ($10\text{ }^\circ C/min$) and held for 5 minutes under $Ar(g)$. Using a T-shaped stopcock, the gas was switched to $HBr(g)$ and an immediate color change from crimson to a black-purple was observed. The compound was reacted for 1 hour under flowing $HBr(g)$ at $150\text{ }^\circ C$ after which the tube was cooled to room temperature under flowing $HBr(g)$. A black $TcBr_3$ powder (86.5 mg, 0.26 mmol, yield: 84%) was obtained after the reaction.

After the reaction, the black $TcBr_3$ powder was placed in a Pyrex tube ($L = 30$ cm) and sealed ($L = 18$ cm) under vacuum (1 mtorr). The sealed tube was placed in a clamshell furnace, heated to $150\text{ }^\circ C$ ($10\text{ }^\circ C/min$), and held there for 24 hours; a small amount of a black amorphous film sublimed to the cooler end of the tube and the remaining powder was characterized by PXRD.

Reaction of $\text{Tc}_2(\text{O}_2\text{CCH}_3)_4\text{Cl}_2$ with $\text{HBr}(\text{g})$ at $300\text{ }^\circ\text{C}$. The reaction of

$\text{Tc}_2(\text{O}_2\text{CCH}_3)_4\text{Cl}_2$ (67.8 mg, 0.16 mmol) with flowing $\text{HBr}(\text{g})$ at $300\text{ }^\circ\text{C}$ was performed using the same method as that above. The apparatus was purged with $\text{Ar}(\text{g})$ for 15 minutes and the temperature was increased ($10\text{ }^\circ\text{C}/\text{min}$) to $150\text{ }^\circ\text{C}$ and held for 5 minutes, after which the atmosphere was switched to $\text{HBr}(\text{g})$ and the temperature was then increased ($10\text{ }^\circ\text{C}/\text{min}$) to $300\text{ }^\circ\text{C}$ and held there for 1 hour. After the reaction, the black TcBr_3 powder (83.4 mg, 0.25 mmol, yield: 77 %) was recovered. The powder was sealed in a Pyrex tube ($L = 18\text{ cm}$) under vacuum and heated in the furnace at $300\text{ }^\circ\text{C}$ for 24 hours; a dark film at the coolest portion of the tube was observed, and the remaining powder was analyzed by PXRD and IR spectroscopy.

Decomposition of TcBr_3 in Pyrex. Technetium tribromide (32.0 mg, 94.5 μmol) was placed in a 30-cm-long Pyrex tube and flame-sealed ($L = 18\text{ cm}$) under vacuum. The resulting tube was placed in a furnace with the solid at the center of the furnace and reacted at $450\text{ }^\circ\text{C}$ for 24 hours. After cooling to room temperature, the reaction yielded a dark crystalline powder, rail spike crystals adjacent to the powder, needle crystals at the cooler end of the tube, and a dark amorphous film at the end of the tube. The rail spike and needle crystals were indexed by SCXRD; the remaining solid was characterized by PXRD.

Decomposition of TcBr_3 in Quartz. Technetium tribromide (32.2 mg, 95.1 μmol) was placed in a 30 cm-long quartz tube and sealed at 18 cm under vacuum. The tube was reacted using the same method as the decomposition in Pyrex for 24 hours at $450\text{ }^\circ\text{C}$. After the reaction, the contents of the cooled tube included a grayish crystalline powder (10.6 mg), metallic purple needle crystals near the cooler portion of the tube, and a dark

amorphous film at the end of the tube. The single crystals were analyzed by SCXRD, and the remaining powder was characterized by PXRD.

4.2.3 Results and Discussion

4.2.3.1 Synthesis of TcBr_3

Technetium tribromide was synthesized from the reaction of $\text{Tc}_2(\text{O}_2\text{CCH}_3)_4\text{Cl}_2$ with flowing $\text{HBr}(\text{g})$ at 150 °C and 300 °C in excellent yields. The experimental setup required the use of two gases (i.e., $\text{Ar}(\text{g})$ and $\text{HBr}(\text{g})$) to prevent the premature release of acetic acid under its boiling point from the reaction $\text{HBr}(\text{g})$ with $\text{Tc}_2(\text{O}_2\text{CCH}_3)_4\text{Cl}_2$. In comparison to the sealed tube method previously used, this synthetic route is an efficient way to prepare TcBr_3 in weighable quantities free of TcBr_4 and/or Tc metal. This will better allow for TcBr_3 to serve as a starting material for other novel compounds [100].

Molecular transition-metal acetate dimers are known for many second- and third-row metals: $\text{M}_2(\text{O}_2\text{CCH}_3)_4$ ($\text{M} = \text{Mo}, \text{W}, \text{Rh}$) and $\text{M}_2(\text{O}_2\text{CCH}_3)_4\text{Cl}_2$ ($\text{M} = \text{Re}, \text{Tc}, \text{Os}$). The reaction of these compounds ($\text{Mo}, \text{Rh}, \text{Re},$ and Tc) with flowing $\text{HX}(\text{g})$ at elevated temperatures is a direct route to binary metal halides (Table 4.3) [176]. For Mo , these reactions yield $\beta\text{-MoX}_2$ ($\text{X} = \text{Cl}, \text{Br}, \text{I}$), whereas for Rh , these reactions result in the formation of RhX_3 and the metal. The same reactions with flowing $\text{HX}(\text{g})$ ($\text{X} = \text{Cl}, \text{Br}, \text{I}$) and $\text{Re}_2(\text{O}_2\text{CCH}_3)_4\text{Cl}_2$ yield Re_3X_9 containing the triangular Re_3^{9+} core [28, 176].

Table 4.3. Products obtained from the reaction of metal-metal bonded acetates with flowing HX(g) (X = Cl, Br, I) at various temperatures. [a] Reaction occurs at 250 °C, [b] Reaction occurs at 340 °C, [c] NR: not reported

Reaction	150 °C/250 °C ^[a]	300 °C/340 °C ^[b]
$\text{Tc}_2(\text{O}_2\text{CCH}_3)_4\text{Cl}_2 + \text{HCl}(\text{g})$ ^[162]	$\text{Tc}_2(\text{O}_2\text{CCH}_3)_2\text{Cl}_4$	Tc_3Cl_9 (α - TcCl_3)
$\text{Tc}_2(\text{O}_2\text{CCH}_3)_4\text{Cl}_2 + \text{HBr}(\text{g})$ ^[21]	TcBr_3	TcBr_3
$\text{Tc}_2(\text{O}_2\text{CCH}_3)_4\text{Cl}_2 + \text{HI}(\text{g})$ ^[21]	TcI_3	TcI_3
$\text{Re}_2(\text{O}_2\text{CCH}_3)_4\text{Cl}_2 + \text{HX}(\text{g})$ (X = Cl, Br, I) ^[28, 176]	$\text{Re}_2(\text{O}_2\text{CCH}_3)_2\text{Cl}_4$ ^[a]	Re_3X_9 ^[b]
$\text{Mo}_2(\text{O}_2\text{CCH}_3)_4 + \text{HX}(\text{g})$ (X = Cl, Br, I) ^[176]	NR	β - MoX_2
$\text{Os}_2(\text{O}_2\text{CCH}_3)_4\text{Cl}_2 + \text{HX}(\text{g})$ ^[c]	NR	NR
$\text{W}_2(\text{O}_2\text{CCH}_3)_4 + \text{HX}(\text{g})$ (X = Cl, Br, I)	NR	NR

4.2.3.2 Characterization of TcBr_3

Infrared Spectroscopy and SEM Analysis

The IR spectrum (Figure 4.16) of the product obtained at 150 °C exhibits weak stretching modes (≈ 1043 and 1022 cm^{-1}) from $\text{Tc}_2(\text{O}_2\text{CCH}_3)_4\text{Cl}_2$, while the product at 300 °C exhibits no stretching modes in this region indicating that the starting compound was no longer present.

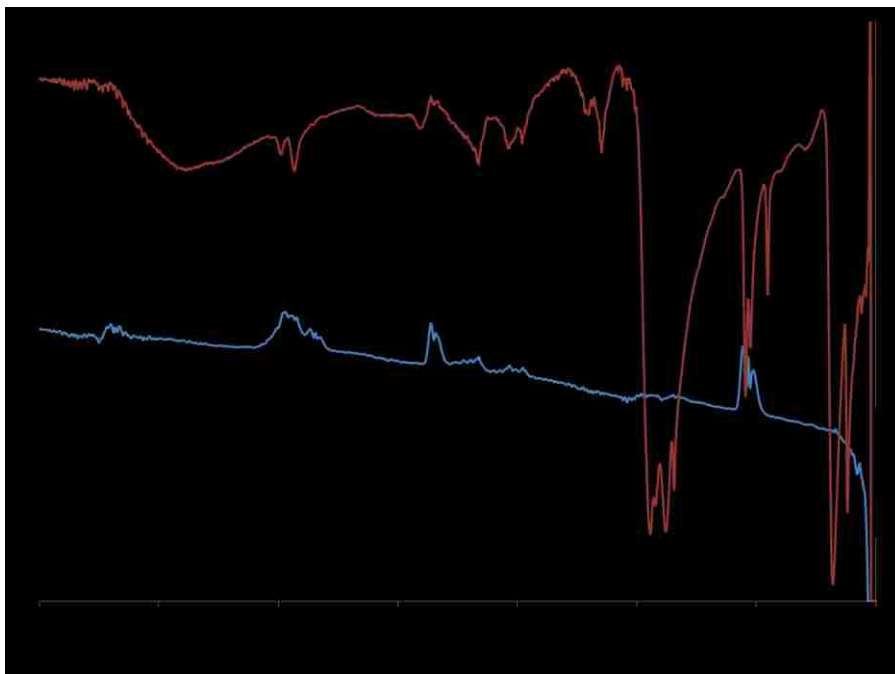


Figure 4.16. IR spectra of $\text{Tc}_2(\text{O}_2\text{CCH}_3)_4\text{Cl}_2$ (burgundy) and the products obtained from reactions of $\text{Tc}_2(\text{O}_2\text{CCH}_3)_4\text{Cl}_2$ and $\text{HBr}(\text{g})$ at $150\text{ }^\circ\text{C}$ (blue) and $300\text{ }^\circ\text{C}$ (black).

The elemental composition of the material obtained at $300\text{ }^\circ\text{C}$ was determined by EDX spectroscopy. The spectrum shows only Tc-L_α and Br-L_α lines, confirming a binary technetium bromide (Figure 4.17). The stoichiometry was determined to be 1:3.1(1) Tc/Br , which is consistent with the TcBr_3 .

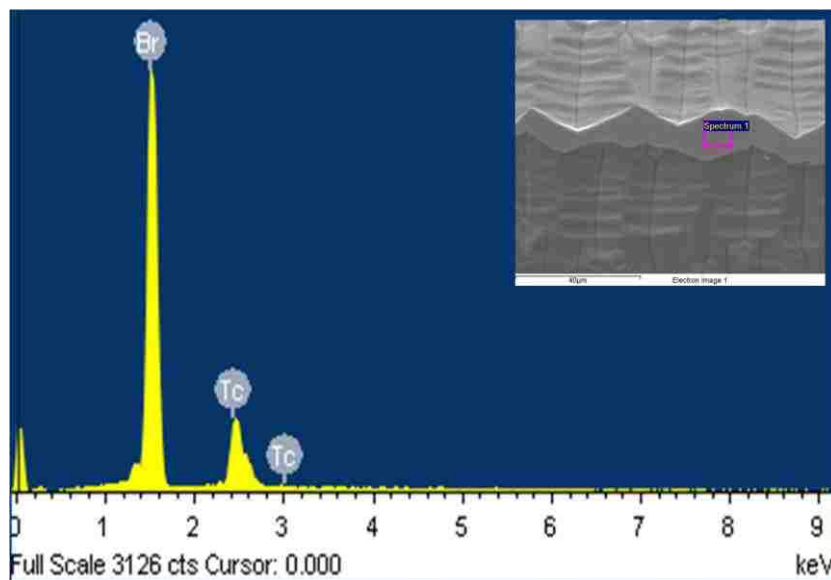


Figure 4.17. EDX spectrum of TcBr_3 displaying Tc-L α , and Br-L α lines; area of TcBr_3 analyzed (top right).

Powder X-ray Diffraction.

The PXRD patterns of the reaction products at 150 °C and 300 °C with HBr(g) are shown in Figure 4.18. Rietveld analyses were performed on the powder patterns at both temperatures and were fitted based on the TiI_3 structure-type. Technetium tribromide obtained from the reaction of $\text{Tc}_2(\text{O}_2\text{CCH}_3)_4\text{Cl}_2$ with flowing HBr(g) at 150 °C and 300 °C ($Pnmm$; $a = 6.4806(3)$ Å, $b = 11.225(8)$ Å, $c = 6.02(3)$ Å and $a = 6.4836(2)$ Å, $b = 11.230(7)$ Å, $c = 6.0207(8)$ Å, respectively) is isostructural to TcBr_3 ($Pnmm$; $a = 6.387(1)$ Å, $b = 11.062(1)$ Å, $c = 5.976(1)$ Å) obtained from reaction of the elements in a sealed tube and consists of infinite chains of face-sharing TcBr_6 octahedra (Figure 4.15). The weak peak at $2\theta = 12.65^\circ$ in the pattern of the product at 150 °C is attributed to an impurity of unreacted $\text{Tc}_2(\text{O}_2\text{CCH}_3)_4\text{Cl}_2$. For Tc, the predicted Tc_3Br_9 structure was not

obtained via this synthetic route; this result contrasts with the one of the HCl system that yields Tc_3Cl_9 with a Tc_3^{9+} core under similar conditions.

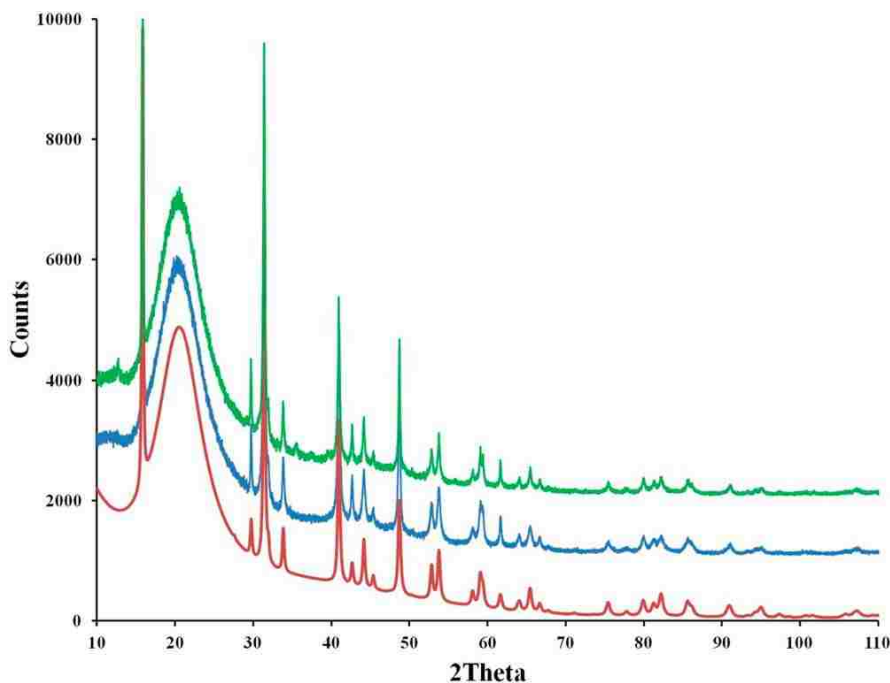


Figure 4.18. PXRD pattern of the products obtained from the reaction of $\text{Tc}_2(\text{O}_2\text{CCH}_3)_4\text{Cl}_2$ with $\text{HBr}(\text{g})$ at 150 °C (green) and 300 °C (blue) and the calculated (red) pattern of TcBr_3 . The amorphous “hump” from $2\theta = 20$ to 30° is due to a radiological containment dome.

4.2.3.3 Thermal Behavior of TcBr_3

The thermal behavior of TcBr_3 , obtained from the reaction of $\text{Tc}_2(\text{O}_2\text{CCH}_3)_4\text{Cl}_2$ with flowing $\text{HBr}(\text{g})$ at 300 °C, was investigated in sealed Pyrex and quartz tubes under vacuum at 450 °C. Decomposition of TcBr_3 in the Pyrex tube (Figure 4.19a) yielded similar results as the decomposition of TcBr_4 ; the rail spike crystals sublimed adjacent to the powder and the needle-shaped crystals (Figure 4.20) at the end of the tube were

identified by SCXRD to be $\text{Na}\{[\text{Tc}_6\text{Br}_{12}]_2\text{Br}\}$ and TcBr_3 , respectively. The PXRD pattern (Figure 4.21) of the resulting powders yielded unreacted TcBr_3 . In contrast, the reaction in quartz tube (Figure 4.19b) resulted in TcBr_3 and Tc metal identified in the remaining powder (Figure 4.22). Because the decomposition in a quartz tube did not provide a crystalline product, this suggests that the source of the Na in the compound originates from the Pyrex tube. It is still an open question whether TcBr_2 is accessible by thermal decomposition routes and whether its structure will be the “naked” $\text{Tc}_6\text{Br}_{12}$ cluster or be similar to TcCl_2 (see section 5.1). Other MBr_3 ($\text{M} = \text{Mo}, \text{Re}, \text{Ru}$) are also susceptible to thermal decomposition: MoBr_3 disproportionates to $\alpha\text{-MoBr}_2$ ($\text{Mo}_6\text{Br}_{12}$) and MoBr_4 at 600 °C [177], whereas ReBr_3 and RuBr_3 decompose to the respective metals and Br_2 at temperatures above 450 °C [178, 179].

a)



b)



Figure 4.19. Resulting tubes from the thermal decomposition of TcBr_3 in a) Pyrex yielding rail spike crystals adjacent to the powder (black circle) and needle crystals at the end of the tube and in b) quartz with only sublimed needle-shaped crystals.



Figure 4.20. SEM image (x35) of TcBr₃ single crystals as individual and clusters of needles ranging in size from 100 μm to 2 mm.

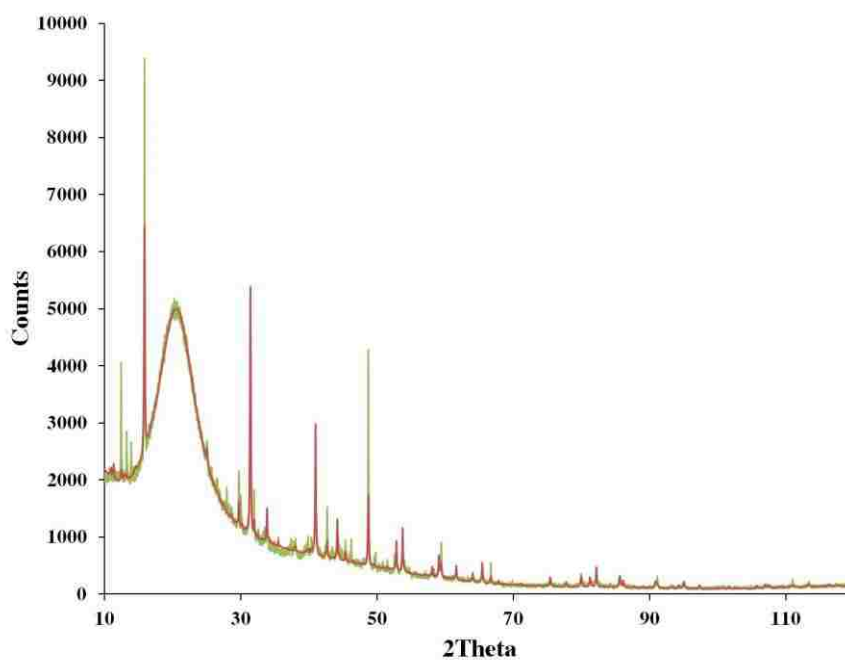


Figure 4.21. PXRD pattern of the products obtained from the decomposition of TcBr₃ in Pyrex at 450 °C (olive green) and calculated (red) pattern fit for TcBr₃.

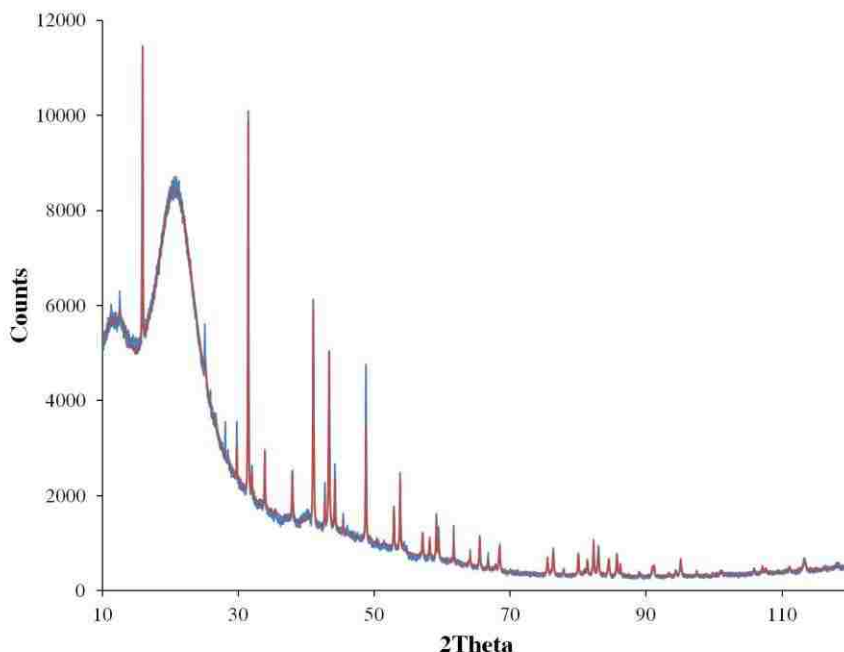


Figure 4.22. PXRD pattern of the products obtained from the thermal decomposition of TcBr_3 in quartz at $450\text{ }^\circ\text{C}$ (blue) and calculated pattern (red) fit with TcBr_3 and Tc metal.

4.2.4 Summary

The reactions of $\text{Tc}_2(\text{O}_2\text{CCH}_3)_4\text{Cl}_2$ with $\text{HBr}(\text{g})$ at $150\text{ }^\circ\text{C}$ and $300\text{ }^\circ\text{C}$ produced TcBr_3 crystallizing in the TiI_3 structure-type. The behavior of $\text{Tc}_2(\text{O}_2\text{CCH}_3)_4\text{Cl}_2$ with $\text{HBr}(\text{g})$ does not follow the one under $\text{HCl}(\text{g})$, and Tc_3Br_9 is not obtained. The TcBr_3 consists of face-sharing TcBr_6 octahedra; this structure is also found for other MBr_3 ($\text{M} = \text{Ru}, \text{Mo}$). The result indicates that the binary bromide chemistry of $\text{Tc}(\text{III})$ is more similar to that of $\text{Mo}(\text{III})$ and $\text{Ru}(\text{III})$ and not to $\text{Re}(\text{III})$, the latter exhibiting the triangular Re_3X_9 clusters in their structure. The thermal behavior of TcBr_3 was investigated under vacuum in sealed tubes at $450\text{ }^\circ\text{C}$. The compound is unstable, and TcBr_3 decomposes to $\text{Na}\{[\text{Tc}_6\text{Br}_{12}]_2\text{Br}\}$ and Tc metal in a Pyrex tube and to Tc metal in a quartz tube. Previous calculations indicate that Tc_3Br_9 should be stable. The current results show that Tc_3Br_9

was not observed in the temperature range 150 °C – 400 °C and that the known TcBr_3 phase decomposes to technetium metal above 450 °C. This suggests that low-temperature routes would be required for the preparation of Tc_3Br_9 . Such routes might include metathesis reactions using $\alpha\text{-TcCl}_3$ as a precursor or thermal decomposition of Ag_2TcBr_6 under vacuum below 150 °C [55].

4.3 Technetium Triiodide

4.3.1 Introduction

Binary transition-metal iodides have been reported for all second- and third-row group IV–XI elements with the exception of Tc [1, 2]. Binary transition-metal iodides can be obtained by either of two methods: (1) the reaction between flowing $\text{HI}(\text{g})$ and a dinuclear acetate complex or (2) the reaction between the elements in a sealed tube. Neither of these reactions has been reported for Tc. Because Tc and I both have isotopes resulting from the fission of U fuel, i.e., ^{99}Tc and ^{129}I , it was also of interest to gain a better understanding of the chemical reactivity of Tc with I for potential nuclear fuel cycle applications [180].

In this section, the reaction of $\text{Tc}_2(\text{O}_2\text{CCH}_3)_4\text{Cl}_2$ with flowing $\text{HI}(\text{g})$ at 150 °C and 300 °C and the reaction of Tc metal with I_2 in sealed Pyrex tubes are presented. The reaction products were characterized using diffraction, microscopic and spectroscopic techniques. The thermal properties of TcI_3 were studied under vacuum in sealed tubes at elevated temperature. Finally, the coordination and synthetic chemistry of TcI_3 is discussed and compared to their Mo, Ru, and Re analogues.

4.3.2 Experimental Details

Reaction of $\text{Tc}_2(\text{O}_2\text{CCH}_3)_4\text{Cl}_2$ with $\text{HI}(\text{g})$ at 150 °C. The reactions were performed in an experimental setup similar to the one used for the reaction with $\text{HBr}(\text{g})$. A $\text{Tc}_2(\text{O}_2\text{CCH}_3)_4\text{Cl}_2$ (74.0 mg, 0.17 mmol) sample was evenly dispersed in a quartz boat lined with a 0.1-mm-thick Au foil [181]. The system was purged with $\text{Ar}(\text{g})$ for 15 minutes at room temperature. The temperature was then increased to 150 °C (10 °C/min) and held for 5 minutes, and the gas was immediately switched to $\text{HI}(\text{g})$. A rapid color change from crimson to deep black upon the introduction of $\text{HI}(\text{g})$ was observed. The compound was reacted for an additional 30 minutes under flowing $\text{HI}(\text{g})$ at 150 °C, after which the tube was cooled to room temperature under flowing $\text{HI}(\text{g})$. After the reaction, the black powder (111.7 mg, yield: 68 %) was analyzed by PXRD, Tc elemental analysis, IR and XAFS spectroscopies.

Following characterization, the remaining powder (47.7 mg) was placed in a Au envelope, which was introduced into a Pyrex tube and sealed under vacuum. The tube was treated at 150 °C (10 °C/min) for 5 days. After the reaction, the black powder (36.4 mg) was characterized by PXRD and EDX spectroscopy.

Reaction of $\text{Tc}_2(\text{O}_2\text{CCH}_3)_4\text{Cl}_2$ with $\text{HI}(\text{g})$ at 300 °C. The same experimental procedure and apparatus as those of the reaction of $\text{HI}(\text{g})$ at 150 °C were used for the reaction at 300 °C. A weighted quantity of $\text{Tc}_2(\text{O}_2\text{CCH}_3)_4\text{Cl}_2$ (58.5 mg, 0.13 mmol) was evenly dispersed in a quartz boat lined with Au foil. The system was purged with $\text{Ar}(\text{g})$ for 15 minutes at room temperature; the temperature was then increased to 150 °C (10 °C/min) and held for 5 minutes under $\text{Ar}(\text{g})$, and the gas was switched to $\text{HI}(\text{g})$. The system was then ramped (10 °C/min) to 300 °C, held for 15 minutes at 300 °C, and cooled to room temperature

under HI(g). The resulting black powder (95.4 mg, yield: 74 %) was analyzed by PXRD. A sample of the compound (59.0 mg) was placed in an Au capsule, sealed in a Pyrex tube, and sintered at 300 °C a week. No single crystals were obtained after the reaction, and the powder (50.4 mg) was analyzed by PXRD.

Reaction of Technetium Metal with Iodine. Technetium metal (36.8 mg, 0.37 mmol) was placed in an Au envelope in a Pyrex tube (L = 43 cm), connected to a Schlenk line, and flamed under vacuum. After backfilling with Ar(g), the tube was removed from the Schlenk line and I₂ (188 mg, 0.74 mmol; Tc:I ■ 1:4) was quickly inserted. The tube was connected to the Schlenk line and flame-sealed (L = 18 cm) under vacuum. The tube was inserted into a clamshell furnace with the metal-end of the sealed tube located in the center of the furnace. The temperature was increased to 400 °C (7.5 °C/min) and held at that temperature for 2 weeks. After cooling to room temperature, a black microcrystalline powder was observed at the cool end of the tube, but no single crystals were obtained. The black powder (78.9 mg, yield: 30%) was analyzed by PXRD.

Decomposition of TcI₃. Technetium triiodide (■24 mg, 0.05 mmol) was inserted into a Au foil capsule, placed in a 30 cm Pyrex tube, and flame-sealed under vacuum. The resulting tube (L = 18 cm) was placed in a clamshell furnace and reacted at 450 °C (10 °C/min) for 16 hours. Once at temperature, the entire tube was bright purple from the release of I₂(g) from the sample. After cooling to room temperature, the tube contained a considerable amount of condensed I₂ at the coolest portion but no crystalline Tc compounds. The resulting grayish-black powder was analyzed by PXRD.

4.3.3 Results and Discussion

4.3.3.1 Synthesis of TcI_3

The preparation of a binary Tc iodide have been investigated using two synthetic approaches: the reaction of $\text{Tc}_2(\text{O}_2\text{CCH}_3)_4\text{Cl}_2$ with flowing $\text{HI}(\text{g})$ at elevated temperatures and the reaction of Tc metal with I_2 in sealed tubes at elevated temperatures. The first method has been used in analogous reactions for the synthesis of the binary Tc chloride (i.e., $\alpha\text{-TcCl}_3$) and bromide (i.e., TcBr_3). This method is the favored route for the rapid production of weighable quantities of pure material. The reaction between Tc metal and I_2 was slow; reactions required long durations (~ 2 weeks) with low yields of conversion of the metal to the iodide. Technetium triiodide obtained from the reaction of $\text{Tc}_2(\text{O}_2\text{CCH}_3)_4\text{Cl}_2$ with $\text{HI}(\text{g})$ at 150 °C and 300 °C is not hygroscopic, but it slowly releases I_2 at room temperature. Technetium triiodide is insoluble in acetone, diethyl ether, dichloromethane, deionized H_2O , and 12 M HCl .

4.3.3.2 Characterization of TcI_3

a. Reaction between $\text{Tc}_2(\text{O}_2\text{CCH}_3)_4\text{Cl}_2$ and Flowing $\text{HI}(\text{g})$

The product obtained from the reaction of $\text{Tc}_2(\text{O}_2\text{CCH}_3)_4\text{Cl}_2$ with flowing $\text{HI}(\text{g})$ at 150 °C was characterized by Tc elemental analysis, IR and XAFS spectroscopies, and PXRD.

Elemental Analysis and Infrared Spectroscopy

For Tc elemental analysis, an aliquot (16.7 mg) of the solid was suspended in 10 mL of concentrated HClO_4 . After 10 days, the solid had dissolved, the Tc concentration was determined by LSC, and was consistent with the stoichiometry $\text{TcI}_{2.97(6)}$. The IR spectrum (Figure 4.23) of TcI_3 shows the absence of stretching from 4000 cm^{-1} to 500

cm^{-1} , confirming completion of the transformation of $\text{Tc}_2(\text{O}_2\text{CCH}_3)_4\text{Cl}_2$ to TcI_3 . The PXRD indicates the compound to be X-ray amorphous, and TcI_3 was characterized by XAFS spectroscopy.

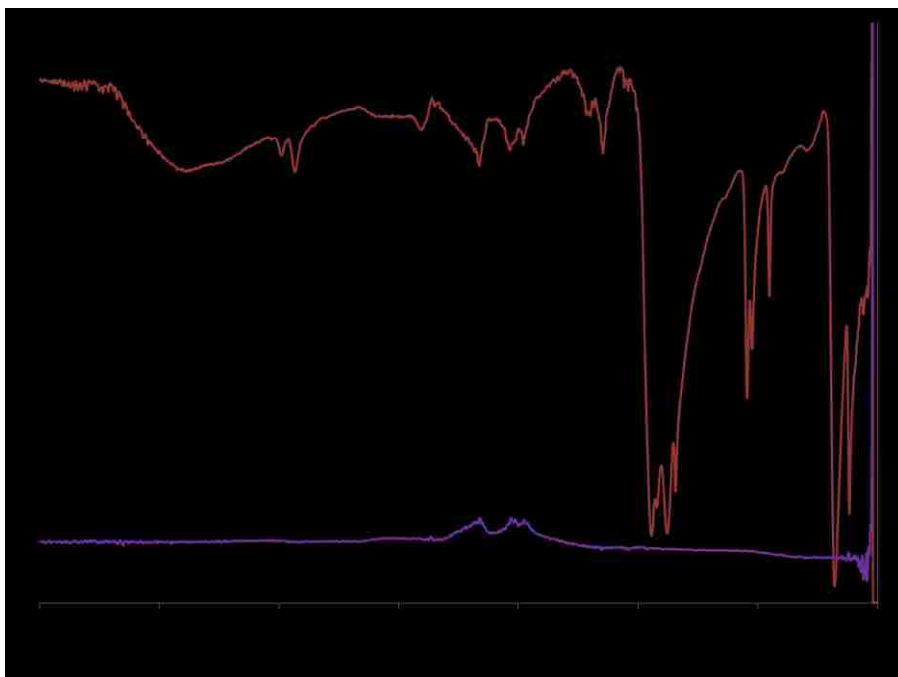


Figure 4.23. IR spectra of $\text{Tc}_2(\text{O}_2\text{CCH}_3)_4\text{Cl}_2$ (burgundy) and the product obtained from reaction of $\text{Tc}_2(\text{O}_2\text{CCH}_3)_4\text{Cl}_2$ and $\text{HI}(\text{g})$ at 150 °C (purple).

X-ray Absorption Fine Structure Spectroscopy

X-ray absorption fine structure spectroscopy has proven to be an efficient technique for the characterization of binary Tc halides. It has previously been used for the characterization of TcCl_4 (see section 3.1.3.2) and $\alpha\text{-TcCl}_3$ (see section 4.1.2) In order to determine the TcI_3 structure and compare it to other trivalent halide species, the compound was analyzed by XAFS spectroscopy. The XANES spectrum of TcI_3 was recorded (Figure 4.24), background-subtracted, and normalized and the Tc K-edge

position determined using the first-derivative method. The position of the Tc K-edge of TcI_3 (21050.8 eV) is lower than the one of Cs_2TcI_6 (21053.0 eV) and similar to the ones of $\alpha\text{-TcCl}_3$ (21051.0 eV) and $\beta\text{-TcCl}_3$ (21050.5 eV); these results are consistent the presence of Tc^{3+} atoms in TcI_3 [139].

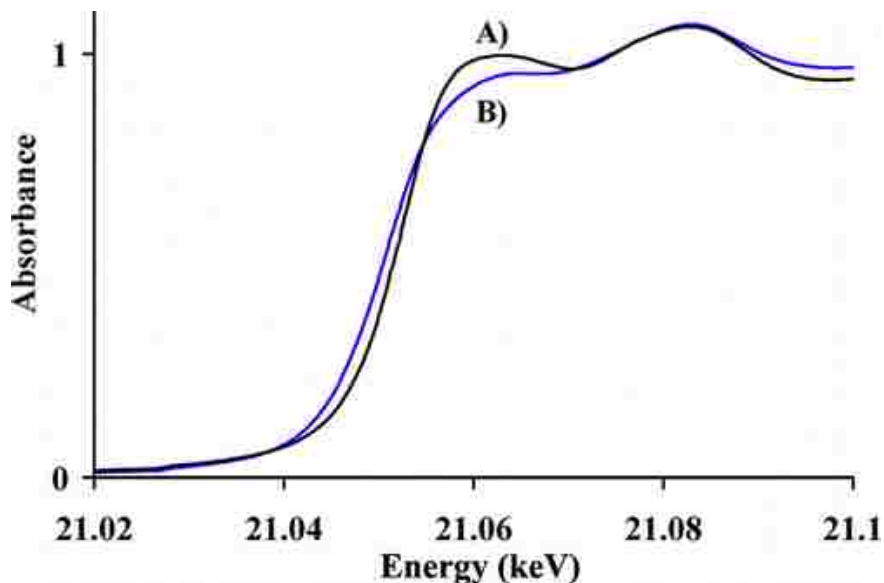


Figure 4.24. Normalized Tc K-edge XANES spectra of Cs_2TcI_6 (A in black) and TcI_3 (B in blue).

The extracted EXAFS spectrum was k^3 -weighted and the Fourier transform performed in the k -range $2 - 14.5 \text{ \AA}^{-1}$. Two different adjustments were performed considering the structure of a Tc_3I_9 cluster that exhibits the Tc_3Cl_9 structure and the structure of TcBr_3 [28]. For the adjustment modeling the structure of ReI_3 , the scattering functions were calculated in a Tc_3I_9 cluster with the Tc_3^{9+} triangular geometry (Figure 4.25a). For the adjustment modeling the structure of TcBr_3 , the scattering functions were calculated in a TcI_3 chain formed from face-sharing TcI_6 octahedron (Figure 4.25b). For the adjustments, the numbers of atoms were fixed at those of the clusters; ΔE_0 was

constrained to be the same value for each wave; all of the other parameters were allowed to vary.

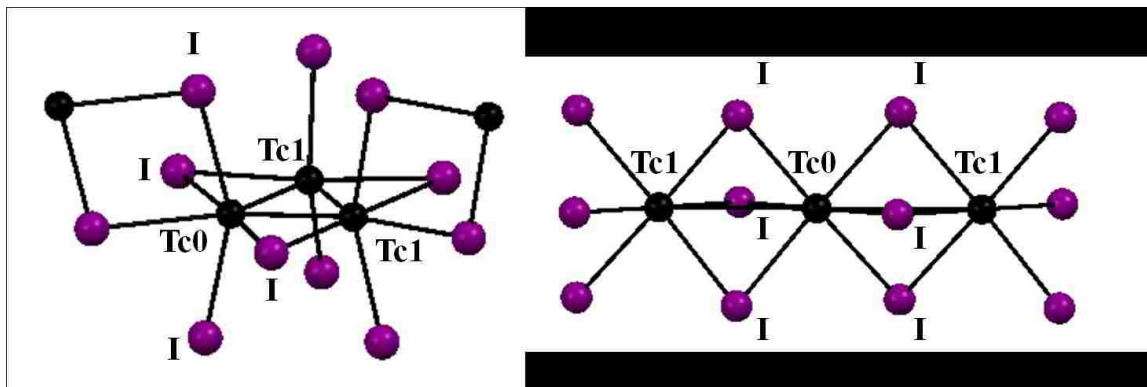


Figure 4.25. Ball-and-stick representations of the clusters used for EXAFS calculations:

(a) cluster with the ReI_3 structure-type; (b) cluster with the TcBr_3 structure-type. Tc and I atoms are in black and blue, respectively. Tc0 represents the absorbing atom.

The best adjustment was obtained by modeling the structure of TcBr_3 (Figure 4.26); further details of the adjustment of the EXAFS spectra of TcI_3 based on the structure of TcBr_3 are presented in Figure 4.26. Adjustment considering the structure of ReI_3 did not provide a suitable fit and resulted in high value of the reduced χ^2 (Figure 4.27).

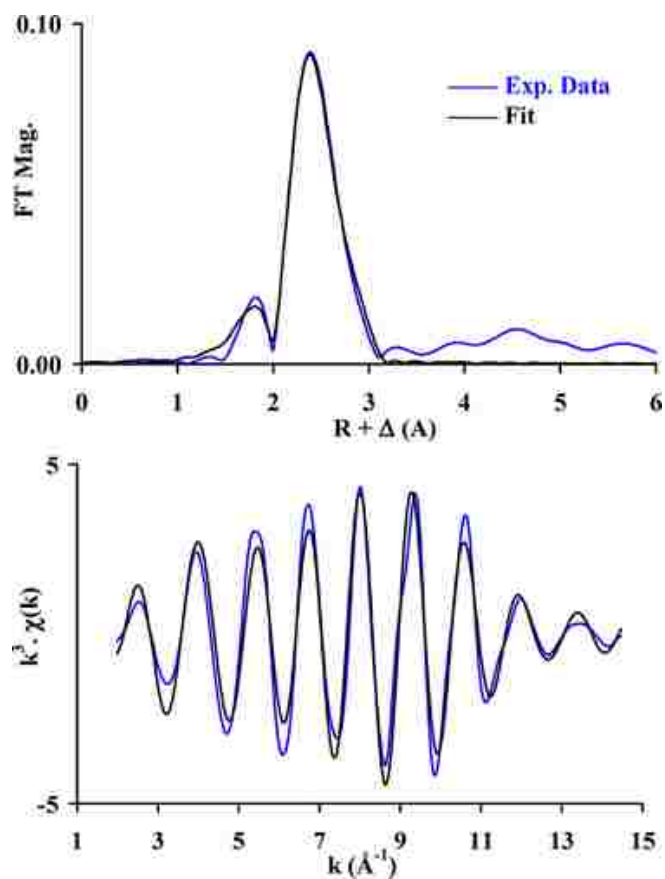


Figure 4.26. Fits of the experimental k^3 -weighted EXAFS spectra (bottom) and Fourier transform of k^3 -weighted EXAFS spectra (top) for the compound obtained from the reaction of $\text{Tc}_2(\text{O}_2\text{CCH}_3)_4\text{Cl}_2$ with $\text{HI}(\text{g})$ at $150\text{ }^\circ\text{C}$. Adjustment was performed between $k = 2$ and 14.5 \AA^{-1} considering the structure of TcBr_3 . Experimental data are in blue, and the fits are in black.

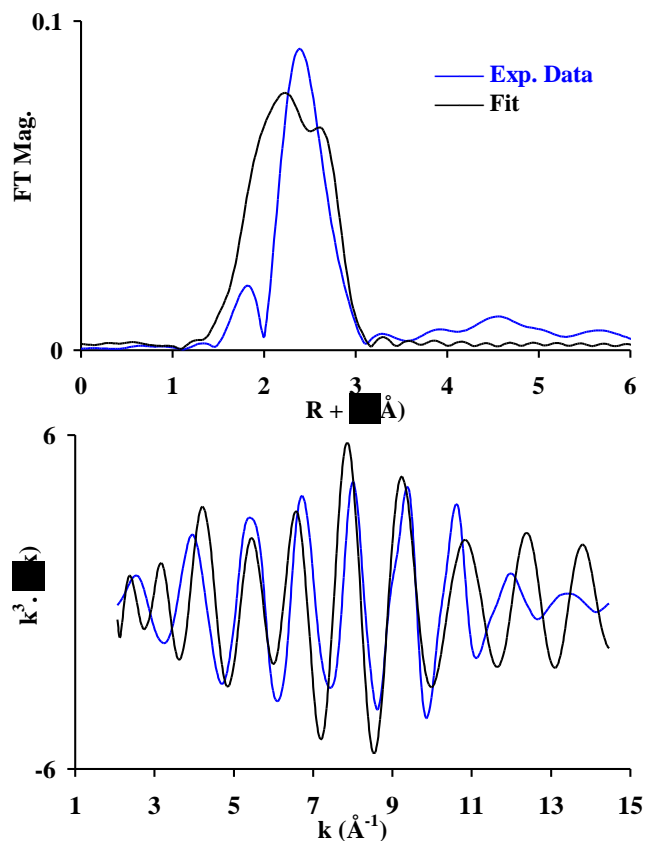


Figure 4.27. Fits of the experimental k^3 -EXAFS spectra (bottom) and Fourier transform of k^3 -EXAFS spectra (top) for the compound obtained from the reaction of $\text{Tc}_2(\text{O}_2\text{CCH}_3)_4\text{Cl}_2$ with $\text{HI}(\text{g})$ at $150\text{ }^\circ\text{C}$. Adjustment performed between $k = [2 - 14.5]\text{ \AA}^{-1}$ considering the structure of ReI_3 . Reduced- $\chi^2 = 9195$. Experimental data are in blue and the fits are in black.

The structural parameters (Table 4.4) found by EXAFS in TcI_3 show the presence of two Tc atoms at $3.10(3)\text{ \AA}$ and six I atoms at $2.67(3)\text{ \AA}$. The Tc–Cl and the Tc–Tc separations are consistent with the presence of face-sharing TcI_6 octahedra with the TcBr_3 structure-type. The separation (d) between the center of two face-sharing regular octahedra (with a = distance from center to vertices) is given by the formula $d = 2a\sqrt{3}/3$.

When this formula is transposed to TcI_6 octahedra ($a = \text{Tc-I}$ and $d = \text{Tc-Tc}$), the Tc-Tc separation between two face-sharing TcI_6 octahedra ($\text{Tc-I} = 2.67 \text{ \AA}$) is calculated to be 3.08 \AA .

Table 4.4. Structural parameters obtained by adjustment of the k^3 -EXAFS spectra of the compound obtained from the reaction of $\text{Tc}_2(\text{O}_2\text{CCH}_3)_4\text{Cl}_2$ with $\text{HI}(\text{g})$ at $150 \text{ }^\circ\text{C}$.

Adjustment between $k = [2 - 14.5] \text{ \AA}^{-1}$ considering the structure of TcBr_3 . $\Delta E_0 (\text{eV}) = -4.09 \text{ eV}$. Reduced- $\chi^2 = 80$.

Scattering	C.N	R (\AA)	$\sigma^2 (\text{\AA}^2)$
$\text{Tc}0 \leftrightarrow \text{I}$	6	2.67(3)	0.0010
$\text{Tc}0 \leftrightarrow \text{Tc}1$	2	3.10(3)	0.0090

Powder X-ray Diffraction and Scanning Electron Microscopy

In order to increase the crystallinity of TcI_3 prepared at $150 \text{ }^\circ\text{C}$, the compound was sealed in a tube and thermally treated at $150 \text{ }^\circ\text{C}$ for 5 days. After the reaction, no single crystals were obtained and the compound was characterized by PXRD, EDX spectroscopy, and SEM.

The PXRD pattern (Figure 4.28) of the thermally treated compound is identical with the one obtained from the reaction at $300 \text{ }^\circ\text{C}$. Neither of the patterns was suitable enough for deriving detailed structural information. The 2θ and d -spacing coordinates are presented in Table 4.5. The EDX spectra (Figure 4.29) show $\text{Tc-L}\alpha$ and $\text{I-L}\alpha$ peaks, which indicate the material to be a binary Tc iodide. The EDX quantification indicates that the compound exhibits the stoichiometry $\text{TcI}_{3.1(3)}$.

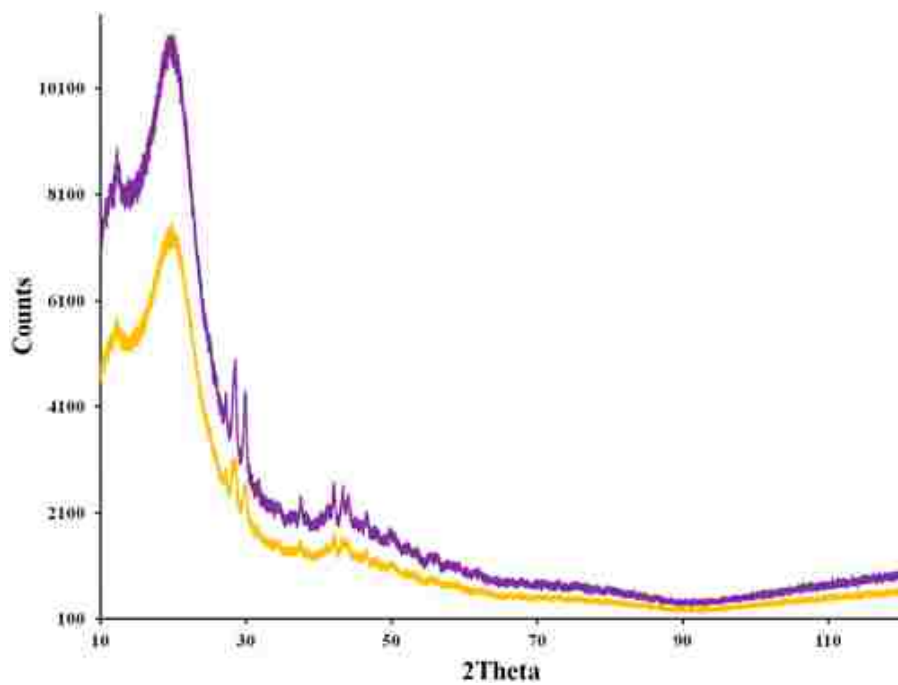


Figure 4.28. PXRD pattern of products obtained from the reaction of $\text{Tc}_2(\text{O}_2\text{CCH}_3)_4\text{Cl}_2$ with $\text{HI}(\text{g})$ at 150 °C (purple) and 300 °C (orange) after sintering for 5 days at the respective temperatures.

Table 4.5. 2θ ($^\circ$) and corresponding d-spacing (\AA) derived from the powder XRD of TcI_3 .

2θ ($^\circ$)	d-spacing (\AA)	Relative Intensity (%)
12.25	7.241	86
27.98	3.185	45
28.50	3.129	100
29.68	3.007	95
37.41	2.401	27
42.07	2.146	41
43.21	2.091	36
43.88	2.061	32
46.52	1.950	23

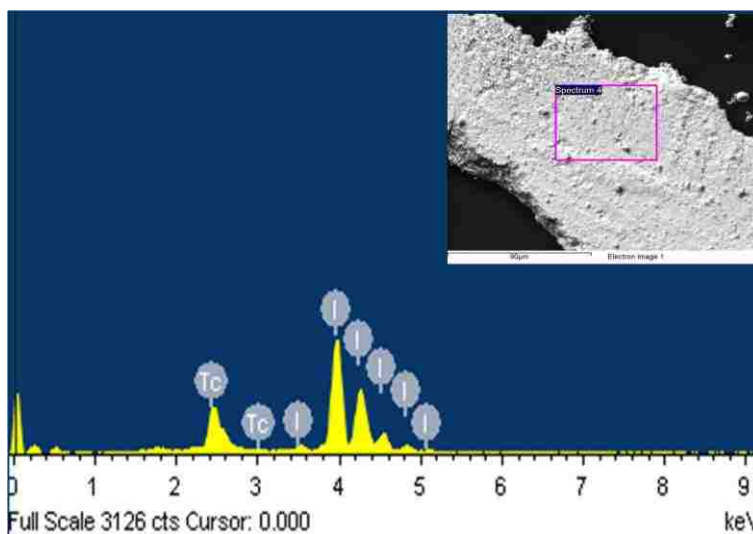


Figure 4.29. EDX spectrum of TcI_3 displaying Tc-L α and I-L α lines; secondary electron image (x500) of TcI_3 sampled shown at top right.

SEM analysis shows TcI_3 to be composed of granulated agglomerates ranging from 10 to 100 μm in size. Within these clumps, single-crystal inclusions ($\approx 5 \mu\text{m}$) with the stoichiometry TcI_3 are randomly dispersed (Figure 4.30).

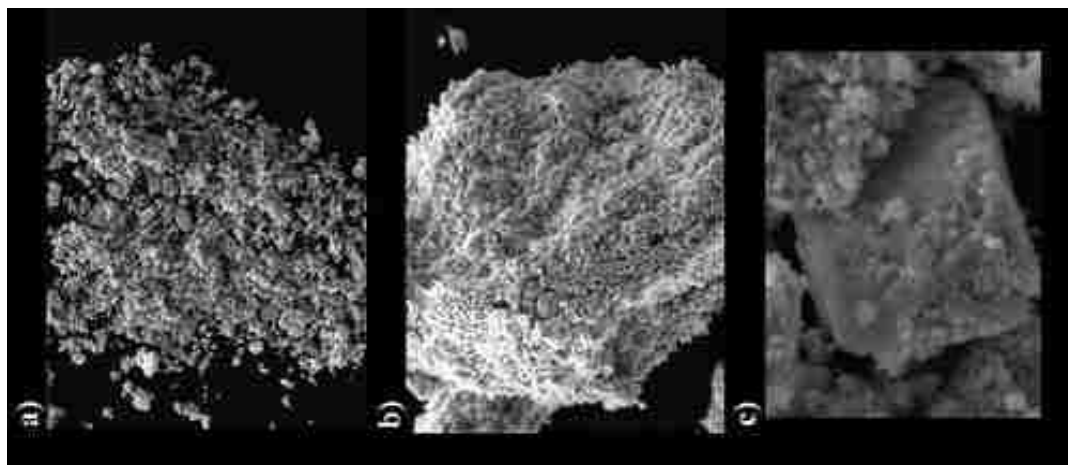


Figure 4.30. SEM images of TcI₃: (a) powder at x200 magnification; (b) individual pieces of powder at x500 magnification; (c) crystalline inclusion of TcI₃ at x5000 magnification.

b. Reaction between Tc Metal and I₂ in a Sealed Tube

The solid-state reaction of Tc metal with I₂ (Tc:I = 1:4) was investigated in sealed Pyrex tubes in the temperature range 250 – 400 °C for 2 weeks. After those reactions, no single crystals were obtained, and the resulting powders were analyzed by PXRD. The PXRD analysis indicates that Tc begins to react with I₂ at 300 °C and higher yields of the product are obtained at 400 °C. After the reaction at 400 °C, the PXRD pattern of the product shows several new peaks (Figure 4.31) that match the ones of TcI₃ synthesized from Tc₂(O₂CCH₃)₄Cl₂ and HI(g). This indicates that TcI₃ is the primary product from the reaction of Tc metal and excess I₂.

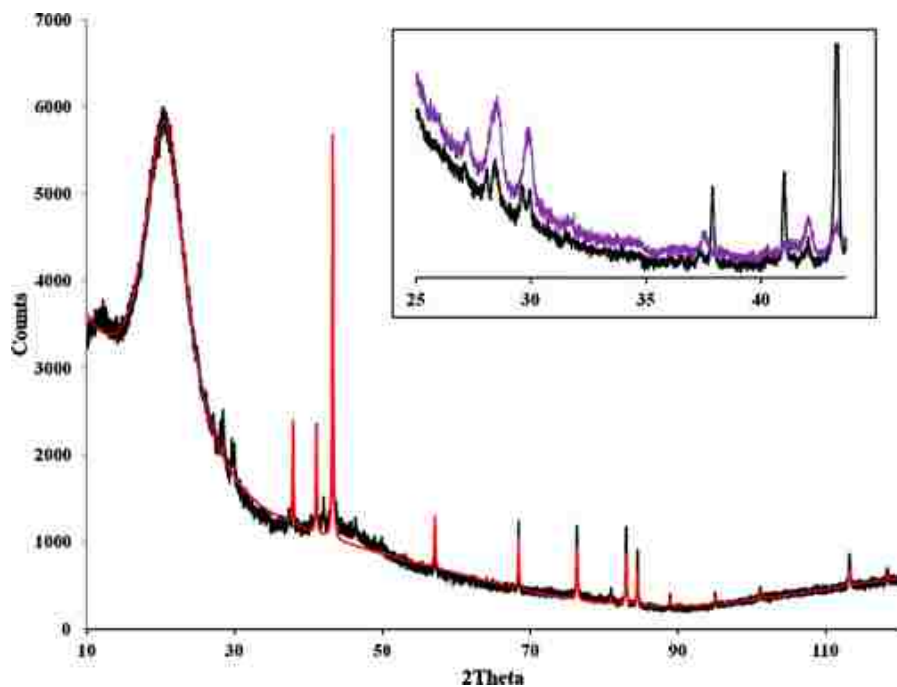


Figure 4.31. PXRD pattern of the products obtained from the reaction of Tc metal and I₂ at 400 °C for 2 weeks (black) and fit with Tc metal (red). Inset: comparison of the product (black) to TcI₃ from the reaction of Tc₂(O₂CCH₃)₄Cl₂ with HI(g) (purple).

4.3.3.3 Thermal Behavior of TcI₃

The thermal behavior of TcI₃ obtained from the reaction of Tc₂(O₂CCH₃)₄Cl₂ with flowing HI(g) at 150 °C was investigated in sealed Pyrex tubes under vacuum at 450 °C. The PXRD pattern indicates that the sample consists of Tc metal as a single phase (Figure 4.32).

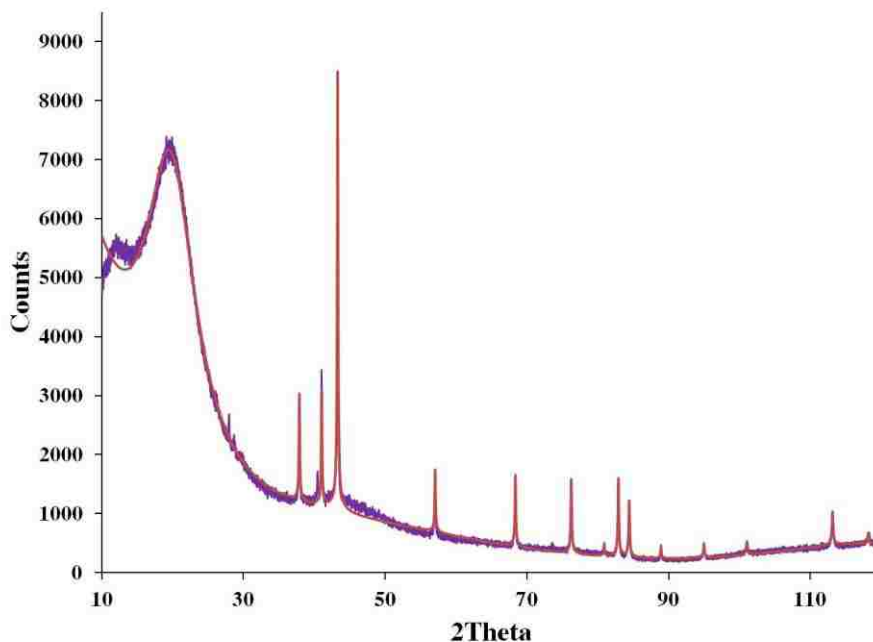


Figure 4.32. PXRD pattern (purple) of the product obtained from the decomposition of TcI_3 under vacuum at $450\text{ }^\circ\text{C}$ in a gold envelope and the fit (red) with Tc metal.

4.3.3.4 Comparison of TcI_3 with Other MI_3 Systems

Technetium triiodide has been obtained from the reaction of $\text{Tc}_2(\text{O}_2\text{CCH}_3)_4\text{Cl}_2$ with flowing $\text{HI}(\text{g})$ at $150\text{ }^\circ\text{C}$ and $300\text{ }^\circ\text{C}$. Its solid-state structure consists of face-sharing TcI_6 octahedra. Concerning Tc neighboring elements, MX_3 ($\text{M} = \text{Mo}, \text{Ru}; \text{X} = \text{Br}, \text{I}$) also exhibit the TiI_3 structure-type, while ReX_3 ($\text{X} = \text{Br}, \text{I}$) consists of Re_3X_9 clusters. This suggests that the chemistry of the heavier Tc halides resemble to their Ru and Mo analogues. The reaction of molecular acetate dimers (Mo, Rh, Re, and Tc) with flowing $\text{HX}(\text{g})$ at elevated temperatures is a direct route to binary metal halides (Table 4.3) [176, 162].

The reaction between Tc metal and I_2 at $450\text{ }^\circ\text{C}$ produces TcI_3 . Similar behavior is observed for Mo, W, and Ru, all of which form triiodide species from analogous

reactions (Table 4.6) [2, 182, 183, 184, 185, 186]. For Re, no reaction between the metal and I₂ in sealed tubes occurred in the temperature range 170–180 °C, which is also observed for Tc at lower reaction temperatures, i.e., 250 °C [187]. For W and Ru, both triiodides can be obtained from the reaction of the elements with I₂ at elevated temperatures [184, 185, 186]. Osmium triiodide has been synthesized from decomposition of (H₃O)₂OsI₆ or the reaction of OsI₂ with I₂ [175a], but no data on the reaction of the Os metal with elemental I₂ were reported.

Table 4.6. Reactions of 2nd and 3rd row transition metals of Group VI, VII, VIII with I₂.

[a] This work. [b] Not reported.

Element	Conditions	Products
Molybdenum	Sealed tube reaction at 500 °C ^{182, 183}	MoI ₃ and α-MoI ₂
Technetium	Sealed tube reaction at 300-400 °C ^[a]	TcI ₃
Ruthenium	Sealed tube reaction at 350 °C ^{184, 185}	RuI ₃
Tungsten	Sealed tube reaction at 500 °C ¹⁸⁶	WI ₃
Rhenium	Flowing I ₂ and sealed tube reaction at 170-180 °C ¹⁸⁷	No reaction
Osmium	NR ^[b]	---

Technetium triiodide consists of face-sharing TcI₆ octahedra, a structure that is also found for the Ru and Mo homologues. Five different structure-types have been identified for the second- and third-row transition-metal triiodides spanning groups 4–10 (d⁰–d⁶) [22]. These triiodides are comprised of either infinite chains or layers (Figure 4.33). The TiI₃ structure is the most common structure-type found for d¹–d⁵ transition-metal MX₃ phases (M = Zr, Hf, β-Nb, Mo, Tc, Ru, X = Br, I; M = Os, X = Br). The TiI₃

structure-type is composed of infinite chains of distorted face-sharing MX_6 octahedra (Figure 4.33a). The distortion within the chain occurs from alternating M–M distances and the correlative formation of M–M pairs, resulting in an “out-of-phase” displacement of the metal atoms and a structural deviation from hexagonal to orthorhombic symmetry [22, 171, 99, 188]. Similar to the other NbX_3 phases ($\text{X} = \text{Cl}, \text{Br}$), $\alpha\text{-NbI}_3$ adopts the “ $\text{Nb}_{3-x}\text{Cl}_8$ ” structure-type (Figure 4.33b), which is a homogeneous mixture of M_3X_8 and MX_4 [189]. For Re, the Re_3X_9 motif is found for the chloride, bromide, and iodide (Figure 4.33c). This structural arrangement consists of a Re_3^{9+} triangular core with $\text{Re}=\text{Re}$ double bonds, which for the bromide and iodide bridge from two adjacent Re atoms, unlike the chloride, which bridges all three atoms, forming layers of sheets [28]. Although the AlCl_3 structure-type (Figure 4.33d) is not predominately found for transition-metal tribromides or triiodides, both d^6 metals Rh and Ir exhibit the AlCl_3 structure-type in their tribromides and triiodides; these are comprised of infinite layers of edge-sharing MX_6 octahedra ($\text{X} = \text{Br}, \text{I}$) [23, 29, 190]. No triiodide has been reported for Pd. For Pt, the structure of PtI_3 is unique and consists of infinite chains of alternating PtI_6 octahedra and PtI_4 tetrahedra (Figure 4.33e) [191]. The compounds WI_3 and TaI_3 have been prepared from the reaction of the respective metals and I_2 , but their X-ray crystallographic structures have not been reported [186, 192].

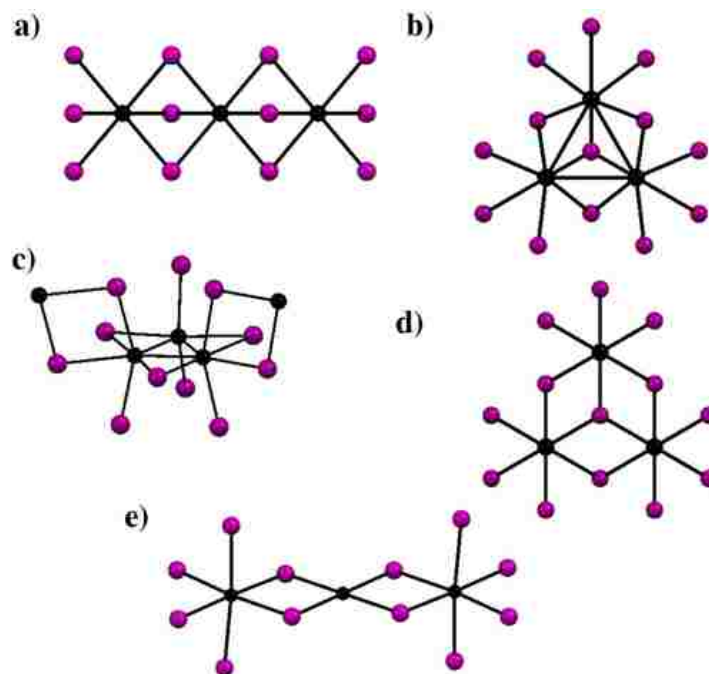


Figure 4.33. Ball-and-stick representations of second- and third-row transition-metal triiodide structure-types for: (a) Zr, Hf, β -Nb, Mo, Tc, Ru, and Os; (b) Nb; (c) Re; (d) Rh and Ir; (e) Pt. Metal atoms are in black, and I atoms are in purple.

An attempt to prepare TcI_2 from the thermal decomposition of TcI_3 was unsuccessful. Technetium triiodide is thermally unstable and decomposes to the metal at 450 °C under vacuum. Direct decomposition to Tc metal also suggests that no other TcI_{3-x} species are thermally stable at 450 °C and that the formation of TcI_3 is thermodynamically unfavorable at these temperatures. In comparison, MoI_3 decomposes to α - MoI_2 (Mo_6I_{12}) at 100 °C [193], while ReI_3 decomposes stepwise to the di- and monoiodides between 320 °C – 420 °C and 420 °C – 470 °C, respectively, and the metal and I_2 at temperatures above 580 °C [194].

4.3.4 Summary

Technetium triiodide, the first binary Tc iodide to be reported, was obtained in the solid-state from the reaction of $\text{Tc}_2(\text{O}_2\text{CCH}_3)_4\text{Cl}_2$ with $\text{HI}(\text{g})$ at 150 °C and 300 °C and from the reaction of Tc metal and I_2 in a sealed tube at 400 °C. Measurements by XAFS indicate the compound to consist of face-sharing TcI_6 octahedra. The behavior of $\text{Tc}_2(\text{O}_2\text{CCH}_3)_4\text{Cl}_2$ with $\text{HI}(\text{g})$ does not follow the one under $\text{HCl}(\text{g})$, and Tc_3I_9 is not obtained. TcI_3 consist of face-sharing TcI_6 octahedra, which is also found for MoI_3 and RuI_3 . In contrast, ReI_3 is composed of Re_3I_9 clusters. The thermal behavior of TcI_3 was investigated under vacuum in sealed tubes at 450 °C; TcI_3 decomposes to Tc metal, and no divalent phases were observed.

4.4 Conclusion

Technetium trichlorides, tribromide and triiodide were synthesized in the solid-state and their solid-state structures and thermal properties are reported. With four known phases (i.e., $\alpha\text{-TcCl}_3$, $\beta\text{-TcCl}_3$, TcBr_3 , and TcI_3), Tc trihalides exhibit the most extensive chemistry among the binary Tc halides.

The compound $\alpha\text{-TcCl}_3$, TcBr_3 , and TcI_3 can be prepared in weighable quantities from the reaction of $\text{Tc}_2(\text{O}_2\text{CCH}_3)_4\text{Cl}_2$ and flowing $\text{HX}(\text{g})$ ($\text{X} = \text{Cl}, \text{Br}, \text{and I}$) at elevated temperatures. The mechanism of formation of $\alpha\text{-TcCl}_3$ mimics the one described for rhenium and $\text{Tc}_2(\text{O}_2\text{CCH}_3)_2\text{Cl}_4$ is formed as an intermediate in the early stage of the reaction. For TcBr_3 and TcI_3 , the reactions differ from the one of rhenium and no $\text{Tc}_2(\text{O}_2\text{CCH}_3)_2\text{X}_4$ ($\text{X} = \text{Br}, \text{I}$) has been observed. The compound $\beta\text{-TcCl}_3$ was obtained

congruently with TcCl_4 and TcCl_2 from the stoichiometric sealed tube reaction between the elements at 450 °C.

The Tc trichlorides exhibit polymorphism. The compound $\alpha\text{-TcCl}_3$ is isostructural with ReCl_3 and composed of infinite layers of interlinked Tc_3Cl_9 clusters. The $\beta\text{-TcCl}_3$ is isostructural with $\alpha\text{-MCl}_3$ ($\text{M} = \text{Mo}, \text{Ru}$) and constituted of infinite layers of edge-sharing TcCl_6 octahedron. In those trichlorides, significant metal-metal interactions occur between Tc atoms and $\text{Tc}=\text{Tc}$ double bonds are formed. Calculations confirm the presence of a $\text{Tc}=\text{Tc}$ double bond with σ and π character for both trichloride. The $\text{Tc}=\text{Tc}$ bond is stronger in $\alpha\text{-TcCl}_3$ than in $\beta\text{-TcCl}_3$. Technetium tribromide and TcI_3 both form infinite chains of face-sharing TcX_6 ($\text{X} = \text{Br}, \text{I}$) octahedra and are isostructural with MX_3 ($\text{M} = \text{Mo}, \text{Ru}; \text{X} = \text{Br}, \text{I}$). This suggests that the chemistry of the heavier Tc halides resemble their Ru and Mo analogues and differ from that of Re.

The thermal behavior of the Tc trihalides has been investigated in sealed tubes under vacuum. The $\beta\text{-TcCl}_3$ converts to $\alpha\text{-TcCl}_3$ at 280 °C after 16 days, and $\alpha\text{-TcCl}_3$ decomposes to TcCl_2 at 450 °C after 14 hours. Technetium tribromide decomposes to $\text{Na}\{[\text{Tc}_6\text{Br}_{12}]_2\text{Br}\}$ in Pyrex and Tc metal in quartz at 450 °C. The compound TcI_3 decomposes to the metal with no intermediates at 450 °C.

Technetium trihalides can find application in inorganic chemistry and/or in the nuclear fuel cycle. Because of its layered structure, $\beta\text{-TcCl}_3$ may exhibit interesting intercalative properties that mimic those of $\alpha\text{-RuCl}_3$ [195]. Similar to its Mo neighbour, $\beta\text{-TcCl}_3$ could be used as a precursor for the synthesis of binary carbides or phosphides, which would find application in the development of Tc waste forms [8]. Rhenium trichloride has been widely used as precursor in the synthesis of other molecular

complexes with the triangular $[\text{Re}_3]^{9+}$ core; it is expected that $\alpha\text{-TcCl}_3$ should also lead to the formation of similar complexes. Technetium triiodide is insoluble in water and organic solvents and decomposes to Tc metal at 450 °C. The thermal and solubility properties of TcI_3 might be of particular interest for nuclear fuel cycle applications i.e., Mo/Tc separation using halide volatility processes and the development of Tc–I waste forms. At a more fundamental level, these studies allow for a better understanding of how the chemistry of Tc trihalides compares to that of its neighboring elements.

Chapter 5

Technetium Dichlorides

In this chapter the new divalent binary technetium chlorides α -TcCl₂ and β -TcCl₂ are reported. The compound β -TcCl₂ has been synthesized from the reaction of the elements in sealed tubes at elevated temperatures while α -TcCl₂ was obtained after thermal treatment of β -TcCl₂ with AlCl₃ in a sealed tube. The crystal structure of the two compounds has been determined using SCXRD. Physical properties (i.e., magnetic susceptibility, band gap and charge transport measurements) of β -TcCl₂ were determined providing a better understanding of the electronic configuration of the material. The thermal properties of β -TcCl₂ have also been investigated in sealed quartz tubes at elevated temperatures. Theoretical calculations were used to further understand the crystallographic and electronic structures as well as the physical properties of these compounds.

5.1 Technetium Dichlorides: α -TcCl₂ and β -TcCl₂

5.1.1 Introduction

Transition metal dichlorides are fundamental compounds that serve as important materials for a variety of industrial and medical applications due to their explicit catalytic, photochemical, and redox properties [1, 2, 196, 197, 198, 199]. Molybdenum dichloride was the first of these compounds discovered in 1859 [200], and to date there have since been six other elements of the second and third row transition metals (Zr [201], Hf [202], W [203], Pd [204], and Pt [205]) that have also been reported to form dichlorides; a total of ten dichloride phases have been structurally characterized. Prior to

2011, there was no known binary dihalide for Tc and no reports of stoichiometric reactions of Tc with Cl_2 [32]. The successful preparation of binary Tc bromides (see Chapter 1) using sealed tube reactions encouraged the exploration of similar reactions with Cl_2 [97]. In the following section, the preparation and characterization of the first binary Tc dihalides, $\alpha\text{-TcCl}_2$ and $\beta\text{-TcCl}_2$ are reported. The crystal structures of $\alpha\text{-TcCl}_2$ and $\beta\text{-TcCl}_2$ were solved by SCXRD. The compound $\beta\text{-TcCl}_2$ was further characterized using PXRD, SEM, EDX, and XAFS spectroscopy. Physical properties of $\beta\text{-TcCl}_2$ were determined and the magnetic susceptibility, band gap, and charge transport measurements are reported. The thermal properties of $\beta\text{-TcCl}_2$ were investigated at elevated temperatures under vacuum. In order to gain a better understanding of the structural and physical properties of the material, theoretical calculations were performed [206, 207]. The synthetic, chemical, and structural properties of Tc dichlorides are compared to those of other 2nd and 3rd row transition metals.

5.1.2 Experimental Details

Preparation of $\beta\text{-TcCl}_2$. Technetium metal (59.5 mg, 0.601 mmol) was placed in a Pyrex tube (L = 43 cm) and flamed under vacuum. After backfilling with Cl_2 , the end of the tube was cooled in liquid nitrogen and the gas (~17 mL, 0.68 mmol) was condensed. The tube was flame-sealed (L = 18 cm) and placed in a clamshell furnace. The temperature of the furnace was increased to 450 °C (10 °C/min) and held for 24 hours. After cooling to room temperature, a dark crystalline powder (83.8 mg) was observed at the end of the tube that contained the metal. On the surface of the tube near the middle some very thin dark needles of $\beta\text{-TcCl}_2$ were present. After the reaction, $\beta\text{-TcCl}_2$ crystals obtained at the center of the tube were analyzed by EDX spectroscopy and used for the

structure determination (SCXRD, EXAFS) and conductivity measurements without any further thermal treatment. The dark crystalline powder obtained at the hot end of the tube was characterized by PXRD and used for magnetic and band gap measurements.

Preparation of α -TcCl₂. The dark crystalline powder (65 mg) prepared in a similar reaction (*vide supra*) was placed in a 30-cm-long Pyrex tube with AlCl₃ (45 mg), the tube was evacuated and flamed-sealed at 17 cm. The tube was placed in the furnace at 450 °C for 4 days (10°C/ min) and black needles, suitable for SCXRD, grew at the end of the tube.

Thermal Behavior of β -TcCl₂. A weighted quantity of β -TcCl₂ (76.5 mg, 0.450 mmol) was transferred into a quartz tube (L = 43 cm), connected to a Schlenk line and evacuated. The tube was lightly flamed to remove any residual O₂ or moisture, and the contents were flame-sealed at 18 cm under vacuum. The tube was placed in a clamshell furnace and the temperature was slowly increased (8 °C/min) to 800 °C and held for 24 hours. During the reaction, a dark colored gas evolved from the powder above 600 °C and sublimed as a reddish black film (i.e., TcCl₄) at the cooler end of the tube. After the reaction, the resulting tube contained a grey powder at the hot portion of the tube and the black film at the opposite end. The powder (21.0 mg) was analyzed by PXRD.

5.1.3 Results and Discussion

5.1.3.1 Preparation of β -TcCl₂

The compound was prepared by reacting Tc metal and Cl₂ (Tc:Cl, 1:2.5) at 450 °C in a Pyrex sealed tube for 24 hours. This method is identical to the one used to obtain β -TcCl₃ (see section 4.1.3.1). In these reactions, the compound β -TcCl₂ is obtained congruently with TcCl₄ and β -TcCl₃ (see section 4.1.4).

5.1.3.2 Characterization of β -TcCl₂

Powder XRD

The powder (Figure 5.1) obtained at the hot end of the tube was characterized by PXRD (Figure 5.2). Results show the powder to contain Tc metal (13 wt.%) and TcCl₂ (87 wt.%).

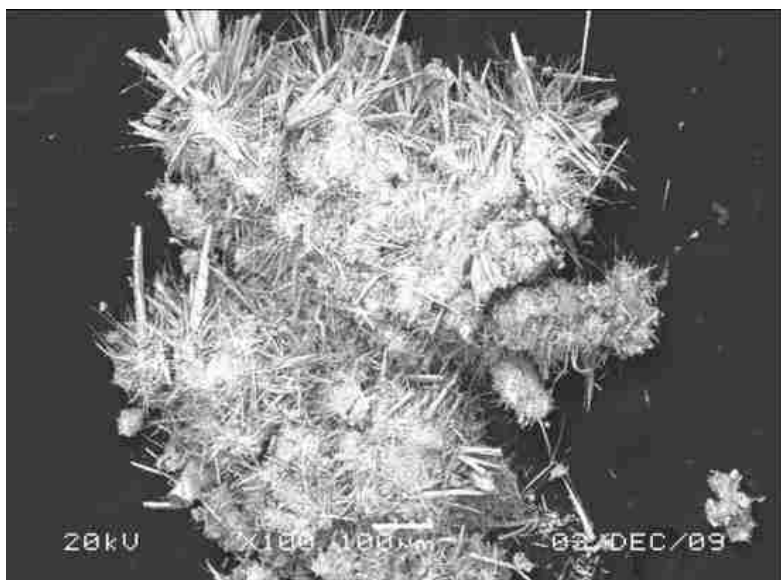


Figure 5.1. SEM image of the TcCl₂/Tc metal powder obtained after the stoichiometric reaction of Tc metal with Cl₂(g) in sealed tubes at 450 °C.

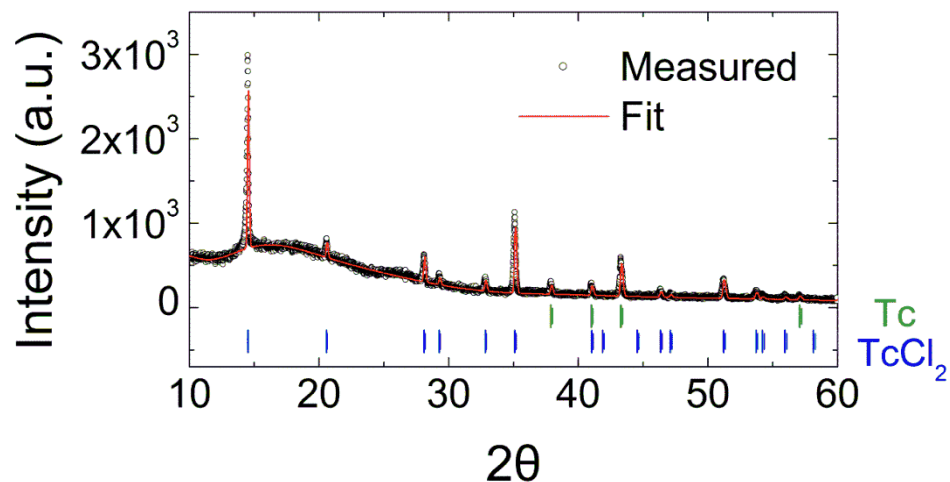


Figure 5.2. PXRD pattern (black open circles) of the powder obtained after reaction of Tc metal and Cl_2 at $450^\circ C$ in a sealed tube. The fit against the experimental pattern is represented in a red solid line. Position of peaks of Tc metal and $TcCl_2$ is marked in green and blue lines, respectively.

EDX Spectroscopy

Analysis by EDX spectroscopy was performed on a needle located in the middle of the tube. (Figure 5.3). Using the ratio of the integrated intensities of the Tc- K_α and Cl- K_α lines, the composition $TcCl_{2.1(2)}$ was found for the needle (Figure 5.4).

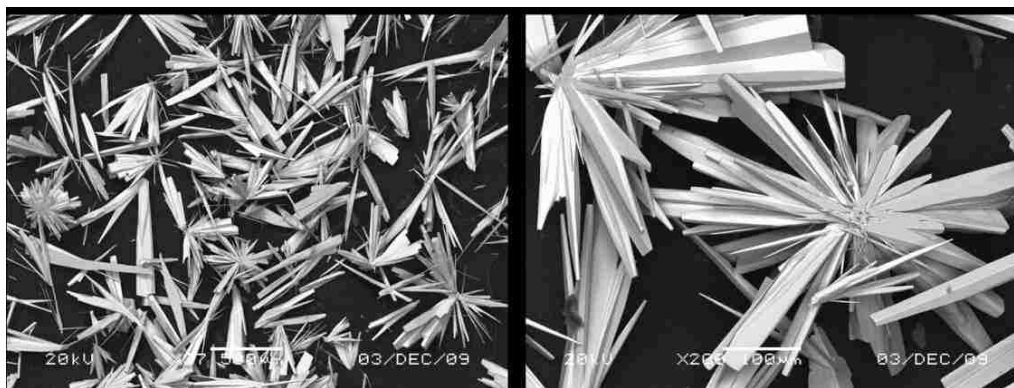


Figure 5.3. SEM images of β - TcCl_2 needles (bottom left, x35; bottom right, x200) obtained after the stoichiometric reaction of Tc metal with $\text{Cl}_2(\text{g})$ in sealed tubes.

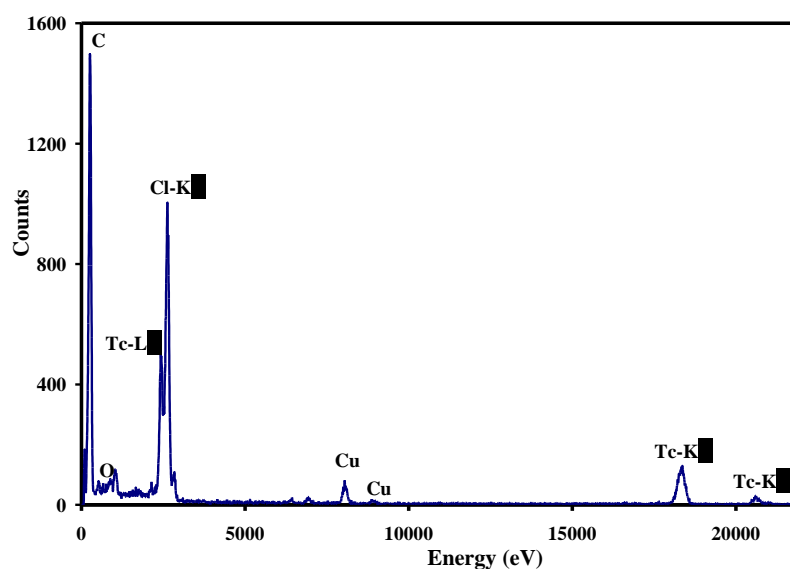


Figure 5.4. The EDX spectrum of β - TcCl_2 . Carbon and Cu peaks are due to the sample holder.

Single Crystal X-ray Diffraction

A single crystal of β - TcCl_2 obtained after the reaction of Tc metal and Cl_2 was used for the structure determination. Based on SCXRD a monoclinic non-isomorphous

supergroup $I2/m$ is proposed with pseudo-tetragonal lattice with cell parameters $a = b = 8.5908(14)$ Å and $c = 3.4251(6)$ Å and $\alpha = \beta = \gamma = 90^\circ$ (additional crystallographic data provided in Appendix II). The structure of β - TcCl_2 consists of infinite chains of face-sharing Tc_2Cl_8 units running along the c -axis (Figure 5.5). The Tc_2Cl_8 units form tetragonal square prisms that are slightly elongated along the c -axis; in those prisms, the height is ~8% longer than the edge of the square basis. In the Tc_2Cl_8 units, the metal–metal separations (i.e., 2.131(2) and 2.142(2) Å) are indicative of $\text{Tc}\equiv\text{Tc}$ triple bonds (*vide infra*). In a chain, two orientations (A and B) of the $\text{Tc}\equiv\text{Tc}$ bonds are observed; the $\text{Tc}\equiv\text{Tc}$ bonds of two adjacent Tc_2Cl_8 units being either parallel or perpendicular (Figure 5.5B). The orientation of the $\text{Tc}\equiv\text{Tc}$ bonds changes every two Tc_2Cl_8 units (i.e., AABBAABB...) and $\text{Tc}\equiv\text{Tc}$ bonds with the same orientation have the same length. The distances between $\text{Tc}\equiv\text{Tc}$ bonds of parallel (i.e., 3.425(2) Å) and perpendicular Tc_2Cl_8 units (i.e., 3.744(2) Å) preclude any metal–metal interaction between adjacent units. The average $\text{Tc}\text{--Cl}$ distance in the Tc_2Cl_8 units is 2.398[3] Å. The average bridging $\langle\text{Tc}\text{--Cl}\text{--Tc}\rangle$ angle between two units with parallel $\text{Tc}\equiv\text{Tc}$ bonds (i.e., 91.25[5]°) is smaller than the one between two units with perpendicular $\text{Tc}\equiv\text{Tc}$ bonds (i.e., 102.65[5]°).

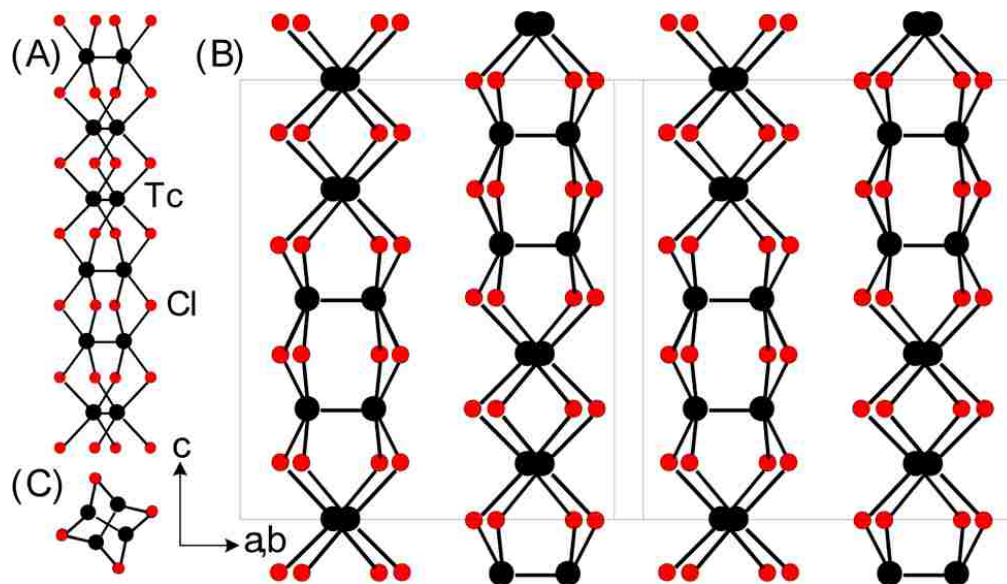


Figure 5.5. Ball-and-stick representation of the structure of β - TcCl_2 . (A) Single β - TcCl_2 chain. The orientation of the $\text{Tc}=\text{Tc}$ bond changes every two Tc_2Cl_8 units within a single chain. (B) View along the c -axis of the $2 \times 2 \times 4$ supercell of β - TcCl_2 showing the packing of the chains. (C) View down the c -axis of a single β - TcCl_2 chain. Tc atoms are in black and chlorine atoms in red.

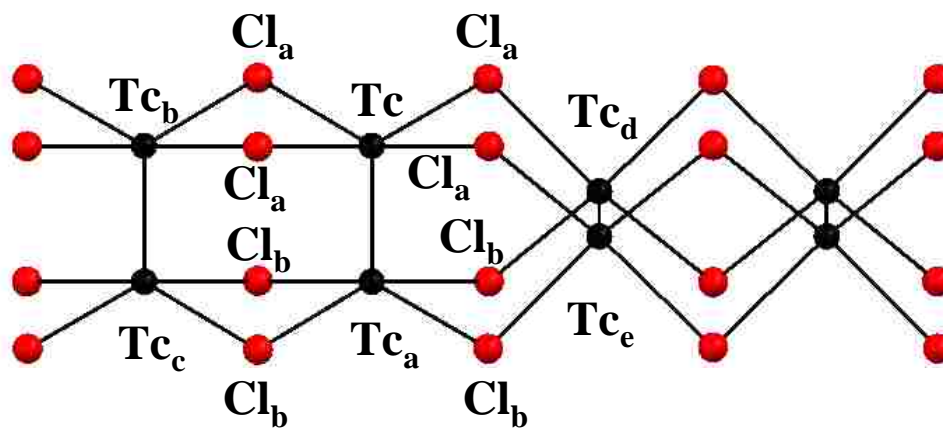


Figure 5.6. Ball-and-stick representation of a portion of a β - TcCl_2 chain. Selected distances (\AA): $\text{Tc}-\text{Tc}_a$ 2.136(3), $\text{Tc}-\text{Tc}_b$ 3.425(2), $\text{Tc}-\text{Tc}_c$ 4.037(3), $\text{Tc}-\text{Tc}_{(d,e)}$ 3.744(2). Tc atoms are in black and chlorine atoms are in red.

X-ray Absorption Fine Structure Spectroscopy

Measurements by EXAFS spectroscopy was also used to investigate the structure of β -TcCl₂. The XANES spectrum of β -TcCl₂ was recorded (Figure 5.7), and the energy of the absorption edge was compared with those of other Tc chloro complexes (Figure 5.8 and Table 5.1). The shift to lower energy observed in the series TcNCl₄⁻, TcOCl₄⁻, TcCl₆²⁻, Tc₂Cl₈²⁻, Tc₂Cl₄(PMe₂Ph)₄, and β -TcCl₂ is correlated with the decrease of the oxidation state of the Tc atoms and is consistent with the presence of divalent Tc in β -TcCl₂ [101].

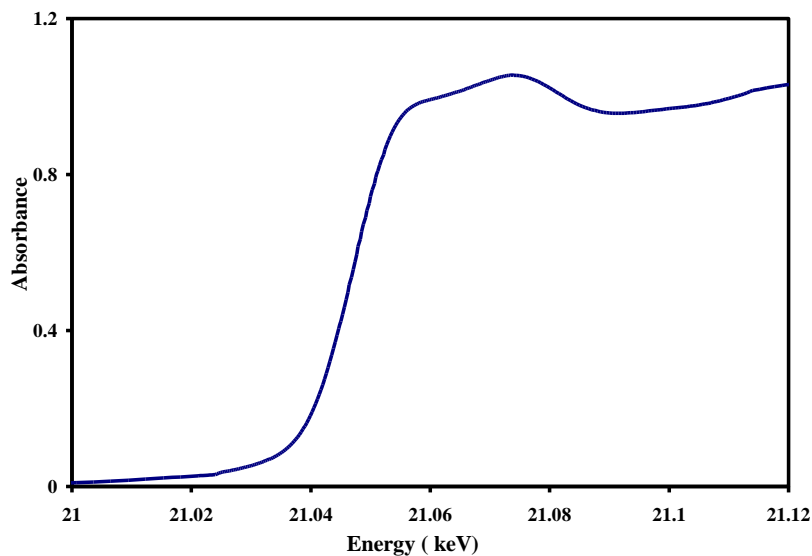


Figure 5.7. The XANES spectrum of β -TcCl₂.

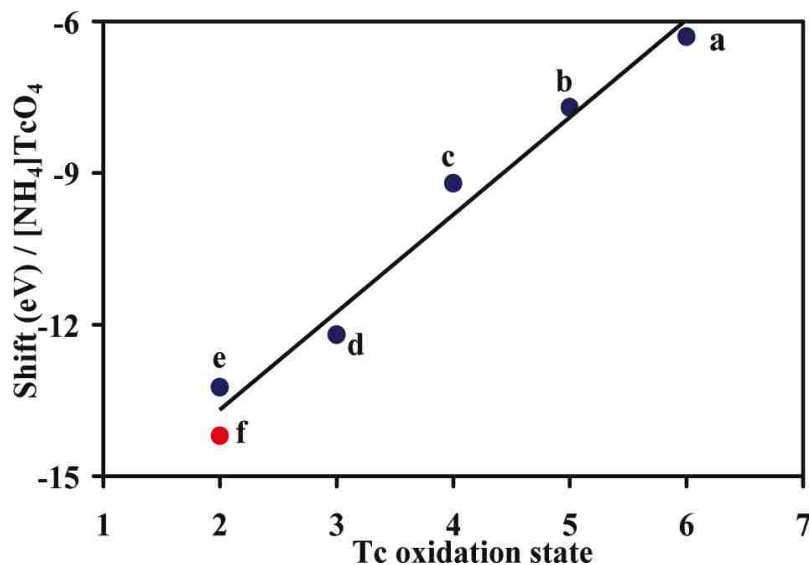


Figure 5.8. Chemical shift ΔE (eV) of the Tc-K edge relative to NH_4TcO_4 versus formal oxidation state for (a) $(n\text{-Bu}_4\text{N})\text{TcNCl}_4$, (b) $(n\text{-Bu}_4\text{N})\text{TcOCl}_4$, (c) $(\text{Me}_4\text{N})_2\text{TcCl}_6$, (d) $(n\text{-Bu}_4\text{N})_2\text{Tc}_2\text{Cl}_8$, (e) $\text{Tc}_2\text{Cl}_4(\text{PMe}_2\text{Ph})_4$, and (f) $\beta\text{-TcCl}_2$ (red dot).

Table 5.1. Chemical shifts (eV) of the technetium K-edge relative to NH_4TcO_4 measured for: $(n\text{-Bu}_4\text{N})\text{TcNCl}_4$, $(n\text{-Bu}_4\text{N})\text{TcOCl}_4$, $(\text{Me}_4\text{N})_2\text{TcCl}_6$, $(n\text{-Bu}_4\text{N})_2\text{Tc}_2\text{Cl}_8$, $\text{Tc}_2\text{Cl}_4(\text{PMe}_2\text{Ph})_4$ [104] and $\beta\text{-TcCl}_2$.

Compound	Shift (eV)	Compound	Shift (eV)
$(n\text{-Bu}_4\text{N})\text{TcNCl}_4$	-6.3	$(n\text{-Bu}_4\text{N})_2\text{Tc}_2\text{Cl}_8$	-12.1
$(n\text{-Bu}_4\text{N})\text{TcOCl}_4$	-7.7	$\text{Tc}_2\text{Cl}_4(\text{PMe}_2\text{Ph})_4$	-13.24
$(\text{Me}_4\text{N})_2\text{TcCl}_6$	-9.2	$\beta\text{-TcCl}_2$	-14.2

For the EXAFS adjustment, the scatterings were calculated in a portion of the $\beta\text{-TcCl}_2$ chain (Figure 5.6). For the fitting procedure, the numbers of atoms were fixed at those of the model; the fitted FT and the k^3 -EXAFS spectra are shown in Figure 5.9. The structural parameters (Table 5.2) found by EXAFS indicate the environment around the absorbing Tc atom to consist of Tc atoms at 2.13(2) Å, 3.45(3) Å, 3.79(4) Å, and 4.02(4)

Å and of Cl atoms at 2.42(2) Å and 3.58(4) Å. The presence of Tc atoms at 3.79(4) Å and 3.45(3) Å confirms that the structure of β -TcCl₂, produced by the reaction of Tc metal and elemental chlorine consists of face sharing Tc₂Cl₈ units, with two orientations of the Tc-Tc vectors, i.e., the Tc-Tc vectors of two adjacent Tc₂Cl₈ units are either parallel or perpendicular. The structural parameters found by EXAFS spectroscopy are in good agreement with the one found by SCXRD.

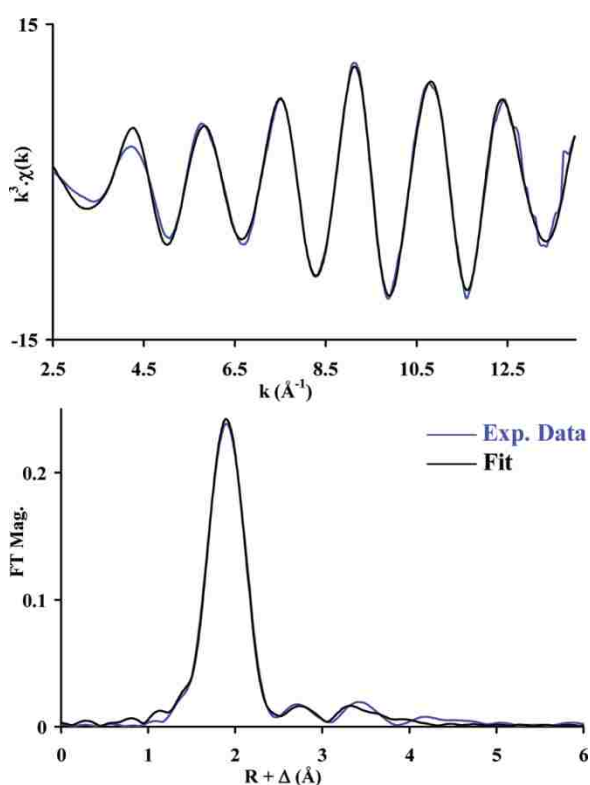


Figure 5.9. Fitted experimental k^3 -EXAFS spectra (top) and Fourier transform of k^3 -EXAFS spectra (bottom) of β -TcCl₂. Adjustment between $k = 2.5$ – 14 Å⁻¹. Experimental data (blue) and fit (black).

Table 5.2. Structural parameters obtained by adjustment of the k^3 -EXAFS spectra of β -TcCl₂. The adjustment was performed between $k = 2.5 - 14 \text{ \AA}^{-1}$. $\Delta E_0 = 1.82 \text{ eV}$. $S_0^2 = 0.9$.

Scattering	C.N	R (\AA)	σ^2 (\AA^2)
Tc \rightleftharpoons Tca	1	2.13(2)	0.0019
Tc \rightleftharpoons Cla	4	2.42(2)	0.0035
Tc \rightleftharpoons Tcb	1	3.45(3)	0.0043
Tc \rightleftharpoons Clb	4	3.58(4),	0.0079
Tc \rightleftharpoons Tcc	1	4.09(4)	0.0084
Tc \rightleftharpoons Tc(d,e)	2	3.79(4)	0.0062

5.1.3.3 Characterization of α -TcCl₂

Single Crystal X-ray Diffraction

The compound α -TcCl₂ was obtained after treatment of β -TcCl₂ at 450 °C in a sealed tube with AlCl₃ for 4 days. After this time, elongated needles were obtained at the cold end of the tube and used for SCXRD (additional crystallographic data provided in Appendix II). The structure of α -TcCl₂ is also a new structure-type and consists of infinite chains of eclipsed Tc₂Cl₈ units running along the c -axis [143]. The Tc-Tc vectors of adjacent units are all parallel, and the distances between Tc atoms of the adjacent units (i.e., 3.417(2) \AA) preclude any metal-metal bonding between these units. The eight Cl atoms form a rectangular prism comprised of two squares and four rectangular faces with the Tc-Tc vector parallel to the square faces. In the chain, the prisms share the square face, and the rectangular face is parallel to the c -axis (Figure 5.10).

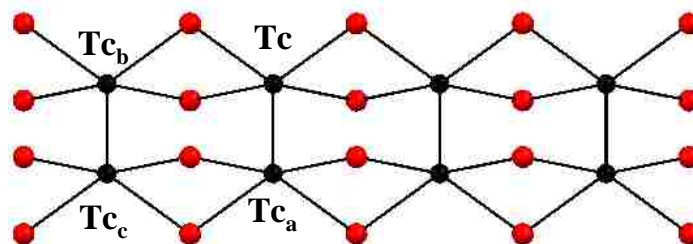


Figure 5.10. Ball-and-stick representation of a portion of a α - TcCl_2 chain. Color of atoms: Tc in black and Cl in red. Selected distances (\AA): Tc-Tc_a 2.136(3), Tc-Tc_b 3.417(2), Tc-Tc_c 4.025(2).

The structure of α - TcCl_2 is closely related to that of β - TcCl_2 ; both dichlorides consist of infinite chains of eclipsed Tc_2Cl_8 units [207, 143]. In the Tc_2Cl_8 units, the average Tc–Tc and Tc–Cl distances for β - TcCl_2 are slightly larger than the ones found for α - TcCl_2 (Table 5.3). For the two compounds, there are four chains in the reduced subcell that run along the c -axis. The volume of the β - TcCl_2 reduced subcell (i.e., 252.78(7) \AA^3) is slightly larger than the one of α - TcCl_2 (i.e., 250.0(2) \AA^3). The interchain Cl \cdots Cl distance in β - TcCl_2 (i.e., 3.534(2) \AA) is larger than the one in α - TcCl_2 (3.522(1) \AA) and slightly less than the sum of van der Waals radii (3.60 \AA).

5.1.3.4 Physical Properties of β - TcCl_2

The magnetic and transport properties of β - TcCl_2 were investigated. For the magnetic properties, the compound obtained as the powder (20.1 mg) was placed in a gelatin capsule and the zero field cooled magnetic susceptibility was measured with an applied field of 0.05 T. The representation of the magnetic susceptibility as a function of the temperature (Figure 5.11A) indicates the compound to be diamagnetic. The measured magnetic susceptibility was corrected for the paramagnetic contribution of unreacted Tc

metal present in the sample. The ratio of Tc/TcCl₂ was refined by PXRD analysis to be 13/87 (Figure 5.2).

The transport properties of β -TcCl₂ were initially studied by diffuse reflectance spectroscopy. This technique is commonly used to determine optical gaps in semiconductor materials [208, 209]. In this method, the optical band gap is determined by fitting the linear portion of the absorption part of the reflectance spectra. For β -TcCl₂, the diffuse reflectance spectrum (Figure 5.11B) was recorded at room temperature on a powder sample. A band gap of 0.12(2) eV was found by fitting the linear portion of the spectrum (Figure 5.11B; fit in red) indicating that the compound is a narrow gap semiconductor. The semiconducting nature of β -TcCl₂ was also verified by high temperature electrical resistivity measurements on a single crystal. The room-temperature resistivity (Figure 5.11C) decreases from 8 to 0.3 $\mu\Omega\cdot\text{cm}$ at 530 K. The corresponding Arrhenius fit (red solid line in Figure 5.11C) indicates a simple mechanism of carrier excitation with an activation energy of 0.17(2) eV. High temperature Seebeck measurements on a β -TcCl₂ single crystal (Figure 5.11D) were positive and in the range of 50 – 70 $\mu\text{V}/\text{K}$ (room temperature to 530 K) suggesting that β -TcCl₂ is a p-type semiconductor with holes being the dominant type of carriers (Figure 5.11D).

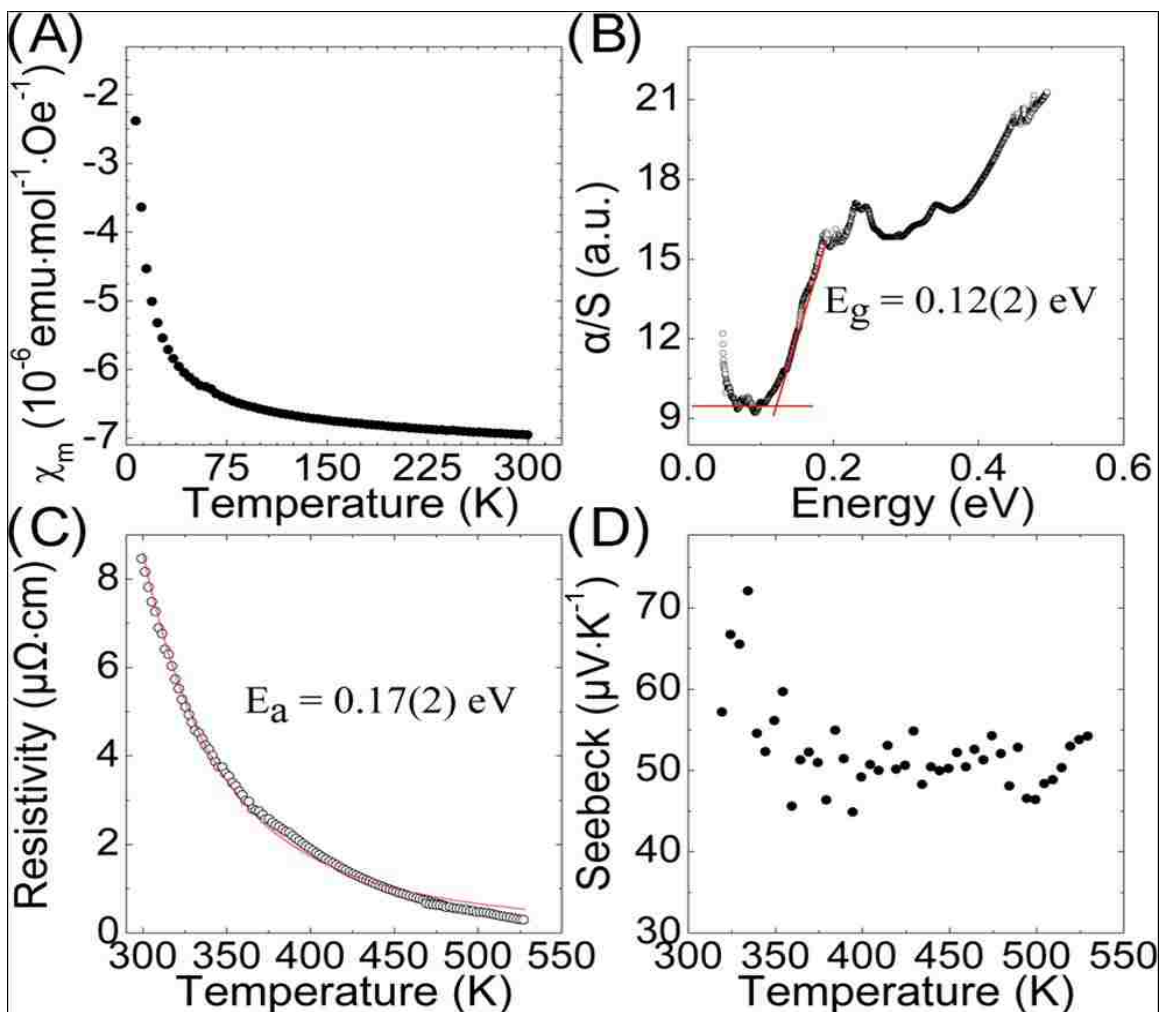
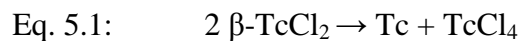


Figure 5.11. (A) Molar magnetic susceptibility of the TcCl_2 powder as a function of temperature. (B) Diffuse reflectance spectrum of the TcCl_2 powder as a function of temperature. Fit of the absorption edge is in red. (C) Resistivity as a function of temperature of a $\beta\text{-TcCl}_2$ single crystal. Red solid line represents the Arrhenius fit with an activation energy of $0.17(2) \text{ eV}$. (D) Seebeck coefficient as a function of temperature of $\beta\text{-TcCl}_2$.

5.1.3.5 Thermal Behavior of β -TcCl₂

The thermal behavior of β -TcCl₂ was investigated in a sealed quartz tube at 800 °C under vacuum for 24 hours. The evolution of a dark gas was observed above 600 °C and after the reaction the tube contained a grey powder and an amorphous black-red film. The recovered mass of the grey powder was consistent with the formation of Tc metal from the disproportionation of β -TcCl₂ (Eq.5.1):



These findings were confirmed by PXRD (Figure 5.12) yielding a pure phase of Tc metal.

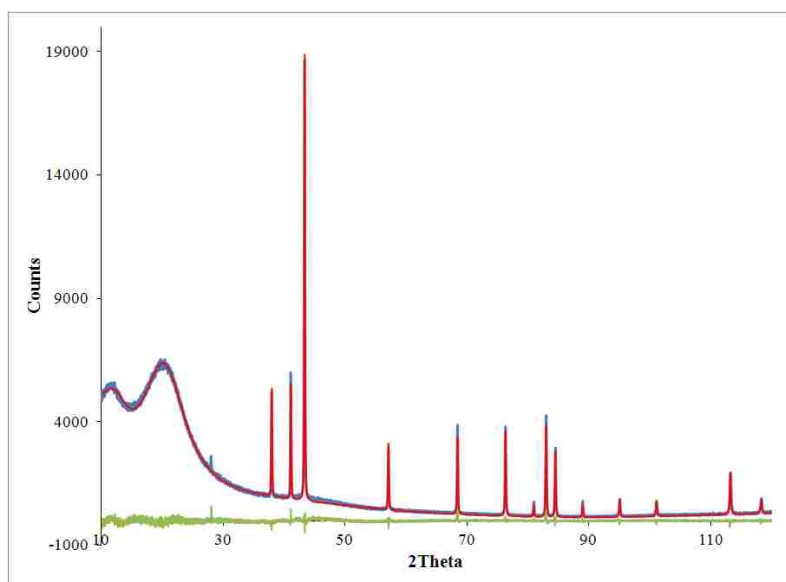


Figure 5.12. PXRD pattern (blue) of the solid obtained after thermal treatment of β -TcCl₂ at 800 °C under vacuum in a sealed tube fit with a homogenous phase of Tc metal (red) and the difference (green).

5.1.3.6 Computational Studies on α -TcCl₂ and β -TcCl₂

To better understand the structure and properties of the Tc dichlorides, electronic calculations were performed on α -TcCl₂ and β -TcCl₂. Calculations performed on a single β -TcCl₂ chain (Figure 5.13) indicate that bond distances (Tc–Tc = 2.073 Å and Tc–Cl = 2.417 Å), are in good agreement ($\pm 5\%$) with the experimental data (Table 5.3). Energetic calculations show a difference of 0.007 eV/f.u. between the α -TcCl₂ and β -TcCl₂ chain, indicating that the β -TcCl₂ chain is energetically slightly more favorable than the α -TcCl₂ chain.

Table 5.3. Average bond distances (Figure 5.6) found by SCXRD, EXAFS [206], and DFT in β -TcCl₂ and found by SCXRD for α -TcCl₂ (Figure 5.10) [143]. ^a Estimated standard deviations are in parentheses. ^b SCXRD measurements were performed at 100 K for β -TcCl₂ and 140 K for α -TcCl₂. ^c No perpendicular units are present in α -TcCl₂.

Bonds	SCXRD ^b β -TcCl ₂	EXAFS β -TcCl ₂	DFT β -TcCl ₂	SCXRD ^b α -TcCl ₂
Tc-Tc[A]	2.136(3)	2.13(2)	2.073	2.127(2)
Tc-Cl[A]	2.398(3)	2.42(2)	2.417	2.372(9)
Tc-Tc[B]	3.425(2)	3.45(3)	3.425	3.417(2)
Tc-Tc[C]	4.037(3)	4.02(4)	4.020	4.025(2)
Tc-Tc[D]	3.744(2)	3.79(4)	3.740	^c

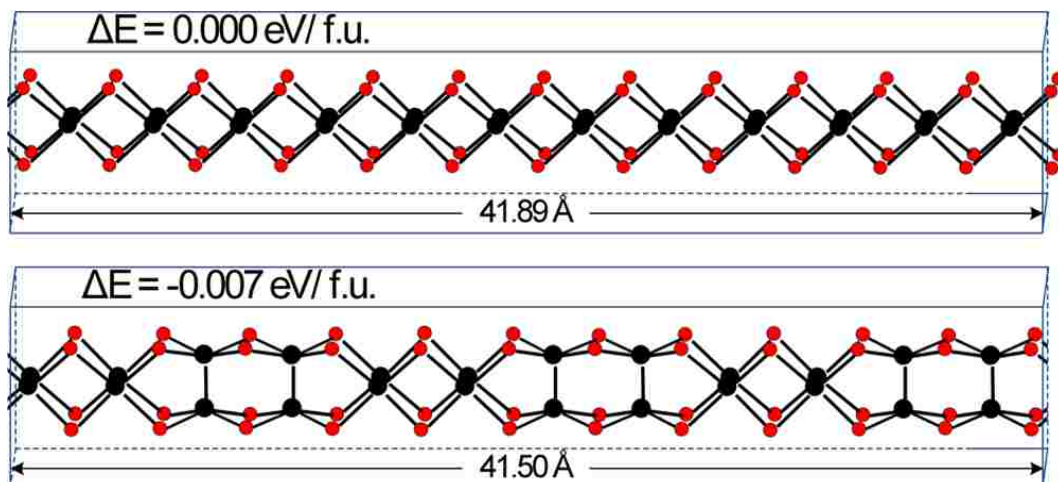


Figure 5.13. Relaxed structures of α -TcCl₂ and β -TcCl₂ chains calculated using spin-polarized density functional theory. The relative total energy difference per formula unit (f.u.), ΔE , is also reported. Tc atoms are in black and Cl atoms are in red.

The nature of metal-metal bonding within the Tc₂Cl₈ unit was investigated by calculations of the NBO occupancy of the Tc-Tc bond. The results indicate a NBO of 5.30 which is consistent with the presence of a Tc≡Tc triple bond (i.e., NBO = 6.00). In agreement with the experimental results, the band structure of β -TcCl₂ indicates an indirect gap of around 0.5 eV which suggests semiconducting behavior.

5.1.3.7 Comparisons of α/β -TcCl₂ with Other Transition Metal Dichlorides

Second and third row transition metal dichlorides can be obtained by many different routes, i.e., reaction between the elements at elevated temperature, thermal decomposition and/or disproportionation of tri- or tetrachloride precursors, reaction between metal-chloride species with gaseous reagents (e.g., Cl₂, HCl) at elevated temperatures, and metallothermic reduction of higher-valent binary chlorides. The

various routes are summarized in Table 5.4. Technetium dichlorides have been obtained by two different routes: (1) reaction between the elements at elevated temperature, and (2) thermal decomposition of TcCl_4 under vacuum.

For the first route, $\alpha\text{-TcCl}_2$ and $\beta\text{-TcCl}_2$ were obtained in sealed tubes for different conditions of pressure, deposition temperature, and reaction time. Single crystals of $\beta\text{-TcCl}_2$ (yield ~5%), located in the center part of the tube ($T \sim 420\text{ }^\circ\text{C}$), were obtained congruently with TcCl_4 and $\beta\text{-TcCl}_3$ after the reaction of Tc metal and Cl_2 at $450\text{ }^\circ\text{C}$ (24 hours) [207, 163]. The $\beta\text{-TcCl}_2$ crystals were characterized by SCXRD and EXAFS spectroscopy [206]. In agreement with the X-ray structure, EXAFS spectroscopy shows the presence of parallel and perpendicular Tc_2Cl_8 units in the compound. Concerning $\alpha\text{-TcCl}_2$, the black powder obtained after the reaction of Tc metal and Cl_2 at $450\text{ }^\circ\text{C}$ was transferred in a second tube, sealed with AlCl_3 and reacted at $450\text{ }^\circ\text{C}$. During this experiment, the pressure of $\text{Al}_2\text{Cl}_6(\text{g})$ in the tube was estimated at $\sim 1.6\text{ atm}$. After 4 days of treatment, single crystals of $\alpha\text{-TcCl}_2$ were obtained at the cold end of the tube ($T \sim 280\text{ }^\circ\text{C}$) and used for SCXRD determination [143]. These results emphasize the role of the experimental parameters (reaction time, deposition temperature, pressure, chemical transport agent) on the structure of Tc dichloride. It is anticipated that varying these parameters will lead to other polymorphs of technetium dichloride.

For the second route, TcCl_4 decomposes stepwise to $\alpha\text{-TcCl}_3$ after 2 h and to TcCl_2 after 14 h at $450\text{ }^\circ\text{C}$ in a sealed tube under vacuum (see section 3.1.3.3) [125]. Because the formation of $\alpha\text{-TcCl}_2$ requires extensive thermal treatment with AlCl_3 , it is expected that the decomposition product of TcCl_4 is $\beta\text{-TcCl}_2$. The thermal behaviors of binary Tc chlorides differ from those of Re and are more similar to those of Pt. For Re,

ReCl_4 disproportionates to ReCl_3 and ReCl_5 , the trichloride volatilizes as the Re_3Cl_9 cluster and no decomposition has been reported [210, 135]. Similar to Tc, PtCl_4 and PtCl_3 decompose to the dichloride ($\beta\text{-PtCl}_2$) [124]. The thermal behavior of TcBr_4 has been reported at 450 °C under vacuum in a Pyrex tube and TcBr_4 yields $\text{Na}\{[\text{Tc}_6\text{Br}_{12}]_2\text{Br}\}$ (see section 3.2.3.1). It is noted that PtBr_3 and PtBr_4 are both unstable and decompose to the dibromide [124].

Table 5.4. Second and third row transition metal MCl_2 phases ($M = \text{Hf, Zr, Mo, W, Tc, Pd, and Pt}$) and their method of synthesis. ^a X-ray structure not reported

MCl_2 phase	Experimental conditions
HfCl_2^a	Disproportionation of HfCl_3 at 450 °C in a evacuated sealed glass tube [202]
ZrCl_2	Reaction between $\text{ZrCl}_4(\text{g})$ and ZrCl at 650-750 °C in a sealed tantalum tube under He atmosphere (≤ 0.5 atm) [201].
$\alpha\text{-MoCl}_2$ ($\text{Mo}_6\text{Cl}_{12}$)	Disproportionation of MoCl_3 at 800 °C in an evacuated, sealed quartz tube [29]. Reduction of MoCl_5 with Al in an evacuated sealed glass tube at 450 °C [211].
$\beta\text{-MoCl}_2$	Reaction of $\text{Mo}_2(\text{O}_2\text{CCH}_3)_4$ with flowing $\text{HCl}(\text{g})$ at 250-350 °C [176].
WCl_2	Disproportionation of WCl_4 at 450°C in an evacuated sealed glass tube [132]. Reaction of WCl_6 with Al in an evacuated sealed glass tube at 450 °C [211].
$\alpha\text{-TcCl}_2$	Reaction between the elements in a glass sealed tube at 450 °C followed by treatment (4 days) of the powder 450 °C with AlCl_3 in a sealed tube [143].
$\beta\text{-TcCl}_2$	Reaction between the elements in a glass sealed tube at 450 °C. Decomposition of TcCl_4 at 450 °C in an evacuated, sealed glass tube [207].
$\alpha\text{-PtCl}_2$	Treatment of $\text{Pt}_6\text{Cl}_{12}$ at 500 °C in an evacuated sealed tube [212]. Reaction between the elements in a sealed tube at 550 °C [212].
$\beta\text{-PtCl}_2$ ($\text{Pt}_6\text{Cl}_{12}$)	Decomposition of PtCl_4 at 350 °C or PtCl_3 at 400 °C [124]. Reaction of $\text{H}_2\text{PtCl}_6 \cdot 6\text{H}_2\text{O}$ with flowing $\text{Cl}_2(\text{g})$ at 475°C [212].
$\gamma\text{-PdCl}_2$	Treatment of Pd metal with aqua regia followed by evaporation to dryness and thermal treatment of the resulting solid at 150 °C [212, 223]
$\alpha\text{-PdCl}_2$	Treatment of $\gamma\text{-PdCl}_2$ at 400 °C in a glass tube under argon [223].
$\delta\text{-PdCl}_2$	Treatment of $\alpha\text{-PdCl}_2$ at 500 °C in a glass tube under argon [223].
$\beta\text{-PdCl}_2$ ($\text{Pd}_6\text{Cl}_{12}$)	Reaction between Pd and SO_2Cl_2 in an evacuated sealed glass tube at 400°C [213]. Reaction between $\text{Pd}_3(\text{O}_2\text{CCH}_3)_6$ with $\text{HCl}(\text{aq})$ in acetic acid [214].

Among the second and third row transition metals, $\alpha\text{-TcCl}_2$ and $\beta\text{-TcCl}_2$ are the 11th and 12th dichloride phases to be structurally characterized, respectively. Notably, both compounds are structurally similar and consist of infinite chains of eclipsed Tc_2Cl_8

units. Polymorphism is common in transition metal dichlorides and two MoCl₂, two PtCl₂ and four PdCl₂ phases have been reported (Table 5.4). Transition metal dichlorides can be classified into one of four categories, *viz.*, those composed of M₂Cl₈ units, those composed of square planar MCl₄ units, those containing M₆Cl₈⁴⁺ hexanuclear clusters, and ZrCl₂. The various motifs encountered in the dichloride phases are presented in Figure 5.14.

Dichlorides composed of M₂Cl₈ units are encountered for Tc (α -TcCl₂, Figure 5.14A and β -TcCl₂, Figure 5.14B) and Mo (β -MoCl₂, Figure 5.14C). For technetium, the structure of α -TcCl₂ and β -TcCl₂ consists of infinite chains of Tc₂Cl₈ units. In the Tc₂Cl₈ units, the metal–metal separation is characteristic of Tc≡Tc triple bonds [157]. Electronic structure calculations on α -TcCl₂ and β -TcCl₂ confirm the presence of a triple bond. In these compounds, the Tc≡Tc triple bond exhibits the $\sigma^2\pi^4\delta^2\delta^{*2}$ electronic configuration, which is also in agreement with the diamagnetism of the compound. The Tc–Tc separation in the Tc₂Cl₈ unit in α/β -TcCl₂ (i.e., Tc–Tc = 2.136(3) Å) is also similar to the one found in the Tc₂Cl₈³⁻ anion (i.e., Tc–Tc = 2.13(1) Å in (NH₄)₃Tc₂Cl₈·2H₂O) [215]. In binary Tc chlorides, the electronic configuration of the Tc atoms has an effect on the metal–metal separation in the coordination polyhedra and the Tc–Tc separation (Δ TcTc) follows the order: Δ TcTc (β -TcCl₂) \approx Δ TcTc (α -TcCl₂) < Δ TcTc (α -TcCl₃) < Δ TcTc (β -TcCl₃) < Δ TcTc (TcCl₄).

For β -MoCl₂, a single crystal X-ray structure is still elusive, but EXAFS measurements revealed the presence of the Mo₄Cl₁₂ unit [206]. The latter consists of two face-sharing Mo₂Cl₈ units, and the Mo(μ -Cl)₂Mo separations are consistent with Mo–Mo single bonds between the Mo₂Cl₈ units. The metal–metal separation in Mo₂Cl₈ (Table

5.5) is indicative of a Mo≡Mo triple bond [157]. The presence of single and triple bonds in β -MoCl₂ is in agreement with the low magnetic susceptibility of the compound [216, 217].

Dichlorides composed of the M₆Cl₈⁴⁺ clusters are found for tungsten and molybdenum (Figure 5.14D). In these compounds, the octahedral M₆¹²⁺ core is coordinated to eight face-capping Cl ligands (M₆Cl₈⁴⁺) and six terminal chlorine ligands [203,29]. The crystallographic and electronic structure of the M₆Cl₈⁴⁺ clusters have been extensively studied, and the results indicate the presence of metal–metal single bonds [218, 219, 220, 221]. The M₆¹²⁺ core has 24 electrons shared between 12 single bonds, which is in agreement with the diamagnetism of the compounds [221].

Dichlorides composed of square planar MCl₄ units are encountered for Pt and Pd. Their structures can either consist of infinite chains of edge-sharing MCl₄ units (α -PtCl₂ [222], α -PdCl₂ [204, 223], δ -PdCl₂ [223], Figure 5.14E), infinite layers of corner-sharing MCl₄ (γ -PdCl₂, Figure 5.14F) [223], or M₆Cl₁₂ cubic clusters composed of four edge-sharing MCl₄ units (β -PtCl₂ [224, 225] and β -PdCl₂ [226, 227], Figure 5.14G). In those phases, the shortest metal–metal separation (Table 5.5) ranges from 3.073(3) Å in α -PtCl₂ [61] to 3.742(2) Å in γ -PdCl₂ [223]; these distances are larger than those expected for Pt–Pt and Pd–Pd single bonds [157]. Analysis of the electronic structure of β -PtCl₂ suggests that minimal metal–metal interaction occurs in the Pt₆Cl₁₂ cubic cluster [228]. In the Pt and Pd dichlorides, the metals have a d⁸ electron configuration and those compounds are diamagnetic [229].

Finally, ZrCl₂ consists of infinite layers of edge-sharing deformed ZrCl₆ octahedra (Figure 7H) [201]. The metal–metal separation (i.e., 3.3819(3) Å) is close to

the one expected for a single Zr–Zr bond [157]. The low magnetic susceptibility of ZrCl₂ is consistent with the presence of discrete metal–metal interactions in the compound [230].

Concerning transport properties, β-TcCl₂ is a semiconductor with a band gap of 0.12(2) eV; it is the lowest band gap reported for a transition metal dichloride. Zirconium dichloride is also a semiconductor and an activation energy of around 0.3 eV has been estimated from resistivity measurements [201]. The semiconducting nature of β-TcCl₂ contrasts with α-MoCl₂ that is an insulator [231]. Concerning PtCl₂ and PdCl₂, no resistivity measurements have been performed.

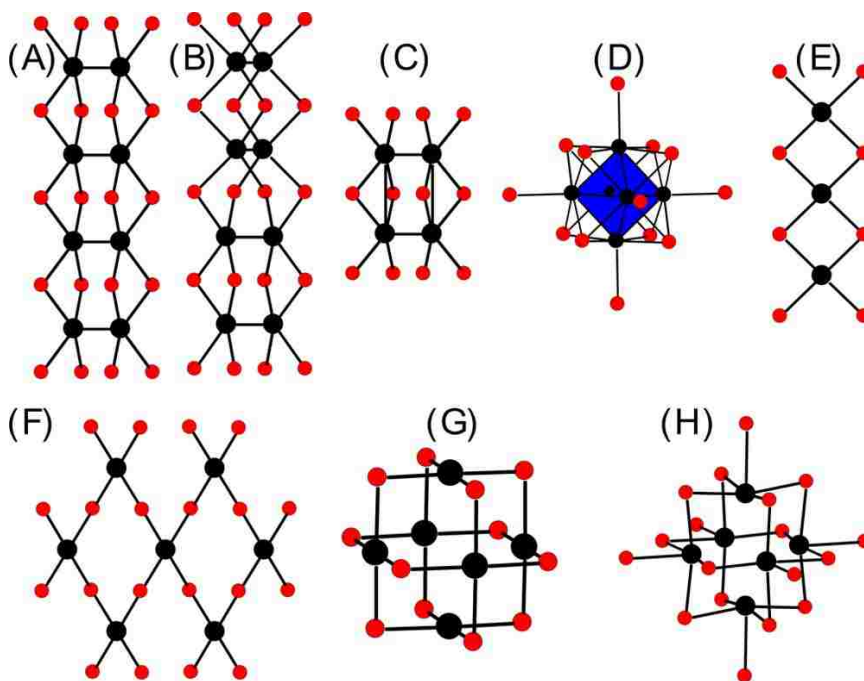


Figure 5.14. Ball and stick representation of the structural motif in 2nd and 3rd transition metal dichlorides: (A) α-TcCl₂; (B) β-TcCl₂; (C) β-MoCl₂; (D) α-MoCl₂, WCl₂; (E) α-PtCl₂, α-PdCl₂, δ-PdCl₂; (F) γ-PdCl₂; (G) β-PdCl₂, β-PtCl₂; (H) ZrCl₂. Metal atoms are in black and Cl atoms are in red.

Table 5.5. Shortest metal-metal separation (M-M in Å) in second and third row transition metal dichlorides.

Phase	M-M (Å)	Phase	M-M (Å)
ZrCl ₂	3.3819(3) ^[201]	α-PtCl ₂	3.073(4) ^[222]
α-MoCl ₂	2.61(1) ^[29]	β-PtCl ₂	3.319(2) ^[224]
β-MoCl ₂	2.21(2) ^[101]	α-PdCl ₂	3.339(2) ^[223]
WCl ₂	NR ^[29]	β-PdCl ₂	3.283(1) ^[226]
α-TcCl ₂	2.129(1) ^[143]	δ-PdCl ₂	3.288(1) ^[223]
β-TcCl ₂	2.131(2) ^[207]	γ-PdCl ₂	3.742(2) ^[223]

5.1.4 Conclusion

Two new dichloride phases α-TcCl₂ and β-TcCl₂ have been reported. The compound β-TcCl₂ was obtained from the reaction of Tc metal and Cl₂ in a sealed tube at 450 °C while α-TcCl₂ after treatment of β-TcCl₂ with AlCl₃ in a sealed tube at 450 °C. Both compounds exhibit new structure-types that consist of infinite chains of face-sharing Tc₂Cl₈ units. Within a β-TcCl₂ chain, the Tc-Tc vectors of two adjacent Tc₂Cl₈ units are either perpendicular or parallel while in an α-TcCl₂ chain, the Tc-Tc vectors are all parallel. The Tc-Tc distances within the Tc₂Cl₈ units are consistent with the presence of a Tc≡Tc triple bond. Further evidence of the triple bond has been shown from natural bond orbital occupancy calculations. The physical properties of β-TcCl₂ have been investigated; in agreement with theoretical calculations, resistivity measurements indicate β-TcCl₂ to be a semiconductor while a magnetic susceptibility measurement shows the compound to be diamagnetic. A Seebeck measurement suggests β-TcCl₂ is a p-type semiconductor. The compound β-TcCl₂ is thermally unstable and disproportionates to Tc metal and TcCl₄ above 600 °C.

Because technetium dichlorides can be obtained from the thermal decomposition of TcCl_4 and/or from the reaction of the elements in a sealed tube, it is still an open question whether TcBr_2 is accessible by these methods and whether its structure will be similar to that of TcCl_2 or a $\text{Tc}_6\text{Br}_{12}$ cluster. The thermal decomposition of TcBr_4 in Pyrex has been studied and yields $\text{Na}\{[\text{Tc}_6\text{Br}_{12}]_2\text{Br}\}$; the latter contains the $\text{Tc}_6\text{Br}_{12}$ trigonal prismatic cluster (see section 3.2.3.2). The reaction between Tc and Br_2 (Tc/Br, 1:2) has not yet been performed. Finally, it is noted that Re and Ru dichlorides are unknown; this is surprising in view of the existence of numerous Re(II) and Ru(II) complexes [232]. It is anticipated that ReCl_2 and RuCl_2 might be obtained from the metallothermic reduction of the trichlorides.

Conclusion

In this work, the synthetic, coordination chemistry, and physico-chemical properties of binary Tc chlorides, bromides, and iodides were investigated. Resulting from these studies was the discovery of five new binary Tc halide phases: α/β -TcCl₃, α/β -TcCl₂, and TcI₃, and the reinvestigation of the chemistries of TcBr₃ and TcX₄ (X = Cl, Br). Prior to 2009, the chemistry of binary Tc halides was poorly studied and defined by only three compounds, i.e., TcF₆, TcF₅, and TcCl₄; today, ten phases are known (Figure 6.1) making the binary halide system of Tc comparable to those of its neighboring elements.

Binary Tc halides were synthesized using three methods: reactions of the elements in sealed tubes, reactions of flowing HX(g) (X = Cl, Br, and I) with Tc₂(O₂CCH₃)₄Cl₂, and thermal decompositions of TcX₄ (X = Cl, Br) and α -TcCl₃ in sealed tubes under vacuum. Binary Tc halides can be found in various dimensionalities such as molecular solids (TcF₆), extended chains (TcF₅, TcCl₄, α/β -TcCl₂, TcBr₃, TcI₃), infinite layers (β -TcCl₃), and bidimensional networks of clusters (α -TcCl₃). Eight structure-types with varying degrees of metal-metal interactions are now known. The coordination chemistry of binary Tc halides can resemble that of the adjacent elements: Mo and Ru (β -TcCl₃, TcBr₃, TcI₃), Re (TcF₅, α -TcCl₃), Pt (TcCl₄, TcBr₄), or can be unique (α -TcCl₂ and β -TcCl₂) in respect to other known binary transition metal halides. Binary Tc halides display a range of interesting physical properties (magnetism, conductivity) that are manifested from their electronic and structural configurations. The

thermochemistry of binary Tc halides is extensive: they can selectively volatilize, decompose, disproportionate, or convert to other phases.

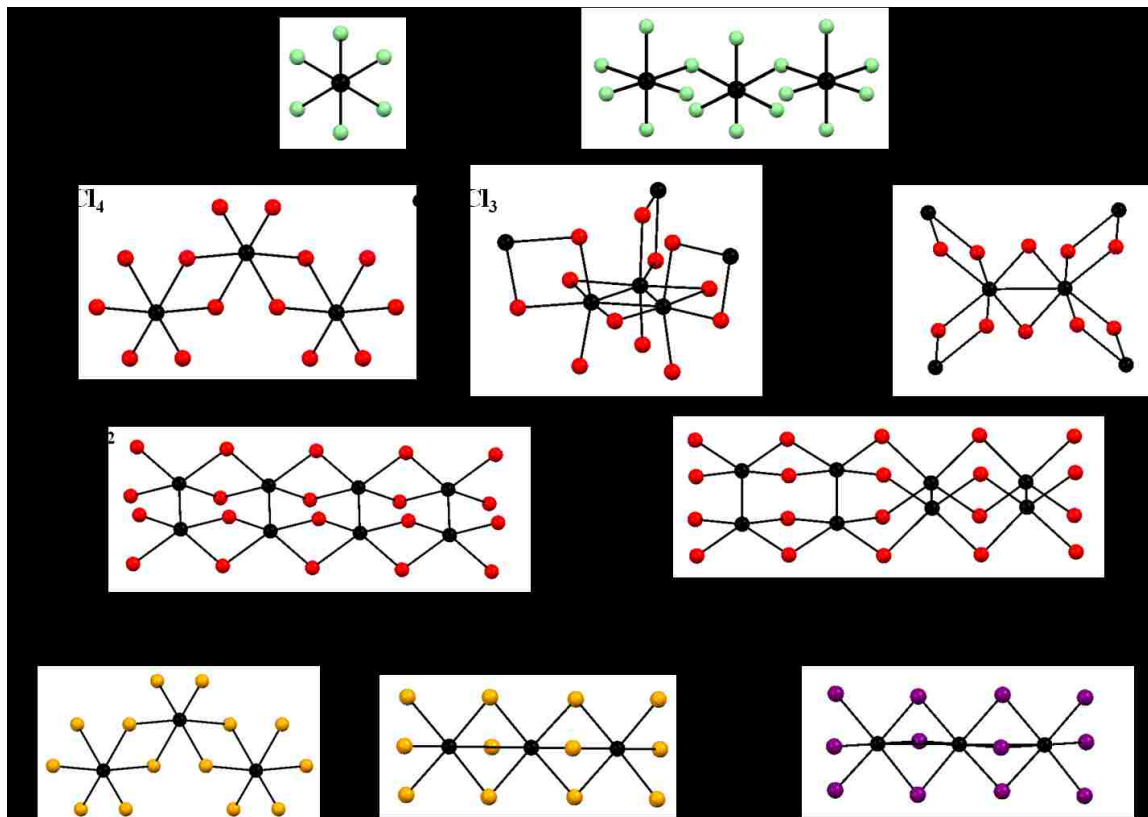


Figure 6.1. Ball-and-stick representations of the ten binary Tc halide phases.

For the binary Tc chlorides (Figure 6.2), stoichiometric sealed tube reactions of Tc metal and Cl_2 at elevated temperatures produced $\beta\text{-TcCl}_2$, $\beta\text{-TcCl}_3$, and TcCl_4 . Reactions performed with a stoichiometric amount of Cl_2 ($\text{Tc}:\text{Cl} \sim 1:2.5$) afforded all three compounds congruently; reactions performed in the presence of excess Cl_2 ($\text{Tc}:\text{Cl} \sim 1:6$) yielded the tetrachloride as a single phase. The compound $\alpha\text{-TcCl}_3$ was prepared using a similar method reported for ReCl_3 from the reaction of flowing $\text{HCl}(\text{g})$ with $\text{Tc}_2(\text{O}_2\text{CCH}_3)_4\text{Cl}_2$ at elevated temperatures.

The crystal structure of each chloride phase was determined by single crystal x-ray diffraction. Technetium tetrachloride is composed of infinite zigzag chains of distorted edge-sharing TcCl_6 octahedra and is isotypic with the Pt analogue. The metal-metal separation in TcCl_4 precludes Tc-Tc interaction.

There are two polymorphs for the Tc trichlorides. The compound $\alpha\text{-TcCl}_3$, which is isostructural to ReCl_3 and constituted of Tc_3Cl_9 clusters, and $\beta\text{-TcCl}_3$ which consists of infinite layers of edge-sharing TcCl_6 octahedra and is isostructural to $\alpha\text{-MCl}_3$ ($\text{M} = \text{Mo}, \text{Ru}$). Electronic calculations on $\alpha/\beta\text{-TcCl}_3$ are consistent with the presence of a $\text{Tc}=\text{Tc}$ double bond; the $\text{Tc}=\text{Tc}$ bond being stronger in $\alpha\text{-TcCl}_3$ than in $\beta\text{-TcCl}_3$.

Two polymorphs are reported for Tc dichloride, $\alpha\text{-TcCl}_2$ and $\beta\text{-TcCl}_2$. Both phases exhibit new structure-types that consist of infinite chains of face-sharing Tc_2Cl_8 units; in the chains, the Tc-Tc vector of adjacent Tc_2Cl_8 units can be perpendicular and parallel to each other ($\beta\text{-TcCl}_2$) or all parallel ($\alpha\text{-TcCl}_2$). Electronic calculations on $\alpha/\beta\text{-TcCl}_2$ are consistent with the presence of the electron rich $\text{Tc}\equiv\text{Tc}$ triple bond ($\sigma^2\pi^4\delta^2\delta^{*2}$) which would make it the highest bond multiplicity reported so far in a binary halide. It is noticeable that the formation of metal-metal bond in binary Tc chlorides is correlated with the electronic configuration of the Tc atom, such as: no metal-metal bond in TcCl_4 (d^3), a double $\text{Tc}=\text{Tc}$ bond in $\alpha/\beta\text{-TcCl}_3$ (d^4), and a triple $\text{Tc}\equiv\text{Tc}$ bond in $\alpha/\beta\text{-TcCl}_2$ (d^5).

The thermal behavior of the Tc chlorides was studied in sealed tubes under vacuum and under flowing argon. Under vacuum, TcCl_4 and $\alpha\text{-TcCl}_3$ both decompose to lower valent halides, $\beta\text{-TcCl}_3$ thermally converts to $\alpha\text{-TcCl}_3$, and $\beta\text{-TcCl}_2$ ultimately disproportionates to the metal and TcCl_4 . Under flowing argon, TcCl_4 volatilizes and no decomposition occurs.

Physical properties were measured for TcCl_4 and $\beta\text{-TcCl}_2$ and predicted from computational calculations for $\alpha\text{-TcCl}_3$ and $\beta\text{-TcCl}_3$. Magnetic measurements on TcCl_4 show the compound to behave as an antiferromagnetic material below 24 K and paramagnetic above 50 K. The magnetic moment of TcCl_4 is consistent with the one of an isolated TcCl_6 octahedron which confirms the absence of metal-metal interactions in the compound. Conversely, $\beta\text{-TcCl}_2$ was determined to be diamagnetic, which is consistent with the electronic configuration of the $\text{Tc}\equiv\text{Tc}$ triple bond ($\sigma^2\pi^4\delta^2\delta^{*2}$). Resistivity and optical band gap measurements indicated $\beta\text{-TcCl}_2$ to be a narrow band gap and p-type semiconductor. For the trichlorides, calculations are consistent with a metallic behaviour for $\beta\text{-TcCl}_3$ and predict $\alpha\text{-TcCl}_3$ to be a semiconductor.

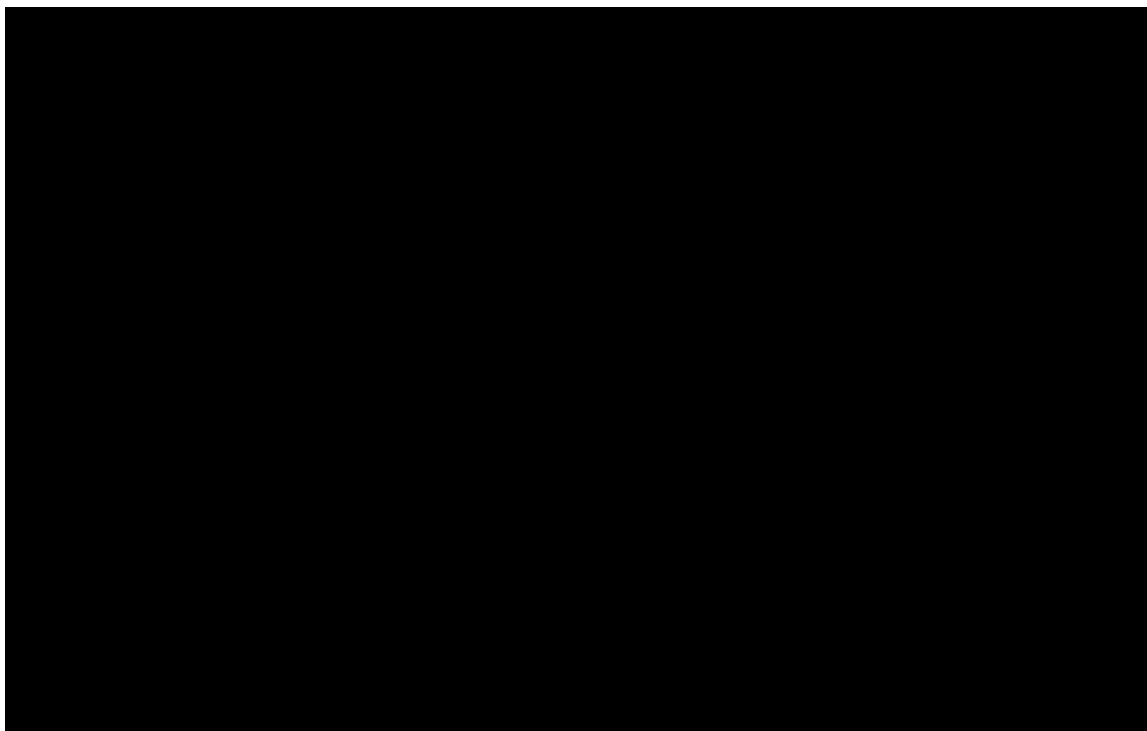


Figure 6.2. Flowchart of the synthetic and thermo-chemistries of binary technetium chlorides.

For the binary Tc bromides, the synthetic chemistry of TcBr_3 and TcBr_4 has been revisited (Figure 6.3). Both compounds can be synthesized congruently from the stoichiometric bromination ($\text{Tc}:\text{Br} \sim 1:3$) of Tc metal in sealed tubes at elevated temperatures. Repetitious reactions performed in the presence of excess Br_2 ($\text{Tc}:\text{Br} \sim 1:5$) yielded TcBr_4 as a single phase. In addition, TcBr_3 can also be synthesized as a homogeneous phase via the reaction of $\text{Tc}_2(\text{O}_2\text{CCH}_3)_4\text{Cl}_2$ with flowing $\text{HBr}(\text{g})$ at elevated temperatures. Technetium tetrabromide is isostructural with TcCl_4 and MBr_4 ($\text{M} = \text{Pt}, \text{Os}$) and consists of infinite zigzag chains of edge-sharing TcBr_6 octahedra. Unlike the Tc trichloride(s), polymorphism was not observed for TcBr_3 ; it forms extended chains of face-sharing distorted TcBr_6 octahedra and is isostructural to MBr_3 ($\text{M} = \text{Mo}, \text{Ru}$). Similar to the chloride system, a correlation between the electronic configuration of the metal atom and the presence of metal-metal interaction is observed in the binary Tc bromides: no metal-metal interaction in TcBr_4 and Tc-Tc interaction in TcBr_3 was determined.

The thermal properties of TcBr_3 and TcBr_4 were investigated under vacuum at elevated temperatures in Pyrex tubes, TcBr_4 and TcBr_3 both decomposed to $\text{Na}\{[\text{Tc}_6\text{Br}_{12}]_2\text{Br}\}$. The $\text{Na}\{[\text{Tc}_6\text{Br}_{12}]_2\text{Br}\}$ salt contains the prismatic hexanuclear $\text{Tc}_6\text{Br}_{12}$ cluster. Within the $\text{Tc}_6\text{Br}_{12}$ cluster, the oxidation state of the Tc atoms is (+2) and calculations indicate the presence of three $\text{Tc}\equiv\text{Tc}$ triple bonds and six Tc-Tc single bonds. It is noted that $\text{Na}\{[\text{Tc}_6\text{Br}_{12}]_2\text{Br}\}$ is the first Group VII compound to contain a trigonal prismatic hexanuclear cluster that was synthesized from a solid-state reaction.

Alternatively, when performed in quartz tubes these reactions yield mixtures of TcBr_3 and Tc metal.

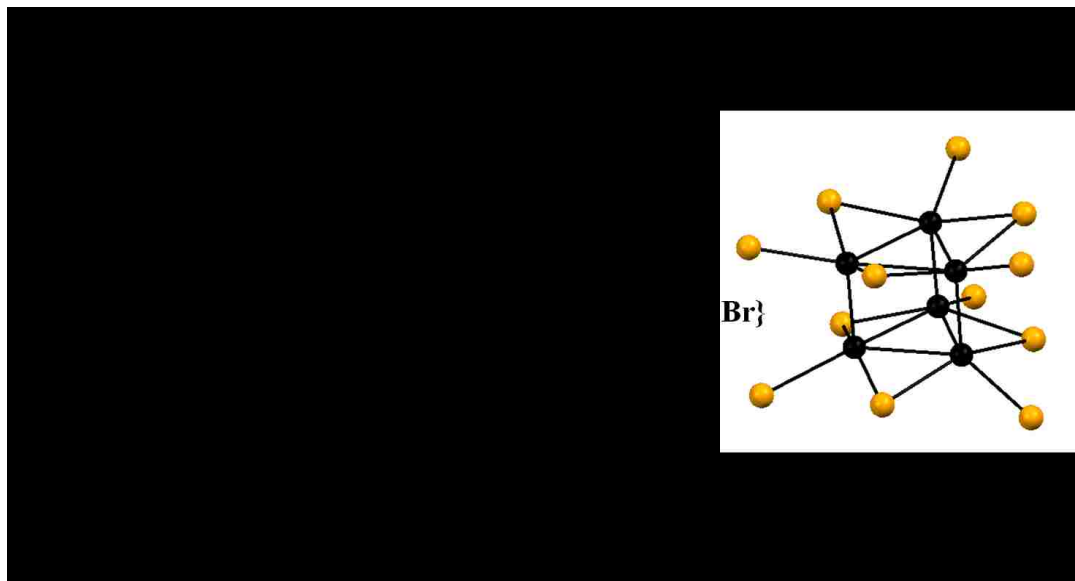


Figure 6.3. Flowchart of the synthetic and thermo-chemistries of binary technetium bromides.

Concerning the iodide system, TcI_3 is the first binary Tc iodide to be reported (Figure 6.4). Technetium triiodide was prepared using two methods: 1) reactions of Tc metal with I_2 in sealed Pyrex tubes and 2) reactions of flowing HI(g) with $\text{Tc}_2(\text{O}_2\text{CCH}_3)_4\text{Cl}_2$. The latter of these two methods produced TcI_3 as a single phase, whereas the prior yielded mixtures of TcI_3 and unreacted Tc metal. The structure of TcI_3 determined from EXAFS spectroscopy is isotopic with its Mo and Ru analogues and consists of face-sharing TcI_6 octahedra. Solubility and thermal properties of TcI_3 were investigated; the compound is insoluble in water and organic solvents and decomposes to the metal at 300 °C.

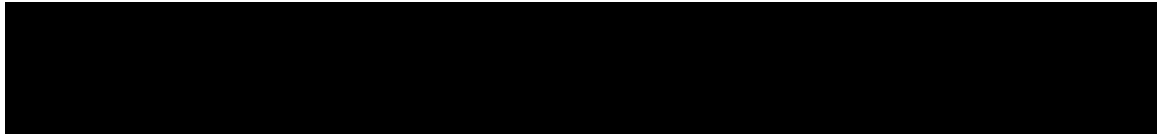


Figure 6.4. Flowchart summarizing the synthetic and thermo-chemistries of TcI_3 .

Binary Tc halides may find application in the nuclear fuel cycle and as precursors in inorganic and organometallic chemistry. The solubility properties of binary Tc halides (TcI_3 and $\beta\text{-TcCl}_2$) might be of particular interest for the development of Tc-halide waste forms. Their thermal properties could potentially be utilized in separation processes via halide volatility, i.e., Mo/Tc separation using iodine volatility processes.

Technetium organometallic complexes with multiple metal-metal bonds are still unknown; those complexes could be prepared using TcX_4 ($\text{X} = \text{Cl}, \text{Br}$) as precursors. For example, $\text{Tc}_2(\text{C}_3\text{H}_5)_4$ could be obtained from the reaction of TcX_4 ($\text{X} = \text{Cl}, \text{Br}$) with $\text{Mg}(\text{C}_3\text{H}_5)\text{Cl}$ in diethyl ether. Technetium clusters with the triangular Tc_3^{9+} core are still unknown, those complexes could be prepared from $\alpha\text{-TcCl}_3$. Salts with the composition $\text{A}_3\text{Tc}_3\text{Cl}_{12}$ ($\text{A} = \text{NH}_4, \text{K}, \text{Rb}, \text{Cs}$) should be obtained from the dissolution of $\alpha\text{-TcCl}_3$ in concentrated HCl followed by precipitation with ACl ($\text{A} = \text{NH}_4, \text{K}, \text{Rb}, \text{Cs}$). Technetium tribromide has already been used in the preparation of new divalent complexes (i.e., $\text{TcBr}_2(\text{PMe}_3)_4$ and $\text{Tc}_2\text{Br}_4(\text{PMe}_3)_4$) and it is expected that similar complexes will be obtained from TcI_3 .

In respect to these studies on the binary Tc halides, there remain many unanswered questions and unexplored facets of research that pertains to these compounds. For example, it will be of particular interest to reinvestigate the binary

fluoride compounds of lower oxidation state, such as TcF_4 or TcF_3 [52,89,168]. For higher oxidation states, theoretical calculations on TcF_7 [88] suggest the compound to be stable and possible to isolate via the fluorination of the metal under high pressures of $\text{F}_2(\text{g})$, which is also the method used for the synthesis of ReF_7 . Other reactions employed for synthesizing 2nd and 3rd row transition metal halides that have not been investigated in this work also provide potential synthetic templates; this would include those used for ReCl_6 [233], OsCl_5 [234], and ReBr_5 [96]. Attempts within this work were also unsuccessful in isolating “ TcBr_2 ”, and it is of interest to whether it can be produced and what chemical and structural relationships it may have with the Tc dichlorides. Lastly, it is hoped that these new finding would have profound significance and be beneficial for the realm of Tc and transition metal chemistry.

Appendix I

An Explanation of the Radioactive Nature of Technetium

The Nuclear Shell Model and Trends in the Chart of the Nuclides

The nuclear shell model is a model of the atomic nucleus that is used to describe the pairing and distribution of nucleons (protons and neutrons) within discrete energy levels, similar to the atomic shell model for electrons.^[13] Proton and neutron shells are filled individually according to the Pauli Exclusion Principle where closed shells result in configurations much more stable in comparison to those with open arrangements. The filled-shell configurations are referred to as “magic numbers,” which correspond to $N = 2, 8, 20, 28, 50, 82,$ and 126 . Whenever the neutron or proton count results in one of these numbers, these nuclides are denoted “magic”. A clear example of magic numbers is tin ($Z = 50$), which has 10 different stable isotopes. When both the number of neutrons and protons result in filled shells, the nuclide is considered as being “doubly magic.” “Magic” and “doubly magic” isotopes illustrate the close relationship between paired nucleons and relative nuclear stability [1].

¹ a) Mayer, M. G.; Jensen, J. H. D. *Elementary Theory of Nuclear Shell Structure*; John Wiley and Sons: New York, 1955. b) *Nuclides and Isotopes of the Nuclides*, 17th ed., Bechtel Marine Propulsion Corp., Knolls Atomic Power Laboratory, Schenectady, NY, 2010.

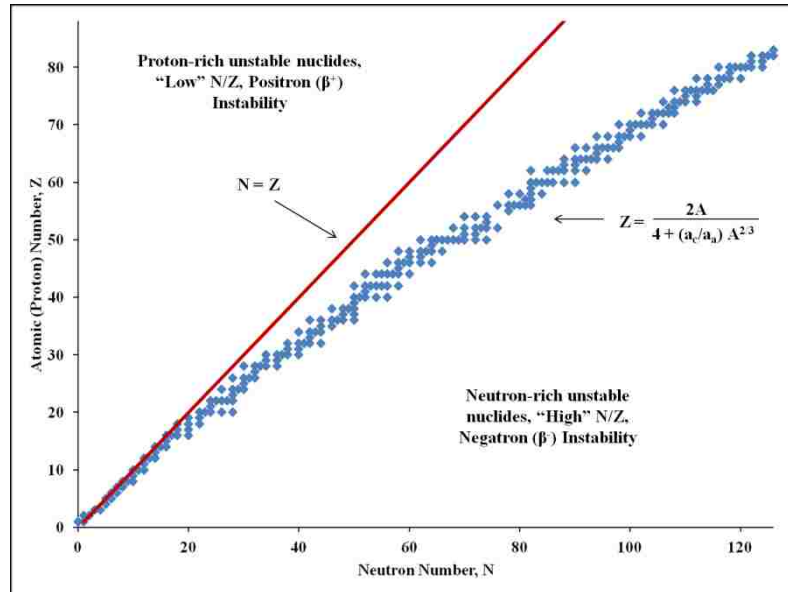


Figure 1. Values of (N, Z) for the stable nuclides in comparison to $N = Z$ [1].

Of the known isotopes, 266 are stable. The values of (N, Z) for the stable nuclides in comparison to $Z = N$ is presented in Figure 2. At low Z numbers ($Z < 7$), the pattern of stable nuclides, otherwise known as the “Valley of Stability”, follows $N = Z$. As the number of protons and corresponding neutrons that inhabit the nucleus are increased, this trend quickly changes and the Valley of Stability moves toward neutron-rich nuclides. This can be explained by the mass compensation of the neutrons in the nucleus needed to overcome the Columbic repulsions of the protons in proximity to each other. Typically, unstable nuclides found above the Valley of Stability (low N/Z or “proton rich”) will decay by emission of a positron (i.e., β^+ decay) or by electron capture, while those below it (high N/Z or “neutron rich”) will decay by emission of an electron (i.e., β^- decay); both types of decay lead to stable nuclides within the Valley of Stability. Empirical evidence shows there are four different ways of classifying stable nuclides by the evenness or oddness of the number of protons and neutrons (Table 1) [1].

Table 1. Distribution of stable nuclides by evenness or oddness of A, Z, and N [1].

A	Z	N	Number of stable nuclides
Even	Even	Even	159
Odd	Even	Odd	53
Odd	Odd	Even	50
Even	Odd	Odd	4

Of the known stable nuclides, the majority (159) are comprised of even A nuclides with even proton and neutron numbers. In the shell model, this behavior is attributed to the absence of unpaired nucleons. In almost equivalent amounts to each other are the odd A stable nuclei with either even Z and odd N or odd Z and even N. Each of these combinations accounts for roughly 1/5 of the existing stable isotopes, and is an outcome of nucleon configurations where even numbers of protons or neutrons result in paired nucleon stability. The fewest stable nuclei fall under the even A with odd Z and odd N with only 4 existing. These four even A nuclides with odd Z, odd N (i.e., ${}^2\text{H}$, ${}^6\text{Li}$, ${}^{10}\text{B}$, ${}^{14}\text{N}$) only exist at low Z numbers where lower energy configurations (i.e., “pairing energy”) are still possible with unpaired nucleons all in the same shell. Beyond ${}^{14}\text{N}$ there are no stable even A (odd Z, odd N) nuclides that exist [1].

These trends within the Chart of the Nuclides allow for assumptions to be made on why there are no stable isotopes of technetium. Hypothetically, if there was a stable isotope of technetium by these trends, it would have to fulfill these characteristics:

1) It would have to fall within the Valley of Stability; for Tc, this ideally ranges from the masses 94 to 102.

2) Because technetium has an odd atomic (proton) number ($Z = 43$), then no even A (even Z, even N) configurations are attainable (even A isotopes would result from odd

Z, odd N, which as discussed earlier only exist in stable configurations at low Z); therefore, the hypothetical stable isotope would have an odd A with an odd Z and even N count. This reduces the possibilities to those with odd A between 95 and 103, i.e., 95, 97, 99, and 101.

However, none of these isotopes are stable. So what else accounts for the inherent radioactive nature of technetium? Mattauch's isobar rule is another empirical trend within the chart of the nuclides that can be used for predicting the stability of an isotope.

Mattauch's Rule

Mattauch's isobar rule states that in general no two adjacent isotopes in an isobar can both be stable *or* that if two isotopes lie on the same isobar and one element is stable, then the other must be radioactive [2]. As previously determined from observable trends within the Chart of the Nuclides, the only stable technetium isotopes that could potentially exist in accordance to the Shell Model would be for those with $A = 95, 97, 99,$ and 101 . For these technetium isotopes to be stable, its neighboring elements on the Chart of the Nuclides, molybdenum ($Z = 42$) and ruthenium ($Z = 44$), must not have stable isotopes with identical masses. Analysis of the chart of the nuclides indicates that molybdenum and ruthenium exhibit seven stable isotopes between $A = 92$ and $A = 104$; for both elements, five of the seven isotopes are consecutively numbered, i.e., ^{94}Mo to ^{98}Mo and ^{98}Ru to ^{102}Ru . The arrangement of these stable isotopes above and below technetium (Figure 2) explains why the remaining possible isotopes ^{95}Tc , ^{97}Tc , ^{99}Tc , and

² Mattauch, J. *Zeit. Fur Physik*. **1934**, *91*, 361-371.

^{101}Tc cannot be stable, specifically because of the existence of stable ^{95}Mo , ^{97}Mo , ^{99}Ru , and ^{101}Ru [2].



Figure 2. An excerpt from the Chart of the Nuclides of isotopes of Mo ($Z = 42$) to Ru ($Z = 44$) illustrating the abundance of stable isotopes of Mo and Ru surrounding technetium. Stable isotopes are in black [1b].

Atomic Mass, Binding Energies, and Mass Parabolas

A more rigorous explanation of the radioactivity of Tc isotopes involves the concepts of binding energies and mass defects. To first order, the mass of a nucleus, A , equals the sum of the number of protons, Z , and neutrons, N . This can be expressed in atomic mass units (AMU) or energy in million electron volts (MeV). In reality, however, the actual mass of a nucleus, M , is less than A by the amount of energy required to dissociate the nucleus into its constituent nucleons, E_B , referred to as the mass defect or binding energy. This is represented in Equation 1, where M_H is the mass of the hydrogen atom (938.77 MeV) and M_N is the mass of the neutron (939.55 MeV).

$$M = ZM_H + (A-Z)M_N - E_B \quad (1)$$

This may be rewritten as

$$M = aZ^2 + bZ + c - \delta A^{-1} \quad (2)$$

where a , b , and c are functions of A reflecting the volume and surface area of the nucleus and Coulomb forces, and δ is related to the pairing energy of the nucleons. For a given isobar (constant A), a , b , and c are constants, so the plot of the constituent masses forms a parabola [3].

Examples of this are seen in Figures 3 and 4. Stable isotopes will occupy the lowest possible energy at a minimum at the bottom of the parabola with unstable nuclei to the left of the bottom β^- decaying and those to the right decaying by β^+ or electron capture both toward stable configurations. Therefore, each mass parabola can be treated as an individual cross-section from the Valley of Stability. For masses with odd A from either odd Z and even N or even Z and odd N , there can be only one minimum value at the bottom of the parabola (Figure 3), i.e., $A = 97$ and 99 . Conversely, even A isotopes can have from one to three stable nuclides/minima for a single isobar (Figure 4), i.e., $A = 98$ [4].

³ Friedlander, G.; Kennedy, J. W.; Miller, J. M. *Nuclear and Radiochemistry*, 2nd ed. Chapter 2; John Wiley and Sons: New York, 1964.

⁴ Choppin, G.; Lijenzin, J.; Rydberg, J.; Ekberg, C. *Radiochemistry and Nuclear Chemistry*, 4th ed.; Elsevier, Inc: Oxford, 2013; Chapter 4.

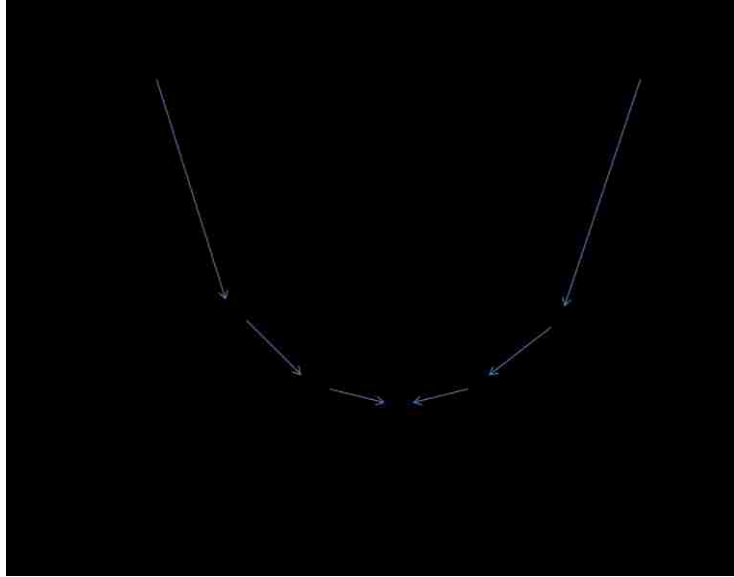


Figure 3. Isobar parabola for odd mass number nuclides demonstrating the tendency of neutron-rich nuclides to successively β^- decay and proton-rich nuclides to successively β^+ or electron capture decay toward a stable nuclide at the minimum or “valley” [1].

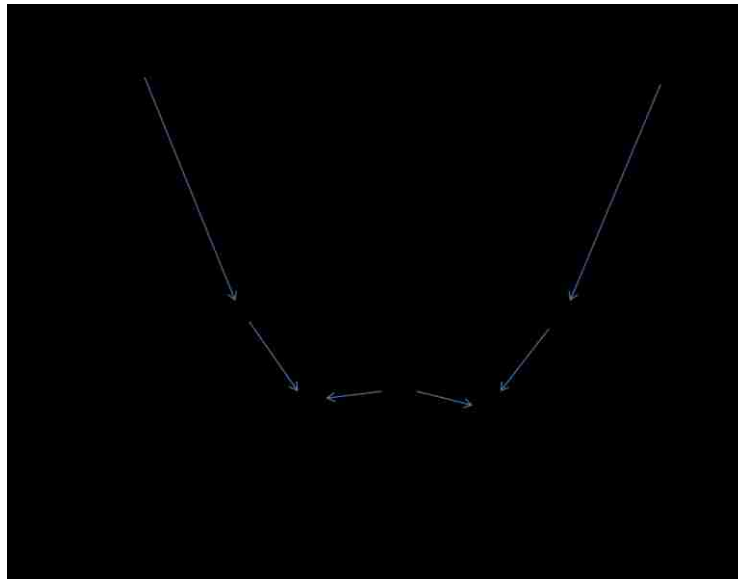


Figure 4. Isobar parabola for even mass number nuclides decaying into two stable nuclides [1].

The energy value on the ordinate could be the actual mass of the nucleus or the mass defect given in MeV. Table 2 lists the mass defects for Mo, Tc, and Ru isotopes 97-101. The most stable nuclei are highlighted in red.

Table 2. Mass Defect Values for Mo, Tc, and Ru Isotopes in MeV.

A =	$_{42}\text{Mo}$	$_{43}\text{Tc}$	$_{44}\text{Ru}$
97	-87.54	-87.22	-86.11
98	-88.11	-86.43	-88.22
99	-85.97	-87.32	-87.62
100	-86.18	-86.02	-89.22
101	-83.51	-86.34	-87.95

The mass parabolas plotted as a function of the atomic mass (amu) and atomic number for the isobars $A = 97, 98,$ and 99 are shown in Figures 5, 6, and 7, respectively. As mentioned previously, for both odd A ($A = 97$ and 99) isobars successive β^- and β^+ decays result in one stable nuclide; for $A = 97$ the final nuclide is ^{97}Mo and for $A = 99$ the end of the chain is ^{99}Ru . The $A = 98$ is noticeably different than the other two isobar chains as there are two stable nuclides, ^{98}Mo and ^{98}Ru . For both the decays of ^{97}Tc and ^{99}Tc , the beta disintegration energies (0.320 and 0.294 MeV, respectively) are relatively small in comparison to that of ^{98}Tc (1.80 MeV). Both ^{97}Tc and ^{99}Tc decay in accordance with other trending isotopes in each isobar, but ^{98}Tc is unusual in that it is reported to undergo β^- decay to ^{98}Ru with no appreciable decay by β^+ or electron capture to ^{98}Mo ; the branching ratio of electron capture to β^- decay is less than 4% [⁵]. The calculated Q_{β^-} for the reported decay of ^{98}Tc is 1.792 MeV, while the Q_{β^+} and Q_{EC} for this isotope to ^{98}Mo are 0.661 and 1.682 MeV, respectively.

⁵ Sueki, K.; Ebihara, M.; Nakahara, H. *Radiochim. Acta.* **1993**, *63*, 29-31.

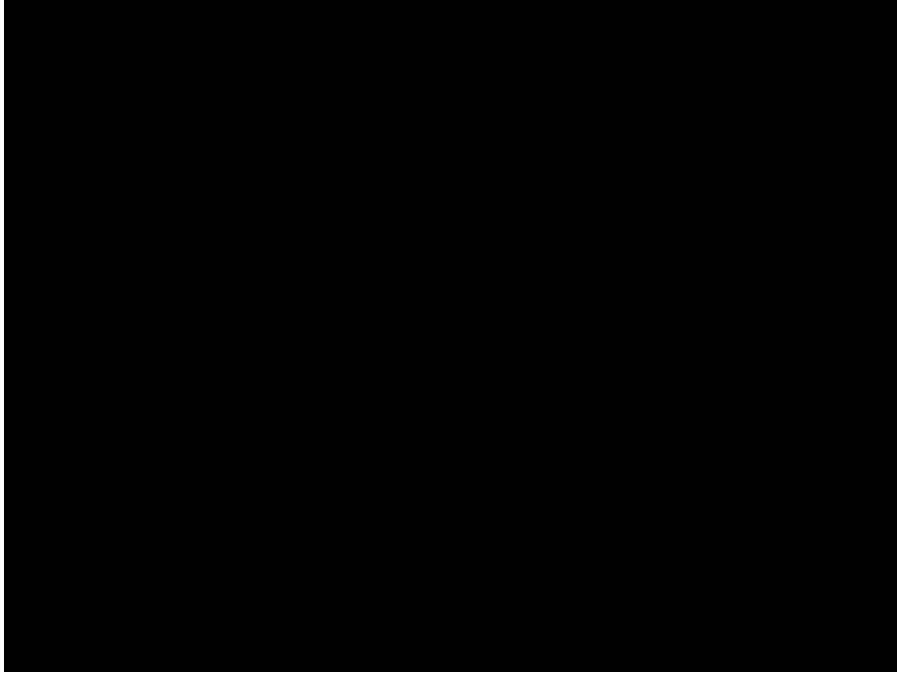


Figure 5. Isobar $A = 97$ decay scheme. No excited states are shown [1b].

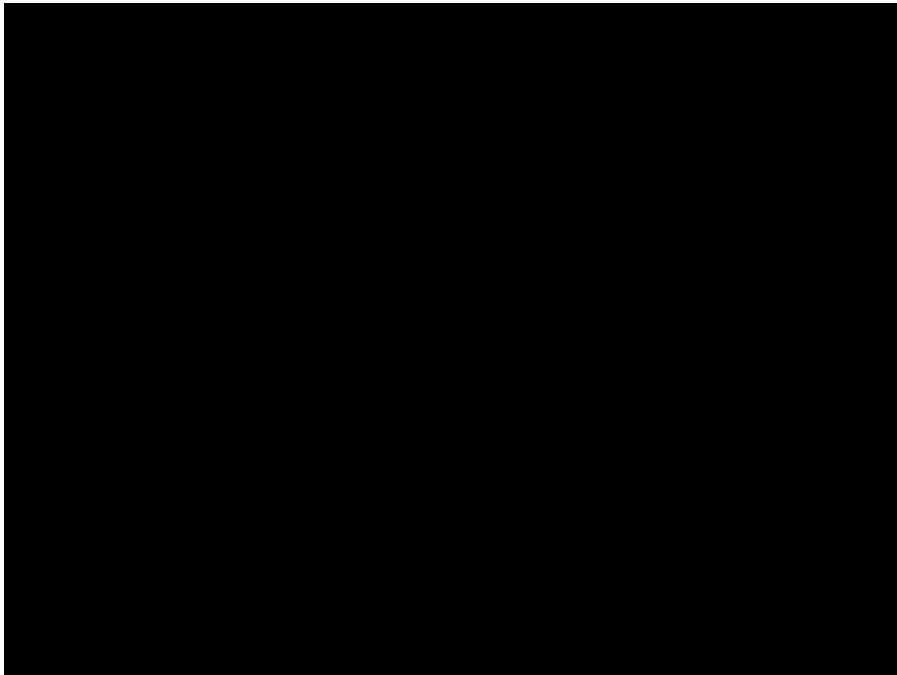


Figure 6. Isobar $A = 98$ decay scheme. No excited states are shown [1b].

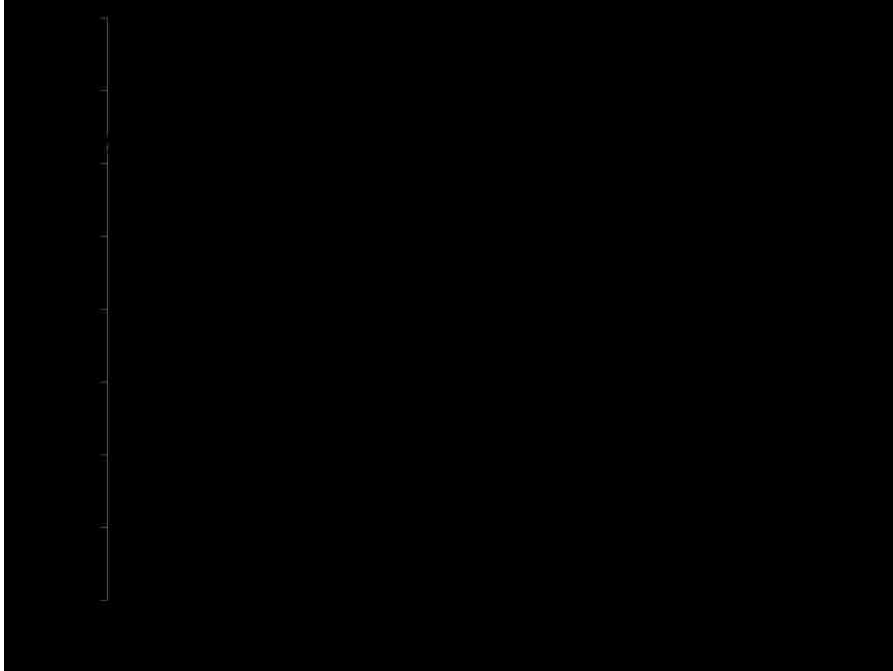


Figure 7. Isobar $A = 99$ decay scheme. No excited states have been shown [1b].

Addition Notable Nuclear Properties of Technetium Isotopes

Spin and parity give information on what nuclear levels are occupied and to what extent by the corresponding neutrons and protons of a nuclide; the highest occupied level and number of occupying nucleons determines the spin and parity. Filled proton or neutron shells have a resultant total angular momentum of zero due to paired nucleons that cancel out corresponding angular momenta where these nuclides have a resultant 0^+ spin and parity. For odd A masses with either odd Z and even N or even Z and odd N , the spin and parity are determined by the unpaired nucleon, and for even A masses with odd Z and N , they are determined by the combined interaction of both unpaired nucleons. The change in spin and parity from the decay of one nuclide to another is dictated by transition probabilities. Interestingly, the measured transitions between low-lying states in ^{99}Tc were determined and properties of the levels could only be explained by models

assuming an oblate deformation of the nucleus [6]. Another interesting observation is that the spin and parity of ^{98}Tc has been loosely predicted as 6^+ , where the calculated value is 1^+ [1b].

Conclusion

The radioactive nature of technetium can be described empirically using a combination of the nuclear shell model and trends within the Chart of the Nuclides including Mattauch's isobar rule. Applying these observations to technetium, an odd- Z element, only isotopes with odd- A could possibly exhibit a stable configuration, but using Mattauch's isobar rule, which states that no two adjacent isobars can both be stable, the remaining isotopes must be radioactive due to the adjacent stable isotopes of molybdenum and ruthenium. A detailed examination of the binding energies of the isobars of Tc graphically represented by the mass parabolas for isobars $A = 97, 98,$ and 99 illustrates that the Mo and Ru isotopes are at the energetically lowest points within the valley of beta stability and all adjacent isobar nuclides are unstable. This explanation clearly shows why technetium has no stable isotopes. The amount of technetium present on the earth is constantly increasing as it is generated in nuclear reactors; knowing this, it is important to increase our knowledge about this fascinating element.

⁶ McDonald, J.; Bäcklin, A. *Nucl. Phys.* **1971**, 162(2), 365-375.

Appendix II

Additional Crystallographic Data

Table 1. Crystal data and structure refinement for TcCl₄ at 100 K.

Empirical formula	Cl ₄ Tc
Formula weight	239.80
Temperature	100(2) K
Wavelength	0.71073 Å
Crystal system	Orthorhombic
Space group	Pbca
Unit cell dimensions	a = 6.0111(4) Å b = 11.5308(9) Å c = 13.9334(10) Å
Volume	965.76(12) Å ³
Z	8
Density (calculated)	3.299 Mg/m ³
Absorption coefficient	4.997 mm ⁻¹
F(000)	888
Crystal size	0.12 x 0.10 x 0.10 mm ³
Theta range for data collection	2.92 to 31.50°.
Index ranges	-8<=h<=8, -16<=k<=16, -20<=l<=20
Reflections collected	15226
Independent reflections	1608 [R(int) = 0.0276]
Completeness to theta = 31.50°	100.0 %
Absorption correction	Semi-empirical from equivalents
Max. and min. transmission	0.7466 and 0.6251
Refinement method	Full-matrix least-squares on F ²
Data / restraints / parameters	1608 / 0 / 46
Goodness-of-fit on F ²	1.208
Final R indices [I>2sigma(I)]	R1 = 0.0224, wR2 = 0.0586
R indices (all data)	R1 = 0.0249, wR2 = 0.0595
Largest diff. peak and hole	1.569 and -0.643 e.Å ⁻³

Table 2. Crystal data and structure refinement for Na{[Tc₆Br₁₂]₂Br} at 100 K.

Empirical formula	Br ₂₅ Na Tc ₁₂
Formula weight	3196.74
Temperature	100(2) K
Wavelength	0.71073 Å
Crystal system	Triclinic
Space group	P-1
Unit cell dimensions	a = 9.5173(5) Å, α = 83.67° b = 10.5233(6) Å, β = 73.72° c = 11.1412(6) Å, γ = 87.49°
Volume	1064.51(10) Å ³
Z	1
Density (calculated)	4.987 Mg/m ³
Absorption coefficient	27.238 mm ⁻¹
F(000)	1402
Crystal size	0.2 x 0.02 x 0.02 mm ³
Theta range for data collection	1.91 to 30.51°.
Index ranges	-13<=h<=13, -15<=k<=15, -15<=l<=15
Reflections collected	17149
Independent reflections	6456 [R(int) = 0.0309]
Completeness to theta = 30.51°	99.5 %
Absorption correction	Semi-empirical from equivalents
Max. and min. transmission	0.7465 and 0.3078
Refinement method	Full-matrix least-squares on F ²
Data / restraints / parameters	6456 / 0 / 175
Goodness-of-fit on F ²	1.079
Final R indices [I>2sigma(I)]	R1 = 0.0252, wR2 = 0.0736
R indices (all data)	R1 = 0.0285, wR2 = 0.0751
Largest diff. peak and hole	1.769 and -1.958 e.Å ⁻³

Table 3. Crystal data and structure refinement for β-TcCl₂ at 100 K.

Empirical formula	TcCl ₂
Formula weight	167.9
Temperature	100 K

Wavelength	0.71073 Å
Crystal system	Monoclinic
Space group	I2/m(1/21/2γ)s0
Unit cell dimensions	a = 8.5908(14) Å, α = 90° b = 8.5908(14) Å, β = 90° c = 3.4251(6) Å, γ = 90°
q-vector(1)	1/2a* + 1/2b* + 1/4c*
Volume	252.78(7) Å ³
Z	4
Density (calculated)	4.4106 g/cm ³
Absorption coefficient	7.399 mm ⁻¹
F(000)	308
Crystal size	0.17 x 0.14 x 0.03 mm ³
θ range for data collection	4.03 to 34.33°
Index ranges	-12 ≤ h ≤ 13, -14 ≤ k ≤ 14, -5 ≤ l ≤ 5, -1 ≤ m ≤ 1
Reflections collected	4977 (1576 main + 3401 satellites)
Independent reflections	1610 (568 main + 1042 satellites) [R _{int} = 0.0542]
Completeness to θ = 30.33°	99%
Refinement method	Full-matrix least-squares on F ²
Data / constrains / restraints / parameters	1610 / 20 / 0 / 55
Goodness-of-fit on F ²	1.99
Final R indices [I > 2σ(I)]	R _{obs} = 0.0787, wR _{obs} = 0.2114
R indices [all data]	R _{all} = 0.0900, wR _{all} = 0.2211
Final R main indices [I > 2σ(I)]	R _{obs} = 0.0480, wR _{obs} = 0.1221
R main indices (all data)	R _{all} = 0.0494, wR _{all} = 0.1237
Final R 1 st order satellites [I > 2σ(I)]	R _{obs} = 0.1288, wR _{obs} = 0.2857
R 1 st order satellites (all data)	R _{all} = 0.1533, wR _{all} = 0.3006
Extinction coefficient	3300(400)
T _{min} and T _{max} coefficients	0.3403 and 0.8447
Largest diff. peak and hole	8.92 and -5.98 e·Å ⁻³

$$R = \frac{\sum ||F_o| - |F_c||}{\sum |F_o|}, wR = \left\{ \frac{\sum [w(|F_o|^2 - |F_c|^2)^2]}{\sum [w(|F_o|^4)]} \right\}^{1/2} \text{ and } w = 1/(\sigma^2(I) + 0.0064I^2)$$

Table 3. Crystal data and structure refinement for α-TcCl₂ at 140 K.

Empirical formula	Cl ₂ Tc
Formula weight	169.90
Temperature	140(1) K

Wavelength	0.71073 Å
Crystal system	Tetragonal
Space group	I 4/m
Unit cell dimensions	a = 8.557(3) Å b = 8.557(3) Å c = 3.417(2) Å
Volume	250.18(19) Å ³
Z	4
Density (calculated)	4.484 Mg/m ³
Absorption coefficient	7.476 mm ⁻¹
F(000)	308
Crystal size	1.50 x 0.06 x 0.04 mm ³
Theta range for data collection	3.37 to 28.15°.
Index ranges	-10 ≤ h ≤ 11, -10 ≤ k ≤ 10, -4 ≤ l ≤ 4
Reflections collected	1330
Independent reflections	170 [R(int) = 0.0094]
Completeness to theta = 25.00°	99.2 %
Absorption correction	Semi-empirical from equivalents
Max. and min. transmission	0.7541 and 0.0315
Refinement method	Full-matrix least-squares on F ²
Data / restraints / parameters	170 / 0 / 13
Goodness-of-fit on F ²	1.261
Final R indices [I > 2σ(I)]	R1 = 0.0335, wR2 = 0.0976
R indices (all data)	R1 = 0.0335, wR2 = 0.0976
Largest diff. peak and hole	0.772 and -0.887 e.Å ⁻³

Bibliography

-
- ¹ Cotton, F. A.; Wilkinson, G.; Murillo, C. A.; Bochmann, M. *Advanced Inorganic Chemistry*, 6th ed.; John Wiley and Sons: New York, **1999**.
- ² Canterford, J. H.; Colton, R. *Halides of the Second and Third Row Transition Metals*; John Wiley and Sons: New York, **1968**.
- ³ Brown, I. *Adv. Inorg. Chem.* **1987**, *31*, 43.
- ⁴ Alderson, T.; Jenner, E. L.; Lindsey, R. V., Jr. *J. Am. Chem. Soc.* **1965**, *87*(24), 5638-5645.
- ⁵ Kobayashi, S; Busujima, T.; Nagayama, S. *Chem.-Eur. J.* **2000**, *6*(19), 3491-3494.
- ⁶ Smidt, J.; Hafner, W.; Jira, R.; Sieber, R.; Sedlmeier, J.; Sabel, A. *Angew. Chem.* **1962**, *74*, 93-102.
- ⁷ Guo, Q.; Miyaji, T.; Hara, R.; Shen, B.; Takahashi, T. *Tetrahedron.* **2002**, *58*(36), 7327-7334.
- ⁸ (a) Nartowski, A. M.; Parkin, I. P.; MacKenzie, M.; Craven, A. J.; MacLeod, I. J. *Mater. Chem.* **1999**, *121*(44), 10426-10427. (b) Hector, A.; Parkin, I. P. *Polyhedron.* **1995**, *14*(7), 913-917. (c) Hector, A. L.; Parkin, I. P. *J. Mater. Chem.* **1994**, *4*(2), 279-283. (d) Martin, M. J.; Qiang, G. H.; Schleich, D. M. *Inorg. Chem.* **1988**, *27*(16), 2804-2808. (e) Hector, A.; Parkin, I. P. *Polyhedron.* **1993**, *12*(15), 1855-1862.
- ⁹ (a) Kauffmann, T.; Fiegenbaum, P.; Papenberg, M.; Wiescholke, R.; Sander, J. *Eur. J. Inorg. Chem.* **1992**, *125*(1), 143-148. (b) Kauffmann, T. *Angew. Chem.* **1997**, *109*(12), 1312-1329.
- ¹⁰ Nugent, W. A. *Inorg. Chem.* **1983**, *22*(6), 965-969.
- ¹¹ (a) Selig, H.; Malm, J. G. *J. Inorg. Nucl. Chem.* **1962**, *24*, 641-644. (b) Osborne, D. W.; Schreiner, F.; Otto, K.; Malm, J. G.; Selig, H. *J. Chem. Phys.* **1978**, *68*, 1108-1118. (c) Drews, T.; Supel, J.; Hagenbach, A.; Seppelt, K. *Inorg. Chem.* **2006**, *45*, 3782-3788.
- ¹² Holloway, J. H.; Hope, E. G.; Stranger, G.; Boyd, D. A. *J. Fluorine Chem.* **1992**, *56*(1), 77-84.
- ¹³ (a) Brisdon, A. K.; Hope, E. G.; Levason, W.; Ogden, J. S. *J. Chem. Soc. Dalton T.* **1989**, 313. (b) Mucker, K.; Smith, G. S.; Johnson, Q. *Acta Cryst. B.* **1968**, *24*(6), 874-879.

-
- ¹⁴ Cotton, F. A.; Kibala, P. A.; Matusz, M.; Sandor, R. B. W. *Acta Cryst.* **1991**, C47, 2435.
- ¹⁵ Edwards, A. J.; Peacock, R. D.; Small, R. W. H. *J. Chem. Soc.* **1962**, 4486-4491.
- ¹⁶ (a) Holloway, J. H.; Peacock, R. D.; Small, R. W. H. *J. Chem. Soc.* **1964**, Feb., 644-648. (b) Casteel, W. J. Jr.; Wilkinson, A. P.; Borrmann, H.; Serfass, R. E.; Bartlett, N. *Inorg. Chem.* **1992**, 31(14), 3124.
- ¹⁷ Paine, R. T.; Asprey, L. B. *Inorg. Chem.* **1975**, 14(75), 1111-1113.
- ¹⁸ Edwards, A. J.; Hugill, D.; Peacock, R. D. *Nature.* **1963**, 200(4907), 672.
- ¹⁹ Johnstone, E. V.; Poineau, F.; Forster, P. M.; Ma, L.; Hartmann, T.; Cornelius, A.; Antonio, D.; Sattelberger, A. P.; Czerwinski, K. R. *Inorg. Chem.* **2012**, 51, 8462-8467.
- ²⁰ Pilbrow, M. F. *J. Chem. Soc. Chem. Commun.* **1972**, 5, 270-271.
- ²¹ Johnstone, E. V.; Poineau, F.; Starkey, J.; Hartmann, T.; Forster, P. M.; Ma, L.; Hilgar, J.; Rodriguez, E. E.; Farmand, R.; Czerwinski, K. R.; Sattelberger, A. P. *Inorg. Chem.* **2013**, 52(24), 14309-14316.
- ²² Lin, J.; Miller, G. J. *Inorg. Chem.* **1993**, 32, 1476-1487.
- ²³ Hillebrecht, H.; Schmidt, P. J.; Rotter, H. W.; Thiele, G.; Zoennchen, P.; Bengel, H.; Cantow, H. J.; Magonov, S. N.; Whangbo, M. H. *J. Alloys Compd.* **1997**, 246, 70.
- ²⁴ Stroganov, E. V.; Ovchinnikov, K. V. *Vestnik Leningrad. Univ.* **1957**, 12 152.
- ²⁵ Muller, U. *Angew. Chem.* **1981**, 93, 697-698.
- ²⁶ Lee, S. C.; Holm, R. H. *Angew. Chem. Int. Edit.* **1990**, 29, 840-856.
- ²⁷ Walton, R. A. *J. Clust. Sci.* **2004**, 15, 559-588.
- ²⁸ (a) Bennett, M. J.; Cotton, F. A.; Foxman, B. M. *Inorg. Chem.* **1968**, 7, 1563-1569. (b) Cotton, F. A.; Mauge, J. T. *Inorg. Chem.* **1964**, 3(10), 1402-1407.
- ²⁹ (a) Schäfer, H.; von Schnering, H. G.; Tillack, J.; Kuhnen, F.; Wöhrle, H.; Baumann, H. Z. *Anorg. Allg. Chem.* **1967**, 353, 281-310. (b) Schäfer, H.; Siepmann, R. *Z. Anorg. Allg. Chem.* **1968**, 357, 273.
- ³⁰ (a) Simon, A.; Schnering, H.; Wöhrle, H.; Schäfer, H. *Z. Anorg. Allg. Chem.* **1965**, 339, 155. (b) Kuhn, P. J.; McCarley, R. E. *Inorg. Chem.* **1965**, 4, 1482.

-
- ³¹ (a) Schäfer, H.; Schnering, H. G.; Niehues, K. J.; Nieder-Vahrenholz, H. G. *J. Less-Common Met.* **1965**, *9*, 95. (b) Simon, A.; Schnering, H. G.; Wöhrle, H.; Schäfer, H. *Z. Anorg. Allg. Chem.* **1965**, *339*, 155. (c) Bauer, D.; von Schnering, H. G. *Z. Anorg. Allg. Chem.* **1968**, *361*, 259.
- ³² Schwochau, K. *Technetium: Chemistry and Radiopharmaceutical Applications*; Wiley-VCH:Weinheim, Germany, **2000**.
- ³³ (a) Perrier, C.; Segrè, E. *J. Chem. Phys.* **1937**, *5*, 712. (b) Perrier, C.; Segrè, E. *Nature.* **1947**, *159*, 24.
- ³⁴ Abram, U.; Alberto, R. *J. Braz. Chem. Soc.* **2006**, *17*(8), 1486-1500. (b) Braband, H. *Chimia.* **2011**, *65*(10), 776-781. (c) Alberto, R. In *Comprehensive Coordination Chemistry II*, McCleverty, J. A.; Mayer, T. J. (eds.). Elsevier, Amsterdam, **2003**, vol. 5, chap. 2. (d) Alberto, R.; Braband, H.; N'Dongo, H. W. P. *Towards Small Molecule Labelling with ^{99m}Tc*. *Curr. Radiopharm.* **2009**, *2*, 254–267.
- ³⁵ Lieser, K. H. *Einführung in die Kernchemie, 3. Auflage*, VCH-Verlagsgesellschaft, Weinheim, **1991**.
- ³⁶ Huber, A.; Baumgärtner, F.; Henkelmann, R.; Gauthier, A. KFK Karlsruhe, Pt UB 15, **355**, **1986**.
- ³⁷ Salaria, G. B. S.; Rulfs, C. L.; Elving, P. J. *J. Chem. Soc.*, **1963**, 2479-2484.
- ³⁸ (a) Lieser, K. H. *Chem. Ztg.* **1986**, *110*, 215-231. (b) Pruett, D. J. *Sep. Sci. Technol.* **1981**, *16*, 1157-1179. (c) Pereira, C., Vandegrift, G. F., Regalbuto, M. C., Aase, S. B., Bakel, A. J., Bowers, D., Byrnes, J. P., Clark, M. A., Emery, J. W., Falkenberg, J. R., Gelis, A. V., Hafenrichter, L., Leonard, R., Quigley, K. J., Tsai, Y., Vander Pol, M. H., Laidler, J. J.: *Lab-scale demonstration of the UREX+2 process using spent fuel*. In *2005 Waste Management Symposium Proceedings*, Tucson, AZ, February 27, 2005.
- ³⁹ Vida, J. *Zum chemischen Verhalten des Technetiums bei der Behandlung des hochradioaktiven Abfalls*, KFK 4642, Karlsruhe, **1989**.
- ⁴⁰ Braband, H. *J. Labelled Compd. Rad.* **2014**, DOI:10.1002/jlcr.3148.
- ⁴¹ (a) Schwochau, K. *Top. Curr. Chem.* **1981**, *96*, 109-147. (b) Mullen, P.; Schwochau, K.; Jorgensen, C. K. *Chem. Phys. Lett.* **1969**, *3*, 49-51.
- ⁴² Poineau, F.; Burton-Pye, B. P.; Maruk, A.; Kirakosyan, G.; Denden I.; Rego, D. B.; Johnstone, E. V.; Sattelberger, A. P.; Fattahi, M.; Francesconi, L. C.; German, K. E.; Czerwinski, K. R. *Inorg. Chim. Acta.* **2013**, *398*, 147-150.
- ⁴³ Boyd, G. E. *Inorg. Chem.* **1978**, *17*, 1808-1810.

-
- ⁴⁴ (a) Boyd, G. E.; Cobble, J. W.; Nelson, C. M.; Smith, W. T., Jr. *J. Am. Chem. Soc.* **1952**, *74*, 556-557. (b) Rodriguez, E. E.; Poineau, F.; Llobet, A.; Thompson, J. D.; Seshadri, R.; Cheetham, A. K. *J. Mater. Chem.* **2011**, *21*(5), 1496-1502.
- ⁴⁵ Krebs, B. *Angew. Chem.* **1969**, *81*, 328-329.
- ⁴⁶ Guest, A.; Lock, C. J. L. *Can. J. Chem.* **1972**, *50*, 1807-1810.
- ⁴⁷ (a) Baldas, J.; Boas, J. F.; Bonnyman, J.; Williams, G. A. *J. Chem. Soc., Dalton Trans.* **1984**, 2395-2400. (b) Baldas, J.; Bonnyman, J.; Williams, G. A. *Aust. J. Chem.* **1985**, *38*, 215-219.
- ⁴⁸ (a) Cotton, F. A.; Davison, A.; Day, V. W.; Gage, L. D.; Trop, H. S. *Inorg. Chem.* **1979**, *18*, 3024-3029. (b) Preetz, W.; Peters, G. *Z. Naturforsch.* **1980**, *35b*, 1355-1358. (c) Davison, A.; Trop, H. S.; Depamphilis, B. V.; Jones, A. G. *Inorg. Synth.* **1982**, *21*, 160-162.
- ⁴⁹ Johnstone, E. V.; Weck, P. F.; Poineau, F.; Kim, E.; Forster, P. M.; Sattelberger, A. P.; Czerwinski, K. R. *Eur. J. Inorg. Chem.* **2013**, *2013*(7), 1097-1104.
- ⁵⁰ (a) Muller, O.; White, W. B.; Roy, R. *J. Inorg. Nucl. Chem.* **1964**, *26*, 2075-2086. (b) Magnénli, A.; Andersson, G. *Acta Chem. Scand.* **1955**, *9*, 1378-1381.
- ⁵¹ (a) Mazzocchin, G. A.; Magno, F.; Bontempelli, G. *Inorg. Chim. Acta.* **1975**, *13*, 209-212. (b) Gorski, B.; Koch, H. *J. Inorg. Nucl. Chem.* **1969**, *31*, 3565-3571. (c) Nelson, C. M.; Boyd, G. E.; Smith, W. T., Jr. *J. Am. Chem. Soc.* **1954**, *76*, 348-352.
- ⁵² (a) Balasekaran, S. M.; Molski, M.; Spandl, J.; Hagenbach, A.; Alberto, A.; Abram, U. *Inorg. Chem.* **2012**, *52*(12), 7094-7099. (b) Elder, R. C.; Estes, G. W.; Deutsch, E. *Acta Cryst.* **1979**, *b40*, 136-137. (c) Vinogradov, I. V.; Zaitseva, L. L.; Konarev, M. I.; Shepel'kov, S. V. *Russ. J. Inorg. Chem.* **1974**, *19*, 1488-1490. (d) Koyama, M.; Kanchiku, Y.; Fujinaga, T. *Coord. Chem. Rev.* **1968**, *3*, 285-291.
- ⁵³ Bandoli, G.; Clemente, D. A.; Mazzi, U. *J. Chem. Soc. Dalton Trans.* **1976**, 125-130.
- ⁵⁴ (a) Mazzi, U.; De Paoli, G.; Di Bernardo, P.; Magon, L. *J. Inorg. Nucl. Chem.* **1976**, *38*, 761-725. (b) Libson, K.; Barnett, B. L.; Deutsch, E. *Inorg. Chem.* **1983**, *22*, 1695-1704.
- ⁵⁵ Fergusson, J. E.; Hickford, J. H. *Aust. J. Chem.* **1970**, *23*, 453-461.
- ⁵⁶ (a) Yang, G. C.; Heitzmann, M. W.; Ford, L. A.; Benson, W. R. *Inorg. Chem.* **1982**, *21*, 3242-3243. (b) Orvig, C.; Davison, A.; Jones, A. G. *J. Labelled Compd. Radiopharm.*

1981, 18, 148. (c) Kirmse, R.; Stach, J.; Abram, U.; Marov, I. N. *Z. Anorg. Allg. Chem.* **1984**, 518, 210-226.

⁵⁷ Brown, D. S.; Newman, J. L.; Thornback, J. R.; Davison, A. *Acta Cryst.* **1987**, C43, 1692-1694.

⁵⁸ Sattelberger, A. P.; Poineau, F. *Comprehensive Organometallic Chemistry III*; Crabtree, R. H.; Mingos, D. M. P., Eds.; Elsevier: Oxford, **2007**; Vol. 5, Chapter 12.

⁵⁹ (a) Hileman, J. C.; Huggins, D. K.; Kaesz, H. D. *Inorg. Chem.* **1962**, 1, 933-938. (b) Kruglov, A. A.; Zaitseva, L. L.; Kotel'nikova, A. S. *Russ. J. Inorg. Chem.* **1981**, 26, 518-519.

⁶⁰ (a) Bryan, J. C.; Sattelberger, A. P. *Comprehensive Organometallic Chemistry II*; Abel, E. W.; Stone, F. G. A.; Wilkinson, G., Eds.; Elsevier: Oxford, **1995**; Vol. 6; Chap. 8, 151. (b) Hileman, J. C.; Huggins, D. K.; Kaesz, H. D. *J. Am. Chem. Soc.* **1961**, 83, 2953. (c) Hieber, W.; Herget, C. *Angew. Chem.* **1961**, 73, 579. (d) Herrmann, W. A.; Alberto, R.; Bryan, J. C.; Sattelberger, A. P. *Chem. Ber.* **1991**, 124, 1107.

⁶¹ Bailey, M. F.; Dahl, L. F. *Inorg. Chem.* **1965**, 4, 1140.

⁶² (a) Schwochau, K. *Handbuch der Präparativen Anorganischen Chemie*; Brauer, G., Ed.; Enke: Stuttgart, **1981**; Vol. 3; 1598. (b) Eakins, J. D.; Humphries, D. G. *J. Inorg. Nucl. Chem.* **1963**, 25, 737. (c) Voltz, R. E.; Holt, M. L. *J. Electrochem. Soc.* **1967**, 114, 128-131. (d) Box, W. D. *Nucl. Appl.* **1965**, 1, 155-157.

⁶³ (a) Peacock, R. D. *The Chemistry of Technetium and Rhenium*. Elsevier: London, **1966**. (b) Spitsyn, V. I.; Golovanov, Y. N.; Balakhovskii, O. A.; Tsvetaev, A. A. *Dokl. Akad. Nauk SSSR.* **1972**, 205, 1421-1424. (c) Spitsyn, V. I. *Z. Chem. [Leipzig]*. **1981**, 21, 131-136.

⁶⁴ Nelson, C. M.; Boyd, G. E.; Smith, W. T., Jr. *J. Am. Chem. Soc.* **1954**, 76, 348-352.

⁶⁵ Marples, J. A. C.; Koch, C. C. *Phys. Lett.* **1972**, 41A, 307-308.

⁶⁶ Daunt, J. G.; Cobble, J. W. *Phys. Rev.* **1953**, 92, 507-508.

⁶⁷ (a) Kubicka, H. *J. Catalysis.* **1968**, 12, 223-237. (b) Spitsyn, V. I.; Pirogova, G. N.; Korosteleva, R. I.; Kalinina, G. E. *Dokl. Akad. Nauk, SSSR.* **1988**, 298, 149-151.

⁶⁸ Sattelberger, A. P. *Multiple Bonds between Metal Atoms*, 3rd ed.; Cotton, F. A.; Murillo, C. A.; Walton, R. A., Eds.; Springer: New York, **2005**; Chap. 7.

⁶⁹ Preetz, W.; Peters, G. *Z. Naturforsch.* **1980**, 35b, 797.

-
- ⁷⁰ Preetz, W.; Peters, G.; Bublitz, D. *J. Cluster Sci.* **1994**, *5*, 83.
- ⁷¹ (a) Cotton, F. A.; Bratton, W. K. *Inorg. Chem.* **1970**, *9*, 789. (b) Cotton, F. A.; Bratton, W. K. *J. Am. Chem. Soc.* **1965**, *87*, 921. (c) Cotton, F. A.; Daniels, L.; Davison, A.; Orvig, C. *Inorg. Chem.* **1981**, *20*, 3051.
- ⁷² Poineau, F.; Forster, P. M.; Todorova, T. K.; Gagliardi, L.; Sattelberger, A. P.; Czerwinski, K. R. *Dalton Trans.* **2012**, *41*, 2869-2872.
- ⁷³ (a) Zaitseva, L. I.; Kotel'nikova, A. S.; Rezvov, A. A. *Russ. J. Inorg. Chem.* **1980**, *25*, 1449. (b) Skowronek, J.; Preetz, W. *Z. Naturforsch.* **1992**, *47B*, 482.
- ⁷⁴ Kerlin, W. M.; Poineau, F.; Czerwinski, K. R.; Forster, P. M.; Sattelberger, A. P. *Polyhedron.* **2013**, *58*, 115-119.
- ⁷⁵ (a) Spitsyn, V. I.; Kuzina, A. F.; Oblova, A. A.; Kryuchkov, S. V.; Belyaeva, L. I. *Dokl. Acad. Nauk. SSSR.* **1977**, *237*, 1412. (b) German, K. E.; Kryuchkov, S. V.; Kuzina, A. F.; Spitsyn, V. I. *Dokl. Chem.* **1986**, *288*, 139.
- ⁷⁶ Kryuchkov, S. V.; Grigoriev, M. S.; Yanovskii, A. I.; Struchkov, Y. T.; Spitsyn, V. I. *Dokl. Chem.* **1988**, *297*, 520.
- ⁷⁷ (a) Kryuchkov, S. V.; Grigoriev, M. S.; Kuzina, A. F.; Gulev, B. F.; Spitsyn, V. I. *Dokl. Chem.* **1986**, *288*, 172. (b) Spitzin, V. I.; Kryuchkov, S. V.; Grigoriev, M. S.; Kuzina, A. F. *Z. Anorg. Allg. Chem.* **1988**, *563*, 136. (c) Koz'min, P. A.; Surazhskaya, M. D.; Larina, T. B. *Dokl. Phys. Chem.* **1982**, *265*, 656. (d) Kryuchkov, S. V.; Grigoriev, M. S.; Yanovskii, A. I.; Struchkov, Y. T.; Spitsyn, V. I. *Dokl. Chem.* **1988**, *301*, 219.
- ⁷⁸ (a) Kryuchkov, S. V.; Grigoriev, M. S.; Kuzina, A. F.; Gulev, B. F.; Spitsyn, V. I. *Dokl. Akad. Nauk. SSSR.* **1986**, *228*, 289-393. (b) Cotton, F. A.; Daniels, L. M.; Falvello, L. R.; Grigoriev, M. S.; Kryuchkov, S. V. *Inorg. Chim. Acta.* **1991**, *189*, 53-54.
- ⁷⁹ Rinke, K.; Klein, M.; Schäfer, H. *J. Less-Common Metals.* **1967**, *12*, 497-503.
- ⁸⁰ (a) Selig, H.; Chernick, C. L.; Malm, J. G. *J. Inorg. Nucl. Chem.* **1961**, *19*, 377. (b) Edwards, A. J.; Hugill, D.; Peacock, R. D. *Nature.* **1963**, *200*, 672. (c) Hugill, D.; Peacock, R. D. *J. Chem. Soc. A.* **1966**, 1339-1341.
- ⁸¹ Selig, H.; Cafasso, F. A.; Gruen, D. M.; Malm, J. G. *J. Chem. Phys.* **1962**, *36*, 3440-3444.
- ⁸² Binenboym, J.; Selig, H. *Inorg. Nucl. Chem.* **1962**, *24*, 641-644.
- ⁸³ Holloway, J. H.; Selig, H. *J. Inorg. Nucl. Chem.* **1968**, *30*, 473-478.

-
- ⁸⁴ Frlec, B.; Selig, H.; Hyman, H. H. *Inorg. Chem.* **1967**, *6*, 1775-1783.
- ⁸⁵ J. E. Till. *Technetium in the Environment*; Desmet, G., Myttenaere, C. Eds.; Elsevier, Appl. Sci. Publ.: New York, **1986**; pp. 1-20.
- ⁸⁶ Edwards, A. J.; Hugill, D.; Peacock, R. D. *Nature*. **1968**, *200*, 672.
- ⁸⁷ Peacock, R. D. *Gmelin Handbook of Inorganic Chemistry*, 8th ed., Supplement Vol. 2; Kugler, H. H., Keller, C. C. Eds.; Springer Verlag: Berlin, **1983**; pp. 78, 79, 84.
- ⁸⁸ Riedel, S.; Renz, M.; Kaupp, M. *Inorg. Chem.* **2007**, *46*(14), 5734-5738.
- ⁸⁹ Weck, P. F.; Kim, E.; Poineau, F.; Rodriguez, E. E.; Sattelberger, A. P.; Czerwinski, K. R. *Inorg. Chem.* **2009**, *48*(14), 6555-6558.
- ⁹⁰ Colton, R. *Nature*, **1962**, *193*, 872.
- ⁹¹ (a) Elder, M.; Penfold, B. R. *Chem. Commun.* **1965**, 309-309. (b) Elder, M.; Penfold, B. R. *Inorg. Chem.* **1966**, *5*, 1197-1200.
- ⁹² Knox, K.; Coffey, E. C. *J. Am. Chem. Soc.* **1958**, *81*, 5-7.
- ⁹³ (a) Fergusson, J. E.; Hickford, J. H. *J. Inorg. Nucl. Chem.* **1966**, *28*, 2293-2296. (b) Hagenbach, A.; Yegen, E.; Abram, U. *Inorg. Chem.* **2006**, *45*, 7331-7338.
- ⁹⁴ Abram, U.; Wollert, R. *Radiochem. Acta.* **1993**, *63*, 149-151.
- ⁹⁵ (a) Fischer, E. O.; Schmidt, M. W. *Chem. Ber.* **1969**, *102*, 1954-1960. (b) Abram, U.; Wollert, R.; Hiller, W. *Radiochim. Acta.* **1993**, *63*, 145-147.
- ⁹⁶ Canterford, J. H.; Waugh, A. B. *Inorg. Nucl. Chem. Lett.* **1971**, *7*, 395-399.
- ⁹⁷ Poineau, F.; Rodriguez, E. E.; Forster, P. M.; Sattelberger, A. P.; Cheetham, A. K.; Czerwinski, K. R. *J. Am. Chem. Soc.* **2009**, *131*, 910-911.
- ⁹⁸ (a) Thiele, G.; Wochner, H.; Wagner, H. *Z. Anorg. Allg. Chem.* **1985**, *530*, 178-186. (b) Pilbrow, M. F. *J. Chem. Soc., Chem. Comm.* **1972**, *5*, 270-271.
- ⁹⁹ (a) Merlino, S.; Labella, L.; Marchetti, F.; Toscani, S. *Chem. Mater.* **2004**, *16*, 3895-3903. (b) Hillebrecht, H.; Ludwig, Th.; Thiele, G. *Z. Anorg. Allg. Chem.* **2004**, *630*, 2199-2204. (c) Lachgar, A.; Dudis, D. S.; Corbett, J. D. *Inorg. Chem.* **1990**, *29*, 2242-2246.
- ¹⁰⁰ Poineau, F.; Weck, P. F.; Forster, P. M.; Sattelberger, A. P.; Czerwinski, K. R. *Dalton Trans.* **2009**, *46*, 10338-10342.

-
- ¹⁰¹ Poineau, F.; Sattelberger, A. P.; Conradson, S. D.; Czerwinski, K. R. *Inorg. Chem.* **2008**, *47*(6), 1991-1999.
- ¹⁰² Skowronek, J.; Preetz, W. *Naturforsch. B.* **1992**, *47*(4), 482-490.
- ¹⁰³ Sheldrick, G. M. *Acta Crystallogr., Sect. A* **2008**, *64*, 112.
- ¹⁰⁴ Almahamid, I.; Bryan, J. C.; Bucher, J. J.; Burrell, A. K.; Edelstein, N. M.; Hudson, E. A.; Kaltsoyannis, N.; Lukens, W. W.; Shuh, D. K.; Nitsche, H.; Reich, T. *Inorg. Chem.* **1995**, *34*, 193– 198.
- ¹⁰⁵ Poineau, F.; Sattelberger, A. P.; Czerwinski, K. R. *J. Coord. Chem.* **2008**, *61*(15), 2356–2370.
- ¹⁰⁶ Ressler, T. *J. Synchrotron Radiat.* **1998**, *5*, 118– 122.
- ¹⁰⁷ Rehr, J. J.; Albers, R. C. *Rev. Mod. Phys.* **2000**, *72*, 621– 654.
- ¹⁰⁸ Ravel, B. *J. Synchrotron Radiat.* **2001**, *8*, 314–316.
- ¹⁰⁹ (a) Kortüm, G. *Reflectance Spectroscopy: Principles, Methods, Applications*; Springer-Verlag: NY, **1969**. (b) Tandon, S. P.; Gupta, J. P. *Phys. Status Solidi B.* **1970**, *38*, 363. (c) Wendlandt, W. W.; Hecht, H. G. *Reflectance Spectroscopy*; Interscience Publishers: New York, **1966**.
- ¹¹⁰ Malliakas, C. D., Specialized scripts written in LabView were utilized to collect an I-V curve of 11 points from +10 to -10 μ A on each temperature point from 300 K to 530 K with a step of 2 K.
- ¹¹¹ Koyama, M.; Kanchiku, Y.; Fujinaga, T. *Coord. Chem. Rev.* **1968**, *3*, 285– 291.
- ¹¹² Kresse, G.; Furthmüller, J. *Phys. Rev. B* **1996**, *54*, 11169.
- ¹¹³ (a) Perdew, J. P.; Chevary, J. A.; Vosko, S. H.; Jackson, K. A.; Pederson, M. R.; Singh, D. J.; Fiolhais, C. *Phys. Rev. B* **1992**, *46*, 6671. (b) Perdew, J. P.; Wang, Y. *Phys. Rev. B* **1992**, *45*, 13244.
- ¹¹⁴ M. J. Frisch et al., Gaussian, Inc., Wallingford CT, **2009**.
- ¹¹⁵ (a) Becke, A. D. *J. Chem. Phys.*, **1993**, *98*, 5648. (b) Lee, C.; Yang, W.; Parr, R. G. *Phys. Rev. B.* **1988**, *37*, 785. (c) Vosko, S. H.; Wilk, L.; Nusair, M. *Can. J. Phys.*, **1980**, *58*, 1200. (d) Stephens, P. J.; Devlin, F.J.; Chabalowski, C.F.; Frisch, M.J. *J. Phys. Chem.*, **1994**, *98*, 11623.

-
- ¹¹⁶ Dunning Jr., T. H.; Hay, P. J. in *Modern Theoretical Chemistry*, Ed. H. F. Schaefer III, Vol. 3; Plenum: New York, **1976**; 1-28.
- ¹¹⁷ Andrae, D.; Haeussermann, U.; Dolg, M.; Stoll, H.; Preuss, H. *Theor. Chem. Acc.* **1990**, *77*, 123.
- ¹¹⁸ Borin, A. C.; Gobbo, J. P.; Roos, B. O. *Mol. Phys.* **2009**, *107*, 1035.
- ¹¹⁹ Peacock, R. D.; Welch, A. J. E.; Wilson, L. F. *J. Chem. Soc.* **1958**, 2901–2902.
- ¹²⁰ Cotton, F. A.; DeBoer, B. G.; Mester, Z. *J. Am. Chem. Soc.* **1972**, *95*, 1159–1163.
- ¹²¹ Casteel, W. J.; Lohmann, D. H.; Bartlett, N. J. *Fluorine Chem.* **2001**, *112*, 165–171.
- ¹²² Mueller, H.; Waschinski, R. *Inorg. Nucl. Chem. Lett.* **1972**, *8*, 413–415.
- ¹²³ Fergusson, J. E.; Robinson, B. H.; Roper, W. R. *J. Chem. Soc.* **1962**, 2113–2115.
- ¹²⁴ Degner, M.; Holle, B.; Kamm, J.; Pilbrow, M. F.; Thiele, G.; Wagner, D.; Weigl, W.; Wodtisch, P. *Transition Met. Chem.* **1976**, *1*, 41–47.
- ¹²⁵ Johnstone, E. V.; Poineau, F.; Forster, P. M.; Ma, L.; Hartmann, T.; Cornelius, A.; Antonio, D.; Sattelberger, A. P.; Czerwinski, K. R. *Inorg. Chem.* **2012**, *51*, 8462–8467.
- ¹²⁶ Blumental, B. H. *The Chemical Behavior of Zirconium*; Van Nostrand: New York, **1958**.
- ¹²⁷ Ruff, O.; Bornemann, F. *Z. Anorg. Allg. Chem.* **1910**, *65*, 429–456.
- ¹²⁸ Kolbin, N. I.; Semenov, I. N.; Shutov, Y. M. *Zh. Neorg. Khim.* **1963**, *8*, 2422–2427.
- ¹²⁹ Wohler, L.; Streicher, S. *Ber. Dtsch. Chem. Ges.* **1913**, *46*, 1591–1597.
- ¹³⁰ Couch, D. E.; Brenner, A. J. *Res. Natl. Bur. Std.* **1959**, *A63*, 185–188.
- ¹³¹ Kepert, D. L.; Mandyczewsky, R. *Inorg. Chem.* **1968**, *7*, 2091–2093.
- ¹³² McCarley, R. E.; Brown, T. M. *Inorg. Chem.* **1964**, *3*, 1232–1236.
- ¹³³ Colton, R.; Martin, R. L. *Nature* **1965**, *205*, 239–240.
- ¹³⁴ Geilmann, W.; Wrigge, F. W.; Blitz, W. *Z. Anorg. Allgem. Chem.* **1933**, *214*, 244–247.
- ¹³⁵ Fraiss, P. W.; Guest, A.; Lock, C. J. L. *Can. J. Chem.* **1969**, *47*, 1069–1072.

-
- ¹³⁶ Brignole, A.; Cotton, F. A. *J. Chem. Soc., Chem. Commun.* **1971**, 13, 706.
- ¹³⁷ Fletcher, J. M.; Gardener, W. E.; Hooper, E. W.; Hyde, K. R.; Moore, F. H.; Woodhead, J. L. *Nature* **1963**, 199, 1089–1090.
- ¹³⁸ Puche, F. *Ann. Chim.* **1938**, 9, 233–322.
- ¹³⁹ Poineau, F.; Johnstone, E. V.; Sattelberger, A. P.; Czerwinski, K. R. *J. Radioanal. Nucl. Chem.* **2013**, DOI: 10.1007/s10967-013-2743-0.
- ¹⁴⁰ Poineau, F.; Sattelberger, A. P.; Conradson, S. D.; Czerwinski, K. R. *J. Radioanal. Nucl. Ch.* **2012**, 292, 989–994.
- ¹⁴¹ Dalziel, J.; Gill, N. S.; Nyholm, R. S.; Peacock, R. D. *J. Chem. Soc.* **1958**, 4012–4016.
- ¹⁴² Figgis, B. N.; Lewis, J.; Mabbs, F. E. *J. Chem. Soc.* **1961**, 3138–3145.
- ¹⁴³ Poineau, F.; Malliakas, C. D.; Weck, P. F.; Scott, B. L.; Johnstone, E. V.; Forster, P. M.; Eunja, K.; Kanatzidis, M. G.; Czerwinski, K. R.; Sattelberger, A. P. *J. Am. Chem. Soc.* **2011**, 133, 8814–8817.
- ¹⁴⁴ Krebs, B. *Angew. Chem.* **1969**, 8, 146–147.
- ¹⁴⁵ Niewa, R.; Jacobs, H. Z. *Kristallogr.* **1995**, 210, 687.
- ¹⁴⁶ Cotton, F. A.; Rice, C. E. *Inorg. Chem.* **1977**, 16, 1865–1867.
- ¹⁴⁷ Taylor, D. R.; Calabrese, J. C.; Larsen, E. M. *Inorg. Chem.* **1977**, 16, 721–722.
- ¹⁴⁸ Bajan, B.; Meyer, H. J. Z. *Kristallogr.* **1996**, 211, 818.
- ¹⁴⁹ Westland, A. D.; Uzelac, V. *Inorg. Chim. Acta.* **1977**, 23, L37–L39.
- ¹⁵⁰ Larson, M. L.; Moore, F. W. *Inorg. Chem.* **1964**, 3, 285–286.
- ¹⁵¹ Shchukarev, S. A.; Novikov, G. I.; Vasil'kova, I. V. *Zh. Neorg. Khim.* **1960**, 5, 1650–1654.
- ¹⁵² Johnstone, E. V.; Grant, D. J.; Poineau, F.; Fox, L.; Forster, P. M.; Ma, L.; Gagliardi, L.; Czerwinski, K. R.; Sattelberger, A. P. *Inorg. Chem.* **2013**, 52(10), 5660–5662.
- ¹⁵³ Kryuchkov, S. V.; Grigoriev, M. S.; Yanovskii, A. I.; Struchkov, Y. T.; Spitsyn, V. I. *Dokl. Chem.* **1987**, 297, 867.

-
- ¹⁵⁴ Koz'min, P. A.; Kotel'nikova, A. S.; Larina, T. B.; Mekhtiev, M. M.; Surazhskaya, M. D.; Bagirov, S. A.; Osmanov, N. S. *Dokl. Phys. Chem.* **1987**, *295*, 647–650.
- ¹⁵⁵ Koz'min, P. A.; Osmanov, N. S.; Surazhskaya, M. D.; Abbasova, T. A.; Larina, T. B.; Tagiev, I. B.; Kotel'nikova, A. S. *Zh. Neorg. Khim.* **1993**, *38*, 449–451.
- ¹⁵⁶ Kryuchkov, S. V. *Russ. Chem. Rev.* **1998**, *67*, 883–904.
- ¹⁵⁷ Pyykko, P.; Atsumi, M. *Chem. Eur. J.* **2009**, *15*, 12770–12779.
- ¹⁵⁸ Batsanov, S. S. *Inorg. Mater.* **2001**, *37*, 871–885.
- ¹⁵⁹ Mingos, D. M. P. *Acc. Chem. Res.* **1984**, *17*, 311.
- ¹⁶⁰ Wade, K. *Chem. Commun.* **1971**, 792.
- ¹⁶¹ (a) Fletcher, J. M.; Gardner, W. E.; Fox, A. C.; Topping, G. *J. Chem. Soc. A.* **1967**, *7*, 1038. (b) Baernighausen, H.; Handa, B. K. *J. Less-Common Metals.* **1964**, *6*, 226.
- ¹⁶² Poineau, F.; Johnstone, E. V.; Weck, P. F.; Kim, E.; Forster, P. M.; Scott, B. L.; Sattelberger, A. P.; Czerwinski, K. R. *J. Am. Chem. Soc.* **2010**, *132(45)*, 15864–15865.
- ¹⁶³ Poineau, F.; Johnstone, E. V.; Weck, P. F.; Forster, P. M.; Kim, E.; Czerwinski, K. R.; Sattelberger, A. P. *Inorg. Chem.* **2012**, *51(9)*, 4915–4917.
- ¹⁶⁴ Esjornson, S. N.; Fanwick, P.E.; Walton, R. A. *Inorg. Chim. Acta*, **1989**, *162* 165–166.
- ¹⁶⁵ Plekhanov, Y. V.; Kryutchkov, S. V. *Russ. J. Coord. Chem.* **1998**, *24*, 617–624.
- ¹⁶⁶ Batsanov, S. S. *Inorg. Mater.* **2001**, *37*, 871–885.
- ¹⁶⁷ Weck, P. F.; Kim, E.; Czerwinski, K. R. *Chem. Phys. Lett.* **2010**, *487*, 190–193.
- ¹⁶⁸ Weck, P. F.; Sergeeva, A. P.; Kim, E.; Boldyrev, A. I.; Czerwinski, K. R. *Inorg. Chem.* **2011**, *50(3)*, 1039–1046.
- ¹⁶⁹ Cotton, F. A.; Feng, X. *Int. J. Quantum Chem.* **1996**, *58*, 671–680.
- ¹⁷⁰ Cavigliasso, G.; Yu, C. Y.; Stranger, R. *Polyhedron* **2007**, *26*, 2942–2948.
- ¹⁷¹ Hillebrecht, H.; Ludwig, Th.; Thiele, G. *Z. Anorg. Allg. Chem.* **2004**, *630*, 2199–2204.
- ¹⁷² Kobayashi, Y.; Okada, T.; Asai, K.; Katada, M.; Sano, H.; Ambe, F. *Inorg. Chem.* **1992**, *31*, 4570–457.

-
- ¹⁷³ Pollini, I. *Phys. Rev. B* **1994**, *50*, 2095–2103.
- ¹⁷⁴ Miroslovov, A. E.; Borisova, I. V.; Sidorenko, G. V.; Suglobov, D. N. *Radiokhimiya*. **1991**, *33(6)*, 14-19.
- ¹⁷⁵ Fergusson, J. E.; Robinson, B. H.; Roper, W. R. *J. Chem. Soc.* **1962**, 2113–2115.
- ¹⁷⁶ (a) Glicksman, H. D.; Hamer, A. D.; Smith, T. J.; Walton, R. A. *Inorg. Chem* **1976**, *15(9)*, 2205-2209. (b) Glicksman, H. D.; Walton, R. A. *Inorg. Chem.* **1978**, *17(1)*, 200–201. c) Santure, D. J.; Huffman, J. C.; Sattelberger, A. P. *Inorg. Chem.* **1985**, *24(3)*, 371-378.
- ¹⁷⁷ Schaefer, H. *Anorg. Allg. Chem.* **1986**, *534*, 206–208.
- ¹⁷⁸ Kolbin, N. I.; Ovchinnikov, K. V. *Zh. Neorg. Khim.* **1968**, *13(8)*, 2306–2307.
- ¹⁷⁹ Shchukarev, S. A.; Kolvin, N. I.; Ryabov, A. N. *Vestn. Leningr. Univ.* **1961**, *16*, 100–104.
- ¹⁸⁰ Prussin, S. G.; Olander, D. R.; Lau, W. K.; Hansson, L. *J. Nucl. Mater.* **1988**, *154(1)*, 25–37.
- ¹⁸¹ Corbett, J. D. *Inorg. Synth.* **1983**, *22*, 13.
- ¹⁸² Lewis, J.; Machin, D. J.; Nyholm, R. S.; Pauling, P.; Smith, P. W. *Chem. Ind.* **1960**, 259–260.
- ¹⁸³ Sato, T.; Fukui, H.; Sasaki, H.; Tachikawa, T. *Denki Kagaku.* **1988**, *56(10)*, 860–863.
- ¹⁸⁴ Schnering, H. G.; Brodersen, K.; Moers, F.; Breitbach, H. K.; Thiele, G. *J. Less-Common Met.* **1966**, *11*, 288–289.
- ¹⁸⁵ Breitbach, H. K. Graduate thesis, received **1965**.
- ¹⁸⁶ Schaefer, H.; Schulz, H. G. *Z. Anorg. Allg. Chem.* **1984**, *516*, 196–200.
- ¹⁸⁷ Rulfs, C. L.; Elving, P. J. *J. Am. Chem. Soc.* **1957**, *72*, 3304.
- ¹⁸⁸ Lachgar, A.; Dudis, D. S.; Corbett, J. D. *Inorg. Chem.* **1990**, *29*, 2242–2246.
- ¹⁸⁹ Simon, A.; von Schnering, H. G. *J. Less-Common Met.* **1966**, *11*, 31–46.

-
- ¹⁹⁰ (a) Hulliger, F. *Structural Chemistry of Layer-Type Phases*; D. Reidel Publishing Co.:Dordrecht, The Netherlands, **1976**; p 164. (b) Babel, D.; Deigner, P. *Z. Anorg. Allg. Chem.* **1965**, 339, 57.
- ¹⁹¹ Thiele, G.; Steiert, D.; Wagner, D.; Wochner, H. *Z. Anorg. Allg. Chem.* **1984**, 207–213.
- ¹⁹² Chizhikov, D. M.; Rabinovich, B. N. *Dokl. Akad. Nauk SSR* **1960**, 134, 368– 370.
- ¹⁹³ Klanberg, F.; Koholschutter, H. W. *Z. Naturforsch.* **1960**, 15b, 616.
- ¹⁹⁴ (a) Drobot, D. V.; Mikhailova, L. G. *Zh. Neorg. Khim.* **1973**, 18(1), 31– 34. (b) Drobot, D. V.; Mikhailova, L. G.; Sushchev, A. V. *Zh. Neorg. Khim.* **1976**, 21(12), 3348–3354
- ¹⁹⁵ Wang, L.; Brazis, P.; Rocci, M.; Kannewurf, C. R.; Kanatzidis, M. G. *Chem. Mater.* **1998**, 10, 3298– 3300.
- ¹⁹⁶ Ghosh, R. N.; Baker, G. L.; Ruud, C.; Nocera, D. G. *Appl. Phys. Lett.* **1999**, 75, 2885.
- ¹⁹⁷ Gray, T. G. *Coord. Chem. Rev.* **2003**, 243, 213.
- ¹⁹⁸ Kamiguchi, S.; Nagashima, S.; Komori, K.-i.; Kodomari, M.; Chihara, T. *J. Cluster Sci.* **2007**, 18, 414.
- ¹⁹⁹ Strobele, M.; Justel, T.; Bettentrup, H.; Meyer, H. J. *Z. Anorg. Allg. Chem.* **2009**, 635, 822.
- ²⁰⁰ Blomstrand, W. *J. Prakt. Chem.* **1859**, 77, 88.
- ²⁰¹ Cisar, A.; Corbett, J. D.; Daake, R. L. *Inorg. Chem.* **1979**, 18, 836.
- ²⁰² Larsen, E. M.; Leddy, J. J. *J. Am. Chem. Soc.* **1956**, 78, 5983.
- ²⁰³ Biltz, W.; Fendius, C. *Z. Anorg. Allg. Chem.* **1928**, 172, 385.
- ²⁰⁴ Wells, A. F. *Z. Kristallogr.* **1938**, 100, 189.
- ²⁰⁵ Brodersen, K. *Angew. Chem.* **1964**, 76, 690.
- ²⁰⁶ Poineau, F.; Johnstone, E. V.; Weck, P. F.; Kim, E.; Conradson, S. D.; Sattelberger, A. P.; Czerwinski, K. R. *Inorg. Chem.* **2012**, 51, 4965.

-
- ²⁰⁷ Malliakas, C. D.; Poineau, F.; Johnstone, E. V.; Weck, P. F.; Kim, E.; Scott, B. L.; Forster, P. M.; Kanatzidis, M. G.; Czerwinski, K. R.; Sattelberger, A. P. *J. Am. Chem. Soc.* **2013**, *135*, 15955–15962.
- ²⁰⁸ Korlann, S. D.; Riley, A. E.; Kirsch, B. L.; Mun, B. S.; Tolbert, S. H. *J. Am. Chem. Soc.* **2005**, *127*, 12516.
- ²⁰⁹ Riley, A. E.; Tolbert, S. H. *J. Am. Chem. Soc.* **2003**, *125*, 4551.
- ²¹⁰ Christodoulakis, A.; Maronitis, C.; Boghosian, S. *Phys. Chem. Chem. Phys.* **2001**, *3*, 5208.
- ²¹¹ Dorman, W. C.; McCarley, R. E. *Inorg. Chem.* **1974**, *13*, 491.
- ²¹² Chusova, T. P.; Semenova, Z. I. *Thermochim. Acta* **2009**, *482*, 62.
- ²¹³ Dillamore, I. M.; Edwards, D. A. *J. Inorg. Nucl. Chem* **1969**, *31*, 2427.
- ²¹⁴ Yatsimirski, A.; Ugo, R. *Inorg. Chem.* **1983**, *22*, 1395.
- ²¹⁵ Bratton, W. K.; Cotton, F. A. *Inorg. Chem.* **1970**, *9*, 789.
- ²¹⁶ Allison, G. B.; Anderson, I. R.; Sheldon, J. C. *Aust. J. Chem.* **1969**, *22*, 1091.
- ²¹⁷ Ryan, T. R.; McCarley, R. E. *Inorg. Chem.* **1982**, *21*, 2072.
- ²¹⁸ Simon, A. *Angew. Chem., Int. Ed. Engl.* **1988**, *27*, 159.
- ²¹⁹ Prokopuk, N.; Shriver, D. F. In *Advances in Inorganic Chemistry*; Sykes, A. G., Ed.; Academic Press: New York, **1998**; Vol. 46, p 1.
- ²²⁰ Cotton, F. A.; Haas, T. E. *Inorg. Chem.* **1964**, *3*, 10.
- ²²¹ Kepert, D. L.; Vrieze, K. *Halogen Chem.* **1967**, *3*, 1.
- ²²² Krebs, B.; Brendel, C.; Schafer, H. *Z. Anorg. Allg. Chem.* **1988**, *561*, 119.
- ²²³ Evers, J.; Beck, W.; Gobel, M.; Jakob, S.; Mayer, P.; Oehlinger, G.; Rotter, M.; Klapotke, T. M. *Angew. Chem., Int. Ed.* **2010**, *49*, 5677.
- ²²⁴ von Schnering, H. G.; Chang, J.-H.; Peters, K.; Peters, E. M.; Wagner, F. R.; Grin, Y.; Thiele, G. *Z. Anorg. Allg. Chem.* **2003**, *629*, 516.
- ²²⁵ Brodersen, K.; Thiele, G.; Schnering, H. G. *Z. Anorg. Allg. Chem.* **1965**, *337*, 120.

-
- ²²⁶ Dell'Amico, D. B.; Calderazzo, F.; Marchetti, F.; Ramello, S. *Angew. Chem., Int. Ed. Engl.* **1996**, *35*, 1331.
- ²²⁷ Schafer, H.; Wiese, U.; Rinke, K.; Brendel, K. *Angew. Chem., Int. Ed. Engl.* **1967**, *6*, 253.
- ²²⁸ Kettle, S. F. A. *Nature* **1966**, *209*, 1021.
- ²²⁹ van Bronswyk, W.; Nyholm, R. *J. Chem. Soc. A* **1968**, 2084.
- ²³⁰ Lewis, J.; Machin, D. J.; Newnham, I. E.; Nyholm, R. S. *J. Chem. Soc.* **1962**, 2036.
- ²³¹ Perrin, C.; Sergent, M. *J. Less-Common Met.* **1986**, *123*, 117.
- ²³² Cotton, F. A.; Murillo, C. A.; Walton, R. A. *In Multiple Bonds between Metal Atoms*; 3rd ed.; Springer: New York, **2005**.
- ²³³ Tamadon, F.; Seppelt, K. *Angew. Chem., Int. Ed.* **2013**, *52*, 767–769.
- ²³⁴ Burns, R. C.; O'Donnell, T. A. *Inorg. Chem.* **1979**, *18*, 3081–3086.

CIRRICULUM VITAE

Name: Erik Vaughan Johnstone

Title: Graduate Assitant

EMPLOYEMENT HISTORY

- 2009 to 2013 Ph.D. student and graduate assistant.
Department of chemistry, University of Nevada Las Vegas.
Subject: “*Synthesis and Characterization of Binary Technetium Halides*”. Supervisor: Professor Kenneth R. Czerwinski. Predicted graduation date February 2014.
- 2007 to 2009 Chemistry stockroom and department assistant.
Chemistry and Biochemistry department, College of Charleston.
- 2006 to 2007 Undergraduate research assistant.
Department of Physics, College of Charleston.
Subject: “*The Use of Photodynamic Therapy for Treating Esophageal Cancers*”.
Supervisor: Dr. Linda Jones
- 2006 Undergraduate research assistant.
Department of Chemistry and Biochemistry, College of Charleston.
Subject: “*The electronic structure of monomeric chlorophyll a as determined from hyperfine sublevel correlation spectroscopy (HYSCORE)*”.
Supervisor: Dr. Michelle Brooks

EDUCATION

- 2009 to present Ph.D. degree in “Radiochemistry” from University of Nevada Las Vegas, Las Vegas, Nevada.

2008 to 2009 Bachelor of Science degree in “Chemistry” from College of Charleston, Charleston, South Carolina.

2004 to 2008 Bachelor of Science degree in “Biochemistry” from College of Charleston, Charleston, South Carolina.

AFFILIATION

Alpha Sigma Chi – chemistry fraternity

American Nuclear Society (ANS) student chapter

SYNERGISTIC ACTIVITIES:

Research mentoring:

- Jenna Starkey, undergraduate student (2012). UNLV nuclear summer school. **Synthesis and characterization of technetium binary bromides.**

- Jeremy Hilgar, undergraduate student (Jan. 2013 to present). UNLV. **Synthesis and characterization of technetium iodides.**

- Jordan Donaldson, undergraduate student (2013). UNLV nuclear summer school. **Metallurgy of technetium: synthesis of binary U-Tc alloys and arc casting transition metals**

AWARDS

1. 2nd place in “Materials Science and Technology” presentations at 2011 ANS Student Conference.
2. 2nd place in “Advanced Materials” for the Innovations in the Fuel Cycle Research 2011.

PUBLICATIONS (15)

1. Poineau, F.; Johnstone, E. V.; Czerwinski, K. R.; Sattelberger, A. P. **Recent Advances in Technetium Halide Chemistry.** *Accounts Chem. Res.* (2014), 47(2), 624-632.
2. Poineau, F.; Johnstone, E. V.; Sattelberger, A. P. Czerwinski, K. R. **Characterization of TcCl_4 and $\beta\text{-TcCl}_3$ by X-ray absorption fine structure spectroscopy.** *J. Radioanal. Nucl. Ch.* (2014), 299(1), 235-239.
3. Habel-Rodriguez, D.; Poineau, F.; Johnstone, E. V.; Czerwinski, K. R.; Sattelberger, A. P.; Kirk, M. **Magnetic Circular Dichroism and Electronic Structure of $[\text{Re}_2\text{X}_4(\text{PMe}_3)_4]^+$ (X = Cl, Br).** *Inorg. Chem.* (2014), 53(3), 1260-1262.
4. Johnstone, E. V.; Poineau, F. P.; Starkey, J.; Hartmann, T.; Forster, P. F.; Ma, L.; Hilgar, J.; Rodriguez, E. E.; Farmand, R.; Czerwinski, K. R.; Sattelberger, A. P. **Synthetic and Coordination Chemistry of the Heavier Trivalent Technetium Binary Halides: Uncovering Technetium Triiodide.** *Inorg. Chem.* (2013) *submitted.*

-
- Malliakas, C. D.; Poineau, F.; Johnstone, E. V.; Weck, P. F.; Kim, E.; Scott, B. L.; Forster, P. M.; Kanatzidis, M. G.; Czerwinski, K. R.; Sattelberger, A. P. **β -Technetium Dichloride: Solid-State Modulated Structure, Electronic Structure, and Physical Properties.** *J. Am. Chem. Soc.* (2013), 135(42), 15955-15962.
 - Mausolf, E.; Johnstone, E. V.; Poineau, F.; Nguyen, S.; Jones, S.; Hartmann, T.; Buck, E.; Czerwinski, K. R. **Formation of Tc metal in 12 M HCl using Zn as a reductant.** *J. Radioanal. Nucl. Chem.* (2013), 298(2), 1315-1321.
 - Johnstone, E. V.; Grant, D. J.; Poineau, F.; Fox, L.; Forster, P. M.; Ma, L.; Gagliardi, L.; Czerwinski, K. R.; Sattelberger, A. P. **A Trigonal-Prismatic Hexanuclear Technetium(II) Bromide Cluster: Solid-State Synthesis and Crystallographic and Electronic Structure.** *Inorg. Chem.* (2013), 52(10), 5660-5662.
 - Poineau, F.; Burton-Pye, B. P.; Maruk, A.; Kirakosyan, G.; Denden, I.; Rego, D. B.; Johnstone, E. V.; Sattelberger, A. P.; Fattahi, M.; Francesconi, L. C.; et al. **On the Nature of Heptavalent Technetium in Concentrated Nitric and Perchloric Acid.** *Inorg. Chem. Acta*, (2013), 398, 147-150.
 - Johnstone, E. V.; Weck, P. F.; Poineau, F.; Kim, E.; Forster, P. M.; Sattelberger, A. P.; Czerwinski, K. R. **X-ray Crystallographic and First-Principles Theoretical Studies of $K_2[TcOCl_5]$ and UV/Vis Investigation of the $[TcOCl_5]^{2-}$ and $[TcOCl_4]^-$ Ions.** *Eur. J. Inorg. Chem.*, (2013), 2013(7), 1097-1104.
 - Poineau, F.; Johnstone, E. V.; Forster, P. M.; Ma, L.; Sattelberger, A. P.; Czerwinski, K. R. **Probing the Presence of Multiple Metal-Metal Bonds in Technetium Chlorides by X-ray Absorption Spectroscopy: Implications for Synthetic Chemistry.** *Inorg. Chem.* (2012), 51(17), 9563-9570.
 - Johnstone, E. V.; Poineau, F.; Forster, P. M.; Ma, L.; Hartmann, T.; Cornelius, A.; Antonio, D.; Sattelberger, A. P.; Czerwinski, K. R. **Technetium Tetrachloride Revisited: A Precursor to Lower-Valent Binary Technetium Chlorides.** *Inorg. Chem.* (2012), 51(15), 8462-8467.
 - Poineau, F.; Johnstone, E. V.; Weck, P. F.; Kim, E.; Conradson, S. D.; Sattelberger, A. P.; Czerwinski, K. R. **On the Structure of β -Molybdenum Dichloride.** *Inorg. Chem.* (2012), 51(9), 4965-4971.
 - Poineau, F.; Johnstone, E. V.; Weck, P. F.; Forster, P. M.; Kim, E.; Czerwinski, K. R.; Sattelberger, A. P. **β -Technetium Trichloride: Formation, Structure, and First-Principles Calculations.** *Inorg. Chem.* (2012), 51(9), 4965-4971.
 - Poineau, F.; Malliakas, C. D.; Weck, P. F.; Scott, B. L.; Johnstone, E. V.; Forster, P. M.; Kim, E.; Kanatzidis, M. G.; Czerwinski, K. R.; Sattelberger, A. P. **Technetium Dichloride: A New Binary Halide Containing Metal-Metal Multiple Bonds.** *J. Am. Chem. Soc.* (2011), 133, 8814-8817
 - Poineau, F.; Johnstone, E. V.; Weck, P. F.; Kim, E.; Forster, P. M.; Scott, B. L.; Sattelberger, A. P.; Czerwinski, K. R. **Synthesis and Structure of Technetium Trichloride.** *J. Am. Chem. Soc.* (2010), 132, 15864-15865.

PRESENTATIONS (15)

- Johnstone, E. V.; Poineau, F.; Starkey, J.; Forster, P. M.; Czerwinski, K. R.; Sattelberger, A. P.; Hartmann, T. **Coordination Chemistry of the Heavier Binary Technetium Halides**, 246th ACS National Meeting & Exposition, Indianapolis, IN, United States, September 8-12, 2013 (2013), NUCL-76.
- Poineau, F.; Johnstone, E. V.; Forster, P. M.; Fox, L.; Grant, D.; Gagliardi, L.; Sattelberger, A. P.; Czerwinski, K. R. **Preparation and characterization of the Tc_6Br_{12} cluster.** 245th ACS National Meeting & Exposition, New Orleans, LA, United States, April 7-11 (2013), NUCL-211.
- Johnstone, E. V.; Weck, P. F.; Poineau, F.; Kim, E.; Forster, P. M.; Czerwinski, K. R.; Sattelberger, A. P. **X-ray crystallographic and first-principle theoretical studies of K_2TcOCl_5 .** 245th ACS National Meeting & Exposition, New Orleans, LA, United States, April 7-11 (2013), NUCL-210.

-
4. Starkey, J. E.; Johnstone, E. V.; Poineau, F.; Czerwinski, K. R. **Characterization and synthesis of binary technetium halides: A new synthetic route to Technetium Tribromide**. 64th Southeast Regional Meeting of the American Chemical Society, Raleigh, NC, United States, November 14-17 (2012), SERM-1161.
 5. E.V. Johnstone, F. Poineau, P.F. Weck, E. Kim, P.M. Forester, B. Scott, T. Hartmann, A.P. Sattelberger, K.R. Czerwinski. **Synthesis and characterization of binary technetium chlorides**. American Nuclear Society (ANS) Student Conference 2012. April 12-15, 2012. Las Vegas, NV.
 6. Sattelberger, Alfred P.; Poineau, Frederic; **Johnstone, Erik V.**; Weck, Phillippe F.; Kim, Eunja; Forster, Paul; Czerwinski, Kenneth R. **Binary technetium chlorides**. 243rd ACS National Meeting & Exposition, San Diego, CA, United States, March 25-29, 2012 (2012), NUCL-110.
 7. F. Poineau, A. P. Sattelberger, B. L. Scott, P. Forster, Ph. Weck, E. Johnstone, K. R. Czerwinski. **Technetium halides: from molecular to extended structures**. 7th International Symposium on Technetium and Rhenium. July 4-8, 2011. Moscow, Russia.
 8. E.V. Johnstone, F. Poineau, P.F. Weck, E. Kim, P.M. Forester, B. Scott, T. Hartmann, A.P. Sattelberger, K.R. Czerwinski. **Synthesis and characterization of low-valent binary technetium chlorides: $TcCl_3$ and $TcCl_2$** . American Nuclear Society (ANS) Student Conference 2011. April 14-17, 2011. Atlanta, GA.
 9. E.V. Johnstone, F. Poineau, P.F. Weck, E. Kim, P.M. Forester, B. Scott, T. Hartmann, A.P. Sattelberger, K.R. Czerwinski. **Synthesis and characterization of low-valent binary technetium chlorides**. 7th International Symposium on Technetium and Rhenium. July 4-8, 2011. Moscow, Russia.
 10. Johnstone, E. V.; Czerwinski, K. R.; Poineau, F.; Sattelberger, A. P. **Synthesis and characterization of low-valent technetium binary chlorides**. 241st ACS National Meeting, Anaheim, CA, United States, March 27-31, 2011.
 11. F. Poineau; A. Sattelberger; P. Forster; P. Weck; E. Johnstone; L. Ma; K. Czerwinski. **Synthesis and characterization of new binary technetium halides**. Pacificchem 2010. December 15-20, 2010. Honolulu, HI, USA.
 12. F. Poineau, A. Sattelberger, P. Forster, P. Weck, E. Johnstone, L. Ma, K. Czerwinski. **Synthesis and Characterization of New Binary Technetium Halides**. International Symposium on technetium and other radiometals in chemistry and medicine. September 8-11, 2010, Bressanone, Italy.
 13. Johnstone, E. V.; Poineau, F.; Czerwinski, K. R.; Sattelberger, A. **Optimization of the synthesis of binary technetium halides**. 240th ACS National Meeting, Boston, MA, United States, August 22-26, 2010
 14. Poineau, F M.; Weck, P; Forster, PM.; Sattelberger, A P.; Czerwinski, K R.; Johnstone, Erik. **Technetium bromides as precursors for the synthesis of low valent complexes**. 239th ACS National Meeting, San Francisco, CA, United States, March 21-25, 2010.
 15. Poineau, F; Czerwinski, Ken R.; Johnstone, Erik V.; Sattelberger, Alfred. **Optimization of the synthesis of technetium binary halides**. 239th ACS National Meeting, San Francisco, CA, United States, March 21-25, 2010